



UNIVERSITAT DE
BARCELONA

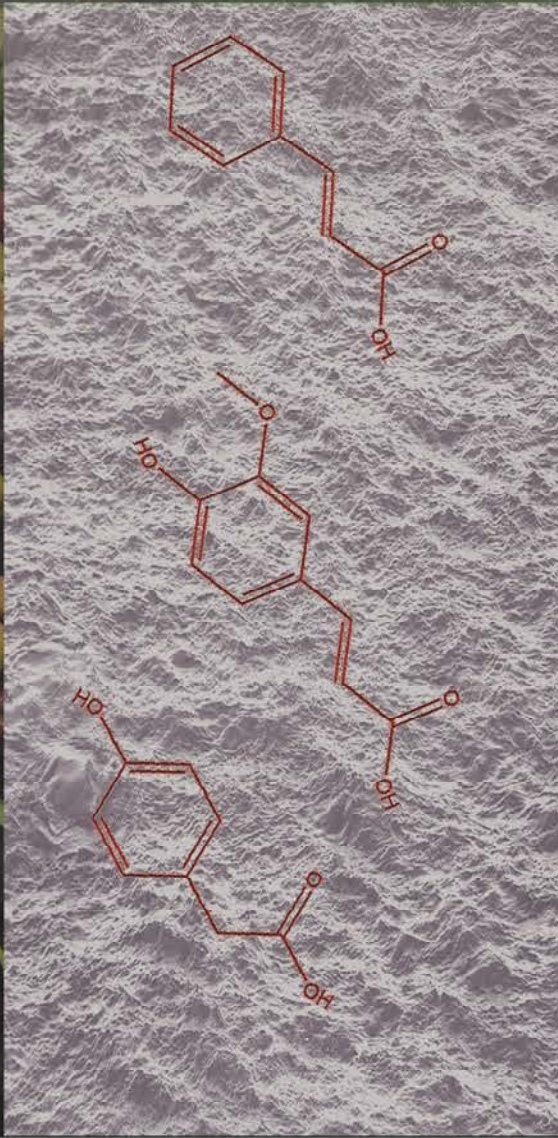
Degradación de contaminantes de aguas residuales de la producción de aceite de oliva mediante procesos electroquímicos de oxidación avanzada

Nelly Esther Flores Tapia

ADVERTIMENT. La consulta d'aquesta tesi queda condicionada a l'acceptació de les següents condicions d'ús: La difusió d'aquesta tesi per mitjà del servei TDX (www.tdx.cat) i a través del Dipòsit Digital de la UB (diposit.ub.edu) ha estat autoritzada pels titulars dels drets de propietat intel·lectual únicament per a usos privats emmarcats en activitats d'investigació i docència. No s'autoritza la seva reproducció amb finalitats de lucre ni la seva difusió i posada a disposició des d'un lloc aliè al servei TDX ni al Dipòsit Digital de la UB. No s'autoritza la presentació del seu contingut en una finestra o marc aliè a TDX o al Dipòsit Digital de la UB (framing). Aquesta reserva de drets afecta tant al resum de presentació de la tesi com als seus continguts. En la utilització o cita de parts de la tesi és obligat indicar el nom de la persona autora.

ADVERTENCIA. La consulta de esta tesis queda condicionada a la aceptación de las siguientes condiciones de uso: La difusión de esta tesis por medio del servicio TDR (www.tdx.cat) y a través del Repositorio Digital de la UB (diposit.ub.edu) ha sido autorizada por los titulares de los derechos de propiedad intelectual únicamente para usos privados enmarcados en actividades de investigación y docencia. No se autoriza su reproducción con finalidades de lucro ni su difusión y puesta a disposición desde un sitio ajeno al servicio TDR o al Repositorio Digital de la UB. No se autoriza la presentación de su contenido en una ventana o marco ajeno a TDR o al Repositorio Digital de la UB (framing). Esta reserva de derechos afecta tanto al resumen de presentación de la tesis como a sus contenidos. En la utilización o cita de partes de la tesis es obligado indicar el nombre de la persona autora.

WARNING. On having consulted this thesis you're accepting the following use conditions: Spreading this thesis by the TDX (www.tdx.cat) service and by the UB Digital Repository (diposit.ub.edu) has been authorized by the titular of the intellectual property rights only for private uses placed in investigation and teaching activities. Reproduction with lucrative aims is not authorized nor its spreading and availability from a site foreign to the TDX service or to the UB Digital Repository. Introducing its content in a window or frame foreign to the TDX service or to the UB Digital Repository is not authorized (framing). Those rights affect to the presentation summary of the thesis as well as to its contents. In the using or citation of parts of the thesis it's obliged to indicate the name of the author.



Nelly Esther Flores Tapia

PhD Thesis

2017

UNIVERSITAT DE BARCELONA

Degradación de contaminantes de aguas residuales de la producción de aceite de oliva mediante procesos electroquímicos de oxidación avanzada

Nelly Esther Flores Tapia

Doctorado en Electroquímica. Ciencia y Tecnología

Universidad de Barcelona

*Departamento de Ciencia de los Materiales y Química Física
-Sección de Química Física-*

***Degradación de contaminantes de
aguas residuales de la producción
de aceite de oliva mediante
procesos electroquímicos de
oxidación avanzada***

Memoria presentada por **Nelly Esther Flores Tapia**
para optar al título de Doctor por la Universidad de Barcelona

Directores de Tesis:

Director

Co-Director

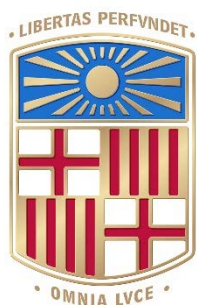
Dr. Enric Brillas Coso

Catedrático de Universidad
Departament de Ciència de
Materials y Química Física de la
Universidad de Barcelona

Dr. Ignacio Sirés Sadornil

Profesor Agregado
Departament de Ciència de
Materials y Química Física de la
Universidad de Barcelona

Barcelona, Septiembre 2017



UNIVERSITAT DE BARCELONA

Degradación de contaminantes de aguas residuales de la producción de aceite de oliva mediante procesos electroquímicos de oxidación avanzada

Nelly Esther Flores Tapia

A Thesis presented for the degree of
Doctor of Philosophy

Departament de Ciència dels Materials i Química-Física
-Secció de Química Física-

Universidad de Barcelona
Septiembre, 2017

Agradecimientos

A todas las personas que han hecho posible la culminación de este trabajo.

A los Directores de la Tesis el Doctor Enric Brillas y el Doctor Ignacio Sirés quienes han compartido sus habilidades y conocimientos para el desarrollo de este trabajo y del manejo dentro del laboratorio. A la Dra. Rosa María Rodríguez por el apoyo con el material del laboratorio y las prácticas en las que me ha dejado participar junto a ella y al Doctor José Antonio Garrido.

A todo el personal del LEMMA por su continua ayuda en todos los momentos dentro del laboratorio.

A los compañeros del laboratorio LEMMA que han pasado a lo largo de los años quienes de una u otra manera ayudaron a aliviar la presión durante las largas horas en el laboratorio, en especial a Laye quien fue más allá de su deber, mil gracias.

A la Doctora Elvira Gómez, gracias a su carta pude ingresar en el programa de Máster y Doctorado y sobre todo porque me puso en contacto con este grandioso grupo de investigación.

A los profesores del Máster "Electroquímica. Ciencia y Tecnología" por sus enseñanzas a lo largo de los años, también a todos los compañeros de aulas en Alicante. Gracias Edu.

Al Doctor Roberts de la University of Calgary, quien me recibió en su laboratorio durante los cuatro meses de mi estancia internacional.

A Farbod y Zoreh, quienes fueron grandes compañeros en Calgary, siendo los que me entrenaron en el uso de los equipos y las técnicas de adsorción con Nyex y grafeno.

Al SENESCYT por proveer con la Beca Convocatoria Abierta 2012 y al ex Presidente Rafael Correa por promover la educación y avance tecnológico en Ecuador. A todos los ciudadanos ecuatorianos quienes con sus impuestos son directos patrocinadores de mis años de estudio, ellos son una razón para volver a mi patria y hacer funcionar los conocimientos adquiridos en España.

Al final, pero jamás los últimos, a mi familia amada, mi papi, nunca dejaste que me cayera, mi mami siempre pendiente de mí, la Mary y sus cachorros (Gabo, Dana y los que vendrán) y a mi hermano Cris.

GLOSARIO DE SIGLAS

Listado de siglas en castellano:

AGG	Disolución de Ácido Glutámico-Glucosa
CE	Comunidad Europea
CEE	Comunidad Económica Europea
COT	Carbono Orgánico Total
DBO₅	Demanda Biológica de Oxígeno medida a los cinco días
DQO	Demanda Química de Oxígeno
EF	Electro-Fenton
FEF	Fotoelectro-Fenton
FEFS	Fotoelectro-Fenton Solar
lpcd	Litros per cápita por día
NT	Nitrógeno Total
OA-H₂O₂	Oxidación Anódica con generación de peróxido de hidrógeno
OOMW	Aguas residuales de la molienda de aceite de oliva
PTFE	Politetrafluoroetileno
ST	Sólidos Totales
STS	Sólidos Totales Suspendidos
SV	Sólidos Volátiles
UE	Unión Europea

Listado de siglas en inglés:

AOP	Advanced Oxidation Processes
COD	Chemical Oxygen Demand
EAOPs	Electrochemical Advanced Oxidation Processes
FDA	Food and Drug Administration
GC-MS	Gas Chromatography coupled to Mass Spectrometry
GDE	Gas Diffusion Electrode
NF	Nanofiltration
OOMW	Olive Oil Mill Wastewater
PTFE	Polytetrafluoroethylene
ROS	Reactive Organic Species
UASB	Upflow Anaerobic Sludge Blanket Reactor
UF	Ultrafiltration

ÍNDICE

1. INTRODUCCIÓN	1
1.1. El agua y su distribución en el planeta	2
1.2. Legislación Española respecto a la gestión y tratamiento de aguas residuales	5
1.3. Producción de aceite de oliva a nivel mundial y su impacto ambiental en los países Mediterráneos	7
1.4. Estudios sobre aguas residuales de la industria productora de aceite de oliva	9
1.4.1. Composición de las OOMW	11
1.4.1.1. Ácido <i>trans</i> -cinámico	13
1.4.1.2. Ácido <i>trans</i> -ferúlico	14
1.4.1.3. Ácido 4-hidroxifenilacético	15
1.5. Tratamientos aplicados a la remediación de las OOMW	16
1.5.1. Tratamientos Físicos	16
1.5.2. Tratamientos Fisicoquímicos	17
1.5.3. Tratamientos de Oxidación Avanzada	18
1.5.4. Tratamientos Biológicos	20
1.5.5. Tratamientos Combinados	21
1.6. Procesos Electroquímicos de Oxidación Avanzada (EAOPs)	22
1.6.1. Ánodo de BDD	23
1.6.2. Electrodo de difusión de aire	25
1.6.3. Oxidación Anódica con H ₂ O ₂ electrogenerado (OA-H ₂ O ₂)	26
1.6.4. Electro-Fenton (EF)	27
1.6.5. Fotoelectro-Fenton (FEF)	29
1.6.6. Fotoelectro-Fenton Solar (FEFS)	30
2. OBJETIVOS	31
2.1. Objetivos Generales	31
2.2. Objetivos Específicos	31
3. PARTE EXPERIMENTAL	33
3.1. Reactivos	33
3.2. Sistemas Electroquímicos	33
3.3. Procedimientos analíticos	35
3.3.1. Cuantificación del H ₂ O ₂	35
3.3.2. Cuantificación del carbono orgánico total (COT)	36
3.3.3. Cuantificación de los aromáticos y ácidos carboxílicos	36
3.3.4. Determinación de la demanda química de oxígeno (DQO)	37
3.3.5. Determinación de la demanda biológica de oxígeno (DBO ₅)	38
3.3.6. Caracterización de aguas residuales	40

4.	HYDROGEN PEROXIDE PRODUCTION	45
5.	MINERALIZACIÓN DEL ÁCIDO <i>TRANS</i>-CINÁMICO	51
	Electrochemical destruction of <i>trans</i> -cinnamic acid by advanced oxidation processes: kinetics, mineralization, and degradation route	55
6.	MINERALIZACIÓN DEL ÁCIDO <i>TRANS</i>-FERÚLICO	67
	Degradation of <i>trans</i> -ferulic acid in acidic aqueous medium by anodic oxidation, electro-Fenton and photoelectro-Fenton	71
7.	MINERALIZACIÓN DEL ÁCIDO 4-HIDROXIFENILACÉTICO EN DISOLUCIONES SINTÉTICAS	81
	Removal of 4-hydroxyphenylacetic acid from aqueous medium by electrochemical oxidation with a BDD anode: Mineralization, kinetics and oxidation products	85
8.	MINERALIZACIÓN DEL ÁCIDO 4-HIDROXIFENILACÉTICO EN OOMW	93
	4-Hydroxyphenylacetic acid oxidation in sulfate and real olive oil mill wastewater by electrochemical advanced processes with a boron-doped diamond anode	97
9.	SUMMARY	107
10.	CONCLUSIONS	117
11.	REFERENCIAS	121

1. INTRODUCCIÓN

“El agua no es necesaria para la vida, sino la vida misma”

Antoine de Saint-Exupéry

Cada 22 de marzo se celebra el día mundial de agua, siendo una fecha que en la mayor parte del planeta pasa desapercibida debido a la escasa conciencia que todavía tiene la sociedad sobre su importancia.

Los seres humanos pensamos que el agua siempre estará ahí para satisfacer nuestras necesidades. Creemos además que el agua es un bien inagotable y que la naturaleza la recicla siguiendo un ciclo infinito. Esta ilusión es más patente en los países con abundantes fuentes hídricas y con un buen sistema de saneamiento y distribución del agua, cosa que no sucede en todo el planeta.

Los esfuerzos de los gobiernos del mundo por concienciar acerca del uso del agua y el mantenimiento de las fuentes hídricas son altamente necesarios.

Hace ya más de diez años, recuerdo ver por televisión un reportaje en el que se citaba a Ismail Serageldin, vicepresidente del Banco Mundial en los años noventa, diciendo que “si las guerras de este siglo son por el petróleo, las del siguiente serán por el agua”. Imaginando este panorama, lo único que viene a la mente es la más horrible, cruenta y despiadada de las guerras, sobre todo si se toman como referencia los varios conflictos relacionados con el agua que ya han sido documentados (Cooley, 1984).

Pero al parecer no todo está perdido. Barnaby (2009), lejos de imaginar un final apocalíptico de la civilización, sugiere que el agua no acarreará guerras ya que la aparente falta de la misma en un país es compensada, por ejemplo, a través de sus importaciones agrícolas, ya que en la práctica éstas conllevan un ahorro relacionado con la producción de esos alimentos. De esta forma, el agua sigue fluyendo entre las naciones en diferentes formas, evitando así conflictos.

Exista o no un riesgo real de guerra por el agua, las preguntas que siguen en el aire siguen siendo: ¿Hasta cuándo podremos sustentar esta paz si día a día contaminamos las efuentes naturales? ¿Qué hacemos con las aguas ya contaminadas? La respuesta a la última pregunta es: tratarlas.

El tratamiento de aguas residuales necesita de mucho esfuerzo y colaboración entre los gobiernos, las industrias y la población en general. Aquí es donde los científicos e ingenieros pueden y deben volcar sus esfuerzos. Como primera iniciativa se puede comenzar mejorando los sistemas de tratamiento de aguas residuales actuales o bien desarrollar nuevas tecnologías que ayuden a este propósito. Por lo cual, estudiar las aplicaciones de los procesos electroquímicos de oxidación avanzada (EAOPs, por sus siglas en inglés) a la descontaminación del agua se convierte en una alternativa más para conseguir solucionar un problema que nos concierne a todos los seres humanos.

1.1. El agua y su distribución en el planeta

La Tierra es llamada el planeta azul por sus grandes extensiones de agua, las cuales abarcan la tercera parte del planeta. Sin embargo, el 97,5% del agua total forma parte de los océanos, de manera que sólo un 2,5% es agua dulce y, además, ésta se encuentra en gran parte en forma de hielo en los polos y en acuíferos. Como resultado, únicamente un 0,01% del total del agua del planeta está disponible para el consumo humano directo (United Nations, 2007).

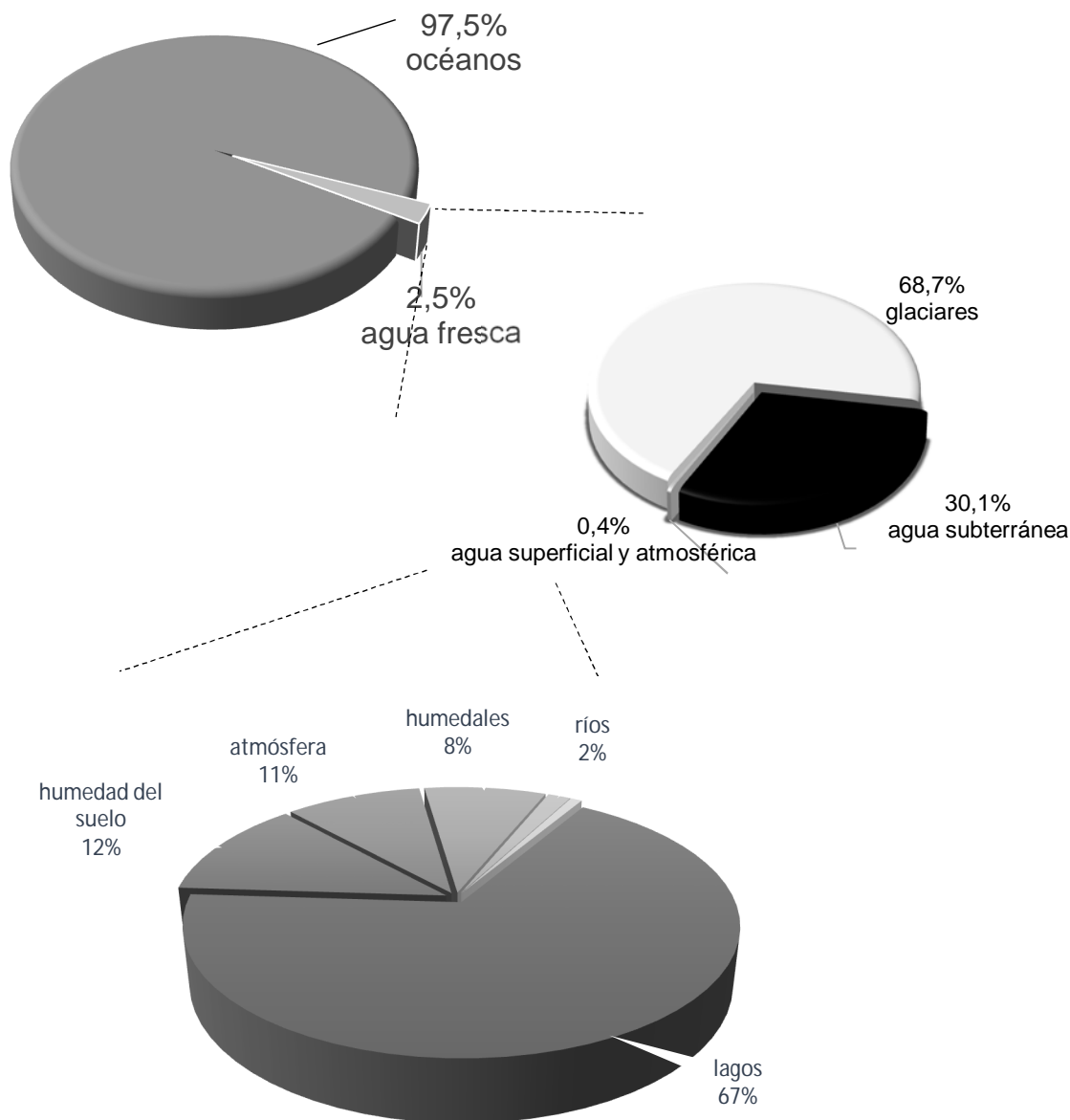


Figura 1. Distribución del agua en el planeta

Fuente: adaptación (United Nations, 2007)

Como se puede ver en la Figura 1, solamente un pequeño porcentaje de agua en el planeta es utilizado para tratar de satisfacer todas las actividades humanas. Según el World Water Council (2000), en el mundo habitan 7 billones de personas, de los cuales 1,4 billones viven en condiciones de extrema pobreza y 1 de cada 5 personas en los países más pobres no tienen acceso a agua saneada a precio

suficientemente bajo.

Actualmente, el agua dulce disponible no cubre las necesidades de todos los seres humanos en el planeta. Sumado a esto, cerca del 80% de las aguas residuales industriales son descargadas a ríos y mares sin previo tratamiento, lo que agrava aún más el problema de abastecimiento de agua (Asociación Española de Abastecimientos de Agua y Saneamiento, 2017).

Otro problema que se suma a la falta de agua en ciertas regiones es su forma de distribución entre la población. Si el reparto del agua se expresa en litros per cápita por día (lpcd), entonces:

- 500 a 800 lpcd va se concentra en ciudades industriales de los EE.UU.,
- 200 a 500 lpcd se distribuyen en grandes centros urbanos mundiales, y
- 90 a 150 lpcd se consume en áreas con suministros restringidos.

Como se observa, la actividad industrial influencia en gran medida el consumo de agua a nivel mundial. En función a los tipos de consumidores de agua, puede dividirse en agua para uso doméstico y no doméstico.

El **consumo doméstico** se relaciona con actividades humanas sin fines comerciales o de producción de insumos. Sirve principalmente para la eliminación de residuos del baño y aseo personal, y uso en la cocina y lavandería, entre otras actividades de los hogares. El consumo doméstico depende de muchos factores, como pueden ser el país analizado, el sistema de distribución del agua, la facilidad de acceso al suministro, el clima, el tamaño de la casa, etc. En la Tabla 1 se compara el consumo doméstico de agua en varios países.

Tabla 1. Consumo doméstico de agua en varios países del mundo.

País	Año	Agua consumida (lpcd)
Argentina	2010	261
Australia	2010	425
España	2014	132*
Francia	2012	120
Gabón	2010	143
Indonesia	2007	90
Japón	2012	225
México	2012	301
EEUU	2012	526

Fuente: Ratnayaka y col. (2009); * Instituto Nacional de Estadística (2017)

Los datos muestran una gran variación en el consumo por país. Cabe notar que los países con mayor desarrollo necesitan mayor cantidad de agua para su día a día, si bien la eficiencia en el consumo también juega un papel importante.

El **consumo no doméstico** comprende el uso industrial, comercial, agrícola y gubernamental. Prácticamente todos los procesos de manufactura necesitan de agua.

Puesto que esta Tesis se enfoca a la remediación de aguas residuales, es más interesante estudiar el volumen de aguas residuales producidas por la industria, más que el consumo de agua de las mismas. La Tabla 2 detalla las toneladas de aguas residuales producidas por día durante el año 2003 y su grado de

contaminación cuantificado como carbono orgánico total (COT) en 13 países pertenecientes a la Unión Europea.

Tabla 2. Niveles de COT en industrias de la UE.

Industria	Ton (día)	COT (kg)
Plantas industriales de pulpa de madera para producir papel o cartón	>20	240771200
Instalaciones para gestión de residuos no peligrosos	>50	123851400
Rellenos sanitarios	>10	
Químicos orgánicos básicos	--	41957238
Mataderos	>50	
Plantas procesadoras de leche	>200	18628850
Materias primas animales	>75	
Materias primas vegetales	>300	
Otros	--	30943

Fuente: WWAP (2006)

El agua está ligada al capital de los países, ya sea como fuente de energía o como parte de los insumos producidos. Esto repercute directamente en el aumento del consumo del agua (United Nations, 1987).

Hasta el año 2050, por ejemplo, se prevé que China e India incrementarán su producción de energía eléctrica entre un 6,6% y un 7,5%. Este crecimiento en la industria eléctrica impulsará un mayor consumo de agua, de tal forma que se piensa que el consumo total del agua en los sectores energéticos comparados con el 2005 aumentará hasta 5 veces en China, 1,5 veces en la Unión Europea, 10,1 veces en India, 1,2 veces en Japón, 3,3 veces en Rusia y 1,4 veces en EEUU (Wan y col., 2016).

La necesidad de agua es mayor conforme pasa el tiempo, pero a la vez estamos en un punto en el cual el abastecimiento de agua está escaseando en cantidad y calidad. Es preocupante que los sistemas acuáticos naturales estén perdiendo su capacidad de diluir los contaminantes y, por tanto, su habilidad de autoregenerarse. Esto podría estar creando un peligroso escenario a futuro, no sólo desde una perspectiva ambiental sino también económica (Arenas-Sánchez y col., 2016).

Durante los años 2007 y 2008, ciudades como Atlanta, Georgia y Barcelona sufrieron escasez de agua debido a una sequía. La situación fue tan difícil que un barco completamente cargado de agua solamente pudo suministrar agua a Barcelona para 32 min (Catley-Carlson, 2011). Esto hace reflexionar sobre los costos que la población de cada ciudad tiene que asumir para la provisión de agua y el gran impacto en la economía de cada región. Por ejemplo, en Cataluña, durante el año 2016, el precio promedio del agua fue de 3,191 €/m³ para un consumo doméstico máximo de 20 m³/mes, mientras que en el sector industrial para el mismo consumo el precio ascendió a 3,324 €/m³; tarifa que se puede reducir hasta 2,586 €/m³ gracias a incentivos que se dan a la gran industria, cuyo consumo asciende a 5000 m³/mes (Agència Catalana de l'Aigua, Generalitat de Catalunya, 2016).

El total de agua dulce con el que cuenta cada país es el total de agua renovable que posee en forma de agua superficial y subterránea. En el caso de España se estima que sus reservas ascienden a 111.000 hm³/año y, de este total, el 80% es empleado en el sector agroindustrial (Montoya y col., 2016). La distribución de

agua por sectores en España en miles de metros cúbicos se resume en la Tabla 3.

Tabla 3. Estadísticas sobre el Suministro y Saneamiento del Agua por grupos de usuarios en 2014.

Usuario	Miles m ³
España	3.214.034
Hogares	2.237.746
Industria	349.320
Servicios	160.375
Usos turísticos y recreativos	137.545
Agricultura y ganadería	25.458
Construcción	12.143
Consumos municipales	291.447

Fuente: Instituto Nacional de Estadísticas (2016)

1.2. Legislación Española respecto a la gestión y tratamiento de aguas residuales

España, como parte de la UE, está obligada al cumplimiento de las leyes y reglamentos expresados en el Acta Única europea de los años setenta, cuyos objetivos y principios están incluidos en los Tratados de Ámsterdam y el Tratado de la Unión Europea, en cuyo apartado 1 del artículo 130R se detallan los objetivos de la política Comunitaria Ambiental.

Los principios a respetar según el artículo 130R.2 del Tratado de la Comunidad Europea incluyen la conservación, la protección, la mejora de la calidad del medio ambiente y de la vida de las personas por medio de un uso racional de los recursos. En el capítulo 1 del Primer Programa de Acción Ambiental de la Comunidad de 1987, aparece el principio de “quien contamina paga”, el mismo que luego se incorporó al Tratado de la Comunidad Europea como una recomendación, la cual finalmente adquirió relevancia en el Tratado de Ámsterdam. Este principio se aplica en el momento de calcular el costo de la contaminación-tratamiento, así como quien deberá cubrirlo. Sin embargo, debido a las diferentes políticas ambientales de cada país perteneciente a la comunidad, este principio ha sido de difícil aplicación (Gutiérrez Duarte y col, 2013).

Referente al recurso hídrico, se puede mencionar la Directiva 91/271/CEE sobre el tratamiento de las aguas residuales urbanas antes de su vertido. Esta Directiva, actualizada con la Directiva 98/15/CE, que determina los sistemas de recolección, tratamiento y vertido de las aguas residuales urbanas, se ha complementado con la normativa española de los Reales Decretos de Ley 11/1995 del 28 de diciembre (BOE núm. 312, de 30 de diciembre), 509/1996 del 15 de marzo (BOE núm. 77, de 29 de marzo), y 2116/199 (MAPAMA, 2016).

En la práctica, el gobierno español aplica la Directiva 91/271/CEE por medio del Plan de Calidad Nacional de las Aguas y su plan de Choque Tolerancia Cero de Vertidos, cuya ejecución está a cargo del Ministerio de Medio Ambiente y la Dirección Nacional de Aguas España (Ministerio de Medio Ambiente, 2007).

Las industrias en España necesitan un permiso para verter sus aguas residuales. Esto se contempla en el Real Decreto 606/2003, en el que se aprueba el Reglamento Público Hidráulico, del 23 de mayo, publicado en el BOE de 6 de junio

de 2003. El vertido directo, la valoración y la eliminación de desechos es competencia de las comunidades autónomas, incluido en el artículo 13 de la Ley 10/1998. La disposición adicional 5ª de la ley también indica que, excepcionalmente, los desechos agrícolas y ganaderos podrán ser reutilizados como fertilizantes (Danés y col., 2007).

Según el Reglamento del Dominio Público Hidráulico (Ministerio de Obras Públicas y Urbanismo, 1989), en su anexo al título IV, las industrias deben considerar el tratamiento de sus residuos acuosos si no alcanzan valores mínimos como los señalados en la Tabla 4, según el sector productivo.

Tabla 4. Límites de contaminación mínimos para que un efluente sea tratado.

Parámetro (Unidad)	Condiciones	Valores Límites		
		1	2	3
pH	La dispersión del efluente a 50 m del punto de vertido debe conducir a un pH comprendido entre 6,5 y 8,5	--	--	5,5-9,5
Sólidos en suspensión (mg L ⁻¹)	Diámetro de partícula menor a 45 µm	300	150	80
Materias sedimentables (mL L ⁻¹)	Medidas en cono Imhoff en 2 h	2	1	0,5
Sólidos gruesos	—	ausentes	ausentes	ausentes
DBO ₅ (mg L ⁻¹)	Para efluentes industriales, con oxidabilidad muy diferente a un efluente doméstico tipo, la concentración límite se referirá al 70 por 100 de la DBO total.	300	60	40
DQO (mg L ⁻¹)	Determinación al bicromato potásico	500	200	160
Temperatura (°C)	En ríos, el incremento de temperatura media de una sección fluvial tras la zona de dispersión no superará los 3 °C	3	3	3
Color	La apreciación del color se estima sobre 10 centímetros de muestra diluida	inapreciable	inapreciable	inapreciable

Fuente: Ministerio de Obras Públicas y Urbanismo (1989)

1.3. Producción de aceite de oliva a nivel mundial y su impacto ambiental en los países Mediterráneos

Según la mitología griega, la Diosa Atenea en competencia con el Dios Poseidón por el patronazgo de la ciudad, ofrecieron regalos a los habitantes de Atenas. La Diosa plantó un olivo mientras que el Dios con su tridente abrió en la tierra un lago, pero éste era salado. Los atenienses, al ver los magníficos beneficios del árbol, proclamaron a Atenea su Diosa patrona y desde entonces el olivo y sus productos han sido el gran tesoro de Grecia y también de los países Mediterráneos.

En la Grecia clásica, Homero trataba al aceite de oliva como “oro líquido” y en la actualidad aún puede seguirse conservando ese título por los beneficios económicos que aún sigue aportando a sus productores. El aceite extra virgen de oliva tiene hoy en día una imagen positiva entre los consumidores por sus beneficios para la salud, sabor y vastas aplicaciones; aunque es un producto de lujo y apenas representa un 2% del total consumido al nivel mundial (Clodoveo y col., 2014). En la Tabla 5 se cita la producción de aceite de oliva a nivel mundial.

Tabla 5. Producción de aceite de oliva a nivel mundial.

País	2015/16 (10 ³ Tm)	2016/2017* (10 ³ Tm)
España	1401,6	1311,3
Grecia	320,0	260,0
Italia	474,6	243,0
Turquía	143,0	177,0
Marruecos	130,0	110,0
Siria	110,0	110,0
Túnez	140,0	100,0
Portugal	109,1	93,6
Argelia	83,5	74,0
Egipto	25,0	27,0
Jordania	29,5	23,0
Australia	20,0	21,0
Chile	16,5	16,5
Palestina	19,5	21,0
Argentina	19,0	15,5
Líbano	23,0	20,0
Libia	18,0	15,5
Israel	15,0	16,0
Albania	10,5	11,0
Irán	5,0	5,5
Chipre	6,0	6,0
Francia	5,0	5,0
Montenegro	0,5	0,5
China	5,0	5,0
EEUU	5,0	5,0
Croacia	5,5	4,0
Eslovenia	0,5	0,4
Arabia Saudí	3,0	3,0
Uruguay	0,5	1,0
Malta	0,1	0,0

Fuente: International Olive Council (2017); *previsión

La UE acapara más del 75% de la producción del aceite de oliva a nivel mundial, siendo España el mayor productor de este aceite con más del 52% de la producción entre los países europeos (International Olive Council, 2017). Otros

grandes productores de aceite de oliva son Italia y Grecia. Grecia tiene la mayor variedad de olivas comparado con otros países, y dedica el 60% de su territorio cultivable a los olivares. Todos estos países tienen protección de denominación de origen en sus productos para diferenciarlos de productos provenientes de otros países. Es interesante notar que si bien los Estados Unidos producen su propio aceite de oliva, su producción no satisface la demanda interna, por lo que también este país es uno de los mayores importadores de aceite de oliva en el mundo (Sabbatini, 2014).

La industria olivera en España aportó 1886 millones de euros entre el 2007 y el 2012. La superficie dedicada al cultivo de olivas en el país es de más de 2 millones y medio de hectáreas, de las cuales el 28% necesita riego. Esta industria da trabajo a 46 mil jornaleros por temporada, por lo que es una fuente muy importante de ingresos para el país (MAPAMA, 2017).

La industria productora de aceite de oliva es una industria que elabora su producto en los meses invernales y comprende varios pasos:

- La fruta, una vez recolectada, debe ser lavada y molida (con molinos mecánicos o artesanales),
- la pasta obtenida es nuevamente mezclada y batida para poder obtener más aceite, y
- finalmente, se separa el aceite del resto de la pasta inicial. Este proceso se puede hacer por prensado o centrifugación en dos o tres fases (Aggoun y col., 2016).

Al final del proceso de extracción se obtienen tres fracciones. La primera es el aceite de oliva extra virgen, la segunda es una pasta (*cake*) sólida que contiene la pulpa, la piel, tierra, etc., y una tercera fracción líquida, denominada aguas residuales de la molienda (OOMW), que arrastra los componentes solubles del fruto, así como algunos sólidos. En España esta actividad se lleva mayoritariamente a cabo en varias pequeñas cooperativas que se hallan muy dispersas por el Mediterráneo. Esto provoca que los residuos sean difíciles de cuantificar con exactitud, lo que dificulta su recolección y tratamiento adecuado (Dermeche y col., 2013).

La caracterización de las dos fases residuales muestra una alta concentración de compuestos fenólicos, carbohidratos, ácidos orgánicos y otros varios compuestos orgánicos de difícil degradación. Estos residuos sin tratar se convierten en un grave problema para los países productores debido a su alta toxicidad, bajo pH, alto DQO superior a 110 g L⁻¹ y DBO superior a 170 g L⁻¹. Además, los grandes volúmenes de OOMW producidos aumentan la peligrosidad de estos efluentes generados a corto plazo (Dermeche y col., 2013).

La liberación de OOMW en el suelo afecta tanto a su fertilidad como a la actividad microbiana sobre él, por lo que no se recomienda como fertilizante sin antes realizar un estudio previo. Tampoco se recomienda el vertido directo de estas aguas residuales por su alta carga contaminante. Esto obliga al tratamiento previo de una OOMW antes de ser considerada apta para el vertido (Mcnamara y col., 2008).

El sistema de extracción de aceite de oliva requiere de mucha cantidad de agua. Por ejemplo, para el prensado se necesitan 40 L kg^{-1} de pasta, mientras que para el sistema de extracción trifásico aproximadamente 50 L kg^{-1} (De Marco y col., 2006). Como resultado de este ingente consumo de agua, anualmente se producen unos 30 millones de metros cúbicos de OOMW en el mundo durante la época de producción del aceite (Borja y col., 1997). Por ejemplo, al estudiar el caso de los dos mayores productores de aceite de oliva, se ha determinado que España produce más de 2 millones de metros cúbicos de OOMW, mientras que Italia produce unos 3 millones de metros cúbicos durante la época de extracción del aceite. Si se suma, además, la producción de otros países Mediterráneos, en total se generan 12 millones de metros cúbicos de OOMW por temporada, los cuales terminarían en la cuenca del mar Mediterráneo, convirtiéndose en un problema ambiental muy grave (Topi y col., 2014).

Ya la Unión Europea, en vista de las particularidades de las OOMW, ha dado recomendaciones sobre el manejo y tratamiento de estas aguas residuales y además ha encargado que se revisen las leyes de los diferentes países productores. Estas recomendaciones pretenden disminuir la contaminación desde la fuente, pero siempre tomando en cuenta la relación de dependencia de los países Mediterráneos con la industria del aceite de oliva (PROSODOL, 2012).

Una de las recomendaciones apremia a que se reutilice el 50% de las OOMW hasta el año 2020. Así mismo, en España se ha prohibido el vertido directo de estas aguas residuales y se ha incrementado el empleo de tecnologías con menor consumo de agua para la extracción del aceite de oliva, mientras que Italia permite el uso de las OOMW en suelos agrícolas previo estudio y en Grecia la práctica habitual implica su neutralización con cal y posterior tratamiento en estanques de evaporación (Ozdemir y col., 2012; Topi y col., 2014).

1.4. Estudios sobre aguas residuales de la industria productora de aceite de oliva

Si se revisa la literatura, se pueden encontrar miles de publicaciones relacionadas con el tratamiento de las OOMW. Existen tratamientos de OOMW que se enfocan en eliminar o reducir la concentración de los contaminantes. En ello se emplean varias técnicas, incluyendo pozos de evaporación, tratamientos biológicos aerobios y anaerobios, procesos fisicoquímicos de filtración con membranas, precipitación y floculación, procesos de oxidación avanzada como UV/H₂O₂, H₂O₂/UV, O₃/UV, métodos electroquímicos y los que combinan una o más de las técnicas anteriores. Algunos tratamientos también se han enfocado a la recuperación de componentes específicos presentes en las OOMW tales como los biofenoles; mientras que otros tratamientos apuntan a la valorización de las OOMW obteniendo de ellos combustibles gaseosos (Fiestas y col., 1997) e incluso reusándolos como fertilizante de suelos (Suna y col., 2011; Barbera y col., 2013; Gebreyohannes y col., 2016). Una opción propuesta por Magdich y col. (2016) consistió en regar con OOMW los campos sembrados con olivares *Chemlali* en dosis variables de 50, 100, y 200 m³ ha⁻¹ año⁻¹ por el lapso de 8 años. Al final determinaron que la práctica no tenía efectos adversos en las plantas si el riego se mantenía por debajo de los 100 m³ ha⁻¹ año⁻¹. Como recomendación final se sugirió que se deben investigar las dosis correctas de OOMW antes de esparcirla sobre los terrenos de cultivo.

Los tratamientos biológicos se han empleado desde siempre en la remediación de aguas residuales. González-González y Cuadros (2015) llevaron a cabo la digestión anaerobia de OOMW sin y con pretratamiento por periodos de 5 y 7 días, logrando una eliminación del 90% de fenoles y de un 65,2 % de la DQO además de recuperar el 30% del agua inicial del proceso después de separarla de los lodos.

Zagklis y col. (2015), utilizaron la técnica de filtración con membranas en tres pasos consecutivos: microfiltración, nanofiltración y ósmosis inversa. Se logró la separación de compuestos orgánicos de bajo peso molecular del resto de la OOMW. Con esta técnica se consiguió bajar la DQO desde 107 hasta 65,5 g L⁻¹ y los sólidos totales de 63,4 hasta 60,4 g L⁻¹. Además, se optimizó un proceso de adsorción con el que se logró hasta un 4,9% de recuperación de fenoles tras la etapa de desorción. Cuando se utiliza la técnica de ultrafiltración seguida por nanofiltración, la DQO se redujo en un 92% y los sólidos totales en un 95% (Ioannou-Ttofa y col., 2017).

Nieto y col. (2011) trataron 1 L de OOMW por oxidación avanzada, mediante la generación de radicales hidroxilos en el medio por la reacción de Fenton empleando cloruro férrico en presencia de peróxido de hidrógeno. Bajo condiciones óptimas llegaron a degradar la materia orgánica disminuyendo la DQO un 61,9%, eliminando además más del 95% de los fenoles, poniendo de manifiesto que el método es muy efectivo para la descontaminación de estas aguas residuales. La viabilidad de los procesos de oxidación avanzada también se han comprobado mediante experimentos a escala de planta piloto, en un reactor agitado en continuo, donde se alcanzó un 99% de eliminación de fenoles mediante la técnica *Fenton-like* utilizando FeCl₃/H₂O₂ (Hodaifa y col., 2013).

Otros tratamientos se enfocan en la recuperación de compuestos específicos de las OOMW, como en el caso de los procesos de adsorción utilizando hidróxidos de doble capa Zn/Al para eliminar los fenoles (De Martino y col., 2011), o también mediante sílices modificadas empleadas para la recuperación de hidroxitirosol (Yangui y col., 2016)

La gran complejidad de las OOMW hace necesario el uso de diversos tratamientos para lograr disminuir la carga orgánica presente. Para ello se pueden combinar varias técnicas que se aplican para eliminar poco a poco contaminantes. Un ejemplo es el acoplamiento de un proceso de coagulación como pre-tratamiento para bajar el contenido de sólidos de la OOMW seguido de un post-tratamiento Fenton (Alver y col., 2015). Se logró reducir un 94% de la DQO, un 86 % del DBO₅, un 96% de sólidos totales y 99,8% de fenoles totales. En el mismo estudio se obtuvieron resultados similares al emplearse una aireación con un reactor Jacto.MRB, ya que la eficiencia de reducción fue del 90% de la DQO, de un 99% de los sólidos totales y de un 80% de fenoles totales.

1.4.1. Composición de las OOMW

La oliva, al ser un fruto dependiente del medio en el que crece, presenta variaciones en su calidad y cantidad cada año. Esto afecta a la composición y características tanto de los productos obtenidos como de las aguas residuales producidas en esta industria, tal como se puede apreciar en la Tabla 6.

Tabla 6. Comparación de diferentes OOMW.

Parámetros	Inan y col. (2004)	Hajjouji y col. (2007)	Ntougias y col. (2013)	[a]	[b]
DQO / mg O ₂ L ⁻¹	48500	135000	--	2368	4369
ST / mg L ⁻¹	1780	168930	44180	5852	2460
COT / mg C L ⁻¹	12600	--	30820	598	1049
pH	4,6	4,8	5,0	6,8	7,1
Fenoles totales / mg L ⁻¹	--	970	3880	9,3	--
Conductividad / mS cm ⁻¹	11,5	44,3	--	1,5	1,4

[a] Datos del agua residual tratada en la presente Tesis, recogida en Octubre 2015

[b] Datos del agua residual tratada en la presente Tesis, recogida en Octubre 2016

La composición de las OOMW depende de varios factores, entre los cuales se pueden enumerar la composición del agua, los procesos de extracción del aceite y el tiempo de almacenaje:

- La composición de las OOMW cambia con las diferentes variedades de la oliva, su madurez, contenido de agua, tierra de cultivo, tiempo de siembra o cosecha, pesticidas, etc.
- La cantidad de agua utilizada en el proceso cambiará la composición del agua residual. Esto depende directamente de los equipos utilizados durante la extracción del aceite, y de la forma en que estos equipos sean utilizados. El agua utilizada en las diferentes etapas de producción del aceite sumada al agua de lavado reduce las concentraciones de los componentes presentes en las aguas residuales.
- El almacenamiento de las OOMW facilitará o no la acción bacteriana. Bajo condiciones adecuadas de almacenamiento puede darse la fermentación aeróbica y/o anaeróbica de los compuestos orgánicos. La descomposición de los compuestos genera volátiles, cambios en el pH y el aumento de la precipitación de sólidos (Niaounakis y Halvadakis, 2006).

Aunque la composición de las aguas residuales varía, generalmente estas OOMW contienen taninos, compuestos fenólicos, polialcoholes, pectinas, sacáridos y lípidos, siendo la fracción fenólica muy abundante y compleja (Chowdhury y col., 2013). Los componentes más frecuentes en este tipo de aguas residuales, de acuerdo con diferentes estudios, se presentan en la Tabla 7.

Tabla 7. Compuestos generalmente encontrados en las OOMW.

Nombre del compuesto	Autor que reporta el compuesto
3,4-Dihidroxifenil glicol	(D'Antuono y col., 2014)
Ácido 3,4-dihidroxifenilacético	(Aggoun y col., 2016)
Ácido 4-hidroxifenilacético	(Dermeche y col., 2013; Aggoun y col., 2016)
Ácido caféico	(Hajjouji y col., 2007; Azaizeh y col., 2012; Dermeche y col., 2013; Aggoun y col., 2016)
Ácido cinámico	(Dermeche y col., 2013)
GÁcido clorogénico	(Aggoun y col., 2016)
Ácido elenólico	(D'Antuono y col., 2014)
Ácido ferúlico	(Azaizeh y col., 2012; Dermeche y col., 2013; Daâssi y col., 2014; Aggoun y col., 2016)
Ácido gálico	(Hajjouji y col., 2007; Dermeche y col., 2013; Aggoun y col., 2016)
Ácido homovanílico	(Dermeche y col., 2013)
Acido <i>p</i> -cumárico	(Hajjouji y col., 2007; Azaizeh y col., 2012; Dermeche y col., 2013; Daâssi y col., 2014; Aggoun y col., 2016)
Ácido quínico	(D'Antuono y col., 2014; Daâssi y col., 2014)
Ácido sinápico	(Dermeche y col., 2013)
Ácido siríngico	(Dermeche y col., 2013)
Ácido vanílico	(Azaizeh y col., 2012; Dermeche y col., 2013; Daâssi y col., 2014; Aggoun y col., 2016)
Ácido verátrico	(Hajjouji y col., 2007)
Apigenina	(Daâssi y col., 2014; Aggoun y col., 2016)
Dihidroxitiroso	(Daâssi y col., 2014)
Dimetil oleuropein	(Dermeche y col., 2013)
Hidroxitiroso	(Azaizeh y col., 2012; Dermeche y col., 2013; Daâssi y col., 2014; Aggoun y col., 2016)
Luteolin	(Aggoun y col., 2016)
Luteolin-7-O-glucósido	(Aggoun y col., 2016)
Oleuropein	(Azaizeh y col., 2012; Dermeche y col., 2013; D'Antuono y col., 2014; Aggoun y col., 2016)
Oleuropein aglicona	(Aggoun y col., 2016)
Tirosol	(Azaizeh y col., 2012; Belaid y col., 2013; Dermeche y col., 2013; Aggoun y col., 2016)

En las OOMW se han identificado alrededor de 50 tipos de fenoles, los cuales según su estructura química se pueden clasificar en: derivados del tiroso y del ácido benzoico, junto ácidos cinámicos (Minh y col., 2007; Torrecilla, 2010).

En vista de su composición, si las OOMW son desechadas directamente al suelo pueden causar fuertes daños afectando a su acidez, salinidad, actividad microbiana, poder de retención de nutrientes, nitrógeno y agua en el suelo. Los efectos no son menos nocivos si se desecha directamente a fuentes naturales de agua, e incluso puede llegar a contaminar aguas subterráneas (Aggoun y col., 2016).

A continuación, se describen brevemente las características de los ácidos presentes en las OOMW que se han estudiado en esta Tesis.

1.4.1.1. Ácido *trans*-cinámico

El ácido cinámico tiene dos isómeros, el *cis* y el *trans*, siendo el más abundante el último de ellos. La fórmula empírica del ácido *trans*-cinámico es $C_9H_8O_2$ (ver estructura en la Figura 2).

También se le conoce como ácido *tert*- β -fenilacrílico, ácido bencenopropenoico y ácido 3-fenil-2-propenoico. Es un sólido cristalino blanco, cuyo peso molecular es $148,16 \text{ g mol}^{-1}$, con una temperatura de fusión de $132\text{-}135 \text{ }^\circ\text{C}$, una temperatura de ebullición de $300 \text{ }^\circ\text{C}$, una temperatura de inflamación de $93,3 \text{ }^\circ\text{C}$ y una densidad de $1,248 \text{ g cm}^{-3}$. Su solubilidad en agua es elevada, llegando a 230 mg L^{-1} (Mota y col., 2008), y su toxicidad LD_{50} en ratas es de $3,57 \text{ g kg}^{-1}$ ingerida por vía oral (95% CI $3,07 - 4,14 \text{ g kg}^{-1}$) (Letizia y col., 2005).

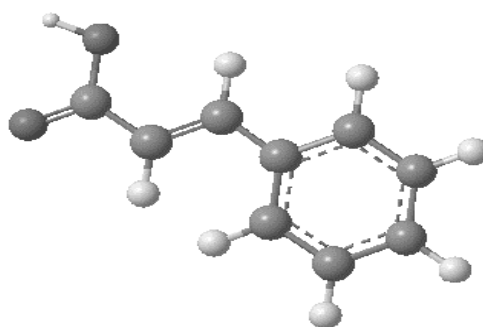


Figura 2. Estructura molecular del ácido *trans*-cinámico.

El ácido *trans*-cinámico es parcialmente absorbido a través de la piel, por lo que es irritante (Niaounakis and Halvadakis, 2006). Este compuesto se encuentra en gran variedad de plantas, vegetales, especias y como parte de los aceites esenciales de la canela china, la albahaca, la *Maleuca bracteata*, *Styrax americana* y *asiática*, hojas de cacao y la *Alpinia galanga*. Industrialmente se obtiene calentando benzaldehído con anhídrido acético y acetato de sodio (Malten, 1976). Es un importante intermedio en la industria de síntesis orgánica, siendo además utilizado como fragancia y saborizante, por ejemplo, en los Estados Unidos donde tiene aprobación por la FDA (21CFR172.515 y 21CFR172.515 182,60), y es reconocido como un compuesto seguro para uso en alimentación. El consumo anual de ácido cinámico a nivel mundial se ha valorado que está entre 1 y 10 toneladas métricas (Bickers y col., 2005).

Este ácido es altamente utilizado en medicina, producción de pesticidas, plásticos y resinas fotosensibles, siendo la mayoría de estos productos peligrosos. Durante la desinfección del agua utilizando cloro activo, el ácido *trans*-cinámico puede generar compuestos clorados, lo que hace que sea muy difícil de mineralizar, contaminando fuentes de agua al ser descargado sin previo post-tratamiento que asegure la detoxificación del efluente (Malten, 1976; Dai y col., 2016).

Este polifenol es un componente que está presente en aguas residuales de la producción de aceite de oliva, como se muestra en la Tabla 7, siendo muy recalcitrante y de difícil extracción (Niaounakis and Halvadakis, 2006; Lafka y col., 2011; Kontos y col., 2014)

1.4.1.2. Ácido *trans*-ferúlico

Su nombre IUPAC es el de ácido (*E*)-3-(4-hidroxi-3-metoxifenil)propil-2-enoico y también puede denominarse como ácido 3-(4-hidroxi-3-metoxifenil)-2-propenoico. Su fórmula empírica es C₁₀H₁₀O₄ (ver estructura en la Figura 3).

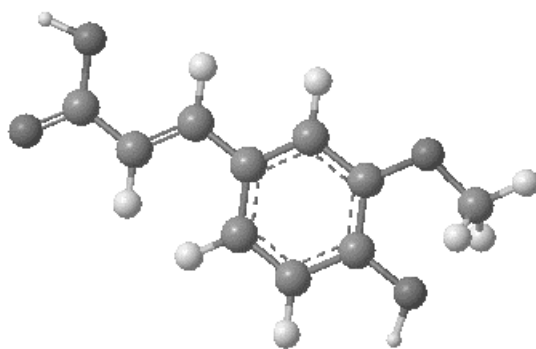


Figura 3. Estructura molecular del ácido *trans*-ferúlico.

El ácido *trans*-ferúlico es un compuesto fenólico derivado del ácido cafeico que se encuentra en vegetales, frutas y hierbas medicinales como la *Angelica sinensis*, la *Cimicifuga racemosa* y la *Ligusticum chuangxiong*. Además, se halla en trazas en bebidas como el café y la cerveza. El ácido *trans*-ferúlico es el isómero que se vende comercialmente y puede convertirse parcialmente a la forma *cis* por la acción de la luz UVA (Hartley and Jones, 1975).

Las propiedades generales del ácido *trans*-ferúlico indican que posee un bajo grado de toxicidad, con una LD₅₀ de 3200 mg kg⁻¹ determinada en ratones (Mancuso and Santangelo, 2014). La solubilidad de este ácido es de 780 mg L⁻¹ a 25 °C (Mota y col., 2008). Es un sólido blanco cristalino de peso molecular 194,18 g mol⁻¹, siendo su temperatura de fusión 448 K si está en su forma cristalina I (Shakeel y col., 2017).

El ácido *trans*-ferúlico presenta un amplio rango de efectos positivos como el de ser antioxidante, antialérgico, anticarcinogénico, antiinflamatorio, antimicrobiano, antiviral, además de actuar como vasodilatador inhibir la agregación plaquetaria, aumentar el flujo sanguíneo coronario, relajar o estimular el músculo liso, poseer efectos antiarrítmicos así como incrementar la viabilidad del esperma (Lu y col., 2005). También se utiliza en la preservación de comida y en protectores solares y lociones para la piel (Zhang y col., 2010). Una aplicación muy importante del ácido *trans*-ferúlico es como precursor de la vainilla mediante su conversión en feruloyl SCoA, usando ATP y coenzima A reducida (Kumar and Pruthi, 2014).

1.4.1.3. Ácido 4-hidroxifenilacético

Otros nombres de este compuesto son los de ácido 2-(4-hidroxifenil)acético y ácido 4-hidroxibencenoacético. Su fórmula empírica es $C_8H_8O_3$ y su peso molecular de $152,15 \text{ g mol}^{-1}$ (ver estructura en la Figura 4).

Este compuesto forma parte de la familia de los 1-hidroxi-2-bencenoides no sustituidos y puede ser preparado a partir del ácido acético. Su apariencia es de un sólido blanco cristalino, con una solubilidad de $60,7 \text{ mg mL}^{-1}$, y tiene un punto de fusión $148-150 \text{ }^\circ\text{C}$. Se encuentra en todos los tejidos y biofluidos humanos, mientras que a nivel celular se halla en el citoplasma (National Center for Biotechnology Information, 2004).

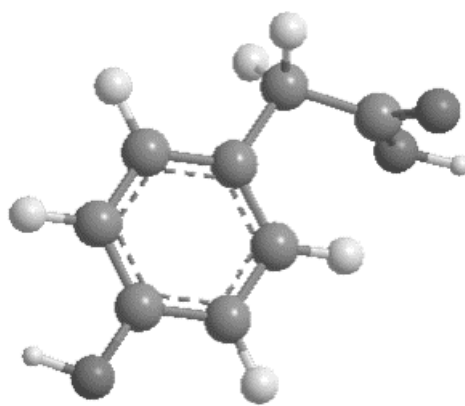


Figura 4. Estructura molecular del ácido 4-hidroxifenilacético.

El ácido 4-hidroxifenilacético es un compuesto fenólico muy común en las aguas residuales agroindustriales, en especial en aguas residuales de la producción de aceite de oliva (Cermola y col., 2004; DellaGreca y col., 2004; Aggoun y col., 2016).

El ácido 4-hidroxifenilacético está presente en varias plantas y también en varios tipos de cervezas (Piazzon y col., 2010). Es un metabolito del kaempferol y un metabolito endógeno de la dopamina, que es un neurotransmisor. Además es un posible marcador biológico de la depresión ya que su disminución en el organismo está relacionado con la depresión y ansiedad (Zabela y col., 2016).

La aciduria por exceso del ácido 4-hidroxifenilacético ha sido detectada en la orina de pacientes que sufren de fibrosis quística de páncreas, de enfermedad celíaca e incluso en pacientes con resección intestinal (Chalmers y col., 1979).

1.5. Tratamientos aplicados a la remediación de las OOMW

1.5.1. Tratamientos Físicos

Los tratamientos físicos se basan en la separación de fases mediante procedimientos mecánicos (Niaounakis and Halvadakis, 2006). Ejemplos de estos tratamientos son:

i) Dilución

Se puede disminuir la concentración de contaminantes del efluente tratado si éste se mezcla con aguas residuales menos contaminadas como, por ejemplo, aguas residuales domésticas (Ochando-Pulido y col., 2017).

ii) Filtración y tecnología de membranas

Se trata de eliminar las partículas sólidas retenidas en las OOMW utilizando telas o membranas de diferente tamaño de poro. La filtración suele ser un proceso de tratamiento inicial de eliminación de sólidos. Su ventaja radica en que la eliminación de los sólidos suspendidos facilita los procesos posteriores. La tecnología de membranas se denomina ultrafiltración (UF) cuando el agua residual se bombea por una membrana filtrante que es capaz de retener compuestos con pesos moleculares de 10000 a 100000 Da. Se logra retener partículas mucho más pequeñas cuando se aplica la nanofiltración (NF) (Ochando-Pulido y Martínez-Ferez, 2015; Ochando-Pulido y col., 2017).

iii) Flotación y Sedimentación

La flotación es una operación unitaria que separa los sólidos de un líquido haciéndolos flotar con un gas que se inyecta en el medio. Las moléculas de gas quedan atrapadas entre las partículas o se adhieren a ellas, disminuyendo de este modo la gravedad específica de los sólidos (Niaounakis and Halvadakis, 2006; Pelendridou y col., 2014). La sedimentación, en cambio, requiere que las moléculas adquieran una gravedad específica mayor y de este modo precipiten al fondo del contenedor. Para esto se necesita que las partículas sólidas sean lo más grandes posible y en la mayoría de los casos se precisa añadir un coagulante. Estas técnicas se puede combinar mutuamente ya sea como pre-tratamiento (Hodaifa y col., 2015) o también como procesos de descontaminación (Teh y col., 2016).

iv) Cristalización

Es una técnica por la cual el soluto se separa de la fase líquida al hacerlo pasar a su forma cristalina. El proceso es muy útil para separar y recuperar polifenoles (Elkacmi y col., 2017), metales y concentrar sales disueltas en las OOMW como NaCl, Na₂SO₄, Na₂CO₃, etc. (Lu y col., 2017).

v) Evaporación, Destilación y Secado

Estos son procesos térmicos que se basan en la separación de fases eliminando el agua. Esto se puede hacer por ebullición mediante destilación o bien en lagunas de grandes extensiones donde el agua se evapora por acción de la luz solar. En ambos casos el problema se presenta en los residuos sólidos que quedan tras del tratamiento (Niaounakis and Halvadakis, 2006; Rozzi and Malpei, 1996).

vi) Combustión

Se aplica a las fases sólidas más cargadas en materia orgánica del procesamiento de la oliva. Los residuos son concentrados en diferentes fases y luego secados para ser utilizados como combustibles según sus propiedades físicas y químicas (Miranda y col., 2006).

1.5.2. Tratamientos Físicoquímicos

Son tratamientos en los que para mejorar la separación de los contaminantes se adicionan productos químicos para lograr la adsorción o la coagulación/floculación/precipitación (Niaounakis and Halvadakis, 2006).

i) Adsorción

Principalmente utilizada para la recuperación de componentes económicamente rentables presentes en las OOMW y que se encuentran muy diluidos, tales como los fenoles. En este proceso se pueden emplear varios agentes adsorbentes como el carbón activado, arcillas, zeolitas, resinas adsorbentes, resinas de intercambio iónico y materiales de desecho reutilizados (Galiatsatou y col., 2002). La eficiencia de la adsorción depende de la composición del adsorbente, su área activa, tamaño de poro y tipo de grupos funcionales superficiales (Soto y col., 2011). Se puede clasificar como un tratamiento puramente físico.

ii) Coagulación/Floculación/Precipitación

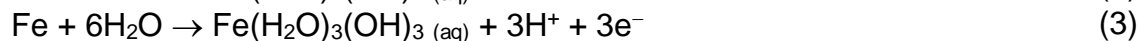
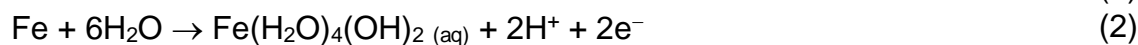
La coagulación aprovecha los productos químicos añadidos que reaccionan con los componentes de las aguas residuales para formar aglomerados y coágulos que dejan de ser solubles en el medio y luego pueden ser separados en su superficie o como lodos con mayor facilidad (Arvanitoyannis y Kassaveti, 2008). La alternativa electroquímica de la coagulación es la **electrocoagulación**. Las cargas eléctricas afectan a la estabilidad de los coloides, suspensiones y emulsiones, así que, cuando se suministran cargas por medio de los electrodos, la carga superficial de las partículas se neutralizan y estas partículas se unen entre sí formando coágulos que precipitan (Tezcan Un y col., 2006). Los iones se liberan directamente en el medio durante la oxidación de uno de los ánodos, que por lo general suelen ser metales de sacrificio como el hierro, el aluminio e incluso el zinc (Fajardo y col., 2015).

Según Moreno y col. (2007), la electrocoagulación tiene lugar según las siguientes etapas:

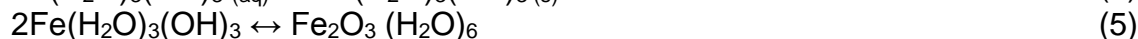
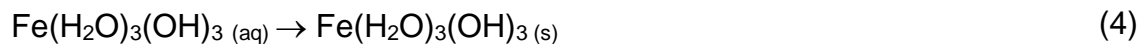
- I. Generación de iones metálicos.
- II. Hidrólisis de los iones y formación de hidróxidos y polihidróxidos.
- III. Electrólisis del agua sobre los electrodos.
- IV. Desestabilización de los contaminantes.
- V. Agregación de las partículas y formación de coágulos.
- VI. Precipitación de los coágulos y partículas formadas en el medio.

Las reacciones con electrodos de hierro que ocurren en este proceso son:

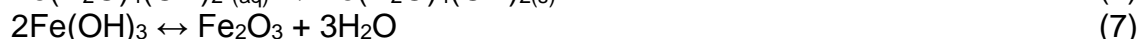
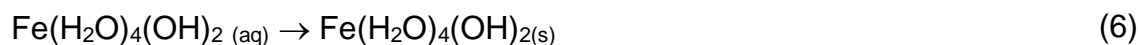
A pH menor que 5:



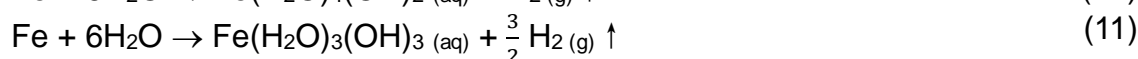
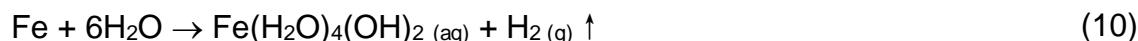
A pH entre 5 a 7:



A pH entre 6 y 8:



A pH mayor que 8:



1.5.3. Tratamientos de Oxidación Avanzada

Se trata de un tipo de oxidación química que conlleva, en muchos casos, la mineralización de la materia orgánica a dióxido de carbono y agua. Todos los procesos de oxidación avanzada (AOPs, por sus siglas en inglés) siempre producen radicales hidroxilo ($\cdot\text{OH}$) que gracias a su poder oxidante son capaces de eliminar la mayor parte de los componentes orgánicos de las aguas residuales o al menos transformarlos en compuestos más inocuos.

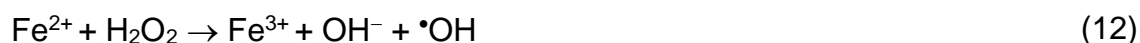
Dentro de los AOPs se pueden estudiar los procesos Fenton ($\text{H}_2\text{O}_2/\text{Fe}^{2+}$), *Fenton-like* ($\text{H}_2\text{O}_2/\text{Fe}^{3+}$), foto-Fenton ($\text{H}_2\text{O}_2/\text{Fe}^{2+}$ /UV), fotocatálisis (TiO_2 /UV) y ozonización asistida ($\text{O}_3/\text{H}_2\text{O}_2$, O_3/UV) (Andreozzi y col., 1999).

El radical hidroxilo es el segundo compuesto conocido con mayor poder oxidante ($E^0 = 2,8 \text{ V vs SHE}$). Puede ser generado por la fotólisis de nitratos, nitritos y peróxido de hidrógeno, formándose a partir de este último bajo la acción de ciertos metales, o también por cavitación ultrasónica, entre otros (Juretic y col., 2015). Los radicales hidroxilo reaccionan de manera no selectiva con muchos contaminantes orgánicos a velocidades de reacción muy elevadas, variando las constantes de reacción entre 10^7 y $10^{10} \text{ M}^{-1} \text{ s}^{-1}$ (Takeda y col., 2017).

i) Proceso Fenton

En 1876, Henry Fenton informó sobre el poder de oxidación del H_2O_2 combinado con el Fe^{2+} aplicado al ácido tartárico. Haber y Weiss (1934) establecieron en 1934 que el radical $\cdot\text{OH}$ era el verdadero responsable de la oxidación de la materia

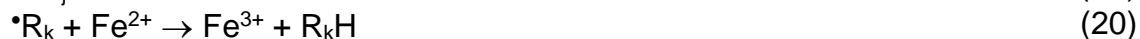
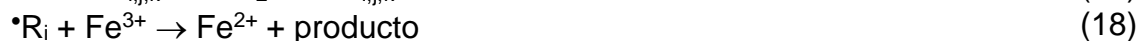
orgánica (Gupta y col., 2016). El proceso Fenton consiste pues en la formación de radicales oxidantes $\bullet\text{OH}$ por reacción entre el ion Fe^{2+} y el peróxido de hidrógeno (Haber y Weiss, 1934):



El proceso es relativamente fácil de repetir en el laboratorio y no requiere de equipos ni sustancias costosas. En condiciones ácidas (pH 2,7-2,8), el Fe^{3+} puede ser reducido a Fe^{2+} según la reacción (16) y actuar como catalizador (Pignatello, 1992). En el tratamiento de aguas residuales, un pH próximo a 3 es el óptimo de la reacción de Fenton (12) (Mert y col., 2010), aunque varios autores también han obtenido buenos resultados a pH neutro e incluso ligeramente básico (Wang y col., 2016).



La reacción de las sustancias orgánicas utilizando el reactivo de Fenton sigue los siguientes pasos (Walling, 1975):

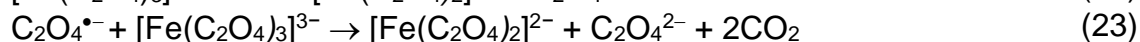
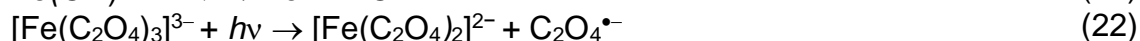


En este caso se formarían tres tipos de radicales orgánicos ($\bullet\text{R}_i$, $\bullet\text{R}_j$, $\bullet\text{R}_k$) por acción del radical hidroxilo, que luego se oxidan, reducen o se dimerizan regenerando los iones Fe^{2+} y Fe^{3+} y continuando con la reacción en cadena.

El proceso Fenton se ha aplicado con buenos resultados al tratamiento de las OOMW, alcanzándose un 70% reducción del COT, pero con la generación de muchos intermedios. El proceso mejora cuando se combina con electro-oxidación con electrodos conductores de diamante obteniéndose una mineralización total (Cañizares y col., 2007).

ii) Proceso foto-Fenton

La reacción de Fenton se acelera por la acción de luz ultravioleta A ($\lambda > 300 \text{ nm}$), que ayuda a la rotura de complejos de hierro que se forman en el medio, como, por ejemplo:

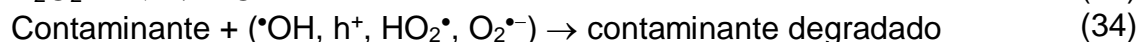
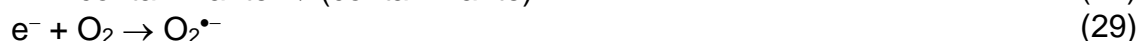


En las reacciones anteriores vemos que la luz UV regenera más catalizador Fe^{2+} o su complejo $[\text{Fe}(\text{C}_2\text{O}_4)_2]^{2-}$ en el medio, el mismo que reacciona con el H_2O_2 para así continuar con la reacción de Fenton (Andreozzi y col., 1999).

El empleo de este proceso en la remediación de las OOMW ha sido recientemente estudiada obteniéndose reducciones del COT, turbidez y fenoles mayores al 90% mediante Fenton/UV/FeCl₃ (Agabo and Hodaifa, 2017) y *Fenton-like* (Hodaifa y col., 2013) en un reactor a escala piloto. En otras investigaciones, los procesos Fenton y *Fenton-like* se combinan con otros procesos fisicoquímicos (Mert y col., 2010) y con tratamientos anaerobios (El-Gohary y col., 2008).

iii) Fotocatalisis

Las moléculas orgánicas, al ponerse en contacto con la superficie de un fotocatalizador como de TiO₂, bajo irradiación de luz se degradan. Pawar y Lee (2015) resumen la fotocatalisis como una serie de pasos que se inician con la formación del par electrón-agujero, seguido de la degradación del contaminante por medio de reacciones con los agujeros y primordialmente con radicales como el superóxido (O₂^{•-}), el hidroperoxilo (HO₂[•]) o el [•]OH.



El tratamiento de OOMW por medio de TiO₂ (1 g L⁻¹)/UV resulta ser muy efectivo porque da lugar a la eliminación del 94% de los fenoles totales, del 57% del color y del 22% de la DQO (Hajjouji y col., 2008). Chatzisyneon y col. (2009b) determinaron que en este tipo de aguas residuales los parámetros más influyentes en la reducción de la DQO eran su concentración inicial y el tiempo de irradiación, mientras que la cantidad de catalizador de TiO₂ y el pH no eran tan significativos. Es más, un exceso de catalizador reflejaba la luz, disminuyendo la degradación de las muestras. El TiO₂ es el catalizador más utilizado para tratar las OOMW y es más eficiente para eliminar el COT y la DQO en comparación con otros como el ZrO₂ y el *composite* FAZA (Badawy y col., 2009).

1.5.4. Tratamientos Biológicos

Son tratamientos en los que se eliminan los compuestos químicos de un residuo gracias a la acción de organismos vivos aprovechando sus procesos metabólicos. Se suelen utilizar hongos, bacterias, enzimas, levaduras (Amaral y col., 2012) y otros microorganismos (Oller y col., 2011).

Las OOMW, por su alto contenido de compuestos fitotóxicos y agentes antibacterianos, presentan gran dificultad para ser degradados por métodos biológicos convencionales. Estos procesos no logran eliminar bien los componentes tóxicos de las OOMW como es el caso de los fenoles, aunque estos componentes pueden ser transformados por catalizadores bióticos y abióticos, como las enzimas fenoloxidasas y peroxidasas, y bajo condiciones adecuadas

también se pueden degradar mediante birnessita y lacasa (Iamarino y col., 2008) o con hongos como los *T. versicolor* (Ergül y col., 2008).

Para aplicar los tratamientos biológicos es necesario diluir la muestra, lo cual constituye una desventaja por el costo de dilución y la contaminación de mayores volúmenes de agua. La digestión anaerobia de muestras diluidas es la más aplicada en el tratamiento de las OOMW, por su menor consumo de energía y menor producción de residuos comparada con el tratamiento aerobio. Además, los biodigestores anaerobios pueden ser utilizados temporalmente, limitándose a los meses de producción de aceite de oliva (Mantzavinos y Kalogerakis, 2005).

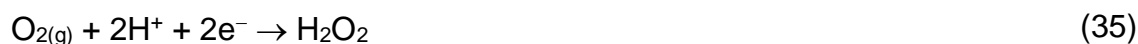
1.5.5. Tratamientos Combinados

La compleja composición de las OOMW dificulta la aplicación de una técnica única para su tratamiento, por eso lo más efectivo es la combinación de diferentes métodos. Existen en la bibliografía muchos tipos de combinaciones entre las que se puede mencionar:

- Coagulación-floculación, antes o después de un proceso de tratamiento biológico aerobio (Jaouani y col., 2005).
- Tratamiento biológico en planta piloto (hongo *P. chrysosporium*) seguido por digestión anaerobia y UF como post-tratamiento (Dhouib y col., 2006).
- Oxidación avanzada utilizando la reacción de Fenton con H_2O_2/Fe^{2+} seguido de un tratamiento anaerobio en un reactor de filtro-prensa (Khoufi y col., 2006). El-Gohary y col. (2009) utilizaron un reactor UASB tras un pre-tratamiento electro-Fenton.
- Oxidación avanzada con O_3 seguida de fotodegradación con luz UV y biodegradación aerobia (Lafi y col., 2009).
- Centrifugación-UF-NF como pre-tratamiento, seguido de ósmosis inversa (Coskun y col., 2010).
- UF con membranas Ceraver, seguida de electrocoagulación con un reactor con electrodos de hierro (Yahiaoui, 2011).
- Procesos consecutivos de coagulación-floculación, extracción con disolvente y oxidación foto-Fenton (Pelendridou y col., 2014).
- Foto-Fenton para reducir los compuestos fenólicos y poder mezclar con residuos sólidos de la producción de aceite de oliva en proporciones adecuadas para utilizar como compost (Zorpas and Costa, 2010).
- UF-NF acopladas a fotocatalisis con TiO_2 en presencia de luz UV (Ochando-Pulido y col., 2015).

1.6. Procesos Electroquímicos de Oxidación Avanzada (EAOPs)

Algunos de los EAOPs que mejores resultados han dado son los que se basan en la producción in situ de radicales hidroxilo en el medio a partir de la electrogeneración de peróxido de hidrogeno, combinado con los radicales hidroxilo que pueden ser generados anódicamente. El H_2O_2 es generado en el cátodo por medio de la reducción del oxígeno que es inyectado o burbujeado como gas puro o en el aire, de acuerdo con la siguiente reacción a pH ácido (Brillas y col., 2009):



En medio alcalino:



En ambos casos, la eficiencia de electrogeneración se ve reducida por las siguientes reacciones parásitas:

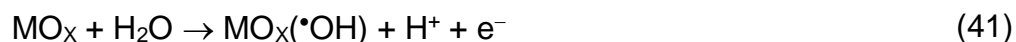


El material más utilizado como cátodo es el carbón en sus diversas formas debido a su alto sobrepotencial para la evolución de hidrógeno, buena estabilidad, buena conductividad y baja acción catalítica para la descomposición del H_2O_2 . Ejemplos de materiales utilizados son el grafito, carbón vítreo reticulado, esponja de carbón, nanotubos de carbón, fibra de carbón activado, fieltro de carbón y electrodos de difusión de gas (GDEs, por sus siglas en inglés) entre otros. Para el ánodo, comúnmente se puede utilizar grafito, platino, óxidos metálicos y diamante dopado con boro (BDD) (Brillas y col., 2009).

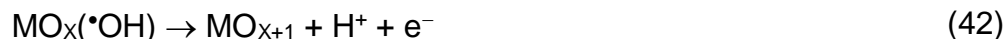
Según el modelo propuesto por Comninellis, la formación y reactividad de las especies activas originadas en el ánodo dependerá del tipo de material utilizado, con lo que se clasifican los ánodos como activos y no activos. Los ánodos activos presentan un bajo sobrepotencial para la evolución del oxígeno, sólo permitiendo la oxidación selectiva de los contaminantes orgánicos. Ejemplos de estos electrodos activos son el grafito, el Pt y los óxidos de Ir y Ru. Por otro lado, los ánodos no activos, como el PbO_2 , óxido de Sn dopado con Sb, y el BDD presentan un alto sobrepotencial de oxígeno y originan radicales hidroxilo que oxidan directamente a la materia orgánica hasta su combustión completa (Comninellis, 1994; Panizza, 2010).

La oxidación de la materia orgánica sobre la superficie de un óxido (MO_x) sigue el siguiente proceso:

- I. Formación de radicales hidroxilo por oxidación del agua:



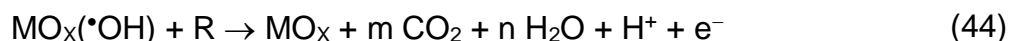
- II. En los electrodos activos, el radical hidroxilo interactúa con la superficie del ánodo formando el superóxido MO_{x+1} :



- III. El par $\text{MO}_x(\bullet\text{OH})/\text{MO}_{x+1}$ denominado “oxígeno activo quimisorbido” actúa como mediador en la conversión selectiva de los orgánicos (R):



- IV. En los electrodos no activos, los radicales hidroxilo llamados “oxígeno activo fisorbido” dan lugar a la combustión de los compuestos orgánicos de forma no selectiva según:



1.6.1. Ánodo de BDD

El diamante, al no ser conductor, no puede ser utilizado como electrodo directamente. Pofperl, Gardner y Angus, en 1973, fueron capaces de producir diamante conductor dopándolo con boro (BDD) vía deposición química en fase vapor, pero fue poco usado por la dificultad de fabricarlo en esos años. El uso del diamante conductor como electrodo data del año 1983, cuando el instituto Raiken de Japón desarrolló un electrodo de diamante con iones Zn implantados, el cual presentaba una amplia ventana de potenciales catódicos en comparación con el carbón vítreo. Años después, en 1987, Pleskov utilizó el diamante semiconductor en procesos fotoelectroquímicos logrando reducciones a potenciales muy negativos.

Los estudios continuaron durante los años 90 revelando más características de este material. Las propiedades que hacen interesante el uso de los electrodos BDD son su gran estabilidad durante el tratamiento de aguas residuales, su amplia ventana electroquímica para la evolución del hidrógeno y del oxígeno, además de su poder para degradar moléculas de residuos orgánicos o inorgánicos (Fujishima y col., 2005; Angus, 2011; Patel y col., 2013).

Otras propiedades importantes de los electrodos BDD son: permiten una alta densidad de corriente, presentan una baja adsorción de compuestos orgánicos, una resistividad de 5 a 100 mΩ cm, baja capacitancia y nula oxidación superficial. La Figura 5 muestra imágenes AFM de la estructura del BDD constituida por C sp^3 junto a una pequeña proporción de C sp^2 . Los electrodos de BDD muestran también propiedades fotoelectroquímicas interesantes a pesar de su ancho *bandgap*, de modo que la luz visible y la radiación UV de onda larga no son capaces de excitar los electrones de valencia hacia la banda de conducción. En algunos casos se forman fotocorrientes significativas mayormente debido a impurezas presentes en el BDD, aunque las impurezas de tipo sp^2 pueden ser desactivadas por oxidación anódica (Kraft, 2007; Luong y col., 2009).

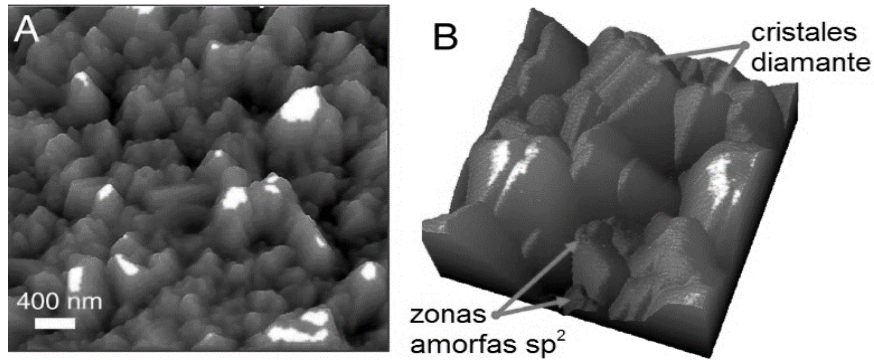
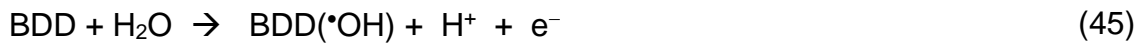


Figura 5. Imágenes superficiales del BDD por AFM. (A) 4000 X 4000 X 150 nm³ y (B) 1000 X 1000 X 150 nm³.

Fuente: Enache y col. (2009)

El alto sobrepotencial de evolución del oxígeno en el BDD permite la producción anódica del radical hidroxilo ($\cdot\text{OH}$) en diferentes electrolitos acuosos. Esto se pudo constatar mediante voltamperometría de pulso diferencial, donde la electrogeneración de radicales hidroxilo aparece asociada a un pico de oxidación debido a la transferencia de un protón y de un electrón en la zona de evolución del oxígeno (Enache y col., 2009) de acuerdo con la reacción:



El platino, por su parte, es un metal muy resistente al ataque químico y a la corrosión por lo que es utilizado en muchas aplicaciones electroquímicas (Kodera y col., 2007), e igual que el BDD sobre su superficie se pueden formar radicales hidroxilo por la reacción (46) (Skoumal y col., 2009), aunque al ser un electrodo activo produce mucha menor cantidad de $\text{Pt}(\cdot\text{OH})$ que $\text{BDD}(\cdot\text{OH})$.



En la Figura 6, se compara el comportamiento de los electrodos de Pt y de BDD.

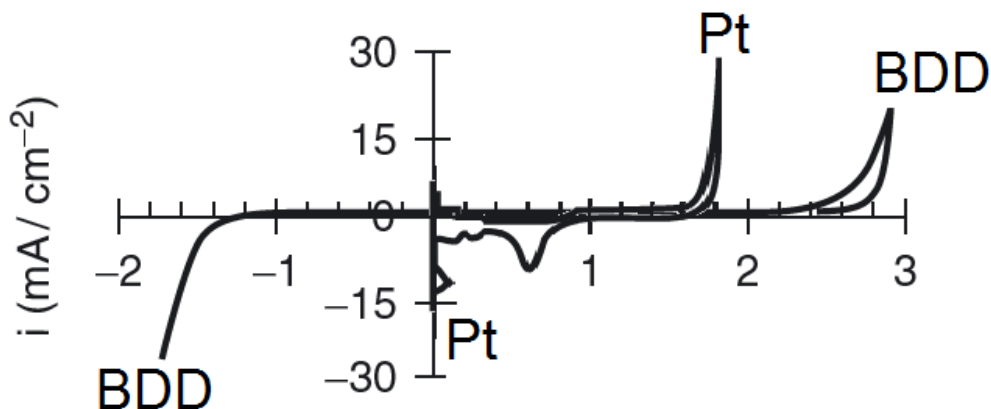


Figura 6. Voltamperometría cíclica de H_2SO_4 0,5 M sobre Pt y BDD vs SHE.

Fuente: Adaptado Angus (2011)

Durante la electrólisis del agua mediante una voltamperometría cíclica en una disolución acuosa 0,5 M de H_2SO_4 , se observa que la ventana electroquímica del electrodo de BDD para la evolución del hidrógeno y del oxígeno (4,5 V) es mucho mayor que la del electrodo de Pt (Angus, 2011).

Chatzisyneon y col. (2009a) utilizó un ánodo y un cátodo de BDD con un área de 70 cm^2 para tratar una OOMW cuya DQO inicial de 40000 mg L^{-1} fue reducida en un 19% después de 15 h de tratamiento a 20 A consumiendo $96 \text{ kW h (kg COD)}^{-1}$. Esto correspondía a un gasto de 10 € por kg de DQO eliminado. Estos autores vieron que el tiempo y la concentración inicial de compuestos orgánicos eran determinantes en cuanto a la eficiencia del proceso.

1.6.2. Electrodo de difusión de aire

Los GDEs, los cátodos carbonosos más utilizados en nuestro grupo de trabajo, constan de tres partes: un colector de corriente eléctrica, por lo general una malla metálica, una capa activa que es un electrocatalizador generalmente de carbón embebido en una matriz polimérica porosa, y una capa externa hidrofóbica que permite la difusión del gas inyectado (Chen, 2004).

Con este tipo de electrodos, como en el caso del carbón-politetrafluoroetileno (C-PTFE), es posible electrogenerar H_2O_2 o HO_2^- a partir de la reducción bielectrónica del O_2 gas en medio ácido por la reacción (35) o en medio alcalino por la reacción (36). Con fines de simplificación, el H_2O_2 y el ion hidroperóxido se interpretan como la misma especie ya que ambas están presentes en el medio por el equilibrio ácido-base ($\text{p}K_a = 11,62$) y seguirán reacciones electroquímicas análogas (Brillas y col., 1995). El poder de degradación aumenta al añadir Fe^{2+} a una disolución ácida para dar lugar a la reacción de Fenton (12) (Brillas y col., 1996).

El electrodo de difusión de aire utilizado en la presente Tesis consiste de un cilindro soporte de polipropileno, el cuerpo del cátodo, que se tapa por sus dos extremos como se ve en la Figura 7. El extremo superior se tapa con un tapón de caucho que tiene: (i) la entrada para el tubo de vidrio por el que ingresa el O_2 /aire, (ii) un agujero para eliminar el exceso de gas inyectado y (iii) el paso de la conexión metálica (alambre de NiCr) por la que circula la corriente eléctrica hasta la malla del conector metálico del electrodo. En el extremo inferior se encuentra la cabeza del cátodo donde se coloca la capa activa del electrodo, en este caso un electrodo poroso de C-PTFE que está en contacto con la malla-conector.

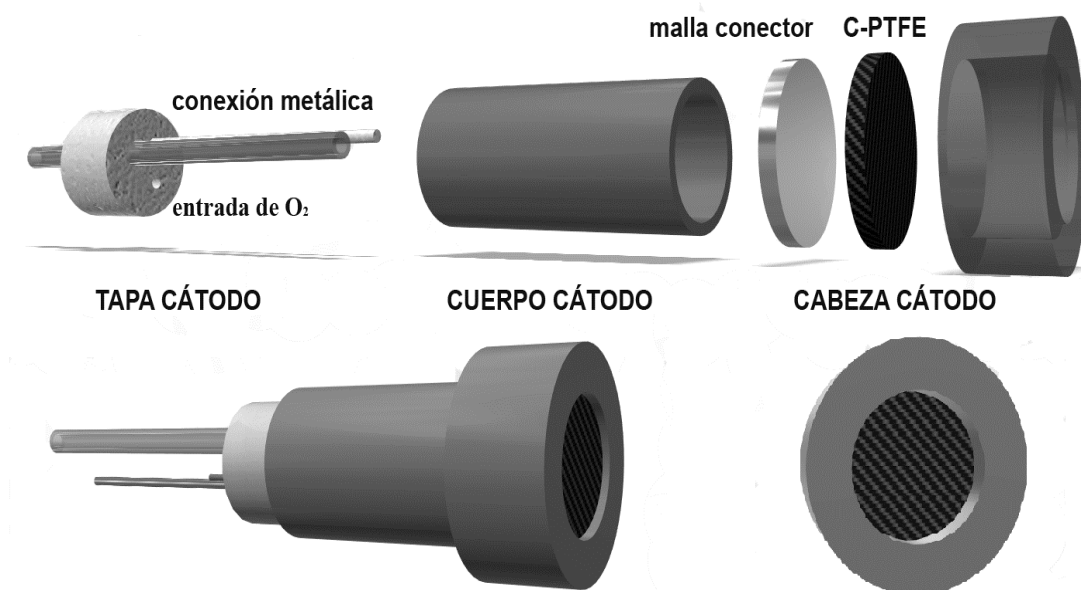


Figura 7. Esquema del cátodo de difusión de oxígeno/aire (C-PTFE).

1.6.3. Oxidación Anódica con H₂O₂ electrogenerado (OA-H₂O₂)

La oxidación anódica (OA) es el método más conocido entre los EAOPs. En este método, los compuestos orgánicos contenidos en una disolución son oxidados por una transferencia de carga directa en el ánodo (M) y por la acción de especies reactivas de oxígeno (ROS) producidas durante la oxidación del agua cuando se aplican altas densidades de corriente. La ROS más importante es el radical hidroxilo fisisorbido sobre la superficie del ánodo (M(*OH)), el cuál es un intermedio que se forma durante la evolución del oxígeno mediante las reacciones:



Los radicales M(*OH) son muy reactivos y pueden dar reacciones parásitas no oxidantes, por ejemplo dimerizándose a H₂O₂ o produciendo oxígeno en el medio según las reacciones (Brillas y col., 2009):



Cuando se genera H₂O₂ en el cátodo, el método se denomina OA con H₂O₂ electrogenerado (OA-H₂O₂). También se conoce como “paired electrocatalysis” ya que los agentes oxidantes se forman tanto en el ánodo (radicales M(*OH)) como en el cátodo (H₂O₂).

La acción oxidante del radical M(*OH) depende de la naturaleza del ánodo, tal como se ha señalado anteriormente. A mayor potencial de evolución del O₂, la interacción entre M y el radical *OH será más débil, lo que significa una mayor reactividad química con los compuestos orgánicos (e inorgánicos) disueltos en el

medio, lo cual conducirá a una mineralización completa de los compuestos aromáticos y ácidos carboxílicos. Si se comparan el Pt, SnO₂, PbO₂, IrO₂, RuO₂ y BDD a altas densidades de corriente, sobre la superficie del BDD se fisisorben mayor cantidad de radical hidroxilo, haciéndolo más eficiente que el resto de electrodos (Brillas y col., 2009; Moreira y col., 2017).

1.6.4. Electro-Fenton (EF)

El proceso EF se basa en la producción continua de peróxido de hidrógeno utilizando un cátodo de difusión alimentado con oxígeno o aire, además de la adición de sales de hierro como catalizador en la disolución. Así, el peróxido de hidrógeno reacciona con el ion Fe²⁺ para producir radicales homogéneos •OH de acuerdo con la reacción de Fenton (12).

La tecnología EF puede utilizar dos o tres electrodos, así como celdas electrolíticas divididas y no divididas. En estas últimas, los contaminantes orgánicos son destruidos competitivamente por los radicales M(•OH) y •OH generados por las reacciones (47) y (12), respectivamente.

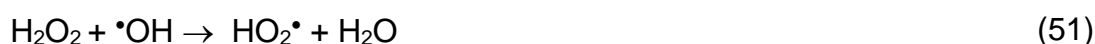
Las ventajas del proceso radican en la generación in situ del peróxido de hidrógeno, evitando su manejo y almacenamiento, la baja cantidad de lodos producidos, la adición de pequeñas cantidades de iones hierro porque éste se regenera en el cátodo, y la consecución de un gran porcentaje de mineralización de los contaminantes orgánicos (Brillas y col., 2009).

El proceso EF puede verse afectado por los siguientes parámetros:

- i) **La concentración del catalizador Fe²⁺**, ya que es indispensable en el proceso. La eficiencia aumenta con el aumento de la concentración del ion Fe²⁺, pero si hay un exceso de catalizador, éste reacciona con los radicales •OH según:



- ii) **La concentración de H₂O₂**. Se trata de una variable clave en EF, ya que una cantidad mayor de H₂O₂ es capaz de eliminar más contaminantes presentes en las aguas residuales al aumentar los radicales •OH generados por la reacción de Fenton (12). Sin embargo, contenidos de peróxido de hidrógeno excesivamente elevados disminuyen la eficiencia del proceso EF debido al efecto secuestrador por parte del H₂O₂ y la recombinación de radicales según las siguientes reacciones:



- iii) **La velocidad de alimentación de O₂ en el cátodo**, siendo un parámetro que limita el proceso. Si se aumenta la velocidad de alimentación del O₂ en un sistema basado en la disolución en el medio, la concentración de O₂ disuelto aumenta y por ende aumentará la concentración de H₂O₂, hasta alcanzar la saturación del gas en el medio. Sin embargo, un exceso de gas de alimentación en un GDE causa su percolación masiva que provoca la formación de burbujas

sobre la superficie electroactiva del cátodo con la consiguiente pérdida de área electroactiva y eficiencia.

iv) **La temperatura.** Para disminuir el consumo energético es mejor llevar a cabo los procesos a temperatura ambiente. Además, el cambio de temperatura es una variable que poco afecta en la eliminación de materia orgánica durante el proceso EF. Un aumento en la temperatura disminuye la acumulación de H_2O_2 en el medio ya que éste no es estable a altas temperaturas y además a mayor temperatura la solubilidad del O_2 en la solución se ve reducida. No conviene operar a temperaturas superiores a $35\text{ }^\circ\text{C}$ pues el agua se evapora y ello provoca errores en las mediciones de los parámetros que sirven para el análisis de la degradación de los contaminantes orgánicos.

v) **El pH de la disolución** es una de las variables que más influyen en la reacción de Fenton (12). La mayor parte de estudios reportan un pH óptimo de 3 para el proceso EF. A pH mayores, los iones hierro precipitan en forma de hidróxidos y a $\text{pH} > 5$ el H_2O_2 se torna inestable y se descompone fácilmente a agua. En cambio, a $\text{pH} < 3$ se forma el ion inactivo H_3O_2^+ por la reacción (54):



Esto puede representar una desventaja si se tiene en cuenta que el pH de las aguas residuales no es el valor óptimo requerido para la reacción Fenton.

vi) **La densidad de corriente aplicada**, ya que afecta a la reducción del O_2 que genera el H_2O_2 . A mayores densidades de corriente se incrementa la producción de H_2O_2 y, por tanto, la cantidad de radicales $\cdot\text{OH}$ originados, aumentando la capacidad de degradación de la materia orgánica y la regeneración del Fe^{2+} disuelto en el medio por reducción catódica del Fe^{3+} . También a mayor densidad de corriente aplicada, mayor es el voltaje y el consumo energético, lo que es una desventaja para este proceso. En general, la eficiencia disminuye una vez alcanzada una densidad de corriente límite, debido a las reacciones parásitas que favorecen la descarga de H_2 en el cátodo y de O_2 en el ánodo.

vii) **La composición del electrolito**, debido a que afecta la conductividad y la producción de las especies. Según el electrolito soporte y su contenido pueden producirse reacciones no deseadas en EF, como por ejemplo si se añade un exceso de sulfato de sodio:



Si el medio contiene ion Cl^- se origina cloro activo que ataca competitivamente a la materia orgánica.

Existen otras variables que también afectan el proceso EF tales como: el transporte de masa a los electrodos, la concentración inicial, la naturaleza del contaminante y la distancia entre electrodos (Nidheesh and Gandhimathi, 2012).

1.6.5. Fotoelectro-Fenton (FEF)

El proceso FEF consiste en la utilización del H_2O_2 electrogenerado en presencia de Fe^{2+} igual que en el EF, pero simultáneamente irradiando la muestra con luz UVA ($\lambda_{\text{max}} = 360 \text{ nm}$). La Figura 8 muestra un esquema del sistema utilizado en EF y FEF. En este proceso se puede notar una mayor regeneración del catalizador y la producción de radicales $\cdot\text{OH}$ adicionales en el medio gracias a la fotólisis del complejo $[\text{Fe}(\text{OH})]^{2+}$, la especie más estable del ion Fe^{3+} , mediante la reacción foto-Fenton (21). Además, la luz UVA puede inducir la fotodescarboxilación de los complejos de Fe(III) producidos en el medio, liberando más Fe^{2+} en el medio. Un ejemplo es la fotólisis de los complejos de Fe(III)-carboxilato (como las especies Fe(III)-oxalato) según la reacción general (22) (Brillas y col. 2009).

Todo esto hace que el FEF sea normalmente más eficiente que el EF para mineralizar la materia orgánica del medio. Algunos autores utilizan una fuente de luz más energética como la luz UVC ($\lambda_{\text{max}} = 254 \text{ nm}$). Esta irradiación puede fotolizar directamente muchos compuestos orgánicos y, sobre todo, da lugar a la fotólisis homogénea del H_2O_2 originando más radicales $\cdot\text{OH}$ (Martínez-Huitle y Brillas, 2009).

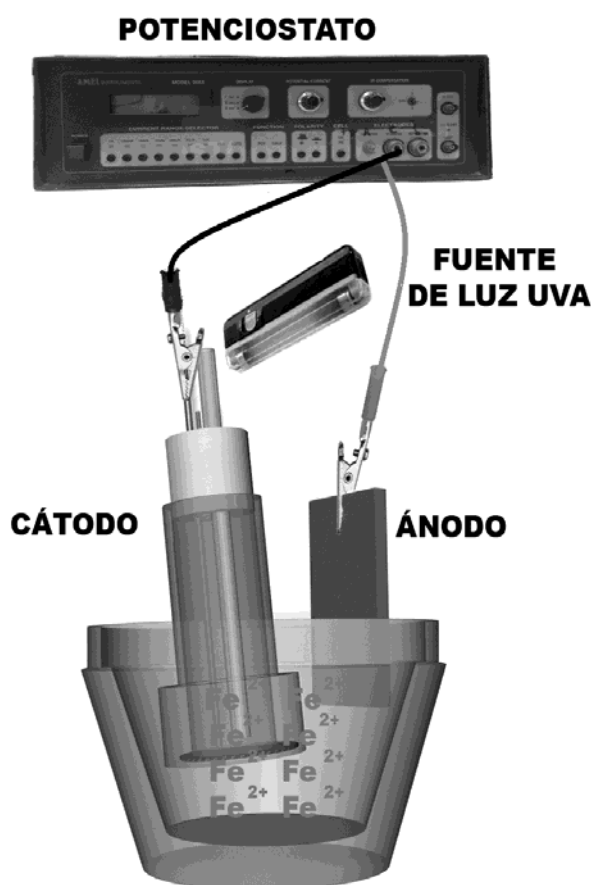


Figura 8. Sistema utilizado para los procesos EF y FEF.

1.6.6. Fotoelectro-Fenton Solar (FEFS)

El proceso FEFS es análogo al proceso FEF, si bien la disolución es irradiada con luz solar renovable y gratuita con una gran parte de su espectro de emisión en el rango UVA ($\lambda > 300$ nm). Este método emergente, desarrollado por el grupo LEMMA, soluciona el problema de gasto energético derivado del uso de las lámparas UV, pudiendo ser aplicado tanto a reactores tipo tanque como a escala de planta piloto de hasta 10 L por su facilidad de implementación (Sirés y Brillas, 2012; Sirés y col., 2014).

Se ha puesto de manifiesto que el proceso FEFS resulta ser más eficiente que los procesos EF y FEF. Así, se ha reportado que las disoluciones de ibuprofeno pueden ser mineralizadas hasta en un 86% en 3 h con un bajo coste energético de $4,3 \text{ kWh m}^{-3}$ (Skoumal y col., 2009). También se han tratado en planta piloto el colorante textil Amarillo Ácido 42 (Espinoza y col., 2016), los herbicidas diuron (Pipi y col., 2014), tebuthiuron, y ametrina (Gozzi y col., 2017) y el fármaco ranitidina (Olvera-Vargas y col., 2015), utilizando un cátodo de difusión de aire junto a ánodos de BDD y Pt.

También se ha aplicado a la descontaminación de aguas residuales de matadero, tratadas primero con un proceso anaerobio seguido de EAOPs. Se pudo comprobar que la capacidad oxidativa de los EAOPs aumentaba en el orden: $\text{EO-H}_2\text{O}_2 < \text{EF} < \text{FEFS}$ con una reducción máxima de la DQO del 95% (Vidal y col., 2016). Si además se combina esta técnica con una celda fotovoltaica, se obtiene un mayor ahorro energético como se mostró en el caso de la degradación del antibiótico trimetoprimo, consiguiendo hasta un 80% de reducción del TOC durante 6 h en condiciones óptimas (Zhang y col., 2016).

2. OBJETIVOS

2.1. Objetivos Generales

El objetivo principal de esta Tesis es estudiar la mineralización de los ácidos *trans*-ferúlico, *trans*-cinámico y 4-hidroxifenilacético, presentes en las aguas residuales de la industria productora de aceite de oliva (OOMW), utilizando Procesos Electroquímicos de Oxidación Avanzada (EAOPs) como la oxidación anódica (OA-H₂O₂), electro-Fenton (EF) y fotoelectro-Fenton (FEF). Para ello se han tratado 100 mL de disoluciones sintéticas de cada ácido con 0,050 M de Na₂SO₄ a pH ácido, empleando un ánodo de BDD y un cátodo de difusión de aire. Además, se ha analizado la mineralización del ácido 4-hidroxifenilacético adicionado a una OOMW real bajo las mejores condiciones determinadas en los ensayos sintéticos.

2.2. Objetivos Específicos

- 2.2.1. Estudiar el proceso de degradación de compuestos orgánicos modelo, típicamente presentes en las aguas residuales de la industria del aceite de oliva, mediante EAOPs en celda tipo tanque operando en *batch* (discontinuo) y utilizando como electrodos un ánodo de BDD y un cátodo de difusión de aire de C-PTFE.
- 2.2.2. Estudiar el efecto de la concentración de los ácidos *trans*-cinámico, *trans*-ferúlico y 4-hidroxifenilacético durante los procesos de OA-H₂O₂, EF y FEF.
- 2.2.3. Estudiar el efecto de la densidad de corriente sobre el descenso del COT en disoluciones de ácidos *trans*-cinámico, *trans*-ferúlico y 4-hidroxifenilacético durante los procesos de OA-H₂O₂, EF y FEF.
- 2.2.4. Estudiar la cinética de degradación de los ácidos *trans*-cinámico, *trans*-ferúlico y 4-hidroxifenilacético mediante HPLC.
- 2.2.5. Determinar mediante GC-MS y HPLC los intermedios que se producen durante la degradación de los ácidos *trans*-cinámico, *trans*-ferúlico y 4-hidroxifenilacético.
- 2.2.6. Recoger y caracterizar químicamente diferentes lotes de OOMW, evaluando su contenido en fenoles, ácidos orgánicos, grasas, pH, DQO, DBO₅, COT, NT, ST, STD, metales e iones inorgánicos, entre otros parámetros.
- 2.2.7. Dopar el agua residual con concentraciones conocidas del ácido 4-hidroxifenilacético y seguir su cinética de degradación para poder evaluar el efecto de la matriz acuosa al aplicar los EAOPs.

3. PARTE EXPERIMENTAL

3.1. Reactivos

Los ácidos *trans*-cinámico (pureza > 99%), *trans*-ferúlico (99% de pureza) y 4-hidroxifenilacético (98% de pureza) y la vainillina (99% de pureza) eran de Sigma-Aldrich. Los ácidos fumárico, acético y oxálico de calidad analítica y el acetonitrilo grado HPLC eran de Merck. El sulfato de Fe(II) heptahidratado y el sulfato de sodio anhidro, ambos de calidad analítica, fueron suministrados por Fluka. Se utilizó ácido sulfúrico analítico de Merck o de Acros Organics para ajustar el pH de la disolución inicial a 3,0. Todos los reactivos químicos se utilizaron directamente del frasco sin tratamiento previo. Todas las disoluciones sintéticas se prepararon con agua de alta pureza filtrada con un sistema Millipore Milli-Q (resistividad > 18 MΩ cm a 25°C). El agua residual de aceite de oliva se obtuvo de un decantador que recolectaba las aguas generadas en las etapas de limpieza durante la producción de aceite de oliva extra virgen en una pequeña cooperativa cercana a Barcelona. Se recogió en Noviembre de 2015 y se mantuvo a 4 °C antes de su uso. Los tratamientos se realizaron después de filtrar la muestra con una malla de 18 μm.

3.2. Sistemas Electroquímicos

La Figura 9 muestra una fotografía del equipo utilizado en las electrólisis. Está compuesto de un reactor cilíndrico tipo tanque de vidrio con una camisa externa por la que puede circular agua que sirve para mantener el sistema a la temperatura escogida mediante un termostato. Las disoluciones se agitaron con una barra magnética controlada por un agitador magnético MR 116 de Schott. En la celda se introdujeron un ánodo y un cátodo, ambos con un área efectiva de 3 cm². Los experimentos se realizaron en modo galvanostático, a densidad de corriente (j) constante suministrada por un potencióstato-galvanostato PAR EG&G modelo 273A.

El ánodo era un recubrimiento delgado de BDD sobre Si suministrado por Adamant Technologies (Le Chaux de Fonds, Suiza). La Figura 10 presenta unas fotografías de este ánodo preparado para operar. Para la medición de la concentración de peróxido de hidrógeno se utilizó un ánodo de Pt con un 99,99% de pureza procedente de SEMPSA (Barcelona). El cátodo de difusión de aire de C-PTFE, suministrado por E-TEK (Somerset, NJ, EEUU), se situó en el extremo inferior del soporte (ver Figura 7) y se alimentó con aire comprimido mediante una bomba a un flujo de 1-5 L min⁻¹. La tela de carbón del cátodo se activó al inicio de su vida útil. Esto se hizo mediante una electrólisis de 100 mL de una disolución acuosa de Na₂SO₄ 0,05 M a pH 3,0 aplicando una $j = 100 \text{ mA cm}^{-2}$ durante 3 h a 25 °C. Este ensayo también se efectuó para limpiar la superficie del ánodo de BDD antes de su uso.

El pH de las disoluciones se ajustó a 3,0 añadiendo las gotas necesarias de H₂SO₄ 0,1 M. En el caso del EF y FEF se añadió a la muestra, antes de ser tratada, 0,50 mM de sulfato ferroso como catalizador de la reacción de Fenton (12). En el proceso FEF, la disolución se expuso a una lámpara UVA de 6 W de la casa Philips, que emite luz UV en la región entre 320 a 400 nm con una $\lambda_{\text{max}} = 360 \text{ nm}$ y una energía de fotoionización de 5 W m⁻², determinada con un radiómetro de la casa

Kipp & Zonen modelo CUV 5 Global.

En todos los ensayos se evitó que la celda quedara expuesta a la acción de la luz ambiental sobre el sistema, recubriéndolo con un plástico opaco.

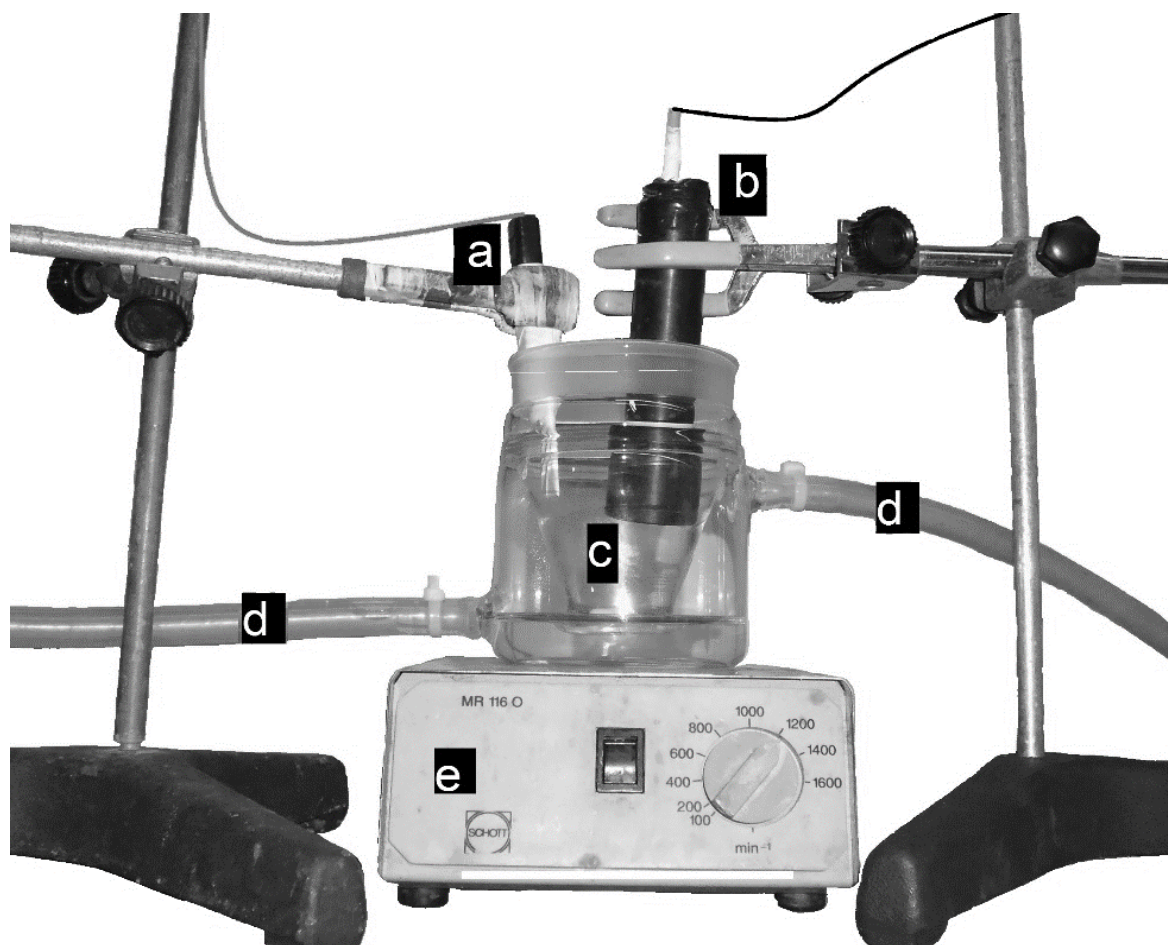


Figura 9. Fotografía del sistema electrolítico. (a) Ánodo, (b) cátodo de difusión de aire de C-PTFE, (c) celda de vidrio, (d) circulación externa de agua y (e) agitador magnético.



Figura 10. Ánodo de BDD utilizado en los ensayos.

3.3. Procedimientos analíticos

3.3.1. Cuantificación del H₂O₂

La medición del H₂O₂ electrogenerado se llevó a cabo utilizando el mismo sistema electrolítico descrito en la sección 3.2, usando un ánodo de Pt y un cátodo de difusión de aire, ambos con un área de 3 cm². Se operó bajo condiciones de OA-H₂O₂, EF y FEF con una disolución de Na₂SO₄ 0,050 M a pH 3,0 y 25 °C aplicando una j de 33,3 a 100 mA cm⁻² durante 7 h. En EF y FEF se añadió a la disolución inicial una cantidad equivalente a 0,50 mM de sulfato ferroso como catalizador.

La concentración de peróxido de hidrógeno acumulada en el medio se determinó mediante medidas espectrofotométricas, utilizando un espectrofotómetro UV-Vis de la casa Unicam modelo UV4 a una $\lambda = 408$ nm y 25 °C. El principio se basa en la formación del complejo de Ti(IV)-H₂O₂ de coloración amarilla (Welcher, 1967), cuya absorbancia es proporcional a la concentración del H₂O₂ (Eisenberg, 1943). El reactivo era una disolución de sulfato de titanio(IV) de concentración 0,5 mM en medio H₂SO₄ 0,5 mM.

Las muestras se tomaron a tiempo 0 y luego cada 30 min hasta que se completaron las 7 h. Para la medición en el espectrofotómetro se introdujo un pequeño volumen de muestra en un matraz de 10 mL, añadiendo después la disolución de Ti(IV) y aforándola con Na₂SO₄ 0,05 M. La concentración de peróxido de hidrógeno se calculó mediante la siguiente ecuación:

$$C_{\text{H}_2\text{O}_2} = \frac{\text{Abs}}{0,7079} * \frac{10 \text{ mL}}{V} \quad (57)$$

donde V es el volumen de la muestra en mL y Abs es su absorbancia. La constante 0,7089 mM⁻¹ corresponde al valor de la pendiente de la recta de calibración del complejo entre el Ti(IV) y el H₂O₂.

Durante la producción de H₂O₂ se determinó la eficiencia de corriente (EC, en %) suponiendo un comportamiento faradaico, de acuerdo con la siguiente ecuación:

$$\text{EC} = \frac{n F V [\text{H}_2\text{O}_2]}{I t} \times 100 \quad (58)$$

donde $n = 2$ es el número de electrones que se intercambian en la reacción (35), F es la constante de Faraday (96487 C mol⁻¹), V es el volumen de la disolución en L, I es la intensidad de corriente en A, $[\text{H}_2\text{O}_2]$ es la concentración del H₂O₂ determinada experimentalmente en M y t el tiempo en s.

3.3.2. Cuantificación del carbono orgánico total (COT)

El COT se determinó directamente en un sistema TOC-V CSH/CSN de la casa Shimadzu. En este equipo, la muestra líquida es aspirada y arrastrada por aire sintético hasta un horno en donde se quema a 720 °C en presencia de un catalizador de Pt, de modo que todo el carbón orgánico se convierte en CO₂. El gas portador que contiene el CO₂ producto de la combustión pasa entonces por el deshumidificador/enfriador del equipo y finalmente llega a un detector de infrarrojos que analiza la señal, la envía al software que la procesa para finalmente mostrar el resultado en forma de picos integrados en la pantalla del equipo (Shimadzu Corporation, 2003). La concentración del COT se determina a partir de la curva de calibración de disoluciones estándar de hidrogenoftalato de potasio.

También se puede obtener la medida del carbono total mediante la ecuación:

$$CT = COT + CIT \quad (59)$$

donde COT es el carbono orgánico total y CIT es el carbono inorgánico total, debido a la presencia de carbonatos, que se elimina cuando se acidifica la muestra y se hace burbujear un gas inerte. En tal caso (método denominado NPOC), el CIT se torna igual a cero ya que los carbonatos se descomponen a CO_{2(g)} y H_{2O(l)}, de modo que:

$$CT = COT \quad (60)$$

Como las muestras podían contener posibles sólidos disueltos y para evitar un malfuncionamiento del analizador del TOC, todas ellas se filtraron con filtros de PTFE de 45 µm de la casa Whatman antes de inyectarlas.

3.3.3. Cuantificación de los aromáticos y ácidos carboxílicos

La reducción de la concentración de los ácidos *trans*-cinámico, *trans*-ferúlico y 4-hidroxifenilacético se siguió por HPLC (*high-performance liquid chromatography*) de fase inversa utilizando un cromatógrafo líquido de Waters, modelo 600 LC, acoplado a un detector UV-visible de fotodiodos Waters modelo 996, que se seleccionó a la longitud de onda λ máxima de cada compuesto. La columna utilizada fue una Hypersil C18 de 6 µm, de dimensiones 250 mm x 4,6 mm, de la casa BDH y termostata a 35 °C. Las muestras de EF y FEF se diluyeron previamente con acetonitrilo en relación 50:50 para detener el proceso de degradación. Todas las muestras se filtraron con un microfiltro PTFE de 45 µm antes de ser inyectadas. Se tomaron alícuotas de 10 µL que se inyectaron al cromatógrafo eluyéndolas en la fase móvil escogida a una velocidad adecuada para cada muestra.

En el caso de los ácidos *trans*-cinámico y *trans*-ferúlico se usó una mezcla 80:20 (v/v) de acetonitrilo/agua eluida a 0,8 mL min⁻¹ como fase móvil. Para el caso del ácido 4-hidroxifenilacético, se utilizó una fase móvil compuesta por una mezcla 60:40 (v/v) de acetonitrilo/agua eluida a 0,6 mL min⁻¹.

Los cromatogramas mostraron un pico para cada ácido a un tiempo característico de retención (t_r), siendo de 3,45 min ($\lambda = 276$ nm) para el ácido *trans*-cinámico, de

3,37 min ($\lambda = 229$ nm) para el ácido *trans*-ferúlico y de 5,0 min ($\lambda = 277$ nm) para el ácido 4-hidroxifenilacético. Además, para la vainillina se encontró un $t_r = 3,89$ min ($\lambda = 229$ nm).

Los ácidos carboxílicos se identificaron por HPLC de exclusión iónica usando el mismo equipo que en el caso de los aromáticos, pero utilizando una columna Aminex HPX 87H, de dimensiones 300 mm x 7,8 mm, de la casa Bio-Rad termostalizada a 35 °C y el detector de fotodiodos seleccionado a $\lambda = 210$ nm. Se inyectaron alícuotas de 10 μ L y la fase móvil fue una disolución acuosa de H₂SO₄ 4 mM a 0,6 mL min⁻¹. Los cromatogramas mostraron picos relacionados con los ácidos oxálico ($t_r = 7,0$ min), acético ($t_r = 14,9$ min) y fumárico ($t_r = 15,6$ min).

Los productos aromáticos primarios del ácido *trans*-cinámico se identificaron a partir del tratamiento OA-H₂O₂ de 100 mL de una disolución de concentración 0,926 mM a $j = 33,3$ mA cm⁻². Se llevaron a cabo varias electrólisis a 30 y 90 min, y los componentes orgánicos se extrajeron con CH₂Cl₂. La fracción orgánica se secó sobre Na₂SO₄ anhidro y se filtró para luego reducir el volumen de la muestra con nitrógeno hasta 1 mL aproximadamente. El mismo procedimiento se aplicó a disoluciones de ácido *trans*-ferúlico de concentración 0,834 mM. En el caso del ácido 4-hidroxifenilacético se trataron disoluciones de concentración 1,03 mM durante 30 y 90 min de EF.

Las mediciones de GC-MS (cromatografía de gases-espectrometría de masas) se efectuaron en un sistema Agilent Technologies, con un GC modelo 6890N y espectrómetro de masas modelo 5975C que opera con un cañón de electrones de 70 eV. El cromatógrafo de gases estaba equipado con una columna no polar J&W HP 5 ms o una columna polar INNOWax HP, ambas de 0,25 μ m y dimensiones 30 m x 0,25 mm, de la casa Agilent. La rampa de temperatura programada fue de 36 °C durante 1 min, 5 °C min⁻¹ hasta los 300 °C para la columna no polar y los 250 °C para la columna polar con un tiempo de espera de 10 min para ambas. La temperatura de la entrada, fuente y línea de transferencia fu de 250, 230 y 280 °C para la columna no polar y de 250, 230 y 250 °C para la polar. Para identificar los compuestos se utilizó el software de Agilent Technologies precargado con la base de datos de espectros de moléculas orgánicas NIST05-MS.

En el caso de las muestras de la OOMW, se liofilizaron y luego se disolvieron en acetato de etilo previamente a inyectarlas en el GC-MS. En este caso, el cromatógrafo de gases se equipó con una columna no polar Sapiens-X5 ms de 0,25 μ m y dimensiones 30 m x 0,25 mm de la casa Teknokroma. La rampa de temperatura fue de 36 °C durante 1 min, 5 °C min⁻¹ hasta 325 °C y el tiempo de espera de 10 min. Las temperaturas de la entrada, fuente y línea de transferencia fueron de 250, 230 y 300 °C, respectivamente.

3.3.4. Determinación de la demanda química de oxígeno (DQO)

Este método se basa en una digestión muy agresiva de la muestra empleando agentes oxidantes muy fuertes como el dicromato de potasio durante largo tiempo a temperatura de ebullición para luego determinar la cantidad de oxidante consumida expresado en mg O₂ L⁻¹ mediante espectrofotometría. La DQO se midió utilizando los viales preparados por HR HACH (EEUU). En concreto, se utilizaron los viales LCK014 que sirven para medir la DQO en el intervalo de 20 a 1500 mg O₂ L⁻¹. Siguiendo el manual de instrucciones, se pipetearon 2 mL de

OOMW que se introdujeron en el vial, agitándolo enérgicamente para homogenizar la mezcla. Finalmente se colocó el vial en una incubadora HACH DRB durante 2 h a 150 °C. La DQO se midió con un colorímetro HACH DR 900, que suministra directamente su contenido en mg O₂ L⁻¹.

3.3.5. Determinación de la demanda biológica de oxígeno (DBO₅)

La determinación de la DBO se basa en la degradación de sustancias orgánicas por medio de microorganismos en presencia de oxígeno y bajo condiciones controladas de temperatura. Se aplica a la determinación de la DBO_n (siendo *n* el número de días del ensayo) de aguas residuales de diferente índole (Eaton y col., 2005).

Existen diferentes metodologías y equipos para la determinación de la DBO_n. En este trabajo se utilizó el método respirométrico con botellas OxiTop® que se colocan en una incubadora a 20 ± 1 ° C por un periodo de cinco días, correspondiendo a la DBO₅. La Figura 11 muestra una fotografía de este sistema. La ventaja de las botellas OxiTop® radica en que permiten medir este parámetro directamente. Su principio de funcionamiento se basa en la medición del consumo de oxígeno de las bacterias durante los cinco días que dura el proceso, midiendo los cambios de presión debido al consumo de O₂ durante la descomposición de la materia orgánica. Como los cambios de la presión parcial son pequeños, es necesario eliminar la interferencia provocada por el CO₂ originado por la respiración de los organismos. Así, se va retirando el CO₂ de la botella haciéndolo reaccionar con dos pastillas de NaOH que se colocan en la base del tapón, verificándose la siguiente reacción:



La eliminación del CO₂ de la botella da lugar a una presión negativa medible. El método respirométrico suministra pues el cambio de presión en un sistema cerrado. La DBO se calcula entonces por la ecuación:

$$\text{DBO} = \frac{M(\text{O}_2)}{\alpha R T_m} \left(\frac{V_t - V_l}{V_l} + \frac{T_m}{T_0} \right) \Delta p(\text{O}_2) \quad (62)$$

donde $M(\text{O}_2)$ es la masa molecular del oxígeno (32000 mg mol⁻¹), R es la constante universal de los gases (83144 L Pa mol⁻¹ K⁻¹), T_0 es la temperatura en el cero absoluto (273,15 K), T_m es la temperatura a la que se realiza la medida (en K), V_t es el volumen de la botella en mL, V_l es el volumen de la muestra en mL, α es el coeficiente de adsorción Bunsen (0,03103) y $\Delta p(\text{O}_2)$ es la diferencia de presión parcial del oxígeno en hPa (WTW, 2001).

Se prepararon distintas disoluciones adaptando la Norma 5210 D del manual Standard Methods:

- i) Disolución estándar de Ácido Glutámico-Glucosa (AGG). Es la disolución recomendada para determinar si el equipo funciona adecuadamente ya que 164 mL de la solución a una concentración de 150 mg L⁻¹ debe dar una DBO₅ de 260 ± 30 mg O₂ L⁻¹.
- ii) Al inicio del análisis, se precisa agua saturada en oxígeno (por lo que se

burbujea aire durante 1 h) a $\text{pH } 7.0 \pm 0,2$, una disolución tampón de NaH_2PO_4 1,5 M a $\text{pH } 7,2$ y 100 mL de disolución de AGG de 3000 mg L^{-1} .

iii) También se necesita NH_4Cl 0.71 M, CaCl_2 0,25 M, MgSO_4 0,41 M y FeCl_3 0,018 M como disoluciones nutrientes, así como KOH 6 M, $\text{Ni}(\text{OH})_2$ 1 M y H_2SO_4 1 M para ajustar el pH.

El procedimiento consistió en añadir 50 mL disolución de AGG a 800 mL de agua en una probeta, seguido de 6 mL de NaH_2PO_4 , 2 mL de NH_4Cl , 2 mL de CaCl_2 , 2 mL de MgSO_4 y 2 mL de FeCl_3 . Inmediatamente después se ajustó el pH a $7,0 \pm 0,2$ con NaOH o H_2SO_4 . Una vez ajustado el pH y verificado que la temperatura del sistema fuese $18 \pm 3^\circ\text{C}$, se añadió el volumen de siembra (agua del decantador secundario de una depuradora municipal), aproximadamente 50 mL, y se completó el litro con agua de dilución. Se trasvasaron 164 mL de la anterior disolución a cada botella Oxitop, colocando un agitador magnético y las gotas de inhibidor. Antes de cerrar el Oxitop, se colocó el capuchón de goma en el cuello de la botella introduciendo en él dos pastillas de NaOH .

La disolución blanco, sirvió para comprobar si las bacterias trabajaban correctamente a 20°C y pH neutro. Ésta se preparó colocando las bacterias y las disoluciones nutrientes en agua saturada en oxígeno, al final de los cinco días la DBO_5 debía ser menor o igual a 2. Para ello, en una probeta se añadieron 800 mL de agua de dilución, 6 mL de NaH_2PO_4 , 2 mL de NH_4Cl , 2 mL de CaCl_2 , 2 mL de MgSO_4 y 2 mL de FeCl_3 , se ajustó el pH a $7,0 \pm 0,2$, se añadió el volumen de siembra con las gotas de inhibidor y se completó el litro con agua de dilución. Se trasvasaron 432 mL del blanco así preparado a una botella, cerrándola como se ha indicado anteriormente.

La muestra se homogeneizó con una licuadora antes del ensayo siempre que no existieran dudas en cuanto a la estabilidad de la muestra. Se seleccionó un volumen de muestra correcto para evitar que la medida fuera tan alta o tan baja que saliera fuera de los rangos de lectura del equipo. Se utilizaron los datos de la Tabla 8 como guía para la elección del volumen correcto de muestra a analizar.

Tabla 8. Valores orientativos para determinar la DBO_5 .

DBO_5 (mg L^{-1})	Tampón (μL)	V (mL)	Inhibidor (gotas)	f
0-40	2590	432	9	1
0-80	2190	365	7	2
0-200	1500	250	5	5
0-400	980	164	3	10
0-800	580	97	2	20
0-2000	260	43,5	1	50
0-4000	140	22,7	1	100

Se añadió la disolución tampón para mantener el pH neutro $7,0 \pm 0,2$ durante el proceso y la siembra de bacterias cuando el agua a analizar lo precisaba. Aproximadamente se añadieron 25 mL de siembra por cada litro de disolución a una temperatura entre 15 y 21°C . En los casos en que la muestra contenía peróxido de hidrógeno, se añadió la cantidad estequiométrica de tiosulfato de sodio sólido para eliminarlo de la solución. Se trasvasó el volumen de la muestra a una botella, sin olvidarse del inhibidor, y finalmente se tapó la botella como ya se ha descrito.

La DBO₅ corregida se obtuvo utilizando la siguiente ecuación:

$$DBO_5 = \left[A - B \frac{V_t - V_e}{V_t} \right] \frac{V_t}{V_e} \quad (63)$$

con $A = M f$

donde DBO₅ es la Demanda Biológica de Oxígeno a los 5 días, M es el valor medido en la tapa del OxiTop tras 5 días (en mg O₂ L⁻¹), f es el factor de dilución del equipo (vea Tabla 8), B es el valor medido del blanco tras 5 días (en mg L⁻¹), V_e es el volumen de la muestra utilizada en el análisis (en mL) y V_t es el volumen total de la disolución analizada (en mL).



Figura 11. Equipo OxiTop® para la medición de la DBO. De izquierda a derecha, tapa medidora de presión, botella OxiTop® e incubadora llena de botellas OxiTop®.

3.3.6. Caracterización de aguas residuales

Filtración de las muestras de OOMW

Se filtró la OOMW dos veces consecutivas utilizando mallas de filtración de 45 y 18 μm de la casa Labopolis (Barcelona). Para ello se utilizó un equipo de filtración al vacío provisto de un embudo Buchner de 250 mL de capacidad. Posteriormente, las muestras se guardaron en una nevera a 4 °C antes de su análisis y ensayos de degradación.

Medición del pH y de la conductividad

El pH de las disoluciones se midió con un pH-metro GLP 22 de la casa Crison y la conductividad mediante un conductímetro de Metrohm modelo 644.

Medición de los Sólidos totales (ST)

Se calentaron cápsulas de Petri o crisoles suficientes a 103 °C durante 3 h y se dejaron enfriar en un desecador. En cada recipiente se trasvasaron 25 mL de la muestra y se taró. Se escogió este volumen de muestra para que quedara después del secado un residuo seco entre 2.5 a 200 mg. La muestra se calentó luego a 103 – 105°C hasta su completa evaporación. Se pesó el recipiente una vez enfriado y se repitió el proceso hasta peso constante (Norma 2540 B del manual Standard Methods).

Los sólidos totales se determinaron mediante la ecuación:

$$ST = \frac{m_1 - m_2}{V} \quad (64)$$

donde m_1 es la masa inicial del recipiente con la muestra y m_2 la masa obtenida al final del secado, respectivamente (en mg), y V es el volumen de la muestra (en L).

Medición de Sólidos Totales Suspendidos (STS)

Se basa en determinar los sólidos que se encuentran en una muestra que tienen un determinado tamaño de partícula y que pueden ser retenidos por un filtro. Utilizando un equipo de filtración al vacío y un filtro de microfibras de vidrio, previamente pesado, se filtra una cantidad de muestra tal que deje un residuo seco mayor que 2,5 mg. En nuestro caso se escogieron 50 y 100 mL de muestra. Al final se seca el filtro de fibra en una cápsula de Petri a $103 \pm 2^\circ\text{C}$ y, una vez seco, se deja enfriar en un desecador y se pesa, repitiendo el proceso hasta que el peso se mantenga constante (Norma 2540 D del manual Standard Methods). Los sólidos totales suspendidos se calculan entonces por la siguiente ecuación:

$$STS = \frac{m_1 - m_2}{V} \quad (65)$$

donde m_1 es la masa del filtro con la muestra retenida después del secado y m_2 es la masa del filtro vacío, ambos en mg, y V es el volumen de la muestra (en L).

Medición de los Sólidos Volátiles (SV)

Se mide el residuo seco que queda tras calcinar una muestra a 550°C hasta peso constante. Para ello se debe calentar un crisol en una mufla a 550°C durante 1 h, dejarlo enfriar en un desecador y pesarlo. A continuación, se introduce un volumen exacto de la muestra en el crisol, el cual se evapora parcialmente antes de introducirlo en la mufla para evitar posteriores ebulliciones bruscas de la muestra. El crisol se calienta en la mufla por un periodo de al menos 1 h, se deja enfriar y se pesa, repitiendo este procedimiento hasta obtener un peso constante (Norma 2540 del manual Standard Methods).

Los sólidos totales se calcularon utilizando la siguiente ecuación:

$$SV = \frac{m_1 - m_2}{V} \quad (66)$$

donde m_1 es la masa del crisol más la muestra al inicio y m_2 su masa al final, ambos en mg, y V es el volumen de la muestra (en L).

Medición de la turbidez

Antes de realizar cualquier medida de la turbidez se tenía que calibrar el turbidímetro TURB 55 IR de la casa WWR, siguiendo su manual. Primero se enjuagaba el portamuestras con la muestra a analizar y luego se introducían 30 mL de muestra en el mismo, procediéndose a realizar la medida, que aparecía en la pantalla del equipo en NTU después de unos segundos.

Medición de los iones totales

Las muestras se filtraron con filtros de $0,45 \mu\text{m}$ antes de su análisis. La

concentración de aniones se determinó por cromatografía iónica con un cromatógrafo líquido de Kontron modelo 465 LC acoplado a un detector de conductividad de Waters modelo 432. Se utilizó una columna de intercambio aniónico IC-PAK de dimensiones 150 mm x 4,6 mm, de Waters termostata a 35 °C. Se eluyó la muestra en una fase móvil de ácido bórico, gluconato de sodio, tetraborato de sodio, acetonitrilo, butanol y glicerina a 2,0 mL min⁻¹.

El contenido de los diferentes cationes se obtuvo con un equipo de plasma de acoplado inductivamente (ICP) a un espectrómetro de emisión óptico OES usando un espectrómetro 3200RL de la casa Optima.

Medición de los fenoles totales

El índice de fenol se obtuvo de acuerdo con el método espectromotométrico directo de la 4-aminoantipirina. Este procedimiento colorimétrico permite determinar la concentración de fenoles y fenoles substituidos en *orto*, *meta* y *para*, exceptuando *para* substituyentes que sean grupos alquilo, arilo, nitro, benzoilo, nitroso o aldehído.

Se prepararon todas las disoluciones analíticas con agua destilada, libre de fenoles y cloro. La disolución madre de fenol contenía 1000 mg L⁻¹ y se preparó en agua destilada añadiendo 10 mL de bromuro-bromato. La concentración de fenol en el blanco se valoró con tiosulfato de sodio 0,025 M, usando almidón como indicador. Se preparó una disolución intermedia de fenol disolviendo 1 mL de la disolución madre en 100 mL de agua. Finalmente, se preparó la disolución estándar de fenol disolviendo 50 mL de la disolución intermedia en 500 mL de agua destilada recién hervida. Estas disoluciones se preparan a diario y antes del análisis. La disolución de bromuro-bromato se preparó disolviendo 2,784 g de KBrO₃ anhidro y 10 g de KBr en 1000 mL de agua.

Como reactivos se emplearon HCl concentrado, hidróxido de amonio (NH₄OH) 0,5 M, una disolución tampón de fosfato conteniendo 104,5 g de K₂HPO₄ y 72,3 g de KH₂PO₄ en 1 L de agua (pH 6,8), una disolución de 4-aminoantipirina, y una disolución de 20 g L⁻¹ de ferricianuro de potasio.

En un vaso de precipitados de 250 mL se colocaron 100 mL de la muestra a analizar, conteniendo una concentración de fenol inferior a 50 mg L⁻¹. Paralelamente se prepararon sendos vasos con la disolución blanco y la estándar. A todas las muestras se les añadió 2,5 mL de 0,5 M de NH₄OH ajustando el pH a 7,9 con la disolución tampón, 1 mL de la disolución de 4-aminoantipirina y 1 mL de la de ferricianuro de potasio. Tras 15 min se midió la absorbancia de la muestra y de la disolución estándar a $\lambda = 500$ nm, usando el blanco preparado (Norma 5330 D del manual Standard Methods).

Medición de las grasas totales

El contenido de aceite y grasa se determinó mediante el método gravimétrico de partición. Este procedimiento permite extraer la grasa disuelta o emulsionada mediante el uso de un disolvente, evitando posibles efectos que dañen las grasas o aumenten el grado de emulsión dentro de la muestra.

Se prepararon los reactivos a utilizar consistentes en H₂SO₄, Na₂SO₄ anhidro y una mezcla de disolventes *n*-hexano/metil-*tert*-butil-éter (MTBE) 80/20 (v/v).

Se introdujo un volumen conocido de la muestra en un embudo de decantación, se añadió el disolvente y se agitó vigorosamente para extraer las grasas. A

continuación se separó la fase orgánica con las grasas y se filtró en un embudo con papel filtro y sulfato de sodio. Se repitió el proceso de extracción y filtración hasta obtener suficiente muestra para destilarla utilizando un baño de agua a 85 °C en un matraz tarado. Una vez eliminado el disolvente, se dejó enfriar en el matraz un desecador y se pesó (Norma 5520 B del manual Standard Methods).

La concentración de grasas totales (en mg L⁻¹) se calcula como:

$$\frac{m_1 - m_2}{V} \quad (67)$$

donde m_1 es la masa del matraz con la grasa extraída y m_2 es la masa del matraz tarado vacío, ambas en mg, y V es el volumen de la muestra (en L).

4. HYDROGEN PEROXIDE PRODUCTION

As an initial step before any degradation, it is necessary to study the accumulation of H₂O₂ electrogenerated with the carbon-PTFE air-diffusion cathode in order to confirm its good performance.

For all the experiments, an undivided electrolytic glass cell equipped with a Pt anode and an air-diffusion cathode, both with a total area of 3 cm², was used. The solution was stirred at 700 rpm along the whole electrolysis.

Under AO-H₂O₂ conditions, the electrolyses were performed with 100 mL of a 0.050 M Na₂SO₄ solution at pH 3.0, 25 °C, and applied j values of 33.3, 66.7 and 100 mA cm⁻². The EF and PEF conditions were reached by adding the required amount of iron(II) salt so as to ensure a concentration of 0.50 mM Fe²⁺, and in PEF the solution was irradiated with a 6 W UVA lamp. The duration of all runs was 420 min, without significant change in the solution pH.

Figure 12a shows an increase of the H₂O₂ concentration in the medium with electrolysis time under AO H₂O₂ conditions at all j values tested. Only at the highest $j = 100$ mA cm⁻² it is possible to see that the H₂O₂ concentration reaches a steady state after 300 min, which occurs when its electrogeneration rate by reaction (35) equals its rate of destruction, primarily due to its anodic destruction to O₂ via reactions (39) and (40) (Brillas y col., 2000). It can also be observed in Figure 12a that a higher accumulation of H₂O₂ was attained as j increased, due to the concomitant acceleration of reaction (35) and hence, of reactions (39) and (40). At 420 min of electrolysis, for example, 60.0, 77.0 and 105.8 mM are accumulated in the medium at 33.3, 66.7 and 100 mA cm⁻², respectively.

Figure 12b shows the change in current efficiency for the results given in Figure 12a. At the beginning of the electrolysis, the efficiency was close to 100% in all cases because of the predominance of reaction (35). As the time was prolonged and more H₂O₂ was present in solution, the rate of reactions (39) and (40) was gradually enhanced, causing a dramatic drop of the efficiency up to a value close to 50% at $j = 33.3$ mA cm⁻², and more drastically up to 31% when increasing j to 100 mA cm⁻². These results demonstrate the capacity of the air-diffusion cathode to largely generate H₂O₂ in this acidic medium.

Figures 13a and 14a highlight the same trend for H₂O₂ accumulation under EF and PEF conditions, respectively, as described above using AO-H₂O₂. The concentration of this compound always grew at higher j and a steady state was always reached around 180-240 min of electrolysis. At j values of 33.3, 66.7 and 100 mA cm⁻², the stationary concentration was about 15, 24 and 45 mM in EF and approximately 14, 20 and 38 mM in PEF, respectively.

These results indicate that the accumulation of H₂O₂ decreases in the sequence AO-H₂O₂ > EF ≥ PEF under comparable experimental conditions. This tendency is also evident from the current efficiency depicted in Figures 13b and 14b, which always decreased with time and in a similar manner at all j values.

This behavior is typical of faradaic reactions of zero order, as expected for reactions

(35), (39) and (40).

The lower H_2O_2 accumulation under EF compared with AO- H_2O_2 can be ascribed to the faster destruction of this species from Fenton's reaction (12). The additional action of the photo-Fenton reaction (21) in PEF, which causes further destruction of H_2O_2 , would explain the lower concentration of this compound with lower current efficiency. However, the fact that PEF only led to a slightly smaller H_2O_2 content compared to EF, suggests a rather poor contribution of reaction (21).

The aforementioned findings allow establishing that a sufficient amount of H_2O_2 is accumulated in these systems and hence, they can be employed to efficiently degrade organic pollutants to be tested in the present Thesis. It should be noted that similar results to those obtained with the Pt/air-diffusion cell are expected for the BDD/air-diffusion one, as has been shown in previous works of our group (Sirés y col., 2007).

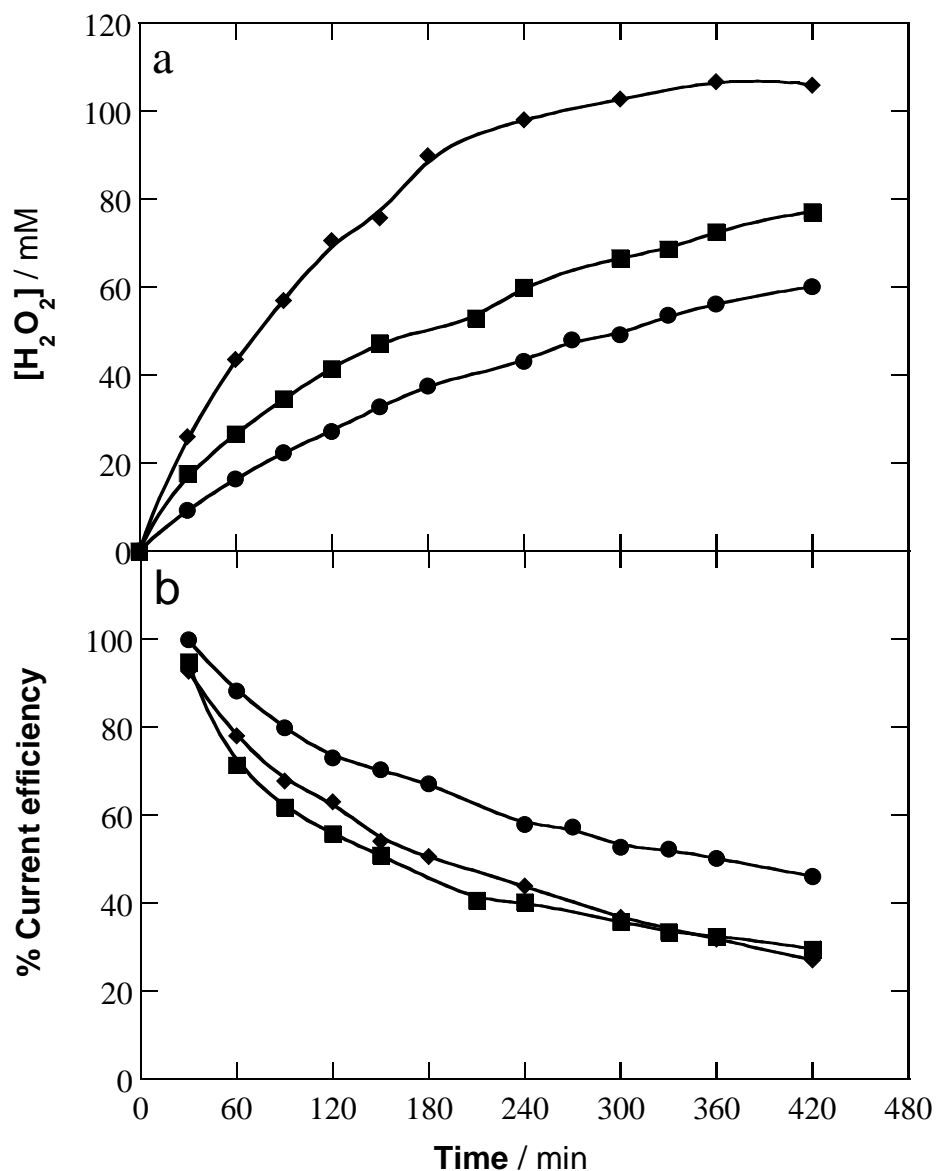


Figure 12. (a) Concentration of accumulated hydrogen peroxide and (b) percentage of current efficiency as a function of time for the AO-H₂O₂ electrolysis of 100 mL of a solution with 0.050 M Na₂SO₄ at pH 3.0 and 25 °C using a stirred tank cell equipped with a Pt anode and an air-diffusion cathode, both of 3 cm² area. Current density: (●) 33.3 mA cm⁻², (■) 66.7 mA cm⁻² and (◆) 100 mA cm⁻².

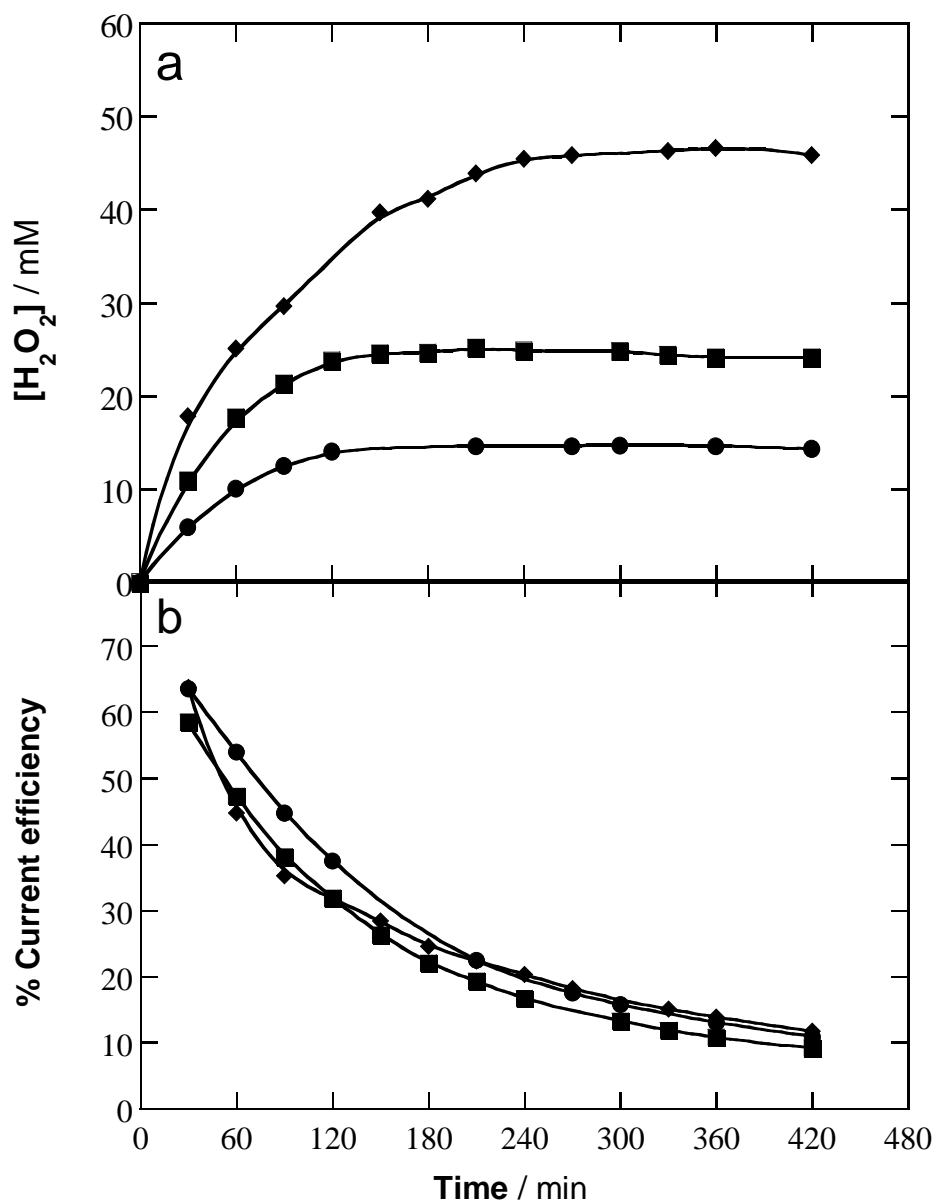


Figure 13. Change of (a) accumulated hydrogen peroxide concentration and (b) percentage of current efficiency with time under EF conditions for the electrolysis of 100 mL of a solution of 0.050 M Na_2SO_4 with 0.50 mM Fe^{2+} at pH 3.0 and 25 °C using a cell equipped with Pt/air-diffusion cell. Current density: (●) 33.3 mA cm⁻², (■) 66.7 mA cm⁻² and (◆) 100 mA cm⁻².

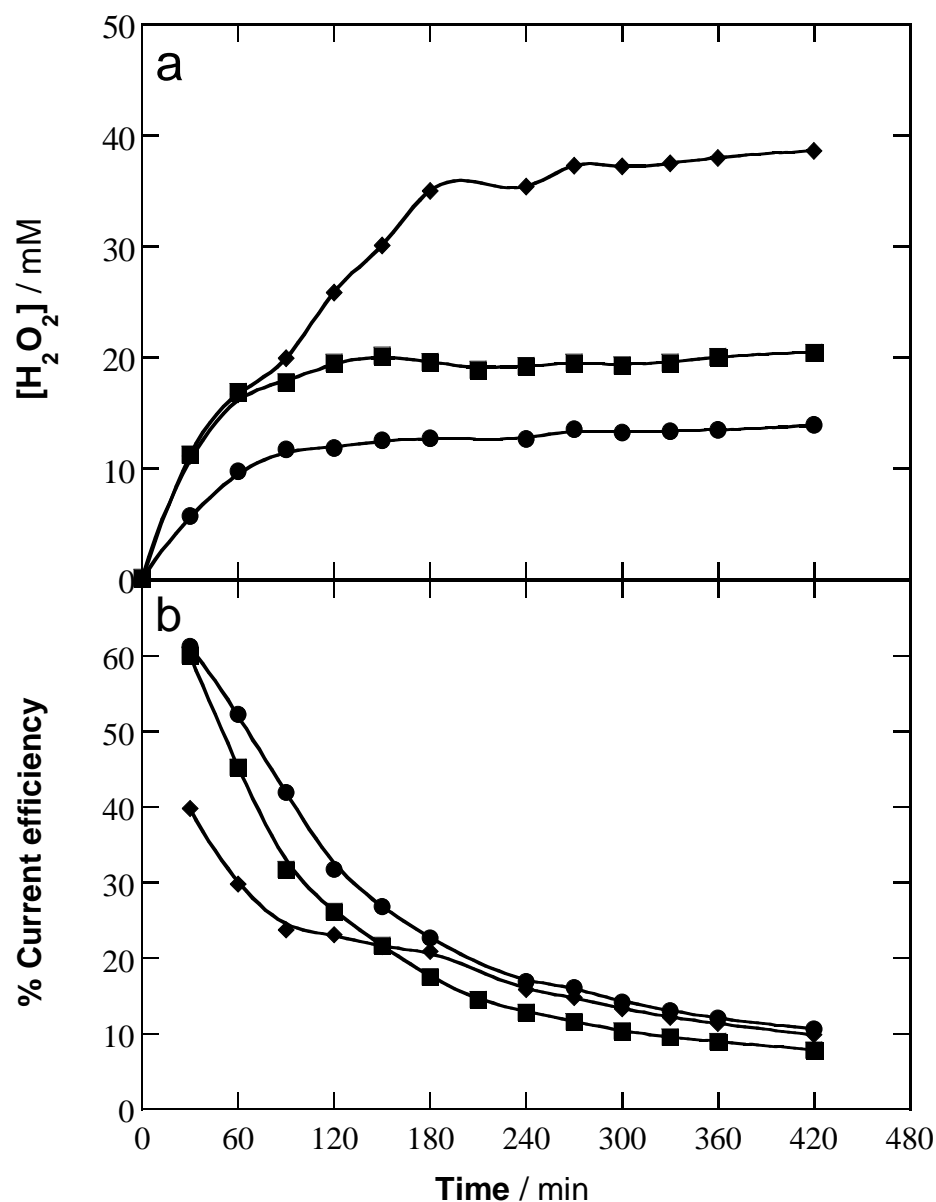
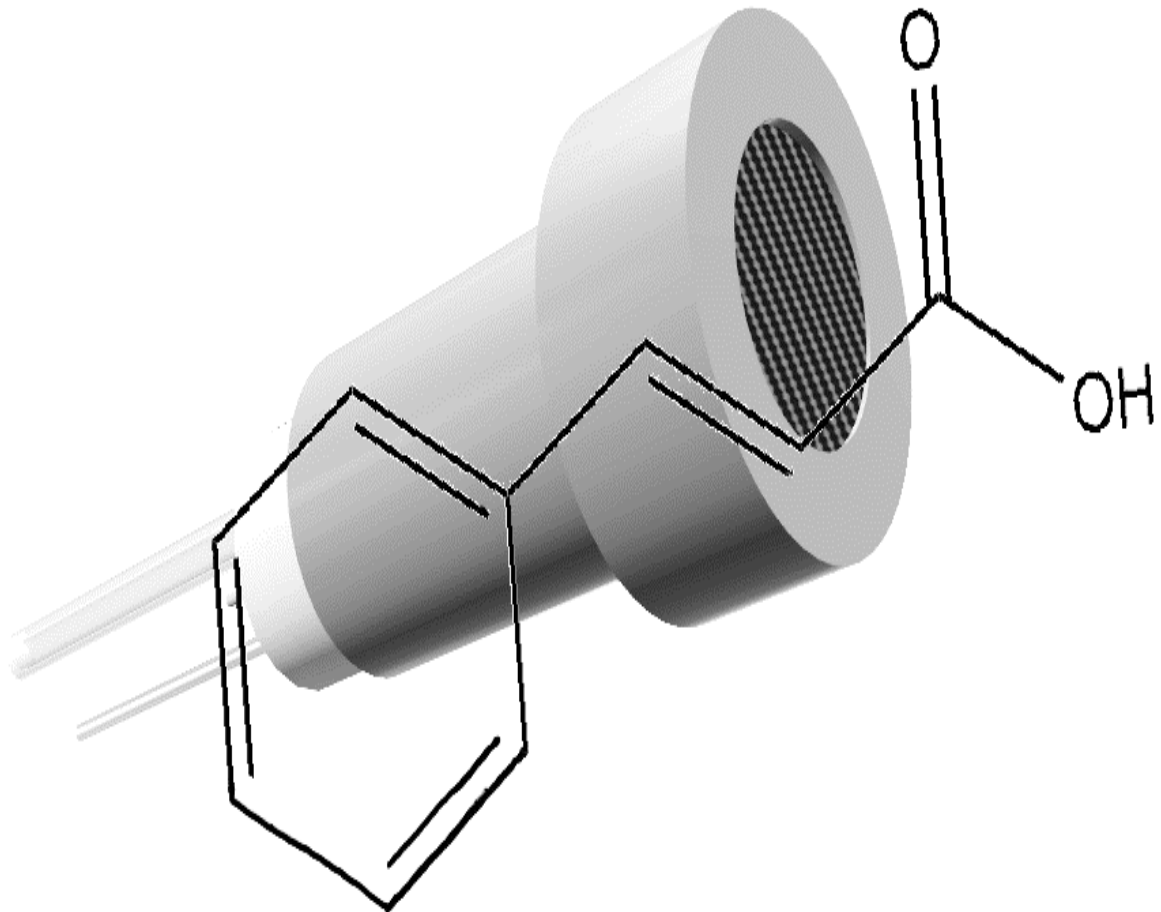


Figure 14. Variation of: (a) accumulated hydrogen peroxide concentration and (b) percentage of current efficiency with time under PEF conditions for the electrolysis of 100 mL of a 0.050 M Na_2SO_4 solution with Fe^{2+} 0.50 mM at pH 3.0 and 25 ° C using a Pt/ air-diffusion cell. The solution was irradiated with a 6 W UVA lamp providing 5 W m^{-2} ($\lambda_{\text{max}} = 360 \text{ nm}$). Current density: (●) 33.3 mA cm^{-2} , (■) 66.7 mA cm^{-2} and (◆) 100 mA cm^{-2} .

5. MINERALIZACIÓN DEL ÁCIDO *TRANS*-CINÁMICO



Publicación 1:

Electrochemical destruction of *trans*-cinnamic acid by advanced oxidation processes: kinetics, mineralization, and degradation route

Las OOMW son residuos muy difíciles de descontaminar. El ácido *trans*-cinámico es un componente común en estas aguas residuales. Las técnicas electroquímicas, especialmente los EAOPs, se aplican en muchos campos incluyendo el tratamiento de aguas residuales industriales con bastante éxito. En este trabajo y por primera vez, se estudió la capacidad de descontaminar el ácido *trans*-cinámico utilizando este tipo de técnicas.

El ácido *trans*-cinámico se degradó en un reactor de tanque agitado equipado con un ánodo de diamante dopado con boro (BDD) y un cátodo de difusión de aire de carbón-PTFE, ambos con un área de 3 cm². En la celda se colocaron 100 mL de una disolución que contenía el ácido y 0,050 M de Na₂SO₄ a pH ácido de 3,0 y a 25 °C. Los EAOPs estudiados fueron la oxidación anódica con H₂O₂ electrogenerado (OA-H₂O₂), el electro-Fenton (EF) y el fotoelectro-Fenton (FEF).

Una disolución 0,962 mM de ácido *trans*-cinámico se trató a 33,3 mA cm⁻², tal como puede verse en las Figuras 1a-c. La eliminación completa del ácido tardó 360 min en OA-H₂O₂, mientras que sólo requirió 42 minutos en EF y FEF. Esto puede explicarse por la rápida reacción del ácido con los radicales [•]OH presentes en el medio producidos durante la reacción de Fenton (12) en EF y FEF, en comparación con la lenta reacción del ácido con los radicales BDD([•]OH) producidos en OA-H₂O₂. Se puede afirmar que la luz UVA no desempeñó un papel importante durante la degradación del ácido *trans*-cinámico. Las constantes aparentes de pseudo-primer orden (k_1) fueron de 0,012 min⁻¹ para OA-H₂O₂, 0,052 min⁻¹ para EF y 0,050 min⁻¹ para FEF. Estos valores confirman que el EF y el FEF son capaces de degradar al ácido *trans*-cinámico más rápidamente gracias a los radicales [•]OH formados en el medio. Se realizaron otros ensayos reduciendo la concentración del ácido a 0,185 y 0,463 mM. Como se esperaba, la disminución de la concentración del ácido disminuyó el tiempo requerido para la eliminación del ácido *trans*-cinámico. Los valores de k_1 aumentaron a 0,014 min⁻¹ en OA-H₂O₂ y a 0,58 min⁻¹ en EF cuando el contenido de ácido *trans*-cinámico fue de 0,185 mM. Esto indica que la reacción no es una verdadera reacción de pseudo-primer orden, ya que k_1 no debería variar con la concentración del sustrato. A una misma j , cabe esperar que se produzcan cantidades similares de [•]OH y/o BDD([•]OH) en los EAOPs y, a mayor concentración de sustrato, un mayor número de estos radicales reaccionan con los compuestos intermedios generados, reduciendo su capacidad para atacar el ácido *trans*-cinámico.

Al aplicar diferentes valores de j desde 16,7 hasta 100 mA cm⁻² a una disolución 0,926 mM de ácido *trans*-cinámico se observó que para todos los EAOPs el TOC bajaba gradualmente a lo largo de la electrólisis. Este comportamiento se muestra en las Figuras 3a-c, especialmente para la OA-H₂O₂ a densidades de corriente menores a 100 mA cm⁻²; aunque se alcanzó un máximo de 66,7% de reducción del TOC al aplicar 100 mA cm⁻². En la Figura 3b se ve que el proceso EF aumentó la velocidad mineralización, hasta alcanzar un 90% a 100 mA cm⁻², valor que era igual al alcanzado en FEF cuando solo se aplicaron 16,7 mA cm⁻². Esto sugiere que casi todos los productos originados en EF eran fotosensibles y por eso, el proceso se tornaba más rápido bajo la acción de la luz UVA, lo que también explica la disminución del TOC hasta un 98% en FEF a los 360 min. Como se ve, la capacidad de oxidación aumenta en el orden: OA-H₂O₂ < EF < FEF. Para cada método, la velocidad y porcentaje de mineralización se

incrementó con el aumento de la densidad de corriente. El proceso más potente, el FEF, logró reducir el TOC en un 98% después de 180 min a 33,3 y 66,7 mA cm⁻², demostrando que la luz UVA es una herramienta poderosa para la descontaminación de este ácido. No obstante, la eficiencia de corriente de mineralización (MCE) para cada EAOP disminuyó al aumentar j . En OA-H₂O₂, los valores de MCE no variaban prácticamente para $j \geq 33$ mA cm⁻² (ver Figura 4a). Los valores máximos de MCE en EF y FEF se encontraron en los primeros 120 min (Figuras 4b y c), indicando la rápida conversión del ácido *trans*-cinámico en productos intermedios, los cuales eran destruidos primordialmente por los radicales $\cdot\text{OH}$ en el medio. Además, en el proceso FEF los compuestos fotosensibles eran eliminados, lo que permitió aumentar el MCE al 73% en 90 min aplicando tan solo 16,7 mA cm⁻².

Otro parámetro importante estudiado fue la concentración inicial del ácido *trans*-cinámico, cuyo efecto sobre la eliminación del TOC se puede observar en las Figuras 5a-c. Para ello, se prepararon disoluciones con concentraciones de 0,185, 0,463, 0,926 y 1,852 mM del ácido, las cuales se trataron a una j de 33,3 mA cm⁻². La cantidad de TOC eliminado creció cuando la concentración de ácido *trans*-cinámico aumentó, en OA-H₂O₂ del 68% al 81%, en EF del 75% al 81% y en FEF del 87% al 97%, al pasar de de 0,185 a 1,852 mM, tornándose el proceso mucho más eficiente, como se puede ver en las Figuras 6a-c. Por ejemplo, al analizar la MCE a 120 min en el anterior intervalo de concentración del ácido, se encontró en OA-H₂O₂ una variación del 8,6% al 60%, del 5,1 al 53% en EF y del 8,6% al 60% en FEF. Este comportamiento puede atribuirse a la menor contribución de las reacciones parasitarias (51)-(53), ya que una cantidad mayor de radicales $\cdot\text{OH}$ es capaz de reaccionar con el ácido y los intermedios formados durante cada tratamiento. Las condiciones óptimas para la eliminación del ácido se obtuvieron en el proceso FEF al tratar una disolución 0,926 mM durante 180 min a 33,3 mA cm⁻², alcanzando una mineralización del 98% y un 16% de MCE. También se observó que a concentraciones más altas de ácido no mejoraba la reducción de TOC.

Se tomaron muestras en la OA-H₂O₂ de una disolución con 0,926 mM de ácido, a los 90 min de ensayos a 33,3 mA cm⁻², las cuales se analizaron por medio de GC-MS. Se identificaron algunos compuestos intermedios tales como la cumarina, el bencenoacetaldehído y el ácido 3-fenilpropanoico que proceden de una ciclación interna del grupo carboxílico, descarboxilación y oxidación de doble enlace del ácido *trans*-cinámico, respectivamente. También se detectaron el ácido 4-hidroxifenilacético, el benzaldehído y el ácido benzoico, todos ellos productos de descomposición del bencenoacetaldehído. La posterior destrucción de estos intermedios dió lugar a una mezcla de ácidos carboxílicos de cadena corta, tales como los ácidos oxálico, acético y fumárico, los cuales se detectaron por HPLC de exclusión iónica. Los dos últimos ácidos se formaron a partir de la ruptura de los anillos bencénico de los derivados aromáticos, oxidándose finalmente a ácido oxálico. Éste se transforma directamente a CO₂ después de 240 min en FEF.

En conclusión, los EAOP demostraron su viabilidad para tratar agua contaminada con ácido *trans*-cinámico, lo que abre las puertas para que estas tecnologías eficaces puedan usarse para el tratamiento de las OOMW.

Electrochemical destruction of *trans*-cinnamic acid by advanced oxidation processes: kinetics, mineralization, and degradation route

Nelly Flores¹ · Abdoulaye Thiam¹ · Rosa María Rodríguez¹ · Francesc Centellas¹ · Pere Lluís Cabot¹ · José Antonio Garrido¹ · Enric Brillas¹ · Ignasi Sirés¹

Received: 7 November 2015 / Accepted: 29 December 2015 / Published online: 14 January 2016
© Springer-Verlag Berlin Heidelberg 2016

Abstract Acidic solutions of *trans*-cinnamic acid at pH 3.0 have been comparatively treated by anodic oxidation with electrogenerated H₂O₂ (AO-H₂O₂), electro-Fenton (EF), and photoelectro-Fenton (PEF). The electrolytic experiments were carried out with a boron-doped diamond (BDD)/air-diffusion cell. The substrate was very slowly abated by AO-H₂O₂ because of its low reaction rate with oxidizing [•]OH produced from water discharge at the BDD anode. In contrast, its removal was very rapid and at similar rate by EF and PEF due to the additional oxidation by [•]OH in the bulk, formed from Fenton's reaction between cathodically generated H₂O₂ and added Fe²⁺. The AO-H₂O₂ treatment yielded the lowest mineralization. The EF process led to persistent final products like Fe(III) complexes, which were quickly photolyzed upon UVA irradiation in PEF to give an almost total mineralization with 98 % total organic carbon removal. The effect of current density and substrate concentration on all the mineralization processes was examined. Gas chromatography–mass spectrometry (GC-MS) analysis of electrolyzed solutions allowed identifying five primary aromatics and one heteroaromatic molecule, whereas final carboxylic acids like fumaric, acetic, and oxalic were quantified by ion exclusion high-performance

liquid chromatography (HPLC). From all the products detected, a degradation route for *trans*-cinnamic acid is proposed.

Keywords Anodic oxidation · Electro-Fenton · Hydroxyl radical · Oxidation products · Photoelectro-Fenton · Photolysis · *trans*-Cinnamic acid · Water treatment

Introduction

trans-Cinnamic acid (*E*-3-phenyl-2-propenoic acid) is an unsaturated carboxylic acid commonly present in many fruits and vegetables. It is obtained from oil of cinnamon and balsams such as storax and shea butter, and it is synthesized in the industry from the base-catalyzed condensation of acetic anhydride and benzaldehyde or from reaction between cinnamaldehyde and benzal chloride. It is largely used worldwide in fragrances including decorative cosmetics, fine fragrances, shampoos, toilet soaps, and other toiletries as well as in non-cosmetic products such as household cleaners and detergents (Letizia et al. 2005). *trans*-Cinnamic acid has antifungal properties, inhibits the toxicity of metals in plants (Hojati et al. 2015), and acts as an antioxidant with very low toxicity in bacteria, animals, and human beings (Letizia et al. 2005; Zeni et al. 2013; Hakkim et al. 2014). It is a main component of toxic and recalcitrant olive oil mill wastewater (OOMWW), where its concentration reaches up to 106 mg L⁻¹ (Deeb et al. 2012), and it has been detected at relatively high contents of 10 µg L⁻¹ in rivers (Lafont et al. 2001). Kontos et al. (2014) described the removal and recovery of *trans*-cinnamic acid from OOMWW by crystallization. Several authors have reported the degradation of this acid and some polyphenolic components of OOMWW using different bacteria strains (Di Gioia et al. 2001) and by several advanced oxidation processes (AOPs) including zero-valent iron

Responsible editor: Bingcai Pan

Article submitted for publication in *Environmental Science and Pollution Research*

✉ Enric Brillas
brillas@ub.edu

¹ Laboratori d'Electroquímica dels Materials i del Medi Ambient, Departament de Química Física, Facultat de Química, Universitat de Barcelona, Martí i Franquès 1-11, 08028 Barcelona, Spain

(Sanchez et al. 2012) and wet oxidation (Lopes et al. 2007; Lopes and Quinta-Ferreira 2010). AOPs are based on the oxidation of pollutants by in situ generated reactive oxygen species (ROS) like hydroxyl radical ($\cdot\text{OH}$). However, much less is known about the treatment of *trans*-cinnamic acid solutions by powerful electrochemical AOPs (EAOPs). Chatzisympson et al. (2009) found a very poor mineralization with 25 % chemical oxygen demand (COD) reduction upon anodic oxidation (AO) treatment of 110 mL of a 5 mM *trans*-cinnamic acid solution in 0.1 M HClO_4 using a Ti/IrO_2 anode after a specific charge consumption of 28 Ah L^{-1} . These authors also describe a similar COD abatement of 30 % for OOMWW with 5 mM NaCl after consuming 43 Ah L^{-1} .

AO is the most popular EAOP and consists in the application of a high current density (j) to the anode M of the cell for the direct anodic oxidation of pollutants or, primordially, for their destruction by physisorbed hydroxyl radical $\text{M}(\cdot\text{OH})$ produced as intermediate of water discharge to O_2 at the anode surface (Marselli et al. 2003; Martínez-Huitle and Ferro 2006; Panizza and Cerisola 2009; Brillas and Martínez-Huitle 2015):



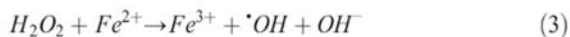
AO is more effective when a boron-doped diamond (BDD) thin-film electrode is employed as anode. This is due to the higher oxidation ability of physisorbed $\text{BDD}(\cdot\text{OH})$ generated by reaction (1) compared to that of other physisorbed $\text{M}(\cdot\text{OH})$ produced at anodes like Pt and PbO_2 (Ciriaco et al. 2009; Guinea et al. 2009; Rodrigo et al. 2010; Cavalcanti et al. 2013), as a result of the low interaction $\text{BDD} \cdot \text{OH}$ and the larger O_2 overpotential of BDD that favors the reaction of $\cdot\text{OH}$ with organics (Panizza and Cerisola 2009).

The oxidation ability of AO with a BDD anode can be enhanced in an undivided cell by electrogenerating H_2O_2 at the cathode from the two-electron reduction of O_2 gas via reaction (2). The so-called AO- H_2O_2 process involves the destruction of organics preferentially by physisorbed $\text{BDD}(\cdot\text{OH})$, with only a minor participation of ROS like H_2O_2 and its anodic oxidation product $\text{HO}_2\cdot$ (Sirés and Brillas 2012; Sirés et al. 2014). Carbon nanotubes (Khataee et al. 2013, 2014), graphite felt (Vatanpour et al. 2009), activated carbon fiber (Wang et al. 2008), carbon modified with metals or metal oxide nanoparticles (Assumpção et al. 2013), carbon felt (Dirany et al. 2012; El-Ghenymy et al. 2014; Yahya et al. 2014), carbon-polytetrafluoroethylene (PTFE) O_2 or air-diffusion (Borràs et al. 2010; Thiam et al. 2014, 2015b), and BDD (Cruz-González et al. 2010, 2012) are considered the most suitable carbonaceous cathodes to electrogenerate H_2O_2 :



The performance of AO- H_2O_2 can be improved by means of EAOPs based on Fenton's reaction chemistry like

electro-Fenton (EF) and photoelectro-Fenton (PEF), which have recently gained increasing interest for wastewater remediation (Sirés and Brillas 2012; Sirés et al. 2014; Vasudevan and Oturan 2014; Brillas and Martínez-Huitle 2015). In the EF process, a small quantity of Fe^{2+} is added to the solution to react with H_2O_2 via Fenton's reaction (3) yielding Fe^{3+} and $\cdot\text{OH}$ in the bulk (Dirany et al. 2012; El-Ghenymy et al. 2014; Thiam et al. 2014, 2015a). Organics are then destroyed by both radicals, $\text{M}(\cdot\text{OH})$ and $\cdot\text{OH}$, at an optimum pH ~ 3 . When the PEF process is applied, the treated solution is irradiated with artificial UVA light that causes the photoreduction of $\text{Fe}(\text{OH})^{2+}$ species to Fe^{2+} and $\cdot\text{OH}$ generation via reaction (4), along with the photodecarboxylation of complexes of $\text{Fe}(\text{III})$ with generated carboxylic acids from reaction (5) (Ruiz et al. 2011; Moreira et al. 2013; Florenza et al. 2014; Thiam et al. 2015a):



In this paper, we present a comparative study on the degradation of *trans*-cinnamic acid solutions of pH 3.0 by AO- H_2O_2 , EF, and PEF using a stirred BDD/air-diffusion cell. The influence of j and substrate content on the performance of these EAOPs was examined to clarify the role of generated hydroxyl radicals and UV light. The abatement of *trans*-cinnamic acid and the evolution of final carboxylic acids were followed by high-performance liquid chromatography (HPLC). Gas chromatography–mass spectrometry (GC-MS) allowed the identification of the primary aromatic intermediates. A plausible route for *trans*-cinnamic acid mineralization including all detected products is proposed.

Experimental details

Chemicals

Analytical grade *trans*-cinnamic acid (purity > 99 %) was supplied by Sigma-Aldrich and used as received. Acetic, fumaric, and oxalic acids were of analytical grade purchased from Panreac. Heptahydrated $\text{Fe}(\text{II})$ sulfate and anhydrous sodium sulfate were of analytical grade supplied by Fluka. Analytical grade sulfuric acid was purchased from Merck and used to adjust the initial solution pH to 3.0. The solutions were prepared with ultrapure water provided by a Millipore Milli-Q system (resistivity > 18.2 $\text{M}\Omega \text{ cm}$ at 25 °C). Other chemicals were of HPLC or analytical grade supplied by Avocado, Fluka, and Merck.

Electrolytic system

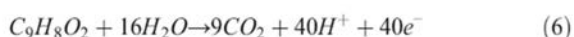
The electrolytic assays were carried out in an open and undivided cylindrical glass cell of 150-mL capacity equipped with a double jacket for recirculating water through a Thermo Electron Corporation HAAKE DC 10 thermostat. All the experiments were made at 25 °C and under vigorous stirring with a magnetic bar at 700 rpm to ensure the solution mixing and the transport of reactants toward/from the electrodes. A 3-cm² BDD thin-film electrode from NeoCoat (La-Chaux-de-Fonds, Switzerland) was used as the anode and a 3-cm² carbon-PTFE air-diffusion cathode from E-TEK (Somerset, NJ, USA) was used as the cathode. The air-diffusion cathode was mounted as described elsewhere (Boye et al. 2003) and was fed with air pumped at 300 mL min⁻¹ for H₂O₂ generation. The interelectrode gap was about 1 cm. The trials were performed at constant *j* provided by an EG&G Princeton Applied Research 273A potentiostat-galvanostat.

Comparative treatment of 100 mL of solutions with *trans*-cinnamic acid and 0.05 M Na₂SO₄ as background electrolyte at pH 3.0 was carried out by AO-H₂O₂, EF and PEF. Electrolyses for the two latter EAOPs were run after addition of 0.50 mM Fe²⁺ as catalyst since this content was found optimal for many organics treated under similar conditions (Ruiz et al. 2011; Moreira et al. 2013; Florenza et al. 2014; Thiam et al. 2015a). For PEF, a Philips TL/6 W/08 fluorescent black light blue tube was placed at 8 cm above the solution. This UVA lamp emitted at λ_{max} = 360 nm and with 5 W m⁻² average power density, as determined with a Kipp&Zonen CUV 5 UV radiometer.

Instruments and analytical procedures

A Crison GLP 22 pH meter was used to measure the solution pH. Total organic carbon (TOC) was determined with a Shimadzu VCSN TOC analyzer. This analysis was performed by filtering the samples withdrawn from treated solutions at regular times with Whatman 0.45 μm PTFE filters and, subsequently, directly injecting 50-μL aliquots into the above analyzer. Reproducible TOC values with ±1 % accuracy were always determined.

Since the total conversion of *trans*-cinnamic acid into CO₂ can be written as follows



the mineralization current efficiency (MCE) for each trial was then estimated from Eq. (7) (Ruiz et al. 2011):

$$MCE(\%) = \frac{nFV\Delta(TOC)_{exp}}{4.32 \times 10^7 mIt} \times 100 \quad (7)$$

where *n* is the number of electrons for total mineralization (40 e⁻ from reaction (6)), *F* is the Faraday constant (96,487 C mol⁻¹), *V* is the solution volume (in L), Δ(TOC)_{exp} is the experimental TOC abatement (in mg L⁻¹), 4.32 × 10⁷ is a conversion factor (3600 s h⁻¹ × 12,000 mg C mol⁻¹), *m* is the number of carbon atoms of *trans*-cinnamic acid (9 C atoms), *I* is the current (in A), and *t* is the electrolysis time (in h).

Reversed-phase HPLC was used to follow the kinetic decay of *trans*-cinnamic acid. These measurements were made by injecting 10-μL aliquots into a Waters 600 LC containing a BDS Hypersil C18 6 μm, 250 mm × 4.6 mm, column at 35 °C, coupled to a Waters 996 photodiode array detector selected at λ = 276 nm. All the samples were filtered with Whatman 0.45 μm PTFE filters, although for the EF and PEF assays, they were previously diluted with acetonitrile (1:1) to stop the degradation process. The mobile phase was an 80:20 (v/v) acetonitrile/water mixture eluted at 0.8 mL min⁻¹ and the chromatograms exhibited a well-defined peak for *trans*-cinnamic acid at retention time (*t_r*) = 3.45 min.

The same LC system was used to detect and quantify the generated carboxylic acids by ion-exclusion HPLC, but with a Bio-Rad Aminex HPX 87H, 300 mm × 7.8 mm, column at 35 °C, and the photodiode array detector set at λ = 210 nm. This analysis was also performed with 10-μL aliquots, circulating 4 mM H₂SO₄ at 0.6 mL min⁻¹ as mobile phase. The chromatograms recorded displayed peaks associated to oxalic (*t_r* = 6.9 min), acetic (*t_r* = 14.9 min), and fumaric (*t_r* = 15.6 min) acids.

The primary aromatic products of *trans*-cinnamic acid were identified from the AO-H₂O₂ treatment of 100 mL of a 0.926 mM substrate solution at 33.3 mA cm⁻². Various electrolyses were run up to 30 and 90 min, and the remaining organic components of each solution were extracted out with CH₂Cl₂ (3 × 25 mL). The resulting organic fractions were dried over anhydrous Na₂SO₄ and filtered and their volume reduced to near 1 mL for further analysis by GC-MS. GC-MS measurements were performed with an Agilent Technologies system composed of a 6890N GC and a 5975C MS operating in electron impact mode at 70 eV. The GC was fitted with either a non-polar Agilent J&W HP-5 ms or a polar HP INNOWax column, both of 0.25 μm, 30 m × 0.25 mm. The temperature ramp was 36 °C for 1 min, 5 °C min⁻¹ up to 300 °C for the non-polar column or 250 °C for the polar one, and hold time 10 min. The temperature of the inlet, source, and transfer line was 250, 230, and 280 °C for the non-polar column and 250, 230, and 250 °C for the polar one. Identified products matched with the mass spectra of standard organics given in a NIST05-MS library.

Results and discussion

Kinetic decay of *trans*-cinnamic acid by AO-H₂O₂, EF, and PEF

The decay kinetics of *trans*-cinnamic acid by the different EAOPs using a BDD/air-diffusion cell was first determined for 100 mL of 0.926 mM substrate solutions in 0.05 M Na₂SO₄ of pH 3.0 at 33.3 mA cm⁻². In AO-H₂O₂ (no catalyst) as well as in EF and PEF (0.50 mM Fe²⁺ as catalyst), the solution pH underwent a slight fall from 3.0 to ~2.7–2.8 after 360 min of electrolysis, which can be ascribed to the production of acidic products such as carboxylic acids (Ruiz et al. 2011; Moreira et al. 2013; Florenza et al. 2014; Thiam et al. 2015a). A preliminary study with the same solution under a 6-W UVA irradiation in the absence of electric current confirmed that the substrate content did not vary with time, as expected if *trans*-cinnamic acid is not directly photolyzed by UVA light.

Figure 1a depicts a very slow abatement of *trans*-cinnamic acid by AO-H₂O₂, requiring 360 min to completely disappear. The reaction rate of this compound with generated ROS, pre-eminently with BDD(•OH) originated from reaction (1), is then very low. In contrast, Fig. 1b depicts a much quicker decay and at similar rate in EF and PEF, being completely removed in about 42 min in both cases. The more rapid disappearance of this compound in such processes can be related to its faster reaction occurring in the bulk with •OH originated from Fenton's reaction (3) compared with the much slower attack of BDD(•OH) confined near the anode. The quite similar removal rate in EF and PEF suggests a very small contribution of both, photolytic reaction (4) and photodegradation of Fe(III)-carboxylate species via reaction (5), to produce greater quantities of •OH.

The concentration decays of Fig. 1a, b were well fitted to a pseudo-first-order kinetic equation, as can be seen in the inset panels. This behavior suggests that *trans*-cinnamic acid is attacked by a steady concentration of BDD(•OH) and/or •OH in each treatment. From this analysis, apparent rate constants (k_1) of 0.012 min⁻¹ (square regression coefficient $R^2=0.991$) for AO-H₂O₂, 0.052 min⁻¹ ($R^2=0.998$) for EF, and 0.050 min⁻¹ ($R^2=0.9990$) for PEF were obtained. The k_1 value in EF and PEF was 4.2–4.3 orders of magnitude greater than that in AO-H₂O₂, corroborating the much larger oxidation ability of •OH compared to BDD(•OH) in the two former EAOPs.

The study of the kinetic decay of *trans*-cinnamic acid was extended to lower concentrations of 0.185 and 0.463 mM by applying 33.3 mA cm⁻². Total removal of the substrate occurred at shorter time as the initial organic load decreased. For example, in AO-H₂O₂, *trans*-cinnamic

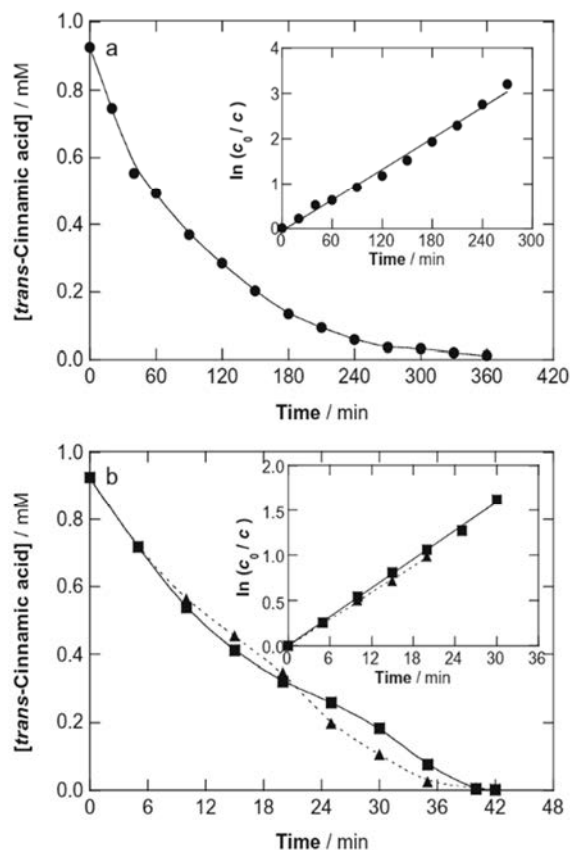


Fig. 1 *trans*-Cinnamic acid content versus electrolysis time for the degradation of 100 mL of a 0.926 mM substrate solution in 0.05 M Na₂SO₄ at pH 3.0 and 25 °C using a BDD/air-diffusion cell of 3-cm² electrode area at 33.3 mA cm⁻². **a** Anodic oxidation with electrogenerated H₂O₂ (AO-H₂O₂). **b** (square) Electro-Fenton (EF) with 0.50 mM Fe²⁺ and (triangle) photoelectro-Fenton (PEF) with 0.50 mM Fe²⁺ using a 6-W UVA light. The pseudo-first-order kinetic analysis for the *trans*-cinnamic acid concentration abatement is shown in the inset panels

acid disappeared at 270, 330, and 360 min for 0.185, 0.463, and 0.926 mM, respectively, whereas its removal in the EF treatment occurred at 8, 20, and 42 min for the same concentrations. According to this trend, a raising k_1 value with decreasing substrate content was obtained from the corresponding pseudo-first-order kinetic analysis. Thus, k_1 grew from 0.012 min⁻¹ ($R^2=0.991$) to 0.014 min⁻¹ ($R^2=0.992$) in AO-H₂O₂ and from 0.052 min⁻¹ ($R^2=0.998$) to 0.58 min⁻¹ ($R^2=0.994$) in EF when changing from 0.926 to 0.185 mM. It is then evident that the kinetic decay of this acid does not obey a true pseudo-first-order reaction, because similar k_1 values should be found independently of its initial content. This change in k_1 can be explained by considering that, since analogous quantities of BDD(•OH) and/or •OH are produced in each EAOP at $j=33.3$ mA cm⁻² regardless of the organic load, a larger proportion of these oxidizing radicals is able to react with the oxidation products

generated, thus decreasing their available quantity to attack the *trans*-cinnamic acid.

Mineralization of *trans*-cinnamic acid solutions by AO-H₂O₂, EF, and PEF

For the above solutions with 0.926 mM *trans*-cinnamic acid of pH 3.0 treated by the EAOPs at 33.3 mA cm⁻², their TOC decay was determined in order to ascertain the relative mineralization ability. Figure 2a highlights a slow and continuous TOC removal under AO-H₂O₂ conditions, reaching a partial mineralization of 68 % after 360 min of electrolysis. A much rapid TOC abatement can be observed in EF, with a final TOC reduction of 78 %. It should be noted that the mineralization process in EF was very fast up to 120 min as a result of the efficient oxidation by [•]OH but, at longer time, it underwent a progressive deceleration suggesting the generation of more recalcitrant products, like Fe(III)-carboxylate complexes, which are very refractory to [•]OH and can only be slowly destroyed by BDD([•]OH) (Sirés et al. 2014). Figure 2a also evidences a very positive effect of UVA irradiation during the PEF process, which yielded a high TOC decay rate to

attain an almost total mineralization with 98 % TOC reduction at 360 min. This large acceleration of the mineralization process can be ascribed to the photolysis of products such as Fe(III)-carboxylate species via reaction (5) (Sirés et al. 2014; Brillas and Martínez-Huitle 2015). These findings indicate that the oxidation ability of the EAOPs to mineralize the *trans*-cinnamic acid increases in the sequence AO-H₂O₂<EF<PEF.

Figure 2b shows the MCE values estimated from Eq. (7) for the assays of Fig. 2a. A higher current efficiency was obtained as the TOC removal of the EAOPs increased. This tendency was more apparent between 60 and 120 min of electrolysis, because of the effect of BDD([•]OH) and [•]OH oxidation and photolysis on the mineralization rate in each treatment. In PEF, the MCE value dropped from 71 % at the beginning of the treatment to 16 % at 360 min. This fall in current efficiency can be explained by the production of more recalcitrant final oxidation products as well as the progressive loss of organic matter (Panizza and Cerisola 2009; Florenza et al. 2014; Thiam et al. 2015b). In the case of EF, the MCE value rose from an initial 14 to 28 % at 120 min, further decaying to 13 %. This is due to the initial formation of some persistent products that react slowly with [•]OH in EF, requiring longer time for their mineralization, whereas their continuous removal caused the increase in MCE at the beginning of this process. In contrast, the MCE values in AO-H₂O₂ remained practically constant between 13 and 15 %, indicating a constant mineralization rate of products upon BDD([•]OH) oxidation.

Effect of applied current density and substrate concentration on the performance of EAOPs

It is well known that the amount of oxidizing hydroxyl radicals acting in each EAOP is limited by the applied *j*. To clarify the influence of this key operation parameter, the mineralization of 0.926 mM *trans*-cinnamic acid solutions was carried out at *j* in the range 16.7–100 mA cm⁻². Figure 3a–c depicts the TOC decay versus electrolysis time measured in the AO-H₂O₂, EF, and PEF assays, respectively. For the former process, Fig. 3a shows a quite similar TOC abatement at 16.7–66.7 mA cm⁻² during about 240 min, whereas the mineralization rate increased more significantly at 100 mA cm⁻². This means that the expected rise in BDD([•]OH) from the acceleration of reaction (1) at higher *j* (Sirés et al. 2014) has little influence on the destruction of organics, indicating that the excess of ROS produced is rather consumed in parasitic reactions, as will be discussed below. The influence of *j* in AO-H₂O₂ was more apparent between 240 and 360 min, when final products like short-linear carboxylic acids are the main accumulated organics. At 360 min, for example, increasing TOC reductions of 64, 68, 76, and 84 % for 16.7, 33.3, 66.7, and 100 mA cm⁻², respectively, were found. A partial

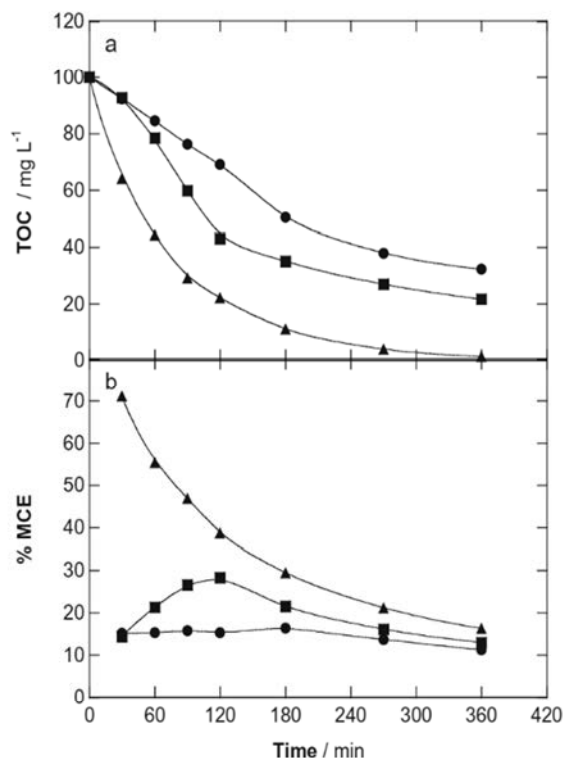


Fig. 2 a TOC removal and b variation of mineralization current efficiency with electrolysis time for the degradation of 100 mL of a 0.926 mM *trans*-cinnamic acid solution in 0.05 M Na₂SO₄ at pH 3.0 and 25 °C using a BDD/air-diffusion at 33.3 mA cm⁻². Method: (circle) AO-H₂O₂, (square) EF with 0.50 mM Fe²⁺, and (triangle) PEF with 0.50 mM Fe²⁺ using a 6 W UVA light

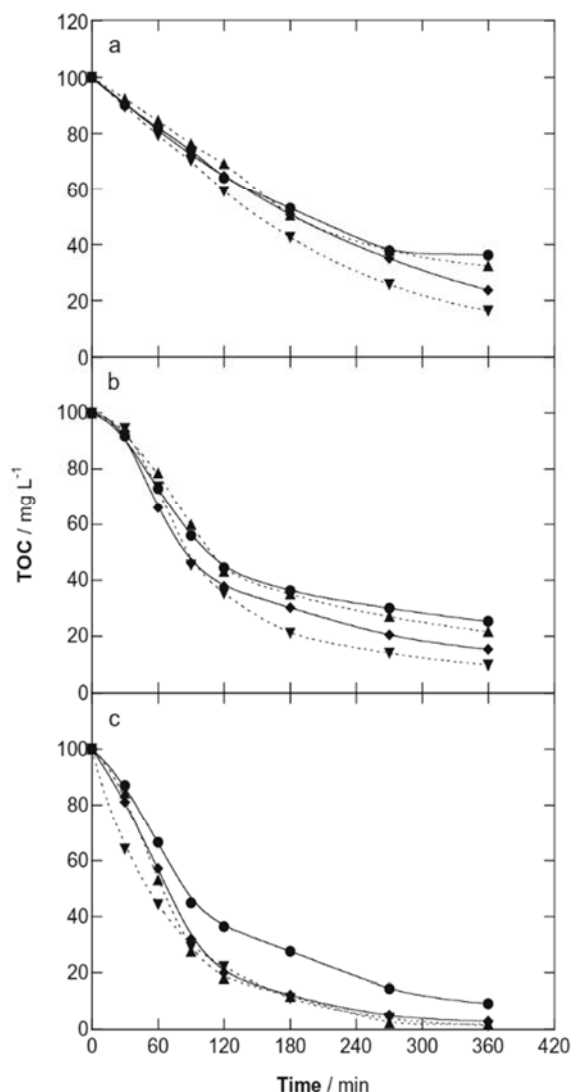


Fig. 3 Effect of current density on TOC decay versus electrolysis time for the treatment of 100 mL of a 0.926 mM *trans*-cinnamic acid solution in 0.05 M Na₂SO₄ at pH 3.0 and 25 °C using a BDD/air-diffusion cell. Method: **a** AO-H₂O₂, **b** EF, and **c** PEF. Applied current density: (circle) 16.7 mA cm⁻², (upright triangle) 33.3 mA cm⁻², (diamond) 66.7 mA cm⁻², and (upside down triangle) 100 mA cm⁻²

mineralization but with greater TOC decay can be seen in Fig. 3b for the comparative EF runs. In this process, higher j originated more quantities of BDD([•]OH) as well as greater amounts of [•]OH in the bulk due to the quicker generation of H₂O₂ by reaction (2) and the concomitant acceleration of Fenton's reaction (3). Both ROS then play a pre-eminent role to destroy the intermediates and their Fe(III) complexes and, thus, greater TOC decay at higher j values can be clearly distinguished in Fig. 3b from 120 min of electrolysis. At the end of these treatments, however, the best j of 100 mA cm⁻² only yielded 90 % mineralization. The behavior was very different when PEF was applied. Figure 3c reveals that the

low production of BDD([•]OH) and [•]OH at 16.7 mA cm⁻² impeded the complete production of photosensitive products and, therefore, only 91 % TOC reduction was achieved at 360 min. In contrast, the use of $j \geq 33.3$ mA cm⁻² favored an effective generation of oxidants, and nearly all the accumulated products were photosensitive and were removed at similar rate yielding an almost total mineralization with 97–98 % TOC reduction at the end of all the treatments. These findings indicate that 33.3 mA cm⁻² can be considered as the best j value for the application of this EAOP to degrade a 0.926 mM *trans*-cinnamic solution.

Figure 4a–c shows a loss in current efficiency for each EAOP as j rose. This tendency is not surprising in view of

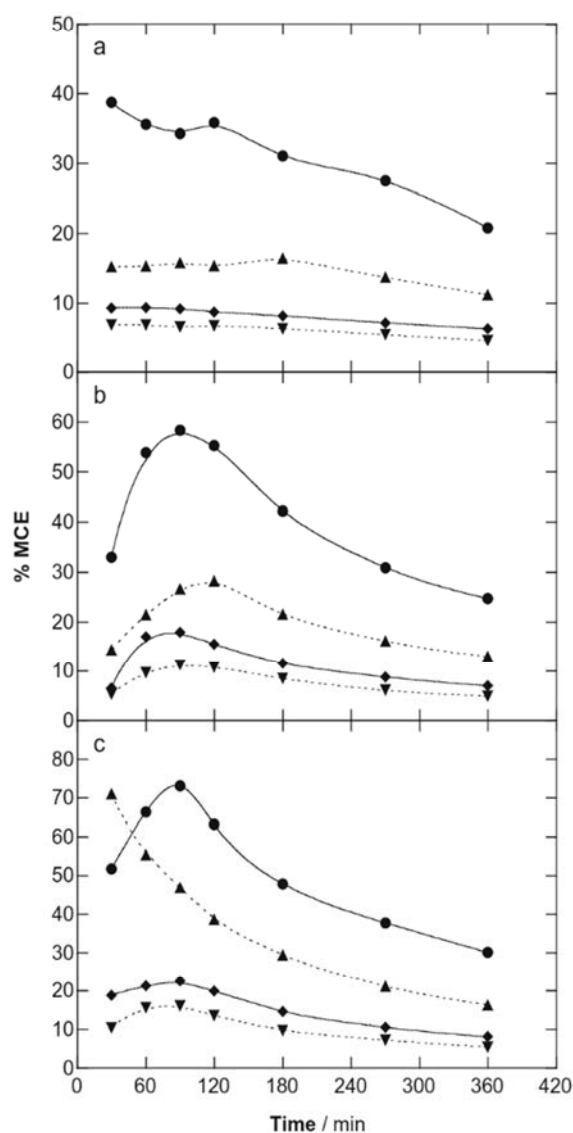
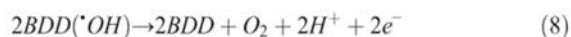


Fig. 4 Mineralization current efficiency versus electrolysis time for the trials of Fig. 3

the low effect of this parameter on the TOC decay of all the treatments, mainly in AO-H₂O₂ and PEF (see Fig. 3a, c). As shown in Fig. 4a, the MCE values in each AO-H₂O₂ at a given $j \geq 33.3 \text{ mA cm}^{-2}$ basically remained unchanged during each run, as expected for a constant mineralization rate of intermediates, whereas at 16.7 mA cm^{-2} , it gradually dropped from 39 to 21 % due to the smaller mineralization ability of the lower amounts of BDD([•]OH) generated. For EF, a maximum MCE value was attained after 90–120 min of all the assays (see Fig. 4b), corroborating the initial formation of several products that are slowly destroyed by hydroxyl radicals while their gradual mineralization largely improves the current efficiency at the beginning of the process. The same phenomenon is shown in Fig. 4c for PEF at 16.7 mA cm^{-2} , since the smaller amounts of BDD([•]OH) and [•]OH produced under these conditions attack slowly the substrate and its products and low quantities of photosensitive species are formed to be removed by UVA light. Current efficiency then grew as these initial recalcitrant products progressively disappeared from the medium. This behavior was not found for greater j values because the mineralization was enhanced by the faster photolysis of larger quantities of products, like Fe(III)-carboxylate species. In all the EF and PEF assays, the current efficiency diminished at long electrolysis time due to two main contributions, the loss of organic load and the formation of more recalcitrant intermediates, as stated above. For the most powerful EAOP, i.e., PEF process, maximum MCE of ~71–73 % was obtained after 90 and 30 min at 16.7 and 33.3 mA cm⁻², respectively.

The decay in MCE as j grows is opposite to the TOC removal trend. This can be associated with the consumption of the excess of generated hydroxyl radicals by waste reactions. Examples are the anodic oxidation of physisorbed BDD([•]OH) to O₂ via reaction (8) and the removal of [•]OH by Fe²⁺ and H₂O₂ via reactions (9) and (10), respectively (Sirés and Brillas 2012; Sirés et al. 2014). It is also expected that the formation of other weaker oxidants at the BDD anode, mainly S₂O₈²⁻ ion from SO₄²⁻ ion of the electrolyte via reaction (11), inhibits the H₂O discharge from reaction (1) (Panizza and Cerisola 2009), becoming largely enhanced as well:



Another important operation parameter in the EAOPs is the substrate concentration since it determines the oxidation ability of hydroxyl radicals and/or their combined action with the photo-oxidation by UVA light. The influence of this parameter was examined for 0.185, 0.463, 0.926, and 1.852 mM of *trans*-cinnamic acid at the best $j = 33.3 \text{ mA cm}^{-2}$ found for PEF, and the results are presented in Fig. 5a–c. Oscillating

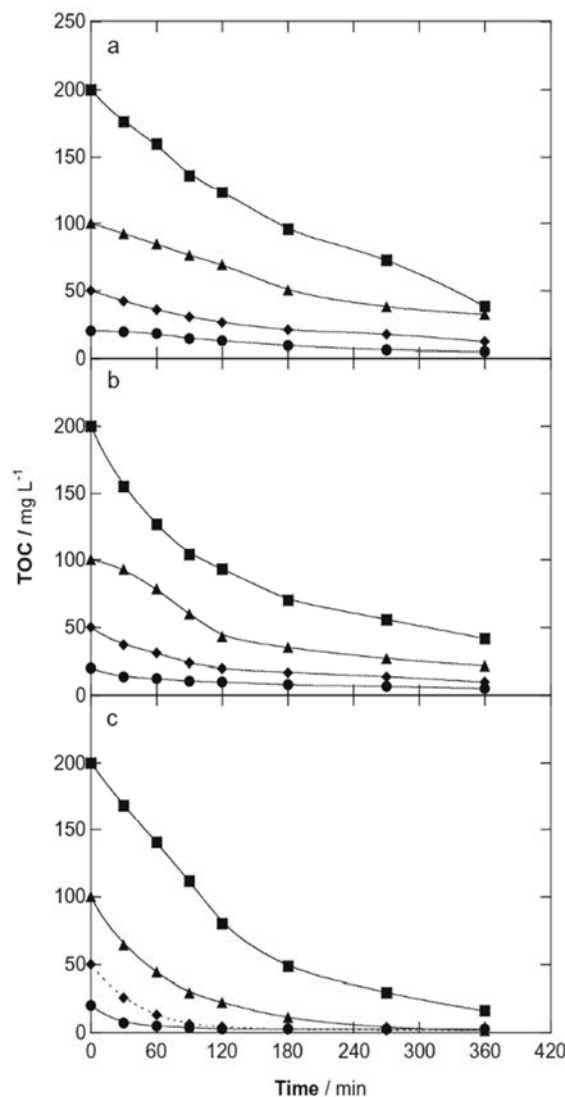
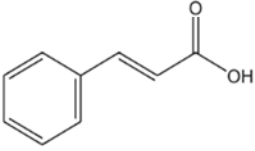
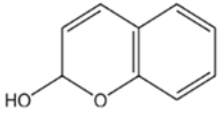
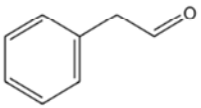
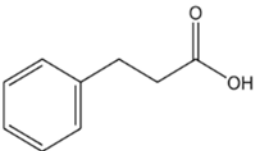
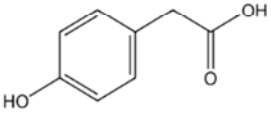
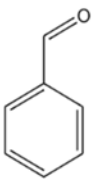
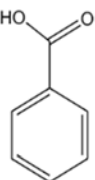


Fig. 5 Effect of *trans*-cinnamic acid concentration on TOC removal with electrolysis time for the degradation of 100 mL of solutions of this substrate in 0.05 M Na₂SO₄ at pH 3.0 using a BDD/air-diffusion cell at 33.3 mA cm⁻² and 25 °C. Method: **a** AO-H₂O₂, **b** EF, and **c** PEF. Content of *trans*-cinnamic acid: (circle) 0.185 mM, (diamond) 0.463 mM, (triangle) 0.926 mM, and (square) 1.852 mM

final percentages of TOC removal were always found for each EAOP with increasing substrate content. For example, at the end of the above treatments, TOC was reduced by 68–81 % in AO-H₂O₂, 75–81 % in EF, and 87–97 % in PEF. Note that quite analogous percentages of TOC abatement were found for the two former treatments up to 0.463 mM, thus showing similar final mineralization values.

For the above assays, however, greater amounts of TOC were always removed with raising the organic load of the solution, and this fact is reflected in Fig. 6a–c from the concomitant enhancement of the corresponding MCE values. At 120 min, for example, operating between 0.185 and

Table 1 Products identified by GC-MS during the electrolysis of 100 mL of a 0.926-mM *trans*-cinnamic acid solution in 0.05 M Na₂SO₄ at pH 3.0 and 25 °C by AO-H₂O₂ using a stirred BDD/air-diffusion cell at 33.3 mA cm⁻²

Number	Name	Molecular structure	<i>t_r</i> (min)	<i>m/z</i>	Electrolysis time (min)
1	<i>trans</i> -Cinnamic acid		26.2 ^a	148 (M ⁺),	30, 90
			42.2 ^b	147, 131, 103	30, 90
2	2 <i>H</i> -1-Benzopyran-2-one or Coumarin		35.7 ^b	146 (M ⁺), 118, 90, 63	30, 90
3	Benzeneacetaldehyde		19.9 ^b	120 (M ⁺), 91, 65	30, 90
4	3-Phenylpropanoic acid		20.5 ^a	150 (M ⁺),	30, 90
			31.3 ^b	135, 107, 77	30, 90
5	4-Hydroxyphenylacetic acid		37.5 ^b	152 (M ⁺), 151, 137, 123, 109, 81	30, 90
6	Benzaldehyde		17.1 ^b	106 (M ⁺), 105, 77	30
7	Benzoic acid		35.3 ^b	122 (M ⁺), 105, 77, 51	30, 90
10	Oxalic acid	COOH-COOH	24.9 ^b	89 ((M-H) ⁻), 71, 50	90

Retention times for: ^a non-polar Agilent J&W HP-5ms and ^b polar HP INNOWax columns.

radicals. In contrast, Fig. 7 shows that the final acid **10** was much more largely accumulated in all the EAOPs, then being the main carboxylic acid generated during the mineralization process of *trans*-cinnamic acid. In AO-H₂O₂, this acid was

progressively accumulated up to 0.137 mM as maximal at 180 min, whereupon it decayed to 0.094 mM. This value accounts for 2.3 mg L⁻¹ TOC, only contributing in 7.2 % to the organic load of the remaining solution (32 mg L⁻¹ TOC,

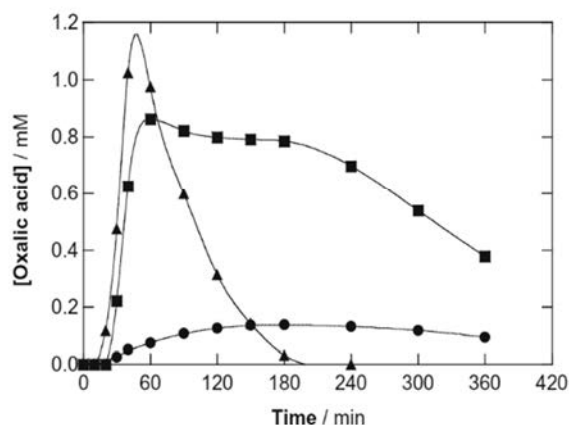


Fig. 7 Time-course of the concentration of oxalic acid (**10**) detected during the treatments shown in Fig. 2. Method: (circle) AO-H₂O₂, (square) EF, and (triangle) PEF

see Fig. 2). This means that the majority of components (93 %) of such solution were recalcitrant products that are slowly destroyed by BDD([•]OH). On the other hand, Fig. 7 reveals a very high accumulation of acid **10** up to 0.86 mM at 60 min in EF and 1.02 mM at 40 min in PEF as a result of the much faster destruction of primary intermediates by [•]OH. At longer time, the evolution of this acid depended on the characteristics of each treatment. In EF, the slow oxidation of Fe(III)-oxalate species mainly by BDD([•]OH) yielded 0.38 mM of **10**, related to 9.1 mg L⁻¹ TOC and a 41 % of the 22 mg L⁻¹ TOC of the final solution (see Fig. 2). The remaining solution of EF then contained 59 % of undetected

products that are highly recalcitrant to hydroxyl radicals. Conversely, the UVA irradiation used in PEF led to rapid and total photodecarboxylation of Fe(III)-oxalate complexes via reaction (5), with all the acid **10** disappearing in only 240 min, although the final solution at 360 min still contained a 2 % of the starting TOC (see Fig. 2). One can infer that the PEF process destroys most of persistent products that cannot be oxidized by hydroxyl radicals in EF, thanks to the photolytic action of UVA light. This behavior along with the total removal of final carboxylic acids justifies the almost total mineralization achieved in PEF.

Degradation route for *trans*-cinnamic acid by EAOPs with BDD

Based on the products identified in this work, a plausible route for *trans*-cinnamic acid mineralization by EAOPs with a BDD anode is proposed in Fig. 8. The oxidation of the substrate and its aromatic and heteroaromatic products occurs by reaction with BDD([•]OH) in AO-H₂O₂ and more rapidly with [•]OH in EF and PEF. The final carboxylic acids and Fe(III)-carboxylate species are preferentially attacked by BDD([•]OH). Other generated oxidants like H₂O₂, HO₂[•], O₃, and S₂O₈²⁻ can oxidize much more slowly some of the products as well. In the proposed path, only the fate of Fe(III)-oxalate complexes is specified for the sake of simplicity. This degradation pathway was more realistic for EF and PEF, due to their higher oxidation ability compared to AO-H₂O₂.

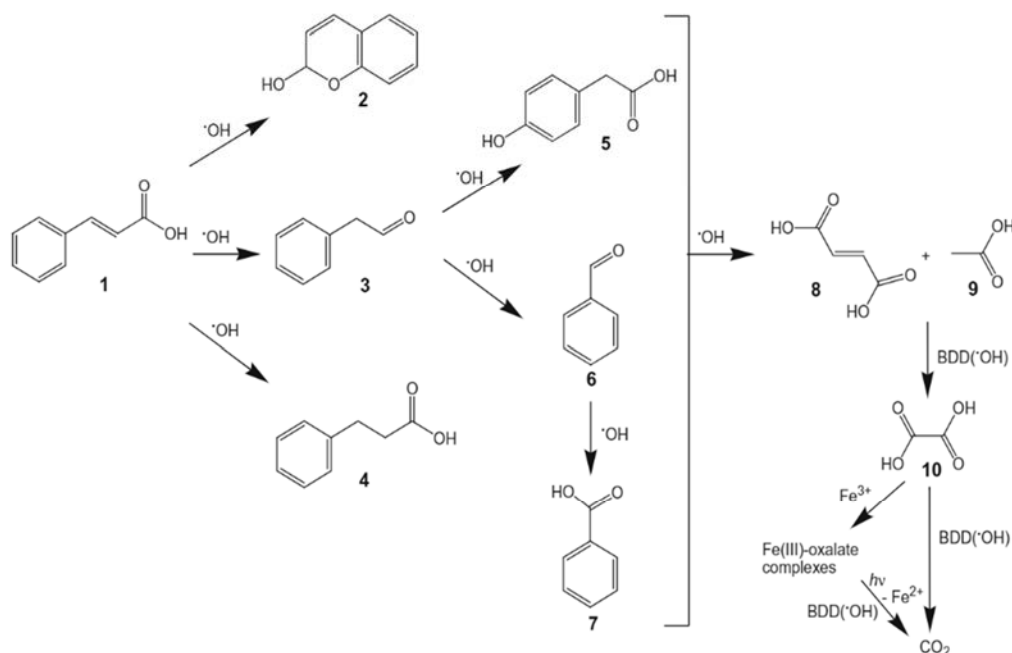


Fig. 8 Route for *trans*-cinnamic acid mineralization by AO-H₂O₂, EF, and PEF using a BDD/air-diffusion cell. The species [•]OH in the sequence of aromatics represents their oxidation by BDD([•]OH) at the BDD surface and/or [•]OH from Fenton's reaction in the bulk

The route is initiated by the attack of hydroxyl radicals over **1** to cause (i) an internal cyclization of its carboxylic group producing the heteroaromatic **2**, (ii) its decarboxylation followed by oxidation to generate the aldehyde **3**, and (iii) the transformation of its double bond giving the saturated carboxylic acid **4**. Subsequent oxidation of **3** yields the saturated acid **5** and benzaldehyde **6**, which is then oxidized to benzoic acid **7**. Further cleavage of the benzene ring of all the above compounds gives a mixture of final acids **8–10**. Acids **8** and **9**, formed to a small extent, are rapidly converted into acid **10**. This acid is transformed into CO₂ by BDD(•OH) in AO-H₂O₂, whereas in EF and PEF, it forms Fe(III)-oxalate species that are slowly mineralized by BDD(•OH) and much more quickly photodecarboxylated by UVA light with Fe²⁺ regeneration via reaction (5).

Conclusions

The PEF degradation of 0.926 mM *trans*-cinnamic acid solutions of pH 3.0 led to an almost total mineralization at $j \geq 33.3 \text{ mA cm}^{-2}$. PEF is much more powerful than EF, which yielded 90 % TOC abatement as maximal at 100 mA cm^{-2} , because of the quick photodegradation of highly recalcitrant products like Fe(III)-carboxylate complexes. The oxidation power of AO-H₂O₂ was always lower than that of EF, indicating the positive combination of BDD(•OH) produced at the anode and •OH formed from Fenton's reaction to remove organics. For each EAOP, increasing j from 16.7 to 100 mA cm^{-2} caused more rapid mineralization with lower current efficiency, whereas the use of more concentrated solutions from 0.185 to 1.852 mM enhanced the amount of TOC abated, which caused a gradual rise of current efficiency at long electrolysis time. Five primary aromatics, one heteroaromatic, and three short final carboxylic acids were identified. Oxalic acid was the most important final product. It presented a large persistence in AO-H₂O₂ and EF but disappeared rapidly in PEF due to the quick photolysis of its Fe(III) complexes that explains the superior oxidation power of this EAOP.

Acknowledgments Financial support from MINECO (Ministerio de Economía y Competitividad, Spain) under project CTQ2013-48897-C2-1-R, co-financed with FEDER funds, and the Ph.D. fellowship awarded to N. Flores by SENESCYT (Secretaría Nacional de Educación Superior, Ciencia, Tecnología e Innovación, Ecuador) are acknowledged.

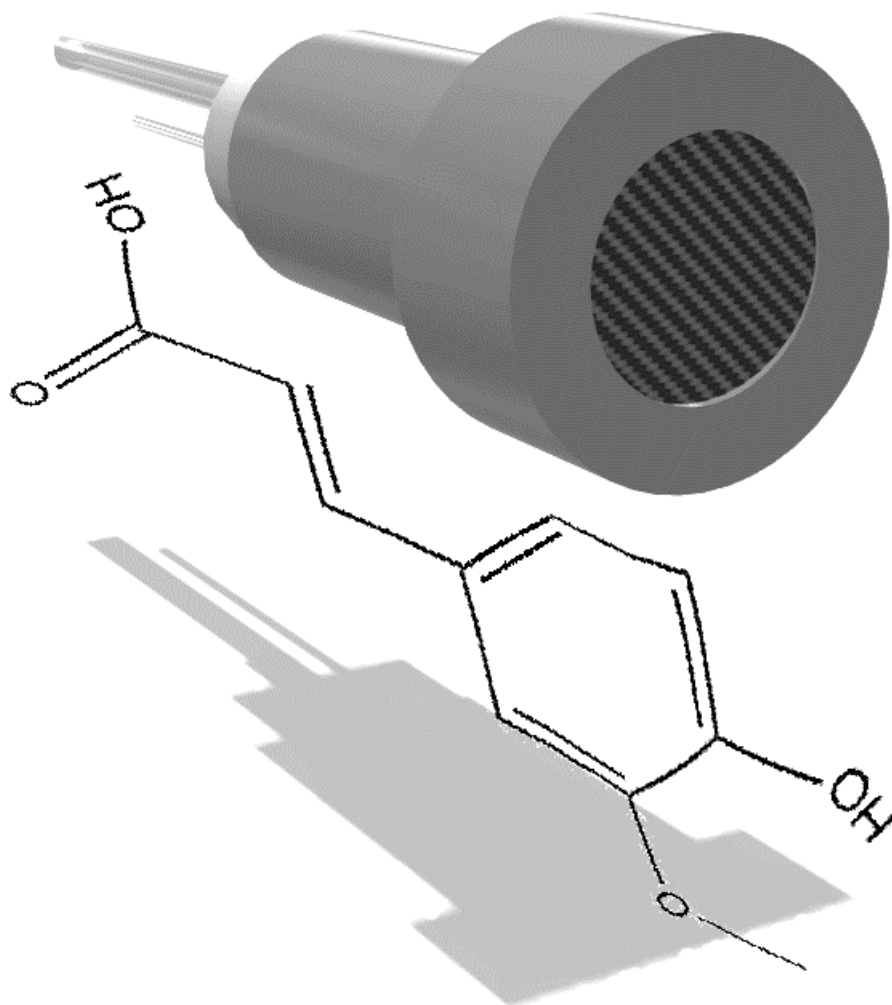
References

Assumpção MHMT, Moraes A, De Souza RFB, Reis RM, Rocha RS, Gaubeur I, Calegario ML, Hammer P, Lanza MRV, Santos MC (2013) Degradation of dipyrone via advanced oxidation processes using a cerium nanostructured electrocatalyst material. *Appl Catal A Gen* 462–463:256–261

- Borrás N, Oliver R, Arias C, Brillas E (2010) Degradation of atrazine by electrochemical advanced oxidation processes using a boron-doped diamond anode. *J Phys Chem A* 114(24):6613–6621
- Boye B, Dieng MM, Brillas E (2003) Electrochemical degradation of 2,4,5-trichlorophenoxyacetic acid in aqueous medium by peroxi-coagulation. Effect of pH and UV light. *Electrochim Acta* 48(7):781–790
- Brillas E, Martínez-Huitle CA (2015) Decontamination of wastewaters containing synthetic organic dyes by electrochemical methods. An updated review. *Appl Catal B Environ* 166–167:603–643
- Cavalcanti EB, Garcia-Segura S, Centellas F, Brillas E (2013) Electrochemical incineration of omeprazole in neutral aqueous medium using a platinum or boron-doped diamond. Degradation kinetics and oxidation products. *Water Res* 47(5):1803–1815
- Chatzisympson E, Dimou A, Mantzavinos D, Katsaounis A (2009) Electrochemical oxidation of model compounds and olive mill wastewater over DSA electrodes: 1. The case of Ti/IrO₂ anode. *J Hazard Mater* 167(1–3):268–274
- Ciríaco L, Anjo C, Correia J, Pacheco MJ, Lopes A (2009) Electrochemical degradation of ibuprofen on Ti/Pt/PbO₂ and Si/BDD electrodes. *Electrochim Acta* 54(5):1464–1472
- Cruz-González K, Torres-López O, García-León A, Guzmán-Mar JL, Reyes LH, Hernández-Ramírez A, Peralta-Hernández JM (2010) Determination of optimum operating parameters for Acid Yellow 36 decolorization by electro-Fenton process using BDD cathode. *Chem Eng J* 160(1):199–206
- Cruz-González K, Torres-López O, García-León A, Brillas E, Hernández-Ramírez A, Peralta-Hernández JM (2012) Optimization of electro-Fenton/BDD process for decolorization of a model azo dye wastewater by means of response surface methodology. *Desalination* 286: 63–68
- Deeb AA, Fayyad MK, Alawi MA (2012) Separation of polyphenols from Jordanian olive oil mill wastewater. *Cromatogr Res Int Article ID* 812127, 8 pp
- Di Gioia D, Bertin L, Fava F, Marchetti L (2001) Biodegradation of hydroxylated and methoxylated benzoic, phenylacetic and phenylpropionic acids present in olive mill wastewaters by two bacterial strains. *Res Microbiol* 152(1):83–93
- Dirany A, Sirés I, Oturan N, Özcan A, Oturan MA (2012) Electrochemical treatment of the antibiotic sulfachloropyridazine: kinetics, reaction pathways, and toxicity evolution. *Environ Sci Technol* 46(7):4074–4082
- Ei-Ghenymy A, Rodríguez RM, Brillas E, Oturan N, Oturan MA (2014) Electro-Fenton degradation of the antibiotic sulfanilamide with Pt/carbon-felt and BDD/carbon-felt cells. Kinetics, reaction intermediates, and toxicity assessment. *Environ Sci Pollut Res* 21(14):8368–8378
- Florenza X, Solano AMS, Centellas F, Martínez-Huitle CA, Brillas E, Garcia-Segura S (2014) Degradation of the azo dye Acid Red 1 by anodic oxidation and indirect electrochemical processes based on Fenton's reaction chemistry. Relationship between decolorization, mineralization and products. *Electrochim Acta* 142:276–288
- Guinea E, Brillas E, Centellas F, Cañizares P, Rodrigo MA, Saez C (2009) Oxidation of enrofloxacin with conductive-diamond electrochemical oxidation, ozonation and Fenton oxidation. A comparison. *Water Res* 43(8):2131–2138
- Hakkim FL, Miura M, Matsuda N, Alharassi AS, Guillemin G, Yamauchi M, Arivazhagan G, Song H (2014) An in vitro evidence for caffeic acid, rosmarinic acid and *trans*-cinnamic acid as a skin protectant against γ -radiation. *Int J Low Rad* 9(4):305–316
- Hojati M, Modarres-Sanavy SAM, Enferadi ST, Majidi M, Ghanati F, Farzadfar S (2015) Differential deployment of parthenolide and phenylpropanoids in feverfew plants subjected to divalent heavy metals and *trans*-cinnamic acid. *Plant Soil*. doi:10.1007/s11104-015-2677-0
- Khataee A, Khataee A, Fathinia M, Vahid B, Joo SW (2013) Kinetic modeling of photoassisted-electrochemical process for degradation

- of an azo dye using boron-doped diamond anode and cathode with carbon nanotubes. *J Ind Eng Chem* 19(6):1890–1894
- Khataee A, Akbarpour A, Vahi B (2014) Photoassisted electrochemical degradation of an azo dye using Ti/RuO₂ anode and carbon nanotubes containing gas-diffusion cathode. *J Taiwan Inst Chem Eng* 45(3):930–936
- Kontos SS, Koutsoukos PG, Paraskeva CA (2014) Removal and recovery of phenolic compounds from olive mill wastewater by cooling crystallization. *Chem Eng J* 251:319–328
- Lafont F, Garcia IM, Aramendia MA, Marinas JM, Urbano FJ, Fernandez JM, Marti V (2001) Automated on-line solid-phase extraction and HPLC-mass spectrometry for rapid determination of phenolic compounds found in olive mill wastewaters. *Adv Mass Spectrom* 15: 875–876
- Letizia CS, Cocchiara J, Lapezynski A, Lalko J, Api AM (2005) Fragrance material review on cinnamic acid. *Food Chem Toxicol* 43(6):925–943
- Lopes RJG, Quinta-Ferreira RM (2010) Assessment of CFD-VOF method for trickle-bed reactor modeling in the catalytic wet oxidation of phenolic wastewater. *Ind Eng Chem Res* 49(6):2638–2648
- Lopes RJG, Silva AMT, Quinta-Ferreira RM (2007) Screening of catalysts and effect of temperature for kinetic degradation studies of aromatic compounds during wet oxidation. *Appl Catal B Environ* 73(1–2):193–202
- Marselli B, Garcia-Gomez J, Michaud PA, Rodrigo MA, Cominellis C (2003) Electrogeneration of hydroxyl radicals on boron-doped diamond electrodes. *J Electrochem Soc* 150(3):D79–D83
- Martínez-Huitle CA, Ferro S (2006) Electrochemical oxidation of organic pollutants for the wastewater treatment: direct and indirect processes. *Chem Soc Rev* 35(12):1324–1340
- Moreira FC, Garcia-Segura S, Vilar VJP, Boaventura RAR, Brillas E (2013) Decolorization and mineralization of Sunset Yellow FCF azo dye by anodic oxidation, electro-Fenton, UVA photoelectro-Fenton and solar photoelectro-Fenton processes. *Appl Catal B Environ* 142–143:877–890
- Panizza M, Cerisola G (2009) Direct and mediated anodic oxidation of organic pollutants. *Chem Rev* 109(12):6541–6569
- Rodrigo MA, Cañizares P, Sánchez-Carretero A, Sáez C (2010) Use of conductive-diamond electrochemical oxidation for wastewater treatment. *Catal Today* 151(1–2):173–177
- Ruiz EJ, Hernández-Ramírez A, Peralta-Hernández JM, Arias C, Brillas E (2011) Application of solar photoelectro-Fenton technology to azo dyes mineralization: effect of current density, Fe²⁺ and dye concentrations. *Chem Eng J* 171(2):385–392
- Sanchez I, Stüber F, Fabregat A, Font J, Fortuny A, Bengoa C (2012) Degradation of model olive mill contaminants of OMW catalysed by zero-valent iron enhanced with a chelant. *J Hazard Mater* 199–200:328–335
- Sirés I, Brillas E (2012) Remediation of water pollution caused by pharmaceutical residues based on electrochemical separation and degradation technologies: a review. *Environ Int* 40:212–229
- Sirés I, Brillas E, Oturan MA, Rodrigo MA, Panizza M (2014) Electrochemical advanced oxidation processes: today and tomorrow. A review. *Environ Sci Pollut Res* 21(14):8336–8367
- Thiam A, Zhou M, Brillas E, Sirés I (2014) Two-step mineralization of Tartrazine solutions: study of parameters and by-products during the coupling of electrocoagulation with electrochemical advanced oxidation processes. *Appl Catal B Environ* 150–151:116–125
- Thiam A, Sirés I, Centellas F, Cabot PL, Brillas E (2015a) Decolorization and mineralization of Allura Red AC azo dye by solar photoelectro-Fenton: identification of intermediates. *Chemosphere* 136:1–8
- Thiam A, Sirés I, Garrido JA, Rodríguez RM, Brillas E (2015b) Decolorization and mineralization of Allura Red AC aqueous solutions by electrochemical advanced oxidation processes. *J Hazard Mater* 290:34–42
- Vasudevan S, Oturan MA (2014) Electrochemistry: as cause and cure in water pollution-an overview. *Environ Chem Lett* 12(1):97–108
- Vatanpour V, Daneshvar N, Rasoulifard MH (2009) Electro-Fenton degradation of synthetic dye mixture: influence of intermediates. *J Environ Eng Manag* 19(5):277–282
- Wang A, Qu J, Liu H, Ru R (2008) Mineralization of an azo dye Acid Red 14 by photoelectro-Fenton process using an activated carbon fiber cathode. *Appl Catal B Environ* 84(3–4):393–399
- Yahya MS, Oturan N, El Kacemi K, El Karbane M, Aravindakumar CT, Oturan MA (2014) Oxidative degradation study on antimicrobial agent ciprofloxacin by electro-Fenton process: kinetics and oxidation products. *Chemosphere* 117:447–454
- Zeni ALB, de Albuquerque CAC, Goncalves F, Latini A, Tasca CI, Podesta R, Pagliosa CM, Duarte FS, de Lima TCM, Maraschin M (2013) Phytochemical profile, toxicity and antioxidant activity of *Aloysia gratissima* (Verbenaceae). *Quim Nov* 36(1):69–73

6. MINERALIZACIÓN DEL ÁCIDO *TRANS*-FERÚLICO



Publicación 2:

Degradation of *trans*-ferulic acid in acidic aqueous medium by anodic oxidation, electro-Fenton and photoelectro-Fenton

El ácido *trans*-ferúlico es un componente de las aguas residuales de la producción de aceite de oliva. Este trabajo presenta la degradación de este contaminante en 100 mL de disoluciones acuosas utilizando la oxidación anódica con H₂O₂ electrogenerado (OA-H₂O₂), el electro-Fenton (EF) y el fotoelectro-Fenton (FEF). Las electrólisis se llevaron a cabo a 35 °C usando un reactor de tanque agitado equipado con un ánodo de diamante dopado con boro (BDD) de 3 cm² y un cátodo de difusión de aire de carbón-PTFE de 3 cm². Se prepararon disoluciones de ácido *trans*-ferúlico en Na₂SO₄ 0,050 M a pH 3 que se electrolizaron a *j* constante durante 360 min hasta alcanzar una mineralización casi total. En los experimentos EF y PEF, se añadió Fe²⁺ 0,50 mM como catalizador de la reacción de Fenton, mientras que en PEF, además, la disolución se irradió con una lámpara UVA de 6 W.

Para determinar la cinética de degradación del ácido *trans*-ferúlico, se trataron disoluciones que contenían 0,167, 0,417, 0,834 y 1,668 mM de ácido a valores de *j* de 16.7, 33.3, 66.7 y 100 mA cm⁻² (ver Tabla 1). La concentración del ácido *trans*-ferúlico se redujo muy lentamente durante la OA-H₂O₂, eliminándose un 95% después de 360 min. En cambio, el ácido desapareció completamente a los 15 min en EF y a los 10 min en FEF (Figura 1), gracias a la potente acción de los radicales •OH en el medio, pero con poca participación de la luz UVA durante el FEF. Las cinéticas de eliminación se ajustaron a una ecuación de pseudo-primer orden, sugiriendo una producción estacionaria de los radicales oxidantes •OH y BDD(•OH). Se obtuvieron valores muy similares de *k*₁ en EF y FEF, de 0,32 y 0,34 min⁻¹ respectivamente, siendo muy superiores a 7,2x10⁻³ min⁻¹ determinada en OA-H₂O₂ cuando se trató una disolución con 0,834 mM del ácido a 33,3 mA cm⁻². Al aumentar la concentración del ácido desde 0,167 a 0,417 mM aplicando 33,3 mA cm⁻², se requirió menor tiempo para reducir su concentración y los valores de *k*₁ aumentaron, lo que indica que la cinética de la degradación del ácido *trans*-ferúlico no obedece realmente una cinética de pseudo-primer orden. Los radicales •OH y BDD(•OH), que se forman con la misma concentración en todos los medios ya que se aplica la misma *j*, eliminan una menor proporción de ácido al aumentar la materia orgánica en el medio.

Después de estudiar la velocidad de degradación del ácido *trans*-ferúlico, se pasó a evaluar la mineralización de la muestra por medio de OA-H₂O₂, EF, FEF y FEFS siguiendo la reducción del TOC con el tiempo de electrólisis. Se encontró que el poder oxidante de los métodos aumentaba en el orden: OA-H₂O₂ < EF < FEF < FEFS, a *j* constante. Al tratar una disolución con 0,834 mM de ácido *trans*-ferúlico a 33,3 mA cm⁻², se consiguió una reducción del TOC del 98% mediante FEF, 80% en EF y 72% en OA-H₂O₂ después de 360 min, lo cual se justifica por la fotólisis de los intermedios como el Fe(III)-carboxilato y la generación de una cantidad adicional de radicales por la reacción (22).

A continuación, se analizó el efecto de la densidad de corriente sobre la mineralización del ácido *trans*-ferúlico, que se muestra en la Figura 3. Para ello, se trató una disolución 0,834 mM del ácido aplicando desde 16.7 hasta 100 mA cm⁻² durante 360 min. Se encontró que el descenso del TOC se aceleraba al ir aumentando *j*. En OA-H₂O₂ este comportamiento puede asociarse a la producción de una mayor concentración de radicales BDD(•OH) y al incremento de H₂O₂ en el cátodo. Esto último beneficia al proceso EF porque provoca la generación de

más radicales $\cdot\text{OH}$ producidos por la reacción de Fenton (12). Sin embargo, el proceso FEF fue más rápido durante los primeros 180 min en los que el TOC disminuyó en más del 95% a todas las j aplicadas. Esto pone de manifiesto una acción fotolítica positiva de la luz UVA para destruir los productos fotosensibles originados. El incremento de j daba lugar a menores valores de la MCE, debido a la destrucción del exceso de radicales hidroxilo por reacciones parásitas como las (51)-(53).

En la Figura 4 se puede apreciar la influencia de la concentración ácido *trans*-ferúlico sobre su mineralización, utilizando disoluciones del ácido desde 0,167 a 1,668 mM electrolizadas a 33,3 mA cm⁻². Analizando los resultados, se observó que a mayor concentración se producía una mayor destrucción del TOC y por tanto, conllevaba una MCE mayor. En disoluciones con 1,668 mM se consiguieron unas reducciones máximas del TOC del 74%, 80% y 98% mediante OA-H₂O₂, EF y FEF, respectivamente, con sus valores de MCE máximos asociados. Como se ve, el proceso FEF era el más potente entre todos. En estos procesos, al aplicar la misma j y aumentar el contenido de materia orgánica, se favorece la acción oxidante de los radicales BDD($\cdot\text{OH}$) y $\cdot\text{OH}$, ralentizando las reacciones parásitas no deseadas.

Los experimentos con FEFS, cuyos resultados pueden verse en la Figura 5, pusieron de manifiesto una rápida destrucción del ácido *trans*-ferúlico, siendo aún más rápida que en FEF con lámpara UVA bajo condiciones similares, debido a la mayor intensidad de los rayos UV proporcionados por la luz solar. Al aplicar una j de 33,3 mA cm⁻² a una disolución con 0,834 mM del ácido su TOC decreció un 93% en 120 min, y sólo tardó 60 min cuando j aumentó a 100 mA cm⁻². Esto es debido a la mayor producción de $\cdot\text{OH}$ en el medio, combinado con la fotólisis de los intermedios formados durante la electrólisis. En el proceso FEFS, cuando la concentración del ácido se redujo a la mitad (0,417 mM) aplicando la misma j , el TOC disminuyó en un 84%. La mejor eficiencia de corriente de mineralización, del 44%, se obtuvo para una disolución con 0,834 mM a los 120 min aplicando 33,3 mA cm⁻², con una reducción de TOC del 93%.

La identificación de productos intermedios durante la mineralización ácido *trans*-ferúlico se realizó por GC-MS a los 30 y 90 min de electrólisis de una disolución con 0,834 mM a 33,3 mA cm⁻². Se detectaron el 2-metoxi-4-vinilfenol, el 4-etil-2-metoxifenol, la 1-(2,4-dihidroxifenil) etanona y la vainillina. El 2-metoxi-4-vinilfenol se formó mediante la descarboxilación del ácido, mientras que el 4-etil-2-metoxifenol y la vainillina se produjeron por su posterior oxidación. Además, mediante la ruptura del anillo bencénico de los compuestos aromáticos, se formaron varios ácidos carboxílicos de cadena corta, que se detectaron mediante HPLC de exclusión iónica, tales como el fumárico, el acético y el oxálico, que se oxidó a CO₂ lentamente. Estos ácidos forman complejos con el Fe(III), los cuales son difíciles de destruir por los radicales BDD($\cdot\text{OH}$) y $\cdot\text{OH}$, y son fotodecarboxilados por la radiación UVA en los procesos FEF y FEFS.

Los resultados anteriores permiten concluir que el tratamiento FEF de disoluciones del ácido *trans*-ferúlico a pH 3,0 es capaz de dar lugar a una mineralización casi total con una reducción del TOC del 98% para contenidos de ácido > 0,843 mM y $j \geq 16,7$ mA cm⁻², siendo mucho más potente que el EF y la OA-H₂O₂. La capacidad de oxidación del método OA-H₂O₂ fue similar a la del EF, a concentraciones > 0,843 mM y $j \geq 33,3$ mA cm⁻².



Degradation of *trans*-ferulic acid in acidic aqueous medium by anodic oxidation, electro-Fenton and photoelectro-Fenton



Nelly Flores, Ignasi Sirés, José Antonio Garrido, Francesc Centellas, Rosa María Rodríguez, Pere Lluís Cabot, Enric Brillas*

Laboratori d'Electroquímica dels Materials i del Medi Ambient, Departament de Química Física, Facultat de Química, Universitat de Barcelona, Martí i Franquès 1-11, 08028 Barcelona, Spain

HIGHLIGHTS

- *trans*-Ferulic acid degradation by EAOPs using a stirred BDD/air-diffusion cell.
- Slow substrate abatement and poor mineralization by AO-H₂O₂.
- 98% Mineralization by PEF, but with rapid and similar substrate decay than by EF.
- Quicker degradation by SPEF due to the more potent photolytic action of sunlight.
- Reaction pathway with four primary aromatic products and three final carboxylic acids.

ARTICLE INFO

Article history:

Received 11 October 2015

Received in revised form

19 November 2015

Accepted 20 November 2015

Available online 2 December 2015

Keywords:

Anodic oxidation

Electro-Fenton

Oxidation products

Photoelectro-Fenton

trans-Ferulic acid

ABSTRACT

Solutions of pH 3.0 containing *trans*-ferulic acid, a phenolic compound in olive oil mill wastewater, have been comparatively degraded by anodic oxidation with electrogenerated H₂O₂ (AO-H₂O₂), electro-Fenton (EF) and photoelectro-Fenton (PEF). Trials were performed with a BDD/air-diffusion cell, where oxidizing •OH was produced from water discharge at the BDD anode and/or in the solution bulk from Fenton's reaction between cathodically generated H₂O₂ and added catalytic Fe²⁺. The substrate was very slowly removed by AO-H₂O₂, whereas it was very rapidly abated by EF and PEF, at similar rate in both cases, due to its fast reaction with •OH in the bulk. The AO-H₂O₂ process yielded a slightly lower mineralization than EF, which promoted the accumulation of barely oxidizable products like Fe(III) complexes. In contrast, the fast photolysis of these latter species under irradiation with UVA light in PEF led to an almost total mineralization with 98% total organic carbon decay. The effect of current density and substrate concentration on the performance of all treatments was examined. Several solar PEF (SPEF) trials showed its viability for the treatment of wastewater containing *trans*-ferulic acid at larger scale. Four primary aromatic products were identified by GC-MS analysis of electrolyzed solutions, and final carboxylic acids like fumaric, acetic and oxalic were detected by ion-exclusion HPLC. A reaction sequence for *trans*-ferulic acid mineralization involving all the detected products is finally proposed.

© 2015 Elsevier B.V. All rights reserved.

1. Introduction

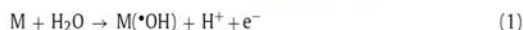
The olive oil industry in Mediterranean countries like Spain, Italy, Greece and Portugal supplies about 77% of the worldwide output of this product. During the extraction of the olive oil, however, a volume of industrial effluents as large as 30 million cubic meters is produced annually in the world. Olive oil mill wastewater (OOMWW) has acidic pH near 5, high chemical and biochemical

oxygen demand up to 110 g L⁻¹ and 170 g L⁻¹, respectively, and total solids contents up to 150 g L⁻¹ [1], which is very harmful for the environment by the negative effects over soil microbial population [2] and aquatic ecosystems [3]. Phenols, lipids, sugars and tannins are the main organic components of OOMWW, representing up to 37% of the total mass [4,5]. One of the most important phenolic compounds is *trans*-ferulic acid (4-hydroxy-3-methoxycinnamic acid), much more abundant than its *cis* isomer. *trans*-Ferulic acid is also present in the plant cell wall of various fruits and vegetables, possesses a high antioxidant activity and low toxicity after oral administration (LD₅₀ = 3200 mg kg⁻¹) and has been detected in rivers, lakes and sea sediments [6]. At indus-

* Corresponding author. Fax: +34 934021231.
E-mail address: brillas@ub.edu (E. Brillas).

trial level, it is used as ingredient in many drug formulations and food additives, being its derivative vanillin of huge commercial importance in the food industry [7]. So far, little information about the degradation of *trans*-ferulic acid for wastewater treatment is available. Several authors have described its oxidation by pyrilium salt photosensitized with sunlight [8] and advanced oxidation processes (AOPs) such as catalytic wet oxidation [9], heterogeneous Fenton [10] and TiO₂ photocatalysis [11], but the use of powerful electrochemical AOPs (EAOPs) for treating water polluted with *trans*-ferulic acid has not yet been reported.

Over the last two decades, EAOPs have received growing attention for the remediation of wastewater contaminated with biorecalcitrant organics [12–16]. The common feature of these methods is the in situ generation of reactive oxygen species (ROS) such as hydroxyl radical ($\bullet\text{OH}$), which can attack most organics up to their mineralization (conversion into CO₂ and inorganic ions) due to its high standard reduction potential ($E^\circ = 2.80\text{ V/SHE}$). The most popular EAOP is anodic oxidation (AO), also so-called electrochemical oxidation. In AO, a high current density (j) is usually applied to the anode M of the cell to produce oxidizing physisorbed hydroxyl radical M($\bullet\text{OH}$) as intermediate of water discharge to O₂ at the anode surface by Reaction (1) [12,17–19]:

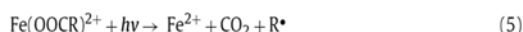
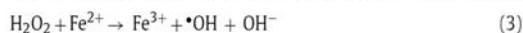


When considering the abatement of aromatic organics and even carboxylic acids, the physisorbed BDD($\bullet\text{OH}$) generated at boron-doped diamond (BDD) anode has higher oxidation ability than M($\bullet\text{OH}$) produced by other common anodes [20–23]. This is due to the larger O₂-overpotential of BDD and the low interaction between its surface and $\bullet\text{OH}$, which favors its reaction with organics [12]. At present, the BDD electrode is the preferred anode for AO.

When an undivided cell is used with a carbonaceous cathode able to electrogenerate H₂O₂, the process is called AO-H₂O₂, where organics are preferentially destroyed by physisorbed M($\bullet\text{OH}$) along with a minor participation of other ROS such as H₂O₂ and its anodic oxidation product HO₂ \bullet [13,14]. It is well-known that H₂O₂ can be efficiently formed from the two-electron reduction of O₂ gas via reaction (2) at cathodes such as activated carbon fiber [24], carbon nanotubes [25,26], graphite felt [27], carbon modified with metals or metal oxides nanoparticles [28], carbon felt [29–31], carbon-polytetrafluoroethylene (PTFE) O₂ or air-diffusion [32–34], and BDD [35,36].



Another widely used EAOP is the electro-Fenton (EF) process, where a catalytic amount of Fe²⁺ is added to the solution to enhance the oxidation power of H₂O₂ via Fenton's Reaction (3) with production of Fe³⁺ and $\bullet\text{OH}$ in the bulk [29–34]. The optimum pH for EF is ~3 and organic pollutants are then destroyed by both kinds of ROS, M($\bullet\text{OH}$) and $\bullet\text{OH}$. In our laboratory, we have been developing other EAOPs like UVA photoelectro-Fenton (PEF) or solar PEF (SPEF) in which the treated solution is irradiated with either artificial UVA light or sunlight, respectively [37–40]. This radiation causes the photoreduction of Fe(OH)²⁺ species to Fe²⁺ with $\bullet\text{OH}$ generation via Reaction (4), as well as the photodecarboxylation of complexes of Fe(III) with generated carboxylic acids according to Reaction (5).



This paper presents a comparative study on the degradation of *trans*-ferulic acid solutions at pH 3.0 by AO-H₂O₂, EF and PEF using a stirred BDD/air-diffusion tank reactor. The mineralization process was also assessed by SPEF in order to check its potentiality at industrial scale. The effect of j and substrate concentration

on the performance of the EAOPs tested was examined to understand the role of the generated hydroxyl radicals and the action of UV light. The decay of *trans*-ferulic acid and the evolution of some products like vanillin and carboxylic acids were monitored by high-performance liquid chromatography (HPLC). Primary aromatic intermediates were identified by gas chromatography–mass spectrometry (GC–MS). Based on the results obtained, a plausible route for *trans*-ferulic acid mineralization by EAOPs is proposed.

2. Experimental

2.1. Chemicals

trans-Ferulic acid (99% purity) and vanillin (99% purity) were supplied by Sigma-Aldrich and used without further purification. Fumaric, acetic and oxalic acids were of analytical grade supplied by Merck. Heptahydrated Fe(II) sulfate and anhydrous sodium sulfate were of analytical grade supplied by Fluka. Analytical grade sulfuric acid purchased from Merck was used to adjust the initial solution pH to 3.0. All the solutions were prepared with high-purity water from a Millipore Milli-Q system (resistivity >18 M Ω cm at 25 °C). Other chemicals used for analysis were of HPLC or analytical grade provided by Avocado, Fluka and Merck.

2.2. Electrolytic systems

All the experiments were performed with an open, undivided, two-electrode cylindrical glass cell of 150 mL capacity. It was equipped with a double jacket for recirculating water at 35 °C by means of a Thermo Electron Corporation HAAKE DC 10 thermostat. This working temperature was chosen because it is the maximum value that can be used without significant water evaporation from the solution. All the assays were made under vigorous stirring with a magnetic bar at 700 rpm to ensure the transport of reactants toward/from the electrodes and homogenization. The electrodes were a BDD (deposited onto *p*-Si) anode purchased from NeoCoat (La-Chaux-de-Fonds, Switzerland) and a carbon-PTFE air-diffusion cathode purchased from E-TEK (Somerset, NJ, USA), both of 3 cm² geometric area and separated about 1 cm. The cathode was mounted as reported elsewhere [41] and was fed with air pumped at 300 mL min⁻¹ for H₂O₂ generation from Reaction (2). The trials were carried out at constant j provided by an EG&G Princeton Applied Research 273A potentiostat-galvanostat.

Solutions of 100 mL containing *trans*-ferulic acid and 0.05 M Na₂SO₄ as background electrolyte at pH 3.0 were comparatively treated by AO-H₂O₂, EF and PEF. In the two latter EAOPs, 0.50 mM Fe²⁺ was added as catalyst since this content has been found optimal for many organics degraded under similar conditions [37–40]. For PEF, a Philips TL/6W/08 fluorescent black light blue tube of $\lambda_{\text{max}} = 360\text{ nm}$ with average power density of 5 W m⁻², determined with a Kipp & Zonen CUV 5 UV radiometer, was placed at 8 cm above the solution surface. Some experiments were also performed by SPEF upon direct exposition of the cell to sunlight irradiation in clear and sunny days of the summer 2015 in our laboratory of Barcelona (latitude: 41°23'N, longitude: 2°9'E). The average UV solar irradiation intensity from 300 to 400 nm was about 30 W m⁻², as measured on the radiometer. Before starting the experiments, the surfaces of the anode and cathode were cleaned and activated, respectively, under polarization in 100 mL of a 0.05 M Na₂SO₄ solution at 100 mA cm⁻² for 180 min.

2.3. Apparatus and analytical methods

The solution pH was measured on a Crison GLP 22 pH-meter. For total organic carbon (TOC) measurements, samples were withdrawn from treated solutions, filtered with 0.45 μm PTFE filters

purchased from Whatman and directly injected into a Shimadzu VCSN TOC analyzer, obtaining reproducible values with $\pm 1\%$ accuracy. From these data and considering that the total mineralization of *trans*-ferulic acid involves its conversion into CO_2 as follows:



the mineralization current efficiency (MCE) for each assay was estimated from Eq. (7) [37]:

$$\text{MCE}(\%) = \frac{nFV\Delta(\text{TOC})_{\text{exp}}}{4.32 \times 10^7 mIt} \times 100 \quad (7)$$

where n is the number of electrons related to the mineralization process (42 e^- according to Reaction (6)), F is the Faraday constant (96487 C mol^{-1}), V is the solution volume (L), $\Delta(\text{TOC})_{\text{exp}}$ is the experimental TOC abatement (mg C L^{-1}), 4.32×10^7 is a conversion factor ($3600 \text{ s h}^{-1} \times 12,000 \text{ mg C mol}^{-1}$), m is the number of carbon atoms of *trans*-ferulic acid (10 C atoms), I is the current (A) and t is the electrolysis time (h).

Treated solutions were analyzed by reversed-phase HPLC using a Waters 600 LC equipped with a BDS Hypersil C18 $6 \mu\text{m}$, $250 \text{ mm} \times 4.6 \text{ mm}$, column at 35°C and coupled to a Waters 996 photodiode array detector. In the EF and PEF assays, the aqueous samples were diluted with acetonitrile to stop the degradation process and then filtered with $0.45 \mu\text{m}$ PTFE filters from Whatman. In all the measurements, $10 \mu\text{L}$ aliquots were injected into the LC and a 80% (v/v) acetonitrile/water mixture was eluted at 0.8 mL min^{-1} as mobile phase. The chromatograms exhibited two well-defined peaks at retention time (t_r) of 3.37 min for *trans*-ferulic acid and $t_r = 3.89 \text{ min}$ for vanillin, monitored at λ of 323 and 229 nm , respectively. Generated carboxylic acids were detected by ion-exclusion HPLC using the above LC fitted with a Bio-Rad Aminex HPX 87H, $300 \text{ mm} \times 7.8 \text{ mm}$, column at 35°C and the photodiode array detector selected at $\lambda = 210 \text{ nm}$. Aliquots of $10 \mu\text{L}$ were also injected into the LC and the mobile phase was $4 \text{ mM H}_2\text{SO}_4$ at 0.6 mL min^{-1} . The chromatograms displayed peaks related to oxalic ($t_r = 6.9 \text{ min}$), acetic ($t_r = 14.9 \text{ min}$) and fumaric ($t_r = 15.6 \text{ min}$) acids.

The primary aromatic products of *trans*-ferulic acid were identified by electrolyzing 100 mL of a 0.834 mM substrate solution at 33.3 mA cm^{-2} by $\text{AO-H}_2\text{O}_2$. Independent electrolyses were run up to 30 and 90 min and the organic components of the remaining solutions were extracted out with CH_2Cl_2 ($3 \times 25 \text{ mL}$). Each organic fraction was dried over anhydrous Na_2SO_4 , filtered and its volume reduced to about 1 mL to be further analyzed by GC-MS using a NIST05-MS library to interpret the mass spectra. GC-MS analysis was performed by coupling a 6890N GC and a 5975C MS from Agilent Technologies, operating in EI mode at 70 eV . The GC was fitted with either a non-polar Agilent J&W HP-5ms or a polar HP INNOWax column, both of $0.25 \mu\text{m}$, $30 \text{ m} \times 0.25 \text{ mm}$. The temperature ramp was: 36°C for 1 min , 5°C min^{-1} up to 300°C or 250°C for the non-polar or polar column, respectively, and hold time 10 min . The temperature of the inlet, source and transfer line was 250 , 230 and 280°C for the non-polar column and 250 , 230 and 250°C for the polar one.

3. Results and discussion

3.1. Decay of *trans*-ferulic acid by $\text{AO-H}_2\text{O}_2$, EF and PEF

A first series of trials was made by treating 100 mL of 0.834 mM *trans*-ferulic acid solutions in $0.05 \text{ M Na}_2\text{SO}_4$ at $\text{pH } 3.0$ by the different EAOPs to determine the decay kinetics of the substrate by reversed-phase HPLC. As a preliminary study, it was found that the substrate concentration of such solutions remained unchanged under a 6 W UVA irradiation in the absence of applied current, as expected if this compound is not directly photolyzed by UVA radiation (data not shown). For the experiments using $\text{AO-H}_2\text{O}_2$ without

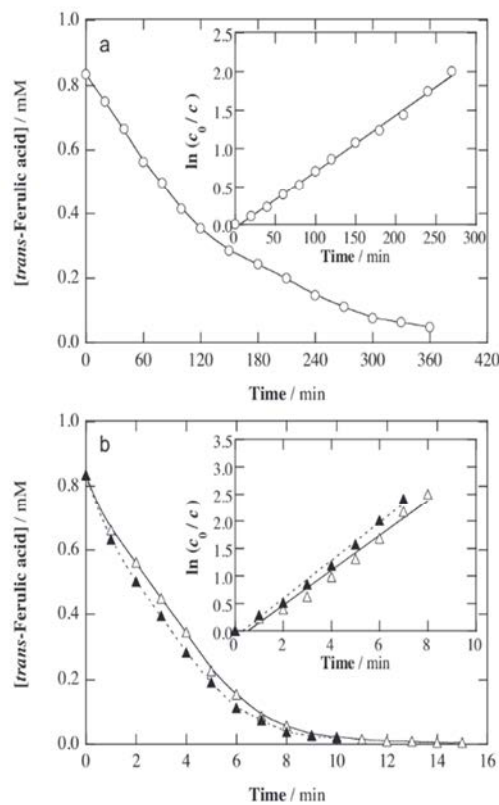


Fig. 1. Variation of *trans*-ferulic acid concentration with electrolysis time for the degradation of 100 mL of a 0.834 mM substrate solution in $0.05 \text{ M Na}_2\text{SO}_4$ at $\text{pH } 3.0$ and 35°C using a BDD/air-diffusion cell of 3 cm^2 electrode area by applying 33.3 mA cm^{-2} . In (a), anodic oxidation with electrogenerated H_2O_2 ($\text{AO-H}_2\text{O}_2$). In (b), (Δ) electro-Fenton (EF) with addition of 0.50 mM Fe^{2+} and (\blacktriangle) photoelectro-Fenton (PEF) with addition of 0.50 mM Fe^{2+} using a 6 W UVA light. The inset panels depict the pseudo-first-order kinetics found for the *trans*-ferulic acid content abatement.

catalyst, as well as for EF and PEF with 0.50 mM Fe^{2+} , the solution pH dropped slightly from 3.0 to a final value near 2.7 – 2.8 after 360 min electrolysis, probably due to the generation of acidic products like final carboxylic acids [37–40].

Fig. 1a depicts a very slow decay of *trans*-ferulic acid by $\text{AO-H}_2\text{O}_2$, attaining 95% removal in 360 min . This means that this compound reacts very slowly with generated ROS, preferentially with BDD($\bullet\text{OH}$) originated from Reaction (1). In contrast, Fig. 1b highlights a much faster abatement of *trans*-ferulic acid by EF and PEF, disappearing in about 15 and 10 min , respectively. The large acceleration can be ascribed to its very fast reaction in the bulk with $\bullet\text{OH}$ formed from Fenton's Reaction (3) compared with the confined reaction taking place with BDD($\bullet\text{OH}$) near the anode. The slight increase in decay rate for PEF compared to EF suggests a very small participation of the photolytic Reaction (4) to induce the production of higher amounts of $\bullet\text{OH}$ in the bulk.

The inset panels of Fig. 1a and b show the good linear fittings obtained for a pseudo-first-order kinetic analysis of the above concentration decays. This behavior suggests the generation of a steady concentration of BDD($\bullet\text{OH}$) and/or $\bullet\text{OH}$ during all treatments. Table 1 collects the apparent rate constants (k_1) and their excellent square regression coefficients (R^2) found for these assays. As can be seen, the k_1 value is quite similar in EF and PEF and approximately 3 orders of magnitude higher than that in $\text{AO-H}_2\text{O}_2$,

Table 1

Pseudo-first-order rate constant for *trans*-ferulic acid decay, along with its square regression coefficient, and percentage of TOC removed and mineralization current efficiency at 360 min determined for the degradation of 100 mL of solutions of this compound in 0.05 M Na₂SO₄ at pH 3.0 and 35 °C by electrochemical advanced oxidation methods using a stirred BDD/air-diffusion cell under different experimental conditions.

Method	[<i>trans</i> -Ferulic acid] (mM)	Current density (mA cm ⁻²)	<i>k</i> ₁ (min ⁻¹)	R ²	% TOC removed at 360 min	% MCE at 360 min
AO-H ₂ O ₂	0.167	33.3	(0.82 ± 0.03) × 10 ⁻²	0.993	74	2.3
	0.417	33.3	(0.74 ± 0.03) × 10 ⁻²	0.989	68	5.3
	0.834	16.7	(0.72 ± 0.01) × 10 ⁻²	0.997	62	19
	33.3	72			11	
	66.7	88			6.9	
	100	94			4.9	
EF ^a	1.668	33.3	0.87 ± 0.05	0.990	67	21
	0.167	33.3			75	2.4
	0.417	33.3			77	6.0
	0.834	16.7			74	23
	33.3	80			13	
	66.7	87			6.7	
PEF ^b	1.668	100	0.32 ± 0.02	0.990	92	4.8
	0.167	33.3			74	23
	0.417	33.3			92	2.9
	0.834	16.7			94	7.3
	33.3	98			31	
	66.7	98			15	
PEF ^b	1.668	100	0.88 ± 0.06	0.988	98	7.7
	0.167	33.3			98	5.1
	0.417	33.3			98	7.7
	0.834	16.7			98	5.1
	33.3	98			7.7	
	66.7	98			5.1	
PEF ^b	1.668	33.3	0.69 ± 0.03	0.993	98	7.7
	0.167	33.3			98	5.1
	0.417	33.3			98	7.7
	0.834	16.7			98	5.1
	33.3	98			7.7	
	66.7	98			5.1	
PEF ^b	1.668	100	0.34 ± 0.02	0.991	98	7.7
	0.167	33.3			98	5.1
	0.417	33.3			98	7.7
	0.834	16.7			98	5.1
	33.3	98			7.7	
	66.7	98			5.1	

^a With addition of 0.50 mM Fe²⁺.

^b With addition of 0.50 mM Fe²⁺ and irradiation with a 6 W UVA light (λ_{max} = 360 nm).

confirming that in the two former EAOPs, *trans*-ferulic acid is slowly oxidized by BDD(•OH) and much more quickly by •OH in the bulk.

The kinetic study of the *trans*-ferulic acid decay was extended to lower concentrations of 0.167 and 0.417 mM operating at 33.3 mA cm⁻². Shorter time was needed for total removal of the substrate as the organic load decreased. For the PEF process, for example, the *trans*-ferulic acid disappeared at 10 min for 0.834 mM, but after only 7 min for 0.167 mM. According to this tendency, the good pseudo-first-order kinetics obtained for all the EAOPs showed an increasing *k*₁ value, as can be seen in Table 1. This behavior clearly indicates that the kinetic decay does not actually obey a true pseudo-first-order reaction, since the same *k*₁ value should be determined regardless of the substrate content. Since quite similar amounts of BDD(•OH) and/or •OH are generated in each EAOP at 33.3 mA cm⁻² when the organic matter content rises, a larger proportion of radicals is expected to react with the oxidation products formed and hence, a smaller quantity of them reacts with *trans*-ferulic acid, thus decelerating its abatement as experimentally found.

3.2. Mineralization of *trans*-ferulic acid solutions by AO-H₂O₂, EF and PEF

The mineralization of 0.834 mM *trans*-ferulic acid solutions at pH 3.0 was comparatively assessed for AO-H₂O₂, EF and PEF at *j* = 33.3 mA cm⁻² by monitoring their TOC abatement. Fig. 2a shows a small but continuous mineralization under AO-H₂O₂ conditions, only achieving 72% TOC removal after 360 min of electrolysis. A much quicker TOC decay can be observed for EF, where TOC was finally reduced by 80%. Note that the mineralization process was very fast up to 90 min of EF because of the efficient action of •OH, whereas it was progressively decelerated at longer time suggesting the formation of more recalcitrant products, like Fe(III)-carboxylate complexes, which are refractory to •OH and slowly attacked by BDD(•OH) [14]. In contrast, Fig. 2a evidences a very positive effect of UVA light in the PEF process since it is able to remove 95% TOC in 180 min, therefore attaining an almost total mineralization with 98% TOC reduction at 360 min. This large enhancement can be related to the photolysis of intermediates involving, for example, the photodecomposition of Fe(III)-carboxylate species via reaction

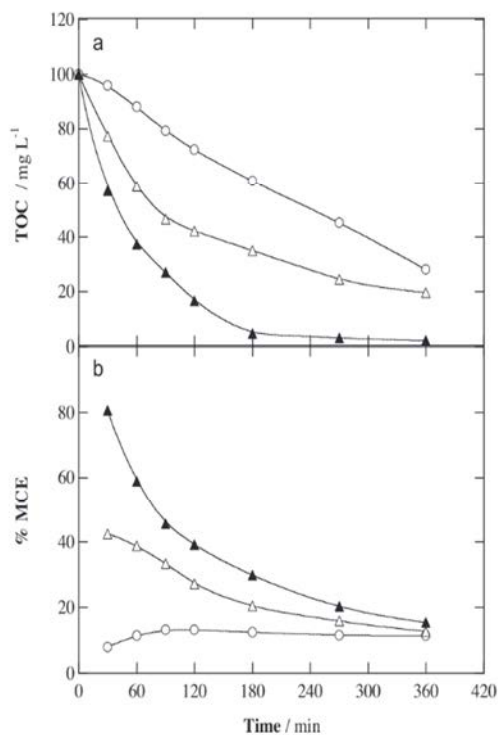


Fig. 2. Change of (a) TOC and (b) mineralization current efficiency with electrolysis time under the same conditions of Fig. 1. Method: (○) AO-H₂O₂, (△) EF and (▲) PEF.

(5) [14–16]. These results clearly indicate that the oxidation ability of the EAOPs grows in the sequence AO-H₂O₂ ≤ EF < PEF.

Fig. 2b depicts the MCE values calculated from Eq. (7) for the trends given in Fig. 2a. As expected, the current efficiency rose as more oxidizing EAOPs were tested, although this behavior was more apparent at short electrolysis time, because the mineralization rate was particularly influenced by the oxidation with •OH and

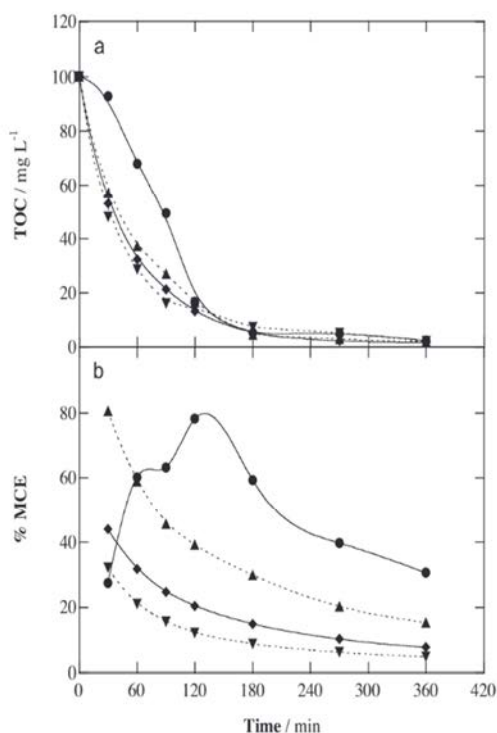


Fig. 3. Influence of current density on (a) TOC decay and (b) mineralization current efficiency vs. electrolysis time for the PEF treatment of 100 mL of a 0.834 mM *trans*-ferulic acid solution in 0.05 M Na₂SO₄ with 0.50 mM Fe²⁺ at pH 3.0 and 35 °C using a BDD/air-diffusion cell. Applied current density: (●) 16.7 mA cm⁻², (▲) 33.3 mA cm⁻², (◆) 66.7 mA cm⁻² and (▼) 100 mA cm⁻².

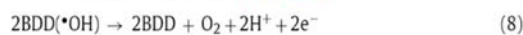
the photolytic action of UVA light. In EF and, especially, the powerful PEF, the MCE values decayed dramatically from 43% and 81% at the beginning of the treatments to 13% and 15% at 360 min, respectively. This fall of current efficiency can be associated not only with the generation of more recalcitrant oxidation products but also with the gradual disappearance of organic matter [12,39,40]. In contrast, the current efficiency acquired a practically constant value of 11–12% during the AO-H₂O₂ run, suggesting a steady mineralization rate of intermediates upon oxidation by BDD(•OH) alone.

Since *j* determines the amount of hydroxyl radicals produced in the EAOPs, the effect of this parameter between 16.7 and 100 mA cm⁻² on the mineralization of 0.834 mM *trans*-ferulic acid solutions was investigated. Table 1 collects the percentage of TOC removed after 360 min of all these treatments. For AO-H₂O₂ and EF, the mineralization degree underwent a progressive rise when *j* increased, as a result of the gradually greater production of oxidizing hydroxyl radicals. This means that the concomitant increase in rate of Reaction (1) yields higher quantities of BDD(•OH) in AO-H₂O₂ while the enhancement of Reaction (2) favors the larger accumulation of H₂O₂ that consequently accelerates the •OH formation from Fenton's Reaction (3) in EF. Note that EF was more powerful than AO-H₂O₂ only up to 33.3 mA cm⁻², with higher *j* values leading to a similar final TOC removal in both cases. This suggests the formation of final products in EF, probably complexes with Fe(III), that are difficultly destroyed by BDD(•OH) and/or •OH, whereas the final species formed in AO-H₂O₂ can be more easily removed by increasing amounts of BDD(•OH). In PEF, Fig. 3a highlights a short activation time at the beginning of the electrolysis at 16.7 mA cm⁻², followed by a quick TOC decay to reach 96% reduction at 180 min, whereby the mineralization was strongly inhibited

to be reduced by 98% at 360 min. However, a similar but faster TOC decay can be observed for greater *j* values, achieving up to 95–97% TOC reduction in 180 min. This is indicative of a very quick photolytic destruction of intermediates that are very slowly destroyed by BDD(•OH) and/or •OH. UVA irradiation is then so potent that, at 33.3 mA cm⁻², sufficient amounts of hydroxyl radicals are produced to yield products that can be completely photolyzed.

The current efficiency for each EAOP always decreased when *j* increased. This tendency can be easily deduced from the MCE values corresponding to the end of all trials, as listed in the last column of Table 1. Fig. 3b exemplifies the MCE-time plots obtained for the powerful PEF process, showing the concomitant drop of current efficiency for all *j* values. The anomalous behavior observed in this figure up to 60–90 min at 16.7 mA cm⁻² is due to the induction period required under such a low *j* value, probably because the poor production of hydroxyl radicals entails a slower appearance of intermediates that can be rapidly photolyzed by UVA light.

The decay in MCE at higher *j* is contrary to the quicker TOC removal found. This behavior is typical of EAOPs and can be ascribed to the destruction of the excess of generated hydroxyl radicals by non-oxidizing wasting reactions. They include the anodic oxidation of physisorbed BDD(•OH) radicals to O₂ by Reaction (8) and the destruction of •OH by H₂O₂ and Fe²⁺ from Reactions (9) and (10), respectively, along with the larger enhancement of the anodic formation of other weaker oxidants such as ozone by Reaction (11) and S₂O₈²⁻ ion from SO₄²⁻ ion by Reaction (12), thus inhibiting the H₂O discharge from Reaction (1) [12–16].



The influence of the substrate concentration in the range 0.167–1.668 mM on the mineralization of *trans*-ferulic solutions upon application of the EAOPs was examined at the best *j* of 33.3 mA cm⁻² found for PEF. A look at Table 1 reveals that TOC removals of 67–74% and slightly higher values of 74–80% were achieved in AO-H₂O₂ and EF, respectively. In fact, AO-H₂O₂ showed lower oxidation ability than EF up to 0.843 mM, whereas both methods had a similar mineralization power for higher substrate concentrations. Despite the similar mineralization attained in each of these EAOPs regardless of the *trans*-ferulic content, a careful inspection of Table 1 indicates a progressive increase of the corresponding final current efficiency when raising the initial substrate amount. For AO-H₂O₂, for example, the MCE grew from 2.3% at 0.164 mM to 21% at 1.668 mM. As mentioned above, similar quantities of hydroxyl radicals are expected to be generated in each EAOP at a given *j* and thus, one can infer that a larger organic matter content favors the reaction of BDD(•OH) and/or •OH with oxidation products, thereby decelerating their wasting Reactions (8)–(12). This also takes place for the PEF process, as can be deduced from the data of Table 1. Fig. 4a depicts the very high oxidation power of this method, which was even able to yield a 98% mineralization for the most concentrated 1.668 mM solution due to the additional quick photodecomposition of intermediates under UVA irradiation. The corresponding MCE-time plots of Fig. 4b highlight again the drop of the current efficiency at prolonged electrolysis because of the gradual generation of highly recalcitrant products and the loss of organic matter, as stated above. The MCE value increased with increasing substrate content as well, due to the larger oxidation with hydroxyl radicals to generate more products that can be rapidly photolyzed. At the end of these PEF treatments, the current efficiency varied from 2.9% for 0.164 mM to a high value of 31% for 1.668 mM. All

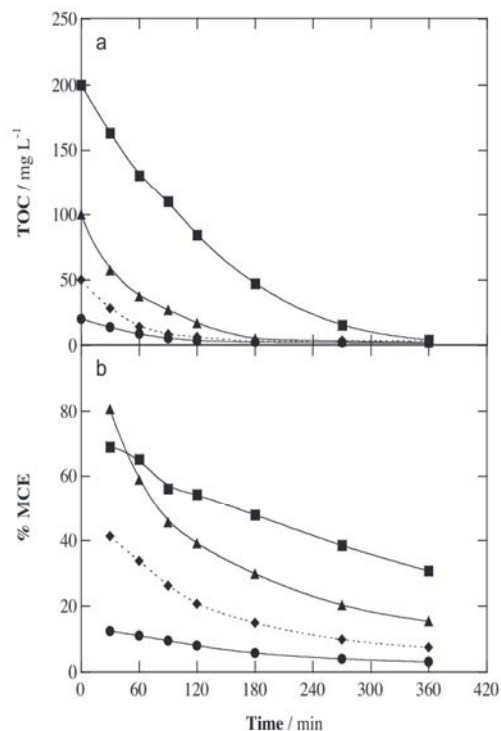


Fig. 4. Effect of *trans*-ferulic acid concentration on (a) TOC removal and (b) mineralization current efficiency vs. electrolysis time for the PEF degradation of 100 mL of solutions of this substrate in 0.05 M Na₂SO₄ with 0.50 mM Fe²⁺ at pH 3.0 using a BDD/air-diffusion cell at 33.3 mA cm⁻² and 35 °C. Content of *trans*-ferulic acid: (●) 0.167 mM, (◆) 0.417 mM, (▲) 0.834 mM and (■) 1.668 mM.

these findings allow concluding that the treatment of more concentrated solutions largely upgrades the mineralization process of *trans*-ferulic acid solutions.

3.3. SPEF treatment of *trans*-ferulic acid solutions

In view of the excellent results found for the PEF process, some experiments were made by degrading *trans*-ferulic acid solutions by SPEF at several j values for 180 min. Fig. 5a presents the quick TOC abatement found in these trials, which was even much faster than that obtained by PEF under comparable conditions (see Fig. 3a and Fig. 4a) because of the higher UV intensity supplied by sunlight. As can be observed, a 0.834 mM substrate solution at 33.3 mA cm⁻² reached 93% mineralization in 120 min, without further TOC removal at longer time. At 100 mA cm⁻², the higher production of hydroxyl radicals along with the quicker photolysis of oxidation products allowed attaining equal final TOC decay in only about 60 min. At that time, a 0.417 mM solution treated at 33.3 mA cm⁻² already reached a steady mineralization with near 84% TOC reduction. The fact that SPEF yielded a smaller final mineralization degree than PEF at the same j values (see Fig. 5a and Table 1) indicates that the quicker photolysis of some intermediates by the more potent sunlight led to a larger accumulation of highly recalcitrant products.

Fig. 5b depicts that the MCE values for the SPEF trials of Fig. 5a showed the same trends already discussed for the other EAOPs, such as a gradual drop of current efficiency (i) at longer electrolysis, (ii) when the initial substrate concentration becomes too low and (iii) at higher j , owing to the reasons pointed out above. For the best SPEF treatment of a 0.834 mM *trans*-ferulic acid solution

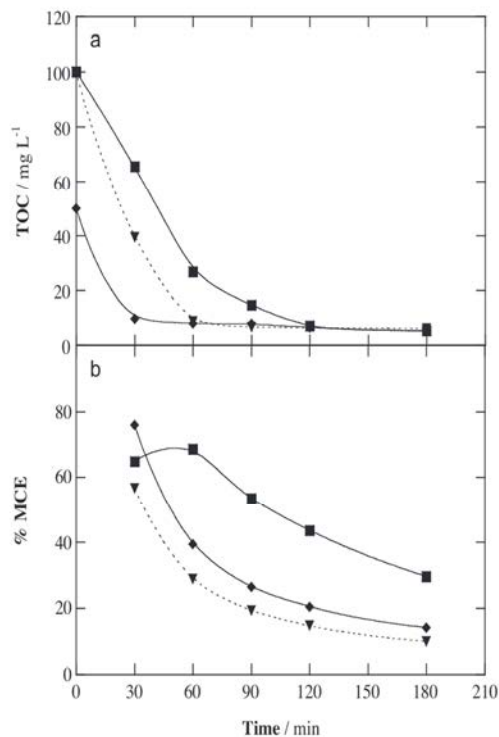


Fig. 5. Variation of: (a) TOC and (b) mineralization current efficiency with electrolysis time for the solar PEF (SPEF) degradation of 100 mL of *trans*-ferulic acid solutions in 0.05 M Na₂SO₄ with 0.50 mM Fe²⁺ at pH 3.0 and 35 °C using a BDD/air-diffusion cell. Content of *trans*-ferulic acid: (■, ▼) 0.834 mM and (◆, ▲) 0.417 mM. Current density: (■, ◆) 33.3 mA cm⁻² and (▼, ▲) 100 mA cm⁻².

at 33.3 mA cm⁻², a 44% MCE was found at 120 min when the maximum 93% TOC removal was reached.

The aforementioned findings corroborate the viability of SPEF for the remediation of wastewater containing *trans*-ferulic acid at industrial level. The method becomes more efficient using concentrated solutions and operating at a low j such as 33.3 mA cm⁻².

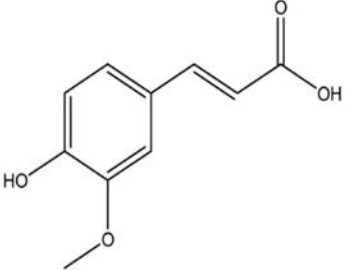
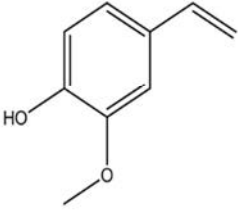
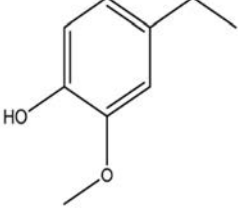
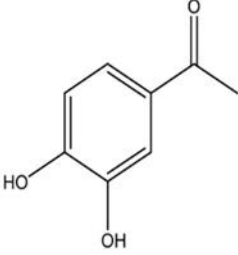
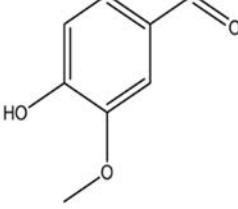
3.4. Identification and evolution of aromatic products and generated carboxylic acids

Table 2 summarizes the characteristics of the four primary aromatic products of *trans*-ferulic acid (**1**) detected by GC-MS at 30 and 90 min of electrolysis of a 0.834 mM solution of pH 3.0 by AO-H₂O₂ at 33.3 mA cm⁻². Compound **2** arises from the decarboxylation of **1**, whereas compounds **3–5** are produced by its further oxidation. It is noticeable that the generation of compound **5** (vanillin) has also been reported during the degradation of *trans*-ferulic acid by •OH radicals originated in TiO₂ photocatalysis [11].

On the basis of the above GC-MS results, the change of the concentration of compound **5** during the degradation of 0.834 mM *trans*-ferulic acid solutions at 33.3 mA cm⁻² under the conditions of Fig. 1 was followed from its characteristic peak recorded by reversed-phase HPLC. Only traces of this product (<0.005 mM) were found under AO-H₂O₂ treatment, suggesting that it was destroyed by BDD(•OH) and produced from the oxidation of **1** at a similar rate. This hypothesis was confirmed from the rapid accumulation and disappearance of **5** under EF and PEF conditions, as shown in Fig. 6a. A similar content of this product can be observed during both treatments, with a maximum value of 0.0030 mM at ca. 6 min and almost total removal at 15 min, i.e., when the parent molecule

Table 2

Aromatic products identified by GC–MS during the electrolysis of 100 mL of a 0.834 mM *trans*-ferulic acid solution in 0.05 M Na₂SO₄ at pH 3.0 and 35 °C by AO-H₂O₂ using a stirred BDD/air-diffusion cell at 33.3 mA cm⁻².

Number	Name	Molecular structure	t _r (min)	m/z	Electrolysis time (min)
1	<i>trans</i> -Ferulic acid		33.9 ^a	194 (M ⁺), 179, 161, 133	30, 90
2	2-Methoxy-4-vinylphenol		20.1 ^a 31.3 ^b	150 (M ⁺), 135, 118, 107, 89, 77	30, 90 30, 90
3	4-Ethyl-2-methoxyphenol or 4-ethylguaiaicol		28.1 ^b	152 (M ⁺), 137, 122, 109, 88	90
4	1-(2,4-Dihydroxyphenyl) ethanone		28.2 ^b	152 (M ⁺), 137, 123, 109, 81	30
5	Vanillin		23.2 ^a 37.5 ^b	152 (M ⁺), 151, 137, 123, 109, 81	90 30, 90

^a Non-polar Agilent J&W HP-5 ms.

^b Polar HP INNOWax columns.

1 had been just removed (see Fig. 1b). These results point to a very quick reaction of **1** and its primary aromatic products with •OH in the bulk, whereas the subsequent products are much more slowly destroyed by hydroxyl radicals, therefore decelerating the mineralization process (see Fig. 2a).

It is well known that the cleavage of the benzene ring of aromatic compounds originates linear products that evolve to short aliphatic carboxylic acids [13–17]. To explore this possibility for

trans-ferulic acid mineralization, the solutions treated under the conditions of Fig. 2 were analyzed by ion-exclusion HPLC. Final carboxylic acids such as fumaric (**6**), acetic (**7**) and oxalic (**8**) were detected and quantified by this technique. While the two former acids are oxidized to the latter one, acid **8** can be directly converted into CO₂ [14,16]. In the EF and PEF treatments, all these acids tend to form Fe(III) complexes, which are slowly oxidized by BDD(•OH) and more difficultly attacked by •OH in the bulk [37–40].

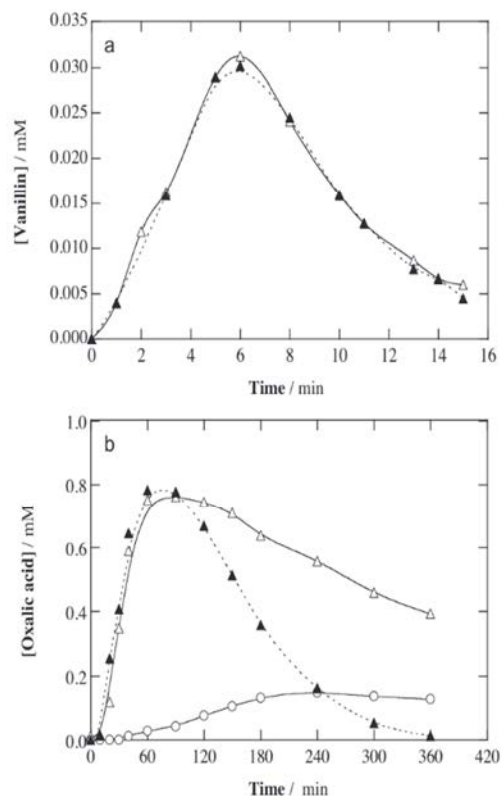


Fig. 6. Time-course of the concentration of (a) vanillin (5) and (b) oxalic acid (8) detected during the treatments shown in Fig. 1. Method: (○) AO-H₂O₂, (△) EF and (▲) PEF.

Low contents of acids **6** and **7** (<0.017 mM) appeared up to 30–60 min in all treatments, as expected from the fast removal of these compounds and their Fe(III) complexes. In contrast, the final acid **8** was much more largely accumulated in all cases evidencing that it was the main carboxylic acid produced in the mineralization process. Fig. 6b shows a progressive accumulation with slow drop of acid **8** up to a final value of 0.13 mM for AO-H₂O₂. This value accounts for 3.1 mg L⁻¹ of TOC, which constitutes 11% of the organic load of the remaining solution (see Table 1). For EF and PEF, Fig. 6b reveals that the much quicker destruction of primary intermediates by •OH led to about 0.76–0.78 mM of acid **8** as maximal at 60–90 min, its further fall depending on the applied treatment. In EF, the slow oxidation of Fe(III)-oxalate complexes by BDD(•OH) yielded 0.39 mM of final acid **8**, corresponding to 9.4 mg L⁻¹ of TOC and a 47% of the organic load of the final solution (see Table 1). This means that the final solution of EF still contained 53% of undetected products that are highly recalcitrant to hydroxyl radicals. On the other hand, the UVA light in PEF caused the quick and overall photodecarboxylation of Fe(III)-oxalate complexes via Reaction (5), as highlighted in Fig. 6b, although a 2% of the starting TOC remained in the final solution (see Table 1). Consequently, the PEF process allows the oxidation of most of undetected recalcitrant products that cannot be destroyed by hydroxyl radicals in EF, thanks to the photolytic action of UVA radiation. This behavior along with the total removal of final carboxylic acids explains the almost total mineralization of *trans*-ferulic acid solutions achieved using the powerful PEF process.

3.5. Plausible reaction pathway for *trans*-ferulic acid treated by EAOPs with BDD

On the basis of the products detected by GC-MS and HPLC, a plausible reaction pathway is proposed in Fig. 7 for *trans*-ferulic acid mineralization by EAOPs with BDD anode. Oxidation of aromatics takes place via reaction with BDD(•OH) in AO-H₂O₂ and much more rapidly with •OH in EF, PEF and SPEF, whereas that of final carboxylic acids and Fe(III)-carboxylate species involves pref-

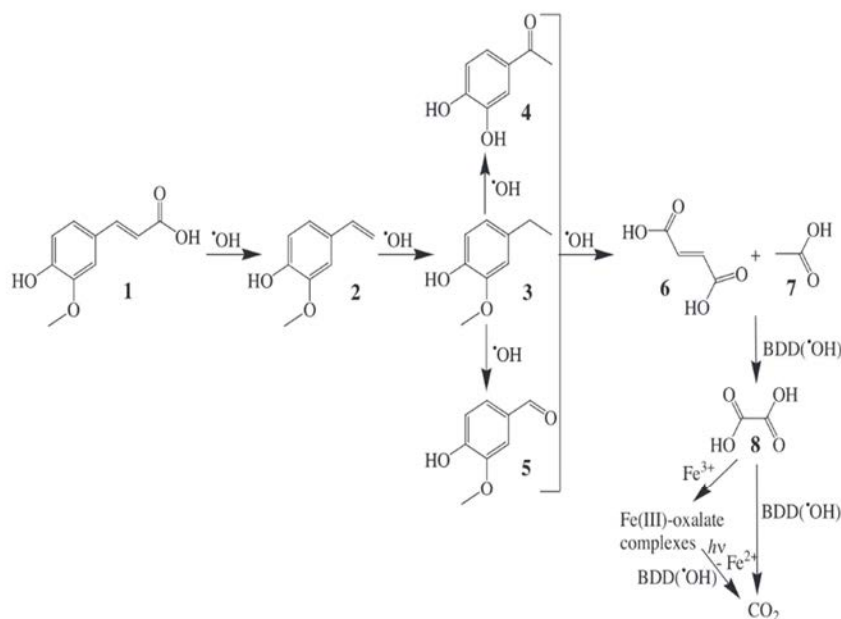


Fig. 7. Reaction pathway proposed for *trans*-ferulic acid mineralization by AO-H₂O₂, EF, PEF and SPEF using a BDD/air-diffusion cell. The species •OH in the sequence of aromatics accounts for by their oxidation by BDD(•OH) at the BDD surface and/or •OH from Fenton's reaction in the bulk.

entially the attack of $\text{BDD}(\cdot\text{OH})$. A much slower degradation with other generated oxidants like H_2O_2 , $\text{HO}_2\cdot$, O_3 and $\text{S}_2\text{O}_8^{2-}$ may occur as well. Only the fate of $\text{Fe}(\text{III})$ complexes with oxalic acid, but not of the other carboxylic acids, is stated for sake of simplicity.

The process starts with the decarboxylation of **1** to yield **2**. Further oxidation of the side vinyl group of **2** yields **3** with a lateral ethyl group, which can then be oxidized either to the ketone **4** with demethylation or to the aldehyde **5**. Subsequent degradation of all these aromatics with cleavage of the benzene ring leads to a mixture of final acids **6–8**. Acids **6** and **7** are formed to a small extent and quickly converted into acid **8**. This acid is directly transformed into CO_2 by $\text{BDD}(\cdot\text{OH})$ in $\text{AO-H}_2\text{O}_2$, but, in EF, PEF and SPEF, it forms $\text{Fe}(\text{III})$ -oxalate species that are slowly mineralized by $\text{BDD}(\cdot\text{OH})$ and much more rapidly photodecomposed under UVA light or sunlight, regenerating Fe^{2+} according to Reaction (5).

4. Conclusions

The PEF treatment of *trans*-ferulic acid solutions of pH 3.0 is able to yield almost total mineralization with 98% TOC reduction for substrate contents ≥ 0.843 mM and $j \geq 16.7$ mA cm^{-2} . It is much more powerful than EF, which allowed 92% TOC abatement as maximal at 100 mA cm^{-2} , because of the enhancement of the destruction of highly recalcitrant products to hydroxyl radicals by UVA irradiation. The oxidation ability of $\text{AO-H}_2\text{O}_2$ was slightly lower than that of EF up to 0.843 mM *trans*-ferulic acid and $j = 33.3$ mA cm^{-2} , both methods possessing similar mineralization power for higher substrate concentrations and j values. The decay of *trans*-ferulic acid concentration by $\text{AO-H}_2\text{O}_2$ was very slow by its poor reaction with $\text{BDD}(\cdot\text{OH})$, being much faster in EF and PEF due to its much quicker reaction with $\cdot\text{OH}$ in the bulk. For each EAOP, increasing j from 16.7 to 100 mA cm^{-2} caused faster mineralization with lower MCE, whereas the change of substrate concentration from 0.167 to 1.668 mM gave similar percentage of final TOC removed with a concomitant growth of current efficiency. The SPEF treatment accelerated the mineralization compared with PEF, although it also promoted the accumulation of a slightly larger proportion of barely oxidizable products. Four aromatic products and three short carboxylic acids were identified. Oxalic acid was the most important product and its total disappearance in PEF in contrast to its large persistence in $\text{AO-H}_2\text{O}_2$ and EF explained the superior oxidation power of the former EAOP.

Acknowledgments

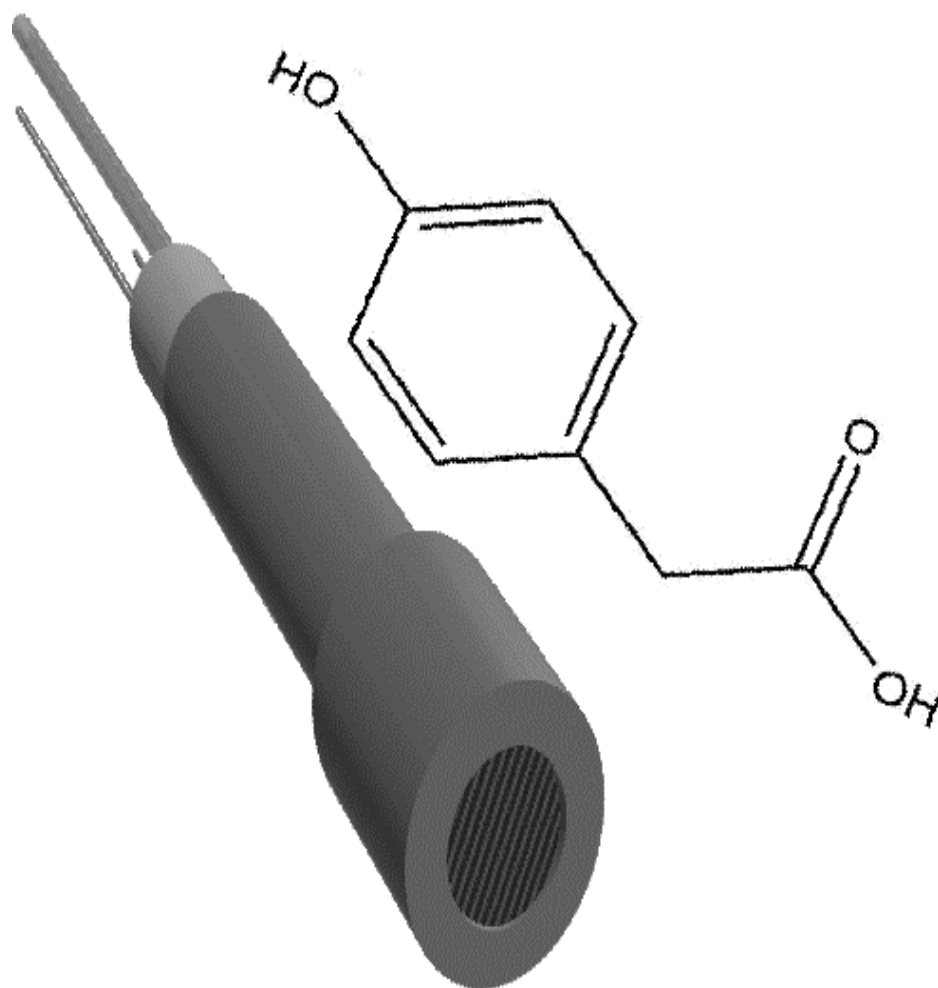
The authors thank MINECO (Spain) for financial support under project CTQ2013-48897-C2-1-R, co-financed with FEDER funds. The Ph.D. fellowship awarded to N. Flores from SENESCYT (Ecuador) is also acknowledged.

References

- [1] U.T. Un, U. Altay, A.S. Kopal, U.B. Ogutveren, Complete treatment of olive mill wastewaters by electrooxidation, *Chem. Eng. J.* 139 (2008) 445–452.
- [2] S. Magdich, C. Ben Ahmed, R. Jarbou, B. Ben Rouina, M. Boukhris, E. Ammar, Dose and frequency dependent effects of olive mill wastewater treatment on the chemical and microbial properties of soil, *Chemosphere* 93 (2013) 1896–1903.
- [3] S. Dermeche, M. Nadour, C. Larroche, F. Moulti-Mati, P. Michaud, Olive mill wastes: biochemical characterizations and valorization strategies, *Process Biochem.* 48 (2013) 1532–1552.
- [4] J.M. Ochando-Pulido, M.D. Victor-Ortega, G. Hodaifa, A. Martinez-Ferez, Physicochemical analysis and adequation of olive oil mill wastewater after advanced oxidation process for reclamation by pressure-driven membrane technology, *Sci. Total Environ.* 503–504 (2014) 113–121.
- [5] M. DellaGrecia, L. Previtera, F. Temussi, A. Zarelli, Low-molecular-weight components of olive oil mill waste-waters, *Phytochem. Anal.* 15 (2004) 184–188.
- [6] C. Mancuso, R. Santangelo, Ferulic acid: pharmacological and toxicological aspects, *Food Chem. Toxicol.* 65 (2014) 185–195.
- [7] N. Kumar, V. Pruthi, Potential applications of ferulic acid from natural sources, *Biotechnol. Rep.* 4 (2014) 86–93.
- [8] M.A. Miranda, F. Galindo, A.M. Amat, A. Arques, Pyrylium salt-photosensitized degradation of phenolic contaminants derived from cinnamic acid with solar light. Correlation of the observed reactivities with fluorescence quenching, *Appl. Catal. B Environ.* 28 (2000) 127–133.
- [9] B.R. Yadav, A. Garg, Catalytic wet oxidation of ferulic acid (a lignin model compound) in the presence of non-noble metal based catalysts at mild conditions, *Chem. Eng. J.* 252 (2014) 185–193.
- [10] R. Andreozzi, M. Canterino, V. Caprio, I. Di Somma, R. Marotta, Use of an amorphous iron oxide hydrated as catalyst for hydrogen peroxide oxidation of ferulic acid in water, *J. Hazard. Mater.* 152 (2008) 870–875.
- [11] V. Augugliaro, G. Camera-Roda, V. Loddo, G. Palmisano, L. Palmisano, F. Parrino, Synthesis of vanillin in water by TiO_2 photocatalysis, *Appl. Catal. B Environ.* 111–112 (2012) 555–561.
- [12] M. Panizza, G. Cerisola, Direct and mediated anodic oxidation of organic pollutants, *Chem. Rev.* 109 (2009) 6541–6569.
- [13] I. Sirés, E. Brillas, Remediation of water pollution caused by pharmaceutical residues based on electrochemical separation and degradation technologies: a review, *Environ. Int.* 40 (2012) 212–229.
- [14] I. Sirés, E. Brillas, M.A. Oturan, M.A. Rodrigo, M. Panizza, Electrochemical advanced oxidation processes: today and tomorrow. A review, *Environ. Sci. Pollut. Res.* 21 (2014) 8336–8367.
- [15] S. Vasudevan, M.A. Oturan, Electrochemistry as cause and cure in water pollution—an overview, *Environ. Chem. Lett.* 12 (2014) 97–108.
- [16] E. Brillas, C.A. Martínez-Huitle, Decontamination of wastewaters containing synthetic organic dyes by electrochemical methods. An updated review, *Appl. Catal. B Environ.* 166–167 (2015) 603–643.
- [17] B. Boye, P.A. Michaud, B. Marselli, M.M. Dieng, E. Brillas, C. Cominellis, Anodic oxidation of 4-chlorophenoxyacetic acid on synthetic boron-doped diamond electrodes, *New Diamond Front. Carbon Technol.* 12 (2002) 63–72.
- [18] B. Marselli, J. Garcia-Gomez, P.A. Michaud, M.A. Rodrigo, C. Cominellis, Electrogeneration of hydroxyl radicals on boron-doped diamond electrodes, *J. Electrochem. Soc.* 150 (2003) D79–D83.
- [19] C.A. Martínez-Huitle, S. Ferro, Electrochemical oxidation of organic pollutants for the wastewater treatment: direct and indirect processes, *Chem. Soc. Rev.* 35 (2006) 1324–1340.
- [20] M. Hamza, R. Abdelhedi, E. Brillas, I. Sirés, Comparative electrochemical degradation of the triphenylmethane dye Methyl Violet with boron-doped diamond and Pt anodes, *J. Electroanal. Chem.* 627 (2009) 41–50.
- [21] L. Ciriaco, C. Anjo, J. Correia, M.J. Pacheco, A. Lopes, Electrochemical degradation of ibuprofen on Ti/Pt/PbO₂ and Si/BDD electrodes, *Electrochim. Acta* 54 (2009) 1464–1472.
- [22] M.A. Rodrigo, P. Cañizares, A. Sánchez-Carretero, C. Sáez, Use of conductive-diamond electrochemical oxidation for wastewater treatment, *Catal. Today* 151 (2010) 173–177.
- [23] E.B. Cavalcanti, S. Garcia-Segura, F. Centellas, E. Brillas, Electrochemical incineration of omeprazole in neutral aqueous medium using a platinum or boron-doped diamond. Degradation kinetics and oxidation products, *Water Res.* 47 (2013) 1803–1815.
- [24] A. Wang, J. Qu, H. Liu, J. Ru, Mineralization of an azo dye Acid Red 14 by photoelectro-Fenton process using an activated carbon fiber cathode, *Appl. Catal. B Environ.* 84 (2008) 393–399.
- [25] A. Khataee, A. Khataee, M. Fathinia, B. Vahid, S.W. Joo, Kinetic modeling of photoassisted-electrochemical process for degradation of an azo dye using boron-doped diamond anode and cathode with carbon nanotubes, *J. Ind. Eng. Chem.* 19 (2013) 1890–1894.
- [26] A. Khataee, A. Akbarpour, B. Vahi, Photoassisted electrochemical degradation of an azo dye using Ti/RuO₂ anode and carbon nanotubes containing gas-diffusion cathode, *J. Taiwan Inst. Chem. Eng.* 45 (2014) 930–936.
- [27] V. Vatanpour, N. Daneshvar, M.H. Rasoulifard, Electro-Fenton degradation of synthetic dye mixture: influence of intermediates, *J. Environ. Eng. Manag.* 19 (2009) 277–282.
- [28] M.H.M.T. Assumpção, A. Moraes, R.F.B. De Souza, R.M. Reis, R.S. Rocha, I. Gaubeur, M.L. Calegario, P. Hammer, M.R.V. Lanza, M.C. Santos, Degradation of dipyrone via advanced oxidation processes using a cerium nanostructured electrocatalyst material, *Appl. Catal. A Gen.* 462–463 (2013) 256–261.
- [29] A. Dirany, I. Sirés, N. Oturan, A. Özcan, M.A. Oturan, Electrochemical treatment of the antibiotic sulfachloropyridazine: kinetics, reaction pathways, and toxicity evolution, *Environ. Sci. Technol.* 46 (2012) 4074–4082.
- [30] M.S. Yahya, N. Oturan, K. El Kacemi, M. El Karbane, C.T. Aravindakumar, M.A. Oturan, Oxidative degradation study on antimicrobial agent ciprofloxacin by electro-Fenton process: kinetics and oxidation products, *Chemosphere* 117 (2014) 447–454.
- [31] A. El-Ghenmy, R.M. Rodríguez, E. Brillas, N. Oturan, M.A. Oturan, Electro-Fenton degradation of the antibiotic sulfanilamide with Pt/carbon-felt and BDD/carbon-felt cells. Kinetics, reaction intermediates, and toxicity assessment, *Environ. Sci. Pollut. Res.* 21 (2014) 8368–8378.
- [32] S. Ammar, R. Abdelhedi, C. Flox, C. Arias, E. Brillas, Electrochemical degradation of the dye indigo carmine at boron-doped diamond anode for wastewaters remediation, *Environ. Chem. Lett.* 4 (2006) 229–233.
- [33] A. Thiam, M. Zhou, E. Brillas, I. Sirés, Two-step mineralization of Tartrazine solutions: study of parameters and by-products during the coupling of electrocoagulation with electrochemical advanced oxidation processes, *Appl. Catal. B Environ.* 150–151 (2014) 116–125.

- [34] A. Thiam, I. Sirés, J.A. Garrido, R.M. Rodríguez, E. Brillas, Decolorization and mineralization of Allura Red AC aqueous solutions by electrochemical advanced oxidation processes, *J. Hazard. Mater.* 290 (2015) 34–42.
- [35] K. Cruz-González, O. Torres-López, A. García-León, J.L. Guzmán-Mar, L.H. Reyes, A. Hernández-Ramírez, J.M. Peralta-Hernández, Determination of optimum operating parameters for Acid Yellow 36 decolorization by electro-Fenton process using BDD cathode, *Chem. Eng. J.* 160 (2010) 199–206.
- [36] K. Cruz-González, O. Torres-López, A. García-León, E. Brillas, A. Hernández-Ramírez, J.M. Peralta-Hernández, Optimization of electro-Fenton/BDD process for decolorization of a model azo dye wastewater by means of response surface methodology, *Desalination* 286 (2012) 63–68.
- [37] E.J. Ruiz, A. Hernández-Ramírez, J.M. Peralta-Hernández, C. Arias, E. Brillas, Application of solar photoelectro-Fenton technology to azo dyes mineralization: effect of current density, Fe^{2+} and dye concentrations, *Chem. Eng. J.* 171 (2011) 385–392.
- [38] F.C. Moreira, S. García-Segura, V.J.P. Vilar, R.A.R. Boaventura, E. Brillas, Decolorization and mineralization of Sunset Yellow FCF azo dye by anodic oxidation, electro-Fenton, UVA photoelectro-Fenton and solar photoelectro-Fenton processes, *Appl. Catal. B Environ.* 142–143 (2013) 877–890.
- [39] X. Florenza, A.M.S. Solano, F. Centellas, C.A. Martínez-Huitle, E. Brillas, S. García-Segura, Degradation of the azo dye Acid Red 1 by anodic oxidation and indirect electrochemical processes based on Fenton's reaction chemistry. Relationship between decolorization, mineralization and products, *Electrochim. Acta* 142 (2014) 276–288.
- [40] A. Thiam, I. Sirés, F. Centellas, P.L. Cabot, E. Brillas, Decolorization and mineralization of Allura Red AC azo dye by solar photoelectro-Fenton: identification of intermediates, *Chemosphere* 136 (2015) 1–8.
- [41] B. Boye, M.M. Dieng, E. Brillas, Electrochemical degradation of 2,4,5-trichlorophenoxyacetic acid in aqueous medium by peroxi-coagulation. Effect of pH and UV light, *Electrochim. Acta* 48 (2003) 781–790.

7. MINERALIZACIÓN DEL ÁCIDO 4-HIDROXIFENILACÉTICO EN DISOLUCIONES SINTÉTICAS



Publicación 3:

Removal of 4-hydroxyphenylacetic acid from aqueous medium by electrochemical oxidation with a BDD anode: Mineralization, kinetics and oxidation products

7. MINERALIZACIÓN DEL ÁCIDO 4-HIDROXIFENILACÉTICO EN DISOLUCIONES SINTÉTICAS

Este trabajo presenta un tratamiento efectivo para disoluciones de ácido 4-hidroxifenilacético mediante oxidación anódica con H_2O_2 electrogenerado (OA- H_2O_2). Los experimentos se llevaron a cabo con un reactor de tanque agitado con un ánodo de diamante dopado con boro (BDD) de 3 cm^2 y un cátodo de difusión de aire de carbón-PTFE de 3 cm^2 . Se electrolizaron 100 mL de disoluciones con una concentración de entre 0,21 y 2,1 mM de este compuesto en Na_2SO_4 0,050 mM como electrolito soporte a pH 3,0 y $35 \text{ }^\circ\text{C}$, a una j constante entre 16,7 y 100 mA cm^{-2} .

Como punto de partida, se estudió el efecto de j sobre la eliminación del TOC. Para ello, se electrolizaron 100 mL de disoluciones que contenían 1,03 mM del ácido, aumentando j desde 16,7 hasta 100 mA cm^{-2} durante 360 min. La Figura 1 muestra que a los valores más altos de j , se obtuvo mayor destrucción del TOC. Ésta varió del 69,1% al 95% para j desde 16,7 a 100 mA cm^{-2} , gracias a la aceleración de las reacciones por la mayor generación de BDD($\cdot\text{OH}$), así como de H_2O_2 en el cátodo.

La mineralización del ácido 4-hidroxifenilacético siguió una cinética de pseudo-primer orden gobernada por el bajo contenido de oxidantes generados y el transporte de masa de los compuestos orgánicos hacia el ánodo. Las constantes k_{TOC} obtenidas fueron $3,4 \times 10^{-3}$, $3,9 \times 10^{-3}$, $6,6 \times 10^{-3}$ y $7,9 \times 10^{-3} \text{ min}^{-1}$ para j de 16,7, 33,3, 66,7 y 100 mA cm^{-2} , respectivamente. La pequeña variación de k_{TOC} con j permite inferir que la eficiencia se reduce a mayor j . Esto se verificó mediante el cálculo de la MCE para las disoluciones con 1,03 mM del ácido 4-hidroxifenilacético a diferente j . En la Figura 2 puede verse que el proceso más eficiente se dio a $16,7 \text{ mA cm}^{-2}$, con una MCE del 28,4% en los primeros 60 min de tratamiento, aunque la eficiencia siempre decaía al prolongar el tiempo. Esto se puede atribuir a la desaparición gradual de la materia orgánica en el medio y a la formación de subproductos que son más difíciles de degradar por los radicales BDD($\cdot\text{OH}$). A mayor j , la velocidad de mineralización del ácido 4-hidroxifenilacético aumentó, pero con disminución de la MCE. Bajo estas condiciones, cabe prever un incremento progresivo de la velocidad de las reacciones parásitas del BDD($\cdot\text{OH}$), con la correspondiente reducción de su concentración relativa.

El consumo específico de energía por unidad de masa de TOC (EC_{TOC}), que se da en la Figura 2b, crecía al ir aumentando j . Se obtuvieron valores finales de $0,325$ y $4,30 \text{ kWh (g TOC)}^{-1}$ para 16,7 y 100 mA cm^{-2} , respectivamente. Estos resultados muestran que es mejor aplicar bajos valores de j a una disolución con 1,03 mM del ácido 4-hidroxifenilacético. El proceso de OA- H_2O_2 más económico resultó a $16,7 \text{ mA cm}^{-2}$, con un coste de 0.030 € por gramo de TOC con una eliminación de TOC del 69% y una MCE del 29,1%.

Para estudiar el efecto de la concentración inicial de contaminante sobre la mineralización de disoluciones del ácido 4-hidroxifenilacético se consideraron concentraciones desde 0,21 hasta 2,06 mM, que se electrolizaron a $j = 33,3 \text{ mA cm}^{-2}$ durante 360 min. Se encontró una mayor degradación del ácido cuando se incrementó su contenido. La eliminación del TOC fue del 67,0%, 82,6%, 75,5% y 64,1% para concentraciones de 0,21, 0,51, 1,03 y 2,06 mM del ácido, respectivamente. En los dos últimos casos se observa una disminución en el porcentaje de reducción de TOC, aunque se eliminó más cantidad de materia

7. MINERALIZACIÓN DEL ÁCIDO 4-HIDROXIFENILACÉTICO EN DISOLUCIONES SINTÉTICAS

orgánica del medio porque un mayor número de moléculas de ácido 4-hidroxifenilacético reaccionaba con más cantidad de BDD(\cdot OH) al decrecer la velocidad de sus reacciones parásitas. Esto es más evidente al analizar la Figura 4^a, donde se ve que los valores de la MCE aumentan con el aumento de concentración del ácido 4-hidroxifenilacético.

Cuando se analizaron los valores de EC_{TOC}, se vio que éstos se reducían gradualmente a mayor concentración, como se observa en la Figura 4b. El proceso de OA-H₂O₂ se tornó más eficiente y con menor consumo de energía, pues, cuando se trataban disoluciones más concentradas.

La cinética de degradación del ácido 4-hidroxifenilacético se siguió mediante HPLC de fase inversa. La Figura 5a muestra que se consigue eliminar prácticamente todo el ácido de una disolución de concentración 1,03 mM en 360 min a $j = 33,3 \text{ mA cm}^{-2}$. Estos datos permitieron determinar una constante de pseudo-primer orden $k_1 = 1,0 \times 10^{-2} \text{ min}^{-1}$ para esta reacción. Ello sugiere que el ácido 4-hidroxifenilacético era degradado por una concentración constante de radicales BDD(\cdot OH). Esto es factible por el corto tiempo de vida de estos radicales, alrededor de 10^{-9} s . Sabiendo que la constante de velocidad absoluta del ácido 4-hidroxifenilacético es de $7,02 \times 10^8 \text{ M}^{-1} \text{ s}^{-1}$, se determinó una concentración de radicales activos BDD(\cdot OH) de $2,4 \times 10^{-13} \text{ M}$ durante el proceso OA-H₂O₂.

Por medio de GC-MS se detectaron los intermedios formados durante la degradación del ácido 4-hidroxifenilacético 1,03 mM a $33,3 \text{ mA cm}^{-2}$. Se encontraron dos intermedios aromáticos, el 4-hidroxibenzenometanol y el 4-hidroxibenzaldehído, además del ácido acético. Esto indica que el ataque de los radicales BDD(\cdot OH) sobre el ácido 4-hidroxifenilacético provoca su descarboxilación e hidroxilación para producir el diol 4-hidroxibencenometanol que luego se oxida a 4-hidroxibenzaldehído. Cabe considerar que el ácido acético era un producto de oxidación de compuestos aromáticos intermedios por la ruptura de su anillo bencénico. Mediante HPLC de exclusión iónica, se detectaron trazas de ácido acético, y la acumulación del ácido oxálico a los 240 min como se ve en la Figura 6.

De todos estos resultados, se concluye que una disolución con 1,03 mM de ácido 4-hidroxifenilacético en medio sulfato a pH 3,0 puede ser casi totalmente mineralizada mediante OA-H₂O₂ bajo las condiciones estudiadas. El uso de bajos valores de j daba lugar a una menor mineralización, pero el proceso era más económico. Los mejores resultados se encontraron a $j = 16,7 \text{ mA cm}^{-2}$, dando lugar a un 29,1% de eficiencia con $0,325 \text{ kWh (g TOC)}^{-1}$, pero consiguiendo tan solo un 67,6% de eliminación de TOC.



Contents lists available at ScienceDirect

Journal of Electroanalytical Chemistry

journal homepage: www.elsevier.com/locate/jelechem

Removal of 4-hydroxyphenylacetic acid from aqueous medium by electrochemical oxidation with a BDD anode: Mineralization, kinetics and oxidation products



Nelly Flores, Ignasi Sirés*, Rosa María Rodríguez, Francesc Centellas, Pere Lluís Cabot, José Antonio Garrido, Enric Brillas*

Laboratori d'Electroquímica dels Materials i del Medi Ambient, Departament de Química Física, Facultat de Química, Universitat de Barcelona, Martí i Franquès 1-11, 08028 Barcelona, Spain

ARTICLE INFO

Article history:

Received 27 June 2016

Received in revised form 29 July 2016

Accepted 31 July 2016

Available online 4 August 2016

Keywords:

Anodic oxidation

By-products

Hydroxyl radical

4-Hydroxyphenylacetic acid

Water treatment

ABSTRACT

The degradation of 100 mL of solutions containing 4-hydroxyphenylacetic acid in 0.050 M Na₂SO₄ at pH 3.0 has been performed by anodic oxidation with electrogenerated H₂O₂ (AO-H₂O₂) using a stirred tank reactor equipped with a boron-doped diamond (BDD) anode and an air-diffusion cathode. An almost total mineralization with 95.5% total organic carbon (TOC) removal was achieved for a 1.03 mM substrate solution at 100 mA cm⁻². The effect of current density between 16.7 and 100 mA cm⁻² and 4-hydroxyphenylacetic acid content between 0.21 and 2.06 mM was examined. Greater current efficiency with lower specific energy consumption and smaller mineralization was found at low current density and high substrate concentration. The TOC abatement as well as the 4-hydroxyphenylacetic acid concentration decay obeyed a pseudo-first-order kinetics. The oxidation role of hydroxyl radical formed from water discharge at the BDD anode is explained on the basis of its electrogeneration rate and competitive wasting reactions. 4-Hydroxybenzenemethanol and its derivative 4-hydroxybenzaldehyde were identified as primary aromatic by-products by gas chromatography-mass spectrometry. Ion-exclusion HPLC allowed the detection of low amounts of the persistent oxalic acid during the AO-H₂O₂ process. The remaining TOC in final electrolyzed solutions is related to the presence of a large proportion of unidentified by-products that are even more recalcitrant than common short-chain aliphatic carboxylic acids.

© 2016 Elsevier B.V. All rights reserved.

1. Introduction

The olive oil production in Mediterranean countries such as Spain, Portugal, Greece and Italy accounts for near 77% of world output. The extraction of olive oil causes the annual release of >30 million cubic meters of industrial effluents worldwide. Olive oil mill wastewater (OOMW) has an acidic pH near 5 and is highly hazardous for the aquatic environment because it presents a chemical oxygen demand up to 110 g L⁻¹, a biochemical oxygen demand up to 170 g L⁻¹ and total solids concentration up to 150 g L⁻¹ [1,2]. The organic components of OOMW include phenols, lipids, sugars and tannins, related to up to 37% of its total mass [3,4]. Several authors have reported the treatment of these effluents by catalytic wet air oxidation [5] and electrochemical degradation with a Pt anode [6,7], which lead to a significant reduction of phenolic derivatives. In order to establish an optimum integral treatment of such wastewater, the degradation of its main single components has to be addressed. 4-Hydroxyphenylacetic acid is one of the most abundant phenolic components detected in OOMW, also found in beer. At industrial level, it is used as intermediate in the production of β -blockers like atenolol and other chemicals. It is a primary product upon oxidation of tyrosol (4-

hydroxyphenylethanol), another phenolic compound in OOMW [8,9]. However, little information is available about the degradation of 4-hydroxyphenylacetic acid for wastewater treatment. Only its removal by several advanced oxidation processes (AOPs) such as zero-valent iron [10] and UV/H₂O₂ and Fenton's reagent [11] has been described, but the use of powerful electrochemical AOPs (EAOPs) for treating wastewater contaminated with 4-hydroxyphenylacetic acid has not been reported yet.

EAOPs are environment-friendly technologies that operate at mild conditions without addition of noxious chemicals since the main oxidant is produced by the electron [12–15]. The great oxidation power of these methods to destroy the organic matter in wastewater is related to the continuous in situ production of reactive oxygen species (ROS), pre-eminently the powerful hydroxyl radical (\bullet OH). This species, the second strongest oxidant known after fluorine, possesses such a high standard reduction potential ($E^\circ(\bullet\text{OH}/\text{H}_2\text{O}) = 2.80 \text{ V/SHE}$) that can non-selectively react with most organics via dehydrogenation and/or hydroxylation up to their mineralization (conversion into CO₂, water and inorganic ions) [13]. Anodic oxidation (AO), also called electrochemical oxidation, is the most popular EAOP. In this procedure, a solution with organic pollutants is placed in the electrolytic cell to be oxidized either by direct charge transfer at the anode M or, if a high current is applied, by adsorbed hydroxyl radical M(\bullet OH) formed as

* Corresponding authors.

E-mail addresses: isires@ub.edu (I. Sirés), brillas@ub.edu (E. Brillas).

intermediate of O₂ evolution from water oxidation [13,16,17]. The oxidation ability of AO depends on the selected anode. It has been found that the most potent one is the boron-doped diamond (BDD) thin-film electrode in which the physisorbed BDD(•OH) is produced from the following reaction [16,18,19]:



The use of the BDD anode presents important technological advantages such as remarkable corrosion stability in harsh media, inert surface with low adsorption of BDD(•OH) and organics and a greater O₂-evolution overvoltage than other anodes. These characteristics significantly upgrade the removal of organic pollutants by hydroxyl radicals [13,16], allowing the mineralization of aromatics [14,18,20–29] and by-products like aliphatic carboxylic acids [30], with much higher oxidation ability than traditional anodes like Pt [31–33] and PbO₂ [34].

An alternative to raw AO relies on its combination with electrogenerated H₂O₂, so-called AO-H₂O₂. In this procedure, H₂O₂ is continuously produced by the two-electron cathodic reduction of injected pure O₂ or air via reaction (2) [12,13]:



Effective cathodes for reaction (2) include carbonaceous materials like BDD [35], activated carbon fiber [36], carbon nanotubes [37], carbon sponge [38], carbon felt [39–41] and carbon-polytetrafluoroethylene (PTFE) gas diffusion composites [14,15,42,43].

AO-H₂O₂ has been developed in our laboratory using a gas-diffusion cathode [12,43], which minimizes the possible cathodic reduction of organics because of the very efficient supply of H₂O₂ to the medium from reaction (2). We have found that the concentration of this species attains a quasi-steady state once its electrogeneration and removal rates equate. H₂O₂ is mainly destroyed upon oxidation to O₂ at the BDD anode, thus forming hydroperoxyl radical from reaction (3). Therefore, in AO-H₂O₂, organic pollutants can be removed by BDD(•OH) and, to much smaller extent, by other weaker oxidants like H₂O₂ and BDD(HO₂•).



This paper reports a study on the degradation of acidic solutions of 4-hydroxyphenylacetic acid by AO-H₂O₂ using a BDD/air-diffusion tank reactor. The influence of current density (*j*) and substrate content on degradation rate, mineralization current efficiency (MCE) and energy consumption was examined. The decay kinetics of 4-hydroxyphenylacetic acid and the evolution of generated carboxylic acids were monitored by high-performance liquid chromatography (HPLC). The degradation process was ascertained by identifying the products using gas chromatography-mass spectrometry (GC-MS).

2. Experimental

2.1. Chemicals

4-Hydroxyphenylacetic acid (98% purity) was purchased from Sigma-Aldrich and used as received. Analytical grade oxalic acid and anhydrous Na₂SO₄ were supplied by Merck and Fluka, respectively. Analytical grade H₂SO₄ purchased from Acros Organics was used to adjust the initial pH to 3.0. All the aqueous solutions were prepared with ultrapure water from a Millipore Milli-Q system (resistivity > 18 MΩ cm at 25 °C). Other chemicals used for analysis were of HPLC or analytical grade provided by Panreac and Merck.

2.2. Electrolytic System

All the trials were carried out in an open, undivided, cylindrical glass cell containing 100 mL solutions. The cell was surrounded with a double jacket where water was recirculated at 35 °C regulated by a Thermo Electron Corporation HAAKE DC 10 thermostat. This temperature was

the maximum value that could be used to avoid significant solvent evaporation. All the assays were performed under vigorous stirring with a magnetic bar at 700 rpm for homogenization and for ensuring maximum mass transport of reactants toward/from the electrodes. A 3 cm² BDD (deposited onto *p*-Si) electrode supplied by NeoCoat (La-Chaux-de-Fonds, Switzerland) was used as the anode and a 3 cm² carbon-PTFE air-diffusion electrode supplied by E-TEK (Somerset, NJ, USA) was used as the cathode. The interelectrode gap was about 1 cm. The cathode was mounted as reported elsewhere [42] and was fed with air pumped at 300 mL min⁻¹ for continuous H₂O₂ generation on site. The experiments were performed at constant *j* provided by an EG&G Princeton Applied Research 273A potentiostat-galvanostat. The surfaces of the anode and cathode were initially cleaned and activated, respectively, under polarization in 100 mL of 0.050 M Na₂SO₄ at 100 mA cm⁻² for 180 min. Aqueous solutions with 0.21–2.06 mM 4-hydroxyphenylacetic acid and 0.050 M Na₂SO₄ at pH 3.0 were treated by AO-H₂O₂ at *j* values between 16.7 and 100 mA cm⁻².

2.3. Analytical Methods

The solution pH was measured with a Crison GLP 22 pH-meter. For total organic carbon (TOC) determinations, samples were withdrawn from treated solutions, filtered with 0.45 μm PTFE filters from Whatman and directly injected into a Shimadzu VCSN TOC analyzer. Reproducible values with ± 1% accuracy were always found.

Assuming the following total mineralization for 4-hydroxyphenylacetic acid:



the MCE values for each trial were estimated as follows [26,29]:

$$\text{MCE}(\%) = \frac{n F V \Delta(\text{TOC})_{\text{exp}}}{4.32 \times 10^7 m I t} \times 100 \quad (5)$$

where *n* = 34 is the number of electrons for the mineralization process, as shown in Eq. (4), *F* is the Faraday constant (96,487 C mol⁻¹), *V* is the solution volume (L), Δ(TOC)_{exp} is the experimental TOC decay (mg C L⁻¹), 4.32 × 10⁷ is a conversion factor to homogenize the units (3600 s h⁻¹ × 12,000 mg C mol⁻¹), *m* = 8 is the number of carbon atoms of 4-hydroxyphenylacetic acid, *I* is the applied current (A) and *t* is the electrolysis time (h).

The specific energy consumption per unit TOC mass (EC_{TOC}) was estimated from Eq. (6) [29,43]:

$$\text{EC}_{\text{TOC}} (\text{kWh}(\text{gTOC})^{-1}) = \frac{E_{\text{cell}} I t}{V \Delta(\text{TOC})_{\text{exp}}} \quad (6)$$

where *E*_{cell} is the average cell voltage (in V) and the rest of parameters have been defined above.

The 4-hydroxyphenylacetic acid abatement was followed by reversed-phase HPLC using a Waters 600 LC fitted with a BDS Hypersil C18 6 μm, 250 mm × 4.6 mm, column at 35 °C and coupled to a Waters 996 photodiode array detector selected at λ = 277.0 nm. Measurements were made by injecting 10 μL aliquots into the LC and eluting an acetonitrile/water (60:40) mixture at 0.6 mL min⁻¹ as mobile phase. The chromatograms exhibited a well-defined peak at retention time (*t*_r) of 5.0 min. Generated carboxylic acids were identified by ion-exclusion HPLC using the same LC fitted with a Bio-Rad Aminex HPX 87H, 300 mm × 7.8 mm, column at 35 °C and the photodiode array detector selected at λ = 210.0 nm. Aliquots of 10 μL were also injected into the LC and the mobile phase was 4 mM H₂SO₄ at 0.6 mL min⁻¹. The chromatograms displayed a well-defined peak related to oxalic acid at *t*_r = 7.0 min.

The organic products generated upon treatment of 1.03 mM 4-hydroxyphenylacetic acid solutions at 30 and 90 min of AO-H₂O₂ at 33.3 mA cm⁻² were identified by GC-MS using a NIST05-MS library to

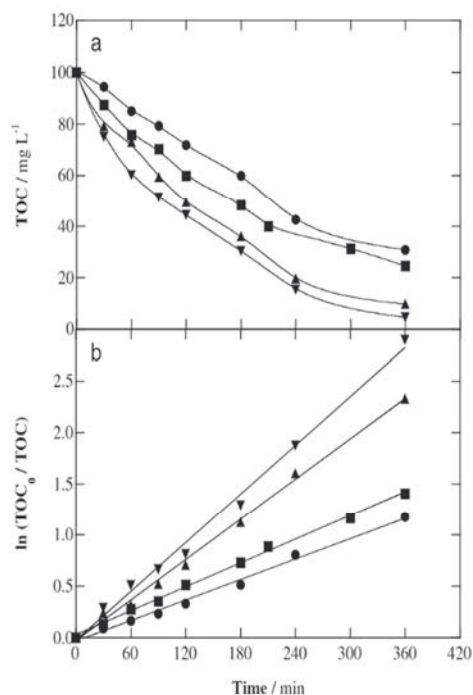


Fig. 1. (a) Effect of current density on TOC removal with electrolysis time for the treatment of 100 mL of a 1.03 mM 4-hydroxyphenylacetic acid solution in 0.050 M Na₂SO₄ at pH 3.0 and 35 °C by anodic oxidation with electrogenerated H₂O₂ (AO-H₂O₂) using a stirred tank reactor with a 3 cm² BDD anode and a 3 cm² air-diffusion cathode. (b) Kinetic analysis for TOC removal assuming a pseudo-first-order decay. Applied current density: (●) 16.7 mA cm⁻², (■) 33.3 mA cm⁻², (▲) 66.7 mA cm⁻² and (▼) 100 mA cm⁻².

interpret the mass spectra. About 100–250 mL aliquots were lyophilized or extracted out with CH₂Cl₂ (3 × 25 mL). After lyophilization, the residue was dissolved in 1 mL of ethyl acetate, whereas after CH₂Cl₂ extraction, the organic volume was reduced to about 1 mL after drying over anhydrous Na₂SO₄ followed by filtration. GC-MS analysis of concentrated samples was carried out on an Agilent system composed of a 6890 N GC and a 5975C MS, operating in EI mode at 70 eV. The GC was fitted with either a non-polar Teknokroma Sapiens-X5ms or a polar HP INNOWax column, both of 0.25 μm, 30 m × 0.25 mm. The temperature ramp was: 36 °C for 1 min, 5 °C min⁻¹ up to 325 °C and hold time 10 min. The temperature of the inlet, source and transfer line was 250, 230 and 300 °C for the non-polar column and 250, 230 and 250 °C for the polar one.

Table 1

Percentage of TOC removal, mineralization current efficiency and specific energy consumption per unit TOC mass for the AO-H₂O₂ treatment of 100 mL of 4-hydroxyphenylacetic acid solutions at pH 3.0 using a BDD/air-diffusion cell under selected conditions.

c ₀ (mM) ^a	j (mA cm ⁻²) ^b	After 120 min of electrolysis			After 360 min of electrolysis		
		% TOC removal	% MCE	EC _{TOC} (kWh (g TOC) ⁻¹)	% TOC removal	% MCE	EC _{TOC} (kWh (g TOC) ⁻¹)
0.21	33.3	21.5	2.05	5.89	67.6	2.15	5.62
0.51	33.3	35.0	8.31	1.44	82.7	6.54	1.83
1.03	16.7	28.2	26.8	0.266	69.1	21.9	0.325
	33.3	40.1	19.1	0.627	75.5	11.5	1.00
	66.7	50.6	12.0	1.39	90.3	7.14	2.34
	100	55.6	8.79	2.46	95.5	5.04	4.30
2.06	33.3	24.7	23.5	0.510	64.1	20.3	0.590

^a Initial substrate concentration.

^b Current density.

3. Results and discussion

3.1. Effect of Current Density on the Degradation of 4-Hydroxyphenylacetic Acid

The current density is a crucial parameter in electrochemical treatments of wastewater because it is expected to determine the amount of oxidant, which is BDD(•OH) in the present study. To test the oxidation ability of AO-H₂O₂ for the decontamination of 4-hydroxyphenylacetic acid solutions and the influence of *j* on the degradation rate, a first series of experiments was performed by electrolyzing 100 mL of solutions containing 1.03 mM of this substrate in 0.050 M Na₂SO₄ at pH 3.0 and at *j* values between 16.7 and 100 mA cm⁻² for 360 min. This acidic pH was chosen for two reasons: (i) to oxidize the neutral form of the molecule, thereby ensuring mineralization since it prevents from possible polymerizations at the anode, as observed for phenolate ions under alkaline conditions [16,19], and (ii) to work under conditions that are optimal for other promising EAOPs, like those based on Fenton's reaction chemistry [12,13], which will be comparatively investigated in the near future. In all these trials, the solution pH remained practically unchanged, becoming slightly more acidic up to 2.6–2.7 probably because of the formation of large quantities of acidic by-products like short-chain aliphatic carboxylic acids [13,29].

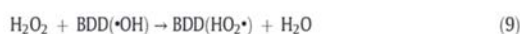
Fig. 1a shows the TOC-time plots obtained for the above assays. A progressive TOC abatement when prolonging electrolysis can be observed in all cases, as expected from the effective mineralization of the parent molecule and its by-products caused by physisorbed BDD(•OH). Moreover, data of Fig. 1a show that increasing *j* from 16.7 to 100 mA cm⁻² yielded a greater TOC decay with the consequent enhancement of the oxidation power of the AO-H₂O₂ process. This tendency can also be deduced from Table 1, where the percentage of TOC removal after 120 and 360 min of electrolysis is summarized. The highest mineralization with 95.5% TOC decay was then found for the greatest *j* of 100 mA cm⁻², whereas TOC was only reduced by 69.1% at the lowest *j* of 16.7 mA cm⁻². The enhancement of TOC abatement at higher *j* can be simply explained by the concomitant acceleration of all electrode reactions, giving rise to a greater quantity of the main oxidant BDD(•OH) from reaction (1), as well as of other weaker oxidants like H₂O₂ from reaction (2).

A look to Fig. 1a reveals an exponential TOC decay for all trials, suggesting that the mineralization process obeyed a pseudo-first-order kinetics, since it was limited by a constant low content of generated oxidants and controlled by mass transport of reactants toward the anode. This behavior was corroborated by representing the corresponding ln(TOC₀/TOC) values versus the electrolysis time, yielding good straight lines as presented in Fig. 1b. The slope of these correlations corresponds to the pseudo-first-order rate constant for TOC removal (*k*_{TOC}), which acquired growing values of 3.4 × 10⁻³, 3.9 × 10⁻³, 6.6 × 10⁻³ and 7.9 × 10⁻³ min⁻¹ for increasing *j* of 16.7, 33.3, 66.7 and 100 mA cm⁻², respectively. The square of the regression coefficient

(R^2) for all these fittings was >0.99 . From these k_{TOC} values, one can infer that the apparent rate constant was upgraded only 2.40-fold when working at 16.7 and 100 mA cm^{-2} , respectively (6-fold increase). This is indicative of a loss in process efficiency at greater j . This point was confirmed from the MCE values calculated from Eq. (5).

The MCE-time curves related to the experiments shown in Fig. 1a are depicted in Fig. 2a. As can be seen, the current efficiency for the AO- H_2O_2 degradation of the 1.03 mM 4-hydroxyphenylacetic acid solution underwent a progressive decrease as j increased. This tendency can also be observed in the MCE values after 120 and 360 min of electrolysis given in Table 1. The most efficient process then occurred at the lowest j of 16.7 mA cm^{-2} , which reached a maximal of 28.4% at 60 min to be further reduced to 21.9% at the end of treatment. Fig. 2a also evidences a greater decay of MCE at long electrolysis time when j became higher. This effect can be ascribed to the progressive disappearance of organic matter in solution, as will be discussed below, along with the formation of by-products that are more hardly destroyed by BDD($\bullet\text{OH}$). This loss in current efficiency is in contrast to the enhancement of the mineralization rate of 4-hydroxyphenylacetic acid with increasing j , and it can be associated with the acceleration of parasitic reactions of BDD($\bullet\text{OH}$). This leads to a smaller generation of available amounts of this oxidant, with the consequent waste of current in reactions that do not contribute to the destruction of organics. The most important of such parasitic reactions is the oxidation of BDD($\bullet\text{OH}$) to O_2 gas via reaction (7), although the dimerization of this radical to H_2O_2 from reaction (8) and its destruction by the latter species from reaction (9) can occur as well [13, 21,26,27]. Apart from the partial destruction of the excess of BDD($\bullet\text{OH}$) produced at higher j under the action of reactions (7)–(9), the larger production of other weaker oxidants at the BDD anode like

the peroxodisulfate ($\text{S}_2\text{O}_8^{2-}$) ion from the oxidation of SO_4^{2-} ion from the electrolyte via reaction (10) and ozone via reaction (11) also reduces the oxidation power of the AO- H_2O_2 process [12,16,18].



The EC_{TOC} is another key parameter to characterize the viability of AO- H_2O_2 for 4-hydroxyphenylacetic acid degradation since cost-effective processes are needed for practical application. For the above trials, Fig. 2b highlights the expected rise in EC_{TOC} determined from Eq. (6) when j increased, as a result of the concomitant growth of E_{cell} . Results of Table 1 also evidence that the specific energy consumption remained practically constant at $j = 16.7 \text{ mA cm}^{-2}$, slightly increasing with electrolysis time at $j = 33.3 \text{ mA cm}^{-2}$ and undergoing a much larger increase at 66.7 and 100 mA cm^{-2} . At this latter j , the final EC_{TOC} value was as high as 4.30 kWh (g TOC)^{-1} , in contrast to 0.325 kWh (g TOC)^{-1} found at $j = 16.7 \text{ mA cm}^{-2}$.

The aforementioned findings demonstrate that the use of low j values is preferable for the AO- H_2O_2 degradation of the 1.03 mM 4-hydroxyphenylacetic acid solution tested, although lower mineralization was achieved compared to that at high j values. Since in Spain the price of the industrial electrical energy is 0.092 € (kWh)^{-1} on average, the cost of the cheapest treatment after 360 min at the lowest j of 16.7 mA cm^{-2} would be around 0.030 € (g TOC)^{-1} , achieving a mineralization of 69.1% with the greatest current efficiency of 29.1%.

3.2. Influence of 4-Hydroxyphenylacetic Acid Concentration on Its Degradation Process

The substrate concentration is an important operation variable that affects the rate of the attack of generated oxidants on organic molecules, which competes with parasitic reactions. The influence of this parameter on the degradation rate for the AO- H_2O_2 treatment of 100 mL of 4-hydroxyphenylacetic acid solutions in 0.050 M Na_2SO_4 at pH 3.0 using a BDD anode was examined for concentrations between 0.21 and 2.06 mM by applying a $j = 33.3 \text{ mA cm}^{-2}$ for 360 min. No significant pH change was observed during these trials, since its value only decreased to 2.6–2.7 due to the formation of acidic by-products, as pointed out above.

Fig. 3a depicts the TOC decay determined for these assays versus the electrolysis time and Table 1 summarizes the percentage of TOC removal at selected times of 120 and 360 min. Different degradation rates can be observed depending on substrate content despite that the same quantity of BDD($\bullet\text{OH}$) was always expected to be generated from reaction (1) at $j = 33.3 \text{ mA cm}^{-2}$. For the lowest content (0.21 mM), the solution was very poorly degraded, especially at the beginning of the process, and its TOC was only reduced by 67.6% after 360 min. This suggests a large influence of parasitic reactions (7)–(9), significantly diminishing the amount of BDD($\bullet\text{OH}$) that is available to react with the low quantity of organic matter present in solution. In contrast, when the concentration was increased to 0.51 mM, the percentage of TOC decay was strongly upgraded (see Table 1), indicating a more effective mineralization of organics by BDD($\bullet\text{OH}$) as a result of the deceleration of reactions (7)–(9). Further treatment of more concentrated solutions up to 2.06 mM caused a progressive drop of the percentage

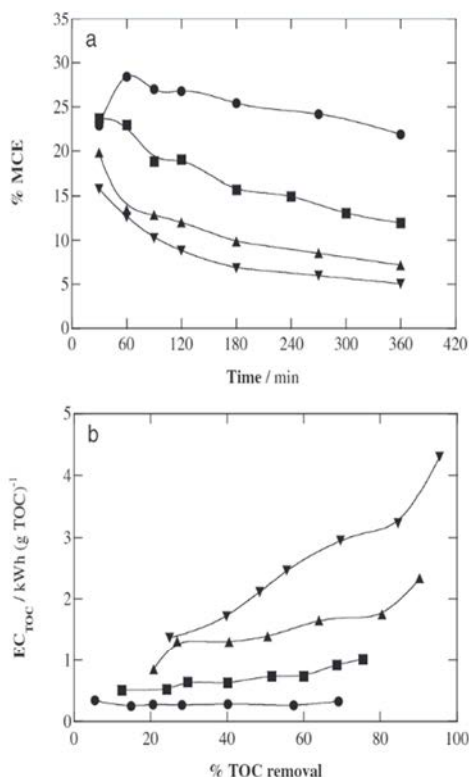


Fig. 2. (a) Mineralization current efficiency vs. electrolysis time and (b) specific energy consumption per unit TOC mass vs. percentage of TOC removal for the trials of Fig. 1.

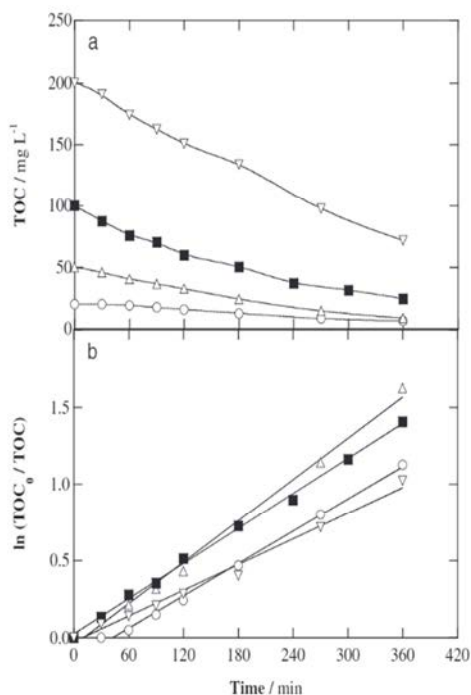


Fig. 3. (a) Influence of pollutant concentration on TOC abatement with electrolysis time for the degradation of 100 mL of 4-hydroxyphenylacetic acid solutions in 0.050 M Na_2SO_4 at pH 3.0 by $\text{AO-H}_2\text{O}_2$ using a BDD/air-diffusion cell at 33.3 mA cm^{-2} and 35°C . (b) Analysis for TOC decay assuming a pseudo-first-order kinetics. 4-Hydroxyphenylacetic acid content: (○) 0.21 mM, (Δ) 0.51 mM, (■) 1.03 mM and (▽) 2.06 mM.

of TOC decay, as can be seen in Table 1, although a larger amount of TOC was gradually removed due to the faster oxidation of organics with greater quantities of available BDD($\cdot\text{OH}$) thanks to the gradual decay in rate of parasitic reactions (7)–(9).

The good linear correlations related to the pseudo-first-order kinetics of TOC abatement for the experiments of Fig. 3a are depicted in Fig. 3b. It should be noted that in the case of 0.21 mM, the linear trend between $\ln(\text{TOC}_0/\text{TOC})$ and electrolysis time started from about 60 min of the $\text{AO-H}_2\text{O}_2$ treatment because no significant mineralization was found at shorter time. The k_{TOC} value under these conditions was $3.5 \times 10^{-3} \text{ min}^{-1}$ ($R^2 = 0.996$), which increased to $4.9 \times 10^{-3} \text{ min}^{-1}$ ($R^2 = 0.990$) for 0.51 mM due to the larger oxidation action of BDD($\cdot\text{OH}$). In contrast, the presence of higher 4-hydroxyphenylacetic acid concentration caused a gradual drop in k_{TOC} , with values of $3.8 \times 10^{-3} \text{ min}^{-1}$ ($R^2 = 0.996$) for 1.03 mM and $2.8 \times 10^{-3} \text{ min}^{-1}$ ($R^2 = 0.990$) for 2.06 mM, because a lower TOC_0/TOC ratio was obtained despite the removal of greater amounts of TOC.

The enhancement of the oxidation power of the $\text{AO-H}_2\text{O}_2$ process with increasing substrate concentration at constant j for the above trials can be more easily deduced from the change of the corresponding MCE values. Fig. 4a highlights that the current efficiency underwent a progressive rise as 4-hydroxyphenylacetic acid content grew from 0.21 to 2.06 mM. This behavior can be pre-eminently accounted for by the more efficient action of reactive physisorbed BDD($\cdot\text{OH}$) due to the deceleration of its parasitic reactions (7)–(9), as stated above. For the most concentrated solution, the MCE value decayed from a maximal value of 24.8% at 60 min to 20.3% at the end of treatment (see Table 1). A drop of current efficiency from 23.7% at 30 min to 11.9% at 360 min was also determined for 1.03 mM, whereas it decreased from 9.1% at 60 min as maximal to a final value of 6.5% for 0.51 mM. In contrast, an MCE value near 2.1% was found for 0.21 mM (see Table 1). These findings corroborate that the decay in current efficiency when

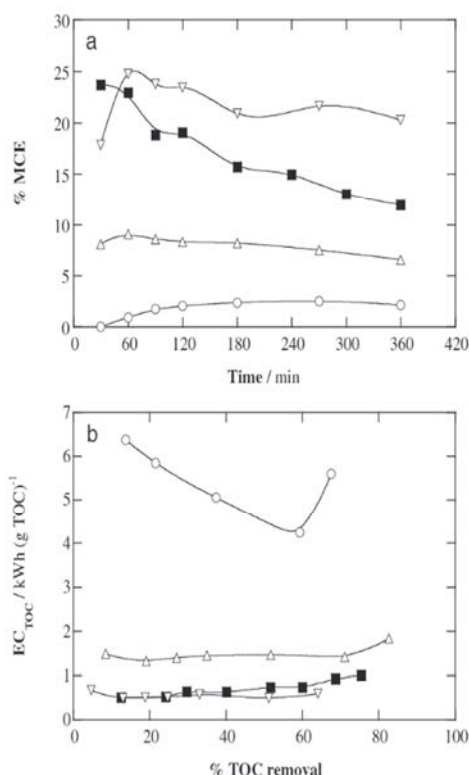


Fig. 4. (a) Time course of mineralization current efficiency and (b) variation of specific energy consumption per unit TOC mass with percentage of TOC removal for the assays of Fig. 3.

prolonging the electrolysis for substrate concentrations ≥ 0.51 mM, shown in Fig. 2a and 4a, is mainly due to the loss of organic matter in solution, although it can be influenced by the gradual formation of more recalcitrant products that makes the degradation process slower.

The very small oxidation power of $\text{AO-H}_2\text{O}_2$ to mineralize the solution of 0.21 mM 4-hydroxyphenylacetic acid was also reflected in the very high EC_{TOC} values required, ranging between 4.3 and 6.4 kWh (g TOC)^{-1} , to attain 67.6% of TOC removal, as can be seen in Fig. 4b. This figure, as well as the data collected in Table 1, shows a gradual reduction of the specific energy consumption when going up to the maximum content of 2.06 mM, which led to a final value of 0.590 kWh (g TOC)^{-1} to remove 64.1% of TOC. These results allow concluding that higher substrate contents are preferable to be mineralized by $\text{AO-H}_2\text{O}_2$ since they lead to greater MCE and lower EC_{TOC} values, but with smaller mineralization of treated solutions.

3.3. Decay Kinetics of 4-Hydroxyphenylacetic Acid

The kinetics of the reaction between 4-hydroxyphenylacetic acid and generated BDD($\cdot\text{OH}$) was followed by reversed-phase HPLC, where this compound presented a well-defined peak. Fig. 5a illustrates the exponential concentration decay for a 1.03 mM substrate solution in 0.050 M Na_2SO_4 at pH 3.0 treated by $\text{AO-H}_2\text{O}_2$ with a BDD anode at $j = 33.3 \text{ mA cm}^{-2}$. Total removal was achieved after approximately 360 min of electrolysis, meaning that the 24.5% of the initial TOC remaining in solution at that time (see Fig. 1a) is due to the accumulated by-products, which are more recalcitrant than the parent molecule. The drop of substrate concentration was well-fitted to a pseudo-first-order kinetic equation, as shown in Fig. 5b. A pseudo-first-order rate constant

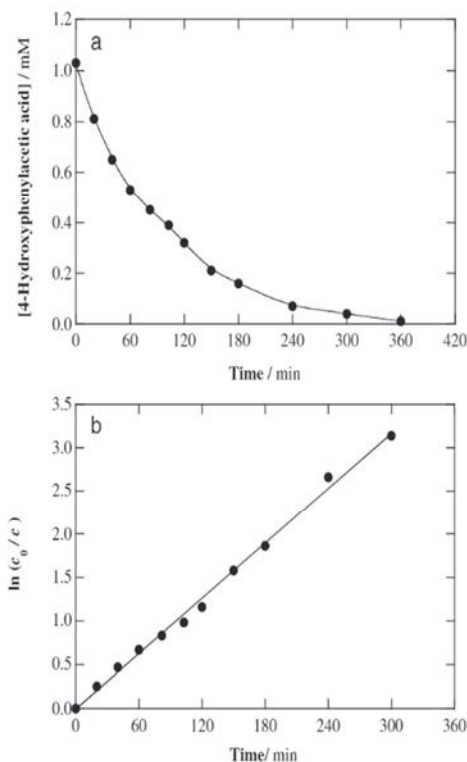


Fig. 5. (a) Decay of 4-hydroxyphenylacetic acid concentration with electrolysis time for the degradation of 100 mL of a 1.03 mM pollutant solution in 0.050 M Na_2SO_4 at pH 3.0 and 35 °C by AO- H_2O_2 using a BDD/air-diffusion cell at 33.3 mA cm^{-2} . (b) Kinetic analysis assuming a pseudo-first-order reaction for 4-hydroxyphenylacetic acid.

(k_1) of $1.0 \times 10^{-2} \text{ min}^{-1}$, with $R^2 = 0.995$, was then determined as slope of the excellent linear trend obtained.

The aforementioned behavior suggests the attack of a constant BDD($\cdot\text{OH}$) concentration on 4-hydroxyphenylacetic acid. This is feasible by the short lifetime of this radical ($\approx 10^{-9} \text{ s}$ [13]) that allows the

presence of a very small steady-state concentration during the AO- H_2O_2 process. Accordingly, the reaction rate (r) between BDD($\cdot\text{OH}$) and the molecule obeys a second-order kinetics, expressed as follows:

$$r = k_2[\text{BDD}(\cdot\text{OH})][\text{R}] = k_1[\text{R}] \quad (12)$$

where $k_2 (= k_1/[\text{BDD}(\cdot\text{OH})])$ is the absolute or second-order rate constant and R symbolizes the 4-hydroxyphenylacetic acid tested. Taking into account that a k_2 value of $7.02 \times 10^8 \text{ M}^{-1} \text{ s}^{-1}$ has been determined for this reaction [11], one can estimate the generation of an average BDD($\cdot\text{OH}$) concentration ($= k_1/k_2$) of near $2.4 \times 10^{-13} \text{ M}$. This radical is expected to act within a small volume near the anode surface owing to its very low adsorption on BDD [16].

3.4. Identification and Evolution of By-products

Table 2 collects the organic products detected by GC-MS for short electrolysis times during the AO- H_2O_2 treatment of a 1.03 mM 4-hydroxyphenylacetic acid solution at pH 3.0 with a BDD anode. Apart from the parent molecule, two primary aromatic by-products (4-hydroxybenzenemethanol and 4-hydroxybenzaldehyde) and one final aliphatic carboxylic acid (acetic acid) were identified by means of this technique. One can then establish that the initial attack of BDD($\cdot\text{OH}$) yields the decarboxylation with hydroxylation of 4-hydroxyphenylacetic acid to produce the diol 4-hydroxybenzenemethanol, which is in turn oxidized to 4-hydroxybenzaldehyde. On the other hand, acetic acid is a final aliphatic carboxylic acid that proceeds from the oxidation of aromatic intermediates with cleavage of their benzenic ring [12,29,39].

The evolution of final carboxylic acids was also followed by ion-exclusion HPLC. These chromatograms only displayed traces of acetic acid ($<0.001 \text{ mM}$), the final by-product identified by GC-MS, at $t_r = 14.9 \text{ min}$. In contrast, they revealed the presence of great amounts of oxalic acid, a usual final aliphatic carboxylic acid that can be directly transformed into CO_2 [21,26,33]. Fig. 6 depicts the time course of oxalic acid concentration during the AO- H_2O_2 degradation of a 1.03 mM 4-hydroxyphenylacetic acid solution at $j = 33.3 \text{ mA cm}^{-2}$. As can be seen, it was progressively accumulated up to a maximum concentration of 0.16 mM at 180–240 min, further being slowly removed to 0.071 mM at the end of the electrolysis. A simple mass balance highlights that this acid content corresponds to 1.70 mg L^{-1} of TOC, which only accounts for 6.9% of the total TOC of the remaining solution (see Fig. 1a). This

Table 2

Organic intermediates detected by GC-MS using different columns and preparation methods for samples withdrawn after 30 and 90 min during the AO- H_2O_2 treatment of 100 mL of a 1.03 mM 4-hydroxyphenylacetic acid solution in 0.050 M Na_2SO_4 at pH 3.0 using a BDD/air-diffusion cell at 33.3 mA cm^{-2} and 35 °C.

Compound	Molecular structure	Electrolysis time (min)	Column	t_r^a (min)	Main fragmentation ions (m/z)
4-Hydroxyphenylacetic acid		30 ^b	Polar	63.7	152, 107, 77
		30 ^b , 30 ^c	Non-polar	26.3	
4-Hydroxybenzenemethanol		30 ^c	Non-polar	20.9	124, 107, 95, 77
4-Hydroxybenzaldehyde		30 ^b , 90 ^c	Polar	43.3	121, 93, 65
		30 ^c , 90 ^c	Non-polar	21.4	
Acetic acid		30 ^b	Polar	15.3	60, 43

^a Retention time.

^b Lyophilized sample.

^c Extraction with CH_2Cl_2 .

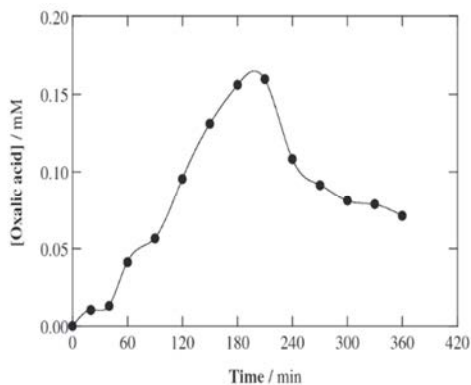


Fig. 6. Evolution of the concentration of oxalic acid detected during the AO-H₂O₂ treatment shown in Fig. 5.

means that the final solution contained a large proportion of unidentified products that are even more hardly oxidized by BDD(•OH) than final aliphatic carboxylic acids.

4. Conclusions

It has been shown that 100 mL of a 1.03 mM 4-hydroxyphenylacetic acid solution in sulfate medium at pH 3.0 can be almost totally mineralized upon AO-H₂O₂ treatment with a BDD/air-diffusion cell. The use of a lower j yielded a lower mineralization, but the process was more cost-effective. The best results were found at $j = 16.7 \text{ mA cm}^{-2}$, leading to 21.9% of current efficiency with $0.325 \text{ kWh (g TOC)}^{-1}$, but with only 67.6% of TOC removal. The efficiency of the process was upgraded and the specific energy consumption became lower when the substrate concentration was increased, although a smaller mineralization was attained. The oxidation role of BDD(•OH) was then a function of its electrogeneration rate at the anode, governed by j , and the extent of its parasitic reactions. TOC removal and substrate concentration decay obeyed a pseudo-first-order kinetics since they were limited by the amount of reactive BDD(•OH) and the mass transport of organics toward the BDD anode. 4-Hydroxybenzenemethanol and its oxidation product 4-hydroxybenzenaldehyde were found as primary aromatic by-products. Ion-exclusion chromatograms revealed the accumulation of low contents of oxalic acid that persist during all the process, highlighting that the final treated solutions contained a large proportion of unidentified, recalcitrant by-products.

Acknowledgements

Financial support from project CTQ2013-48897-C2-1-R (MINECO, FEDER, EU) and the PhD fellowship awarded to N. Flores by SENESCYT (Ecuador) are acknowledged.

References

- [1] S. Magdich, C. Ben Ahmed, R. Jarbouli, B. Ben Rouina, M. Boukhris, E. Ammar, Dose and frequency dependent effects of olive mill wastewater treatment on the chemical and microbial properties of soil, *Chemosphere* 93 (2013) 1896–1903.
- [2] S. Dermeche, M. Nadour, C. Larroche, F. Mouti-Mati, P. Michaud, Olive mill wastes: biochemical characterizations and valorization strategies, *Process Biochem.* 48 (2013) 1532–1552.
- [3] M. DellaGrecia, L. Previtiera, F. Temussi, A. Zarrelli, Low-molecular-weight components of olive oil mill waste-waters, *Phytochem. Anal.* 15 (2004) 184–188.
- [4] J.M. Ochando-Pulido, M.D. Victor-Ortega, G. Hodaifa, A. Martinez-Ferez, Physico-chemical analysis and adequation of olive oil mill wastewater after advanced oxidation process for reclamation by pressure-driven membrane technology, *Sci. Total Environ.* 503–504 (2014) 113–121.
- [5] D. Pham Minh, P. Gallezot, S. Azabou, S. Sayadi, M. Besson, Catalytic wet air oxidation of olive oil mill effluents, *Appl. Catal. B Environ.* 84 (2008) 749–757.

- [6] C. Belaid, M. Kallel, M. Khadhraou, G. Lalleve, B. Elleuch, J.F. Fauvarque, Electrochemical treatment of olive mill wastewaters: removal of phenolic compounds and decolorization, *J. Appl. Electrochem.* 36 (2006) 1175–1182.
- [7] C. Belaid, M. Khadhraoui, S. Mseddi, M. Kallel, B. Elleuch, J.F. Fauvarque, Electrochemical treatment of olive mill wastewater: treatment extent and effluent phenolic compounds monitoring using some uncommon analytical tools, *J. Environ. Sci.* 25 (2013) 220–230.
- [8] P.P. Liebgott, M. Labat, A. Amouric, J.L. Tholozan, J. Lorquin, Tyrosol degradation via the homogenous acid pathway in a newly isolated *Halomonas* strain from olive processing effluents, *J. Appl. Microbiol.* 105 (2008) 2084–2095.
- [9] S. Ammar, M.A. Oturan, L. Labiadh, A. Guersalli, R. Abdelhedi, N. Oturan, E. Brillas, Degradation of tyrosol by a novel electro-Fenton process using pyrite as heterogeneous source of iron catalyst, *Water Res.* 74 (2015) 77–87.
- [10] I. Sanchez, F. Stueber, A. Fabregat, J. Font, A. Fortuny, C. Bengoa, Degradation of model olive mill contaminants of OMW catalysed by zero-valent iron enhanced with a chelant, *J. Hazard. Mater.* 199–200 (2012) 328–335.
- [11] F.J. Benitez, J.L. Acero, F.J. Real, F.J. Rubio, A. Leal, The role of hydroxyl radicals for the decomposition of *p*-hydroxy phenylacetic acid in aqueous solutions, *Water Res.* 35 (2001) 1338–1343.
- [12] I. Sirés, E. Brillas, Remediation of water pollution caused by pharmaceutical residues based on electrochemical separation and degradation technologies: a review, *Environ. Int.* 40 (2012) 212–229.
- [13] I. Sirés, E. Brillas, M.A. Oturan, M.A. Rodrigo, M. Panizza, Electrochemical advanced oxidation processes: today and tomorrow. A review, *Environ. Sci. Pollut. Res.* 21 (2014) 8336–8367.
- [14] A. Thiam, I. Sirés, J.A. Garrido, R.M. Rodríguez, E. Brillas, Decolorization and mineralization of Allura Red AC aqueous solutions by electrochemical advanced oxidation processes, *J. Hazard. Mater.* 290 (2015) 34–42.
- [15] A. Thiam, I. Sirés, F. Centellas, P.L. Cabot, E. Brillas, Decolorization and mineralization of Allura Red AC azo dye by solar photoelectro-Fenton: identification of intermediates, *Chemosphere* 136 (2015) 1–8.
- [16] M. Panizza, G. Cerisola, Direct and mediated anodic oxidation of organic pollutants, *Chem. Rev.* 109 (2009) 6541–6569.
- [17] S. Vasudevan, M.A. Oturan, Electrochemistry: as cause and cure in water pollution—an overview, *Environ. Chem. Lett.* 12 (2014) 97–108.
- [18] B. Boye, P.A. Michaud, B. Marselli, M.M. Dieng, E. Brillas, C. Cominellis, Anodic oxidation of 4-chlorophenoxyacetic acid on synthetic boron-doped diamond electrodes, *New Diamond Front. Carbon Technol.* 12 (2002) 63–72.
- [19] B. Marselli, J. Garcia-Gomez, P.A. Michaud, M.A. Rodrigo, C. Cominellis, Electrogeneration of hydroxyl radicals on boron-doped diamond electrodes, *J. Electrochem. Soc.* 150 (2003) D79–D83.
- [20] P. Cañizares, J. Lobato, R. Paz, M.A. Rodrigo, C. Sáez, Electrochemical oxidation of phenolic compound wastes with BDD anodes, *Water Res.* 39 (2005) 2687–2703.
- [21] E. Brillas, I. Sirés, C. Arias, P.L. Cabot, F. Centellas, R.M. Rodríguez, J.A. Garrido, Mineralization of paracetamol in aqueous medium by anodic oxidation with a boron-doped diamond electrode, *Chemosphere* 58 (2005) 399–406.
- [22] A. Özcan, Y. Şahin, A.S. Kopalal, M.A. Oturan, Prophan mineralization in aqueous medium by anodic oxidation using boron-doped diamond anode. Experimental parameters' influence on degradation kinetics and mineralization efficiency, *Water Res.* 42 (2008) 2889–2898.
- [23] V. Santos, J. Diogo, M.J.A. Pacheco, L. Ciriaco, A. Morão, A. Lopes, Electrochemical degradation of sulfonated amines on Si/BDD electrodes, *Chemosphere* 79 (2010) 637–645.
- [24] M.A. Rodrigo, P. Cañizares, A. Sánchez-Carretero, C. Sáez, Use of conductive-diamond electrochemical oxidation for wastewater treatment, *Catal. Today* 151 (2010) 173–177.
- [25] N. Oturan, E. Brillas, M.A. Oturan, Unprecedented total mineralization of atrazine and cyanuric acid by anodic oxidation and electro-Fenton with a boron-doped diamond anode, *Environ. Chem. Lett.* 10 (2012) 165–170.
- [26] A. El-Ghenymy, J.A. Garrido, R.M. Rodríguez, P.L. Cabot, F. Centellas, C. Arias, E. Brillas, Degradation of sulfanilamide in acidic medium by anodic oxidation with a boron-doped diamond anode, *J. Electroanal. Chem.* 689 (2013) 149–157.
- [27] C.I. Brinzila, N. Monterio, M.J. Pacheco, L. Ciriaco, I. Siminiceanu, A. Lopes, Degradation of tetracycline at a boron-doped diamond anode: influence of initial pH, applied current intensity and electrolyte, *Environ. Sci. Pollut. Res.* 21 (2014) 8457–8465.
- [28] E.V. dos Santos, C. Sáez, C.A. Martínez-Huitle, P. Cañizares, M.A. Rodrigo, The role of particle size on the conductive diamond electrochemical oxidation of soil-washing effluent polluted with atrazine, *Electrochem. Commun.* 55 (2015) 26–29.
- [29] A. Bedolla-Guzman, I. Sirés, A. Thiam, J.M. Peralta-Hernández, S. Gutiérrez-Granados, E. Brillas, Application of anodic oxidation, electro-Fenton and UVA photoelectro-Fenton to decolorize and mineralize acidic solutions of Reactive Yellow 160 azo dye, *Electrochim. Acta* 206 (2016) 307–316.
- [30] P. Cañizares, R. Paz, C. Sáez, M.A. Rodrigo, Electrochemical oxidation of alcohols and carboxylic acids with diamond anodes. A comparison with other advanced oxidation processes, *Electrochim. Acta* 53 (2008) 2144–2153.
- [31] I. Sirés, P.L. Cabot, F. Centellas, J.A. Garrido, R.M. Rodríguez, C. Arias, E. Brillas, Electrochemical degradation of clofibrac acid in water by anodic oxidation. Comparative study with platinum and boron-doped diamond electrodes, *Electrochim. Acta* 52 (2006) 75–85.
- [32] M. Hamza, R. Abdelhedi, E. Brillas, I. Sirés, Comparative electrochemical degradation of the triphenylmethane dye Methyl Violet with boron-doped diamond and Pt anodes, *J. Electroanal. Chem.* 627 (2009) 41–50.
- [33] E.B. Cavalcanti, S. Garcia-Segura, F. Centellas, E. Brillas, Electrochemical incineration of omeprazole in neutral aqueous medium using a platinum or boron-doped diamond. Degradation kinetics and oxidation products, *Water Res.* 47 (2013) 1803–1815.

- [34] L. Ciriaco, C. Anjo, J. Correia, M.J. Pacheco, A. Lopes, Electrochemical degradation of ibuprofen on Ti/Pt/PbO₂ and Si/BDD electrodes, *Electrochim. Acta* 54 (2009) 1464–1472.
- [35] K. Cruz-González, O. Torres-López, A. García-León, E. Brillas, A. Hernández-Ramírez, J.M. Peralta-Hernández, Optimization of electro-Fenton/BDD process for decolorization of a model azo dye wastewater by means of response surface methodology, *Desalination* 286 (2012) 63–68.
- [36] A. Wang, J. Qu, H. Liu, J. Ru, Mineralization of an azo dye Acid Red 14 by photoelectro-Fenton process using an activated carbon fiber cathode, *Appl. Catal. B Environ.* 84 (2008) 393–399.
- [37] A. Khataee, A. Akbarpour, B. Vahi, Photoassisted electrochemical degradation of an azo dye using Ti/RuO₂ anode and carbon nanotubes containing gas-diffusion cathode, *J. Taiwan Inst. Chem. Eng.* 45 (2014) 930–936.
- [38] N. Daneshvar, S. Aber, V. Vatanpour, M.H. Rasoulifard, Electro-Fenton treatment of dye solution containing Orange II: influence of operational parameters, *J. Electroanal. Chem.* 615 (2008) 165–174.
- [39] A. Dirany, I. Sirés, N. Oturan, A. Özcan, M.A. Oturan, Electrochemical treatment of the antibiotic sulfachloropyridazine: kinetics, reaction pathways, and toxicity evolution, *Environ. Sci. Technol.* 46 (2012) 4074–4082.
- [40] A. El-Ghenemy, R.M. Rodríguez, E. Brillas, N. Oturan, M.A. Oturan, Electro-Fenton degradation of the antibiotic sulfanilamide with Pt/carbon-felt and BDD/carbon-felt cells. Kinetics, reaction intermediates, and toxicity assessment, *Environ. Sci. Pollut. Res.* 21 (2014) 8368–8378.
- [41] M.S. Yahya, N. Oturan, K. El Kacemi, M. El Karbane, C.T. Aravindakumar, M.A. Oturan, Oxidative degradation study on antimicrobial agent ciprofloxacin by electro-Fenton process: kinetics and oxidation products, *Chemosphere* 117 (2014) 447–454.
- [42] I. Sirés, F. Centellas, J.A. Garrido, R.M. Rodríguez, C. Arias, P.L. Cabot, E. Brillas, Mineralization of clofibrac acid by electrochemical advanced oxidation processes using a boron-doped diamond anode and Fe²⁺ and UVA light as catalysts, *Appl. Catal. B Environ.* 72 (2007) 373–381.
- [43] E.J. Ruiz, A. Hernández-Ramírez, J.M. Peralta-Hernández, C. Arias, E. Brillas, Application of solar photoelectro-Fenton technology to azo dyes mineralization: Effect of current density, Fe²⁺ and dye concentrations, *Chem. Eng. J.* 171 (2011) 385–392.

8. MINERALIZACIÓN DEL ÁCIDO 4-HIDROXIFENILACÉTICO EN OOMW



Publicación 4:

4-Hydroxyphenylacetic acid oxidation in sulfate and real olive oil mill wastewater by electrochemical advanced processes with a boron-doped diamond anode

Este último trabajo presenta la mineralización de disoluciones del ácido 4-hidroxifenilacético mediante oxidación anódica con H_2O_2 electrogenerado (OA- H_2O_2), electro-Fenton (EF) y fotoelectro-Fenton (FEF) en diferentes matrices. Los experimentos se llevaron a cabo en un reactor de tanque agitado con un ánodo de diamante dopado con boro (BDD) y un cátodo de difusión de aire, ambos de 3 cm^2 . Se electrolizaron 100 mL de disoluciones de concentración de 0,21 a 2,1 mM de este compuesto en Na_2SO_4 0,050 M como electrolito a pH 3,0 y $35 \text{ }^\circ\text{C}$, a densidades de corriente constante entre 16,7 y 100 mA cm^{-2} . Se añadió una concentración 0,50 mM de Fe^{2+} como catalizador de la reacción de Fenton para los procesos EF y FEF. Se usó además una lámpara de luz UVA de 6 W para el proceso FEF. Con el objetivo de estudiar la viabilidad de estos EAOPs para el tratamiento de aguas reales, se estudió el efecto de la matriz sobre la degradación del ácido 4-hidroxifenilacético añadiendo 1,03 mM de ácido 4-hidroxifenilacético a mezclas de OOMW/agua con porcentajes desde el 20% al 100% v/v de OOMW, que se electrolizaron a $16,7 \text{ mA cm}^{-2}$ durante 540 min.

Los experimentos con disoluciones de 1,03 mM del ácido en Na_2SO_4 0,050 M a $j = 16,7 \text{ mA cm}^{-2}$ exhibieron una reducción gradual del TOC durante 360 min (ver Figura 1 y 2), alcanzando un máximo del 69%, 86% y 98% mediante OA- H_2O_2 , EF y FEF, respectivamente. Ello indica que el FEF fue el tratamiento más eficaz para eliminar el TOC presente en el medio. Este comportamiento está relacionado con los agentes reactivos en cada método: BDD($\cdot\text{OH}$) en OA- H_2O_2 , los radicales $\cdot\text{OH}$ adicionales producidos por la reacción de Fenton (12) en EF, y los fotones UV que causan la fotólisis y fotorreducción de complejos de Fe(III) en FEF.

La influencia de j se evaluó para una disolución acuosa que contenía 1,03 mM del ácido, aumentándose desde 16,7 a 100 mA cm^{-2} . La Figura 2 revela que se producía una mayor eliminación del TOC a mayores valores de j . En EF, por ejemplo, se obtuvo un 85,7%, 90,1%, 93,5% y 94,8% de reducción del TOC a 16,7, 33,3, 66,7 y 100 mA cm^{-2} , respectivamente. La misma tendencia se observó para el FEF, pero con mineralizaciones superiores al 97,5% a todas las j aplicadas. El proceso FEF eliminaba más rápidamente los contaminantes por la mayor formación de intermedios fotosensibles que se mineralizaban más velozmente por la luz UVA.

Los resultados de MCE de la Figura 3 presentan una caída de los valores de eficiencia con el aumento de j para todos los procesos. En todos los casos, la MCE disminuía casi exponencialmente a lo largo de los últimos 180 min de electrólisis debido a la pérdida de carga orgánica y a la formación de subproductos recalcitrantes. Esta relación entre MCE y j puede asociarse a la aceleración de reacciones parasitarias tales como (51)-(53).

Los resultados de los ensayos para el aumento del contenido de substrato de 0,21 a 2,1 mM a $j = 33,3 \text{ mA cm}^{-2}$ de la Figura 4 confirmaron de nuevo que el proceso FEF era el tratamiento más eficaz para eliminar el ácido 4-hidroxifenilacético, lográndose una mineralización de hasta del 98%. A los 360 min, el TOC decreció hasta en un 72,1% y 79,3% en EF y un 92,2% y 88,8% en FEF para 0,21 y 2,1 mM de ácido, respectivamente.

La reacción del ácido 4-hidroxifenilacético con los oxidantes generados se siguió mediante HPLC de fase inversa (ver Figura 6). La concentración inicial de 1,03 mM del ácido decayó exponencialmente al ser tratadas las disoluciones mediante EF y FEF a $33,3 \text{ mA cm}^{-2}$. El ácido 4-hidroxifenilacético desapareció a los 60 min

en EF y a los 45 min en FEF, indicando que la oxidación se debió principalmente a los radicales $\bullet\text{OH}$ en el medio acrecentada por la acción fotolítica de luz UVA sobre las especies $\text{Fe}(\text{OH})^{2+}$ en el proceso FEF. La destrucción del ácido siguió una cinética de pseudo-primer orden con una k_1 de 1.4×10^{-3} y $1.9 \times 10^{-3} \text{ s}^{-1}$ para el EF y el FEF. Esto sugiere que el ácido 4-hidroxifenilacético era atacado preferencialmente por una concentración constante y baja de $\bullet\text{OH}$ originada en el medio por la reacción de Fenton (12).

Se cuantificó la acumulación de ácido oxálico durante los tratamientos EF y FEF del ácido 4-hidroxifenilacético por HPLC de exclusión iónica. Se encontró que para un contenido de 1,03 mM a $33,3 \text{ mA cm}^{-2}$, este ácido era completamente mineralizado a tiempos ≥ 270 min en ambos casos.

El siguiente paso consistió en estudiar la mineralización del ácido 4-hidroxifenilacético en disoluciones que contenían OOMW. La muestra fue suministrada por una empresa local de extracción de aceite de oliva y se filtró con una malla de $18 \mu\text{m}$. Su caracterización se resume en la Tabla 1. El análisis de GC-MS reveló la presencia de varios compuestos fenólicos, el ácido 4-hidroxifenilacético, un alcohol heteroalifático, así como 4 ácidos carboxílicos aromáticos y 4 alifáticos (1 cíclico y 3 lineales), que se detallan en la Tabla 2.

Al tratar la OOMW filtrada a $j = 16,7 \text{ mA cm}^{-2}$ se encontraron reducciones del TOC de 71,8% en OA- H_2O_2 , del 79,5% en EF y del 83,4% en FEF. La capacidad de los EAOPs incrementaba en la secuencia OA- $\text{H}_2\text{O}_2 < \text{EF} < \text{FEF}$, de acuerdo con la capacidad oxidante de los radicales BDD($\bullet\text{OH}$) y $\bullet\text{OH}$ generados y/o de la luz UVA. Esto también ocurrió al añadir ácido 4-hidroxifenilacético a la OOMW.

El estudio de la degradación de 1,03 mM de ácido 4-hidroxifenilacético en matrices que contenían OOMW mostró que la eliminación del TOC aumentaba ligeramente cuando disminuía el porcentaje de OOMW. La mineralización más rápida del ácido ocurrió en 20% v/v OOMW, reduciendo el TOC un 82,5% en OA- H_2O_2 , un 83,0% en EF y un 86,4% en FEF. Dado que el TOC inicial disminuyó al diluir la OOMW, puede decirse que todos los tratamientos fueron más eficientes a mayor contenido de carga orgánica debido a la desaceleración de reacciones parásitas.

La cinética de degradación del ácido 4-hidroxifenilacético por HPLC de fase inversa aparentaba ajustarse linealmente a una reacción de pseudo-primer orden en todos los casos (ver Figura 9). El ácido desapareció después de 540 min de OA- H_2O_2 en todas las matrices que contenían OOMW, requiriendo solo 360 min en la matriz de Na_2SO_4 0,050 M. La degradación era más rápida con un menor contenido de compuestos orgánicos en el medio. Los valores de k_1 aumentaron desde $7.3 \times 10^{-5} \text{ s}^{-1}$ en 100% OOMW hasta $2,0 \times 10^{-4} \text{ s}^{-1}$ en Na_2SO_4 0,050 M. En el caso del FEF, el ácido desapareció en sólo 50 min para Na_2SO_4 0,050 M y en 100 min para 100% OOMW con $k_1 = 1.4 \times 10^{-3} \text{ s}^{-1}$. El proceso FEF fue el EAOP más potente para tratar el ácido 4-hidroxifenilacético en cualquier matriz analizada. La rápida mineralización en este método se producía por la acción fotolítica de la radiación UVA sobre subproductos fotoactivos y la eliminación de los complejos de Fe(III)-oxalato formados. El aumento de j aceleraba la mineralización en todos los medios, pero con pérdida de MCE debido a las reacciones parasitarias que consumían los radicales $\bullet\text{OH}$. Al aumentar la carga orgánica aumentaba la capacidad de oxidación de todas las EAOP, con el consiguiente incremento de la MCE. Por último, el proceso FEF también aumentó la biodegradabilidad de las muestras.



4-Hydroxyphenylacetic acid oxidation in sulfate and real olive oil mill wastewater by electrochemical advanced processes with a boron-doped diamond anode



Nelly Flores, Pere Lluís Cabot, Francesc Centellas, José Antonio Garrido, Rosa María Rodríguez, Enric Brillas*, Ignasi Sirés*

Laboratori d'Electroquímica dels Materials i del Medi Ambient, Departament de Química Física, Facultat de Química, Universitat de Barcelona, Martí i Franquès 1-11, 08028 Barcelona, Spain

HIGHLIGHTS

- Degradation of 4-hydroxyphenylacetic acid spiked in 0.050 M Na₂SO₄ and in real OOMW.
- Quicker mineralization in the order AO-H₂O₂ < EF < PEF in all media using a BDD anode.
- Pseudo-first-order decay of 4-hydroxyphenylacetic acid in all treatments.
- Almost total mineralization achieved by the powerful PEF process in 0.050 M Na₂SO₄.
- Up to 80% mineralization with strong biodegradability enhancement in the real OOMW matrix.

ARTICLE INFO

Article history:

Received 3 August 2016
Received in revised form
22 September 2016
Accepted 23 September 2016
Available online 24 September 2016

Keywords:

BDD anode
Electro-Fenton
4-Hydroxyphenylacetic acid
Olive oil mill wastewater
Photoelectro-Fenton

ABSTRACT

The degradation of 4-hydroxyphenylacetic acid, a ubiquitous component of olive oil mill wastewater (OOMW), has been studied by anodic oxidation with electrogenerated H₂O₂ (AO-H₂O₂), electro-Fenton (EF) and photoelectro-Fenton (PEF). Experiments were performed in either a 0.050 M Na₂SO₄ solution or a real OOMW at pH 3.0, using a cell with a boron-doped diamond (BDD) anode and an air-diffusion cathode for H₂O₂ generation. Hydroxyl radicals formed at the BDD surface from water oxidation in all processes and/or in the bulk from Fenton's reaction between added Fe²⁺ and generated H₂O₂ in EF and PEF were the main oxidants. In both matrices, the oxidation ability of the processes increased in the order AO-H₂O₂ < EF < PEF. The superiority of PEF was due to the photolytic action of UVA radiation on photosensitive by-products, as deduced from the quick removal of Fe(III)-oxalate complexes. The effect of current density and organic content on the performance of all treatments was examined. 4-Hydroxyphenylacetic acid decay obeyed a pseudo-first-order kinetics. The PEF treatment of 1.03 mM 4-hydroxyphenylacetic acid in 0.050 M Na₂SO₄ allowed 98% mineralization at 360 min even at low current density, whereas 80% mineralization and a significant enhancement of biodegradability were achieved with the real OOMW.

© 2016 Elsevier B.V. All rights reserved.

1. Introduction

The olive oil produced in Spain and other Mediterranean countries accounts for more than 75% of total world production. This, in turn, entails a huge annual release of industrial olive oil mill wastewater (OOMW). These effluents are usually acidic and extremely hazardous for the aquatic environment due to their very large organic matter contents and high turbidity levels, which cause

a poor oxygenation and light penetration [1,2]. OOMW mainly contains phenols, acids, lipids, sugars and tannins [3,4]. A limited number of works have described the treatment of these effluents by catalytic wet air oxidation [5] and electrolysis with a Pt anode [6,7], showing a significant destruction of phenolic components. More research efforts are then needed to degrade OOMW and its main single components to devise an optimum integral treatment for such industrial wastewater.

4-Hydroxyphenylacetic acid is a typical phenolic component routinely found in OOMW. It is a primary product formed upon oxidation of tyrosol (4-hydroxyphenylethanol), which is a well known phenolic compound in OOMW as well [8,9]. On the other hand,

* Corresponding author.

E-mail addresses: brillas@ub.edu (E. Brillas), lsires@ub.edu (I. Sirés).

4-hydroxyphenylacetic acid is useful for the industrial synthesis of various end products like the β -blocker atenolol, among others. However, the information on its degradation routes and fate in the field of wastewater treatment is scarce. The removal of 4-hydroxyphenylacetic acid by advanced oxidation processes (AOPs) like zero-valent iron [10] and UV/H₂O₂ and Fenton's reagent [11] has been reported. Conversely, as far as we know, its destruction by powerful electrochemical AOPs (EAOPs) has not been reported yet.

Over the last fifteen years, the EAOPs have received increasing attention to remove toxic and/or non-biodegradable organic pollutants from wastewater [12–15]. These methods are particularly viable owing to their environmental compatibility, high energy efficiency, versatility, amenability of automation, safe operation under mild conditions and easy scale-up. The great oxidation power of EAOPs is based on the continuous in situ generation of reactive oxygen species (ROS) like hydroxyl radical ($\cdot\text{OH}$), the second strongest oxidant known after fluorine. A high standard reduction potential ($E^\circ(\cdot\text{OH}/\text{H}_2\text{O}) = 2.80 \text{ V/SHE}$) explains its ability to non-selectively react with most organics up to mineralization to CO₂, water and inorganic ions [13,14].

The boron-doped diamond (BDD) thin-film anodes yield the quickest mineralization of organics in the EAOPs. This anode possesses larger oxidation ability than conventional Pt [16–18] and PbO₂ [19] ones as a result of the low adsorption of both, $\cdot\text{OH}$ formed at its surface and organics, as well as its greater O₂-evolution over-voltage. These properties allow the mineralization of aromatics [12,20–27] and by-products like short-chain linear carboxylic acids [28]. The oxidation ability of EAOPs may be upgraded when H₂O₂ is continuously generated at the cathode from the two-electron reduction of O₂, as follows [13,14]:



Anodic oxidation with electrogenerated H₂O₂ (AO-H₂O₂), electro-Fenton (EF) and photoelectro-Fenton (PEF) are the most important EAOPs based on H₂O₂ electrogeneration. They use effective carbonaceous cathodes for Reaction (1) like BDD [29], activated carbon fiber [30], carbon nanotubes [31], carbon sponge [32], carbon felt [9,24,33–35] and carbon-polytetrafluoroethylene (PTFE) gas-diffusion devices [27,36–39].

This paper presents a study on the oxidation of 4-hydroxyphenylacetic acid, spiked in either synthetic sulfate solutions with ultrapure water or real OOMW solutions, by AO-H₂O₂, EF and PEF using a BDD/air-diffusion tank reactor. Very worth mentioning, no previous studies have addressed the treatment of real OOMW by EAOPs with an air-diffusion cathode, which is mandatory aiming to scale-up these promising technologies. The effect of current density (j) and substrate content on the degradation rate and mineralization current efficiency (MEC) was examined. The kinetics for the substrate decay and the evolution of generated carboxylic acids were monitored by high-performance liquid chromatography (HPLC). The change in biodegradability was determined during the treatment of OOMW. Gas chromatography-mass spectrometry (GC-MS) was used to identify the main organic components of the raw OOMW.

2. Experimental

2.1. Chemicals

4-Hydroxyphenylacetic acid (98% purity) was purchased from Sigma-Aldrich. Analytical grade oxalic acid was supplied by Merck. Iron(II) sulfate heptahydrate and anhydrous sodium sulfate were of analytical grade supplied by Fluka. Analytical grade sulfuric acid from Acros Organics was used to adjust the initial pH to 3.0.

Aqueous solutions were prepared with high purity water from a Millipore Milli-Q system (resistivity > 18 M Ω cm at 25 °C). Other chemicals were of HPLC or analytical grade provided by Panreac and Merck.

2.2. Real OOMW sample

The real OOMW was obtained from a decanter receiving wastewater generated upon cleaning stages during the premium extra virgin olive oil production at a small size oil mill in north-eastern Spain. It was collected in November of 2015 and kept at 4 °C before use. The treatments were made after filtration of the OOMW sample with an 18 μm filter, spiking or not 1.03 mM 4-hydroxyphenylacetic acid, without or with dilution with Milli-Q water.

2.3. Electrolytic system

All the trials were carried out with an open, undivided, cylindrical glass cell containing 100 mL solutions under vigorous stirring with a magnetic bar at 700 rpm. The cell was surrounded with a double jacket where thermostated water was recirculated at 35 °C. This was the maximum temperature that could be used avoiding significant solvent evaporation. A 3 cm² BDD (deposited onto *p*-Si) electrode supplied by NeoCoat (La-Chaux-de-Fonds, Switzerland) was used as the anode and a 3 cm² carbon-PTFE air-diffusion electrode supplied by E-TEK (Somerset, NJ, USA) as the cathode. The interelectrode gap was about 1 cm. The cathode was mounted as reported elsewhere [27] and was fed with air pumped at 300 mL min⁻¹ for continuous H₂O₂ generation on site. The experiments were performed at constant j provided by an EG&G Princeton Applied Research 273A potentiostat-galvanostat. The surfaces of the anode and cathode were initially cleaned and activated, respectively, under polarization in 100 mL of 0.050 M Na₂SO₄ at 100 mA cm⁻² for 180 min.

Solutions with 0.21–2.06 mM 4-hydroxyphenylacetic acid and 0.050 M Na₂SO₄ at pH 3.0 were comparatively treated by AO-H₂O₂, EF and PEF at j values between 16.7 and 100 mA cm⁻². These EAOPs were also applied to degrade the filtrated OOMW sample at pH 3.0, either raw or diluted with ultrapure water, in the absence and presence of 1.03 mM 4-hydroxyphenylacetic acid. For EF and PEF, 0.50 mM Fe²⁺ was added as Fenton's catalyst since it was found optimal for many organics degraded under similar conditions [36–39]. For PEF, a Philips TL/6W/08 fluorescent black light blue tube of $\lambda_{\text{max}} = 360 \text{ nm}$ placed at 8 cm above the solution surface was used. The average power density of this lamp was 5 W m⁻², as determined with a Kipp&Zonen CUV 5 UV radiometer.

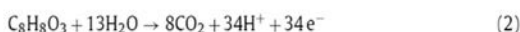
2.4. Analytical methods

The pH and conductance of synthetic sulfate solutions and real OOMW samples were measured with a Crison GLP 22 pH-meter and a Metrohm 644 conductometer, respectively. The turbidity was determined with a WTW TURB 55 IR turbidimeter. The chemical oxygen demand (COD) was measured with Hach Lange LCK014, LCK514 and LCK614 COD cuvette tests using a Hach DR 3900 UV-vis spectrophotometer. Other parameters of the OOMW were determined according to the Standard Methods [40]. The 5-day biochemical oxygen demand (BOD₅) was obtained following a respirometric method with a WTW Oxitop 12 system using seed from a municipal wastewater treatment plant (method 5210 D). Total solids (TS) and total suspended solids (TSS) were determined upon evaporation and drying to constant weight in an oven at 103–105 °C (methods 2540 B and C). Phenol index was obtained according to the 4-aminoantipyrine direct spectrophotometric method 5530 D. Oil and grease content was measured via the

partition-gravimetric method 5520 B. Anions concentration was obtained by ion chromatography with a Kontron 465 LC equipped with a Waters IC-PAK, 150 mm × 4.6 mm, anion-exchange column at 35 °C and coupled with a Waters 432 conductivity detector. A mixture of boric acid, sodium gluconate, sodium tetraborate, acetonitrile, butanol and glycerine was eluted at 2.0 mL min⁻¹ as the mobile phase. The cations content was found by inductively coupled plasma (ICP-OES) using an Optima 3200RL spectrometer.

For total organic carbon (TOC) determinations, 1 mL samples were withdrawn from treated solutions, filtered with 0.45 μm Whatman PTFE filters and 50 μL directly injected into a Shimadzu VCSN TOC analyzer. Reproducible values with ±1% accuracy were found.

Assuming the following total mineralization for 4-hydroxyphenylacetic acid:



the mineralization current efficiency (MCE) for each trial was estimated as follows [41]:

$$MCE(\%) = \frac{nFV \Delta(TOC)_{exp}}{4.32 \times 10^7 mIt} \times 100 \quad (3)$$

where $n=34$ is the number of electrons of the mineralization process, F is the Faraday constant (96,487 C mol⁻¹), V is the solution volume (L), $\Delta(TOC)_{exp}$ is the TOC decay (mg L⁻¹), 4.32×10^7 is a conversion factor to homogenize units (3600 s h⁻¹ × 12,000 mg C mol⁻¹), $m=8$ is the number of carbon atoms of 4-hydroxyphenylacetic acid, I is the current (A) and t is the electrolysis time (h).

The 4-hydroxyphenylacetic acid abatement was followed by reversed-phase HPLC using a Waters 600 LC fitted with a BDS Hypersil C18 6 μm, 250 mm × 4.6 mm, column at 35 °C and coupled with a Waters 996 photodiode array detector set at $\lambda=277.0$ nm. The samples of EF and PEF were immediately diluted with acetonitrile to stop the degradation process and filtered prior to injection. Measurements were made by injecting 10 μL aliquots into the LC and eluting an acetonitrile/water (60:40) mixture at 0.6 mL min⁻¹ as mobile phase. The chromatograms exhibited a peak for the parent compound at retention time (t_r) of 5.0 min. Final carboxylic acids were identified by ion-exclusion HPLC using the same LC fitted with a Bio-Rad Aminex HPX 87H, 300 mm × 7.8 mm, column at 35 °C and the photodiode array detector set at $\lambda=210.0$ nm. Aliquots of 10 μL were injected into the LC and the mobile phase was 4 mM H₂SO₄ at 0.6 mL min⁻¹. The chromatograms displayed a peak related to oxalic acid at $t_r=7.0$ min.

The organic components of the real OOMW sample after filtration were identified by GC-MS using a NIST05-MS library to interpret the mass spectra. Aliquots were lyophilized and the residue was dissolved in 1 mL of ethyl acetate. GC-MS analysis was performed on an Agilent system composed of a 6890N GC and a 5975C MS, operating in EI mode at 70 eV. The GC was fitted with a non-polar Teknokroma Sapiens-X5 ms 0.25 μm, 30 m × 0.25 mm, column. The temperature ramp was 36 °C for 1 min, 5 °C min⁻¹ up to 325 °C and hold time 10 min. The temperature of the inlet, source and transfer line was 250, 230 and 300 °C, respectively.

3. Results and discussion

3.1. Comparative degradation by AO-H₂O₂, EF and PEF in sulfate medium

First assays to degrade solutions of 1.03 mM 4-hydroxyphenylacetic acid (100 mg L⁻¹ TOC) in 0.050 M Na₂SO₄ at pH 3.0 aimed at comparing the relative oxidation ability of AO-H₂O₂, EF and PEF at 16.7 mA cm⁻². The solution pH did not

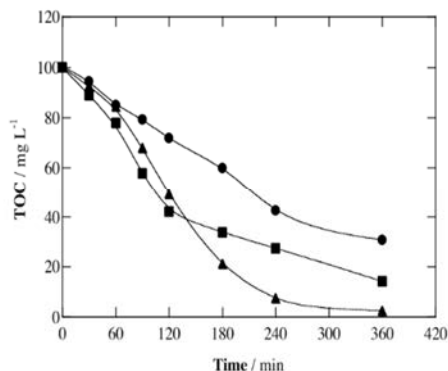
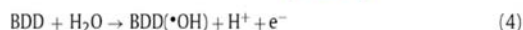


Fig. 1. TOC abatement with electrolysis time for the treatment of 100 mL of 1.03 mM 4-hydroxyphenylacetic acid solutions in 0.050 M Na₂SO₄ at pH 3.0 using a tank reactor equipped with a 3 cm² BDD anode and a 3 cm² air-diffusion cathode at 16.7 mA cm⁻² and 35 °C. Method: (●) anodic oxidation with electrogenerated H₂O₂ (AO-H₂O₂), (■) electro-Fenton (EF) with 0.50 mM Fe²⁺ and (▲) photoelectro-Fenton (PEF) with 0.50 mM Fe²⁺ and 6 W UVA radiation.

changed significantly, slightly decreasing to 2.7–2.8 owing to the generation of acidic by-products [13,14,38].

Fig. 1 depicts a gradual TOC abatement over electrolysis time in all cases, attaining a final reduction of 69%, 86% and 98% for AO-H₂O₂, EF and PEF, respectively. A slightly faster mineralization can be observed in EF compared to PEF up to 120 min. These findings allow concluding that the power of EAOPs rises in the order AO-H₂O₂ < EF < PEF for electrolysis times >120 min, reaching an almost total mineralization with powerful PEF.

The good oxidation ability of AO-H₂O₂ can be related to the pre-eminent action of physisorbed hydroxyl radical formed from water oxidation at the BDD anode surface [12,42,43]:



In AO-H₂O₂, organics can be simultaneously degraded by other ROS like H₂O₂ and its oxidation product, HO₂• [14]. Moreover, other weak species like peroxodisulfate ion (S₂O₈²⁻) and O₃ formed at the BDD anode via Reactions (5) and (6), respectively, can be formed [12,43]:



The enhancement of the degradation using EF can be explained by the additional production of •OH in the bulk through homogeneous catalysis with added Fe²⁺ via Fenton's Reaction (7) [14,15,27,33]. Organics are then destroyed by heterogeneous and homogeneous oxidants, i.e., BDD(•OH) and •OH.



The faster mineralization in PEF is due to the photolysis of some by-products upon UVA light irradiation, which induces the photoreduction of Fe(OH)²⁺ to Fe²⁺ via Reaction (8) and the photolysis of Fe(III) complexes with final carboxylic acids by Reaction (9) [36–39,41]:



The fact that the mineralization rate in EF is slightly higher than that in PEF up to 120 min of electrolysis (see Fig. 1) suggests the formation of more recalcitrant benzenic by-products at the beginning of the PEF process under the action of UVA light, which are more hardly oxidizable by BDD(•OH) and •OH. This behavior is also

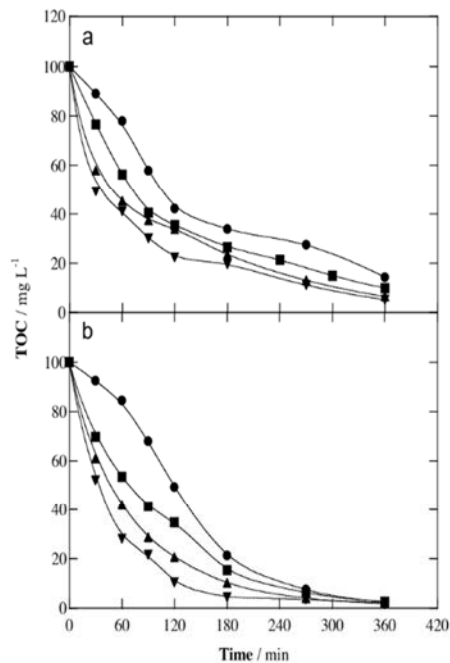


Fig. 2. Effect of current density on TOC decay with electrolysis time for the (a) EF and (b) PEF treatments of 100 mL of a 1.03 mM 4-hydroxyphenylacetic acid solution in 0.050 M Na₂SO₄ with 0.50 mM Fe²⁺ at pH 3.0 and 35 °C using a BDD/air-diffusion cell. Applied current density: (●) 16.7 mA cm⁻², (■) 33.3 mA cm⁻², (▲) 66.7 mA cm⁻² and (▼) 100 mA cm⁻².

indicative of little influence of additional •OH formed from Reaction (8) on TOC decay. In contrast, the faster degradation of PEF at longer times confirms a strong photolytic action of UVA light over the remaining by-products, probably Fe(III) complexes.

The above findings reveal the superiority of PEF for degrading 4-hydroxyphenylacetic acid in sulfate medium. The influence of the main operation parameters on its performance is discussed below, as compared with EF to better clarify the specific role of UVA light.

3.2. Effect of operation parameters on EF and PEF processes in sulfate medium

The concentration of generated hydroxyl radicals in EAOPs and hence, their oxidation ability for wastewater remediation, depends on the applied *j*. The influence of this parameter on the EF and PEF treatments of 1.03 mM 4-hydroxyphenylacetic acid in 0.050 M Na₂SO₄ at pH 3.0 was assessed in the range 16.7–100 mA cm⁻².

For EF, Fig. 2a shows a greater TOC decay at higher *j*. Final TOC reductions of 85.7%, 90.1%, 93.5% and 94.8% were obtained at 16.7, 33.3, 66.7 and 100 mA cm⁻², respectively. This enhancement can be related to the progressive generation of larger amounts of BDD(•OH) and •OH by the concomitant increase in rate of Reactions (4) and (1), thus accelerating Fenton's Reaction (7). The same behavior can be observed in Fig. 2b for PEF, although yielding an almost total mineralization (97.5%–98.3%) for all *j* values. The effect of this parameter was more evident at short times. For example, at 180 min of electrolysis increasing TOC reductions of 78.8%, 84.6%, 89.2% and 95.5% were found at growing *j* values. Comparison of Fig. 2a and b allows concluding not only the superiority of PEF at each *j*, but also the greater relative importance of UVA light as *j* was raised. After 180 min at 16.7 mA cm⁻², for example, 66.2 mg L⁻¹ TOC were abated in EF, rising to 78.8 mg L⁻¹ in PEF. This difference is lower than 15.1 mg L⁻¹ TOC found at 100 mA cm⁻². This finding

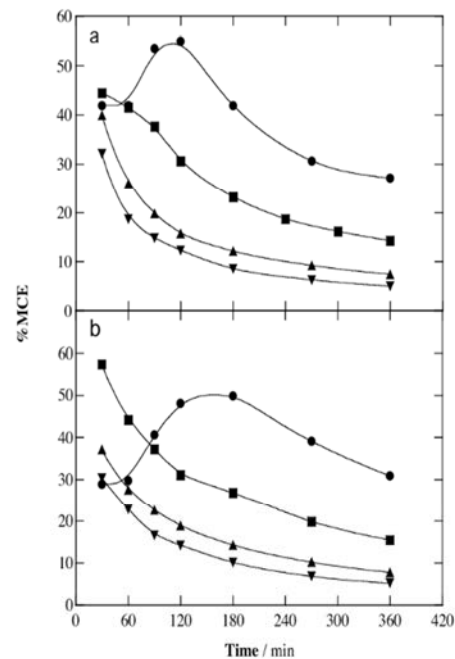
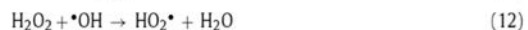
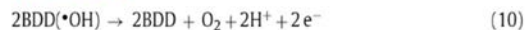


Fig. 3. Mineralization current efficiency vs. electrolysis time for the trials of Fig. 2.

can be explained by the formation of larger quantities of photosensitive by-products at higher *j*, being more rapidly removed upon UVA irradiation.

Fig. 3a and b depict a drop in MCE values with increasing *j* for both, EF and PEF, in contrast to its positive contribution to TOC removal. Maximum current efficiencies of 54.9% for EF and 49.9% for PEF were then found at the lowest *j*, dropping to 27.1% and 30.8%, respectively. In all cases, the MCE values decreased at prolonged time due to the loss of organic load and the formation of more recalcitrant by-products [12,13]. It is also noticeable that only the MCE-*t* plots at the lowest *j* of 16.7 mA cm⁻² presented a marked maximal at 120 min for EF (see Fig. 3a) and at about 180 min for PEF (see Fig. 3b). This can be related to the smaller amounts of BDD(•OH) and •OH radicals produced at this low *j*, which destroy slowly the primary recalcitrant benzenic by-products. As a result, species that are more prone to being mineralized are gradually generated up to reach the maximum value of current efficiency, whereas the loss of organic load and the formation of Fe(III)-carboxylate products cause a progressive decay in current efficiency at longer time.

The decay in MCE with rising *j* can be related to the acceleration of parasitic reactions of BDD(•OH) and •OH, leading to smaller available quantities. Examples include the following ones [12–14,36–39]:



The substrate concentration is another important variable since it affects the attack of oxidants on organic molecules in competition with parasitic reactions. To study the effect of this parameter on the performance of the EF and PEF treatments, solutions with 0.21–2.06 mM of the pollutant in 0.050 M Na₂SO₄ at pH 3.0 were treated at 33.3 mA cm⁻² for 360 min. Fig. 4a and b confirm the superiority of PEF over EF to remove 4-hydroxyphenylacetic acid and its

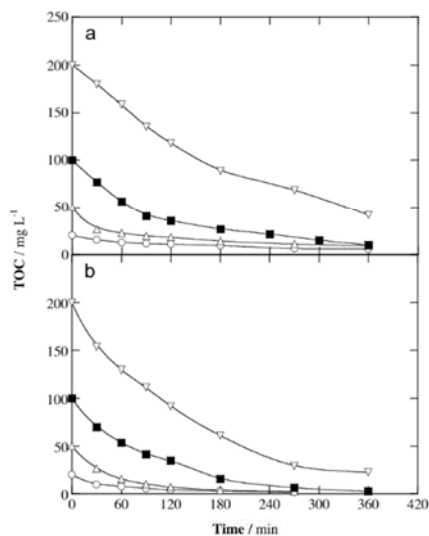


Fig. 4. Influence of pollutant concentration on TOC removal with electrolysis time for the degradation of 100 mL of 4-hydroxyphenylacetic acid solutions in 0.050 M Na_2SO_4 with 0.50 mM Fe^{2+} at pH 3.0 using a BDD/air-diffusion cell at 33.3 mA cm^{-2} and 35°C . Method: (a) EF and (b) PEF. 4-Hydroxyphenylacetic acid concentration: (○) 0.21 mM, (△) 0.51 mM, (■) 1.03 mM and (▽) 2.06 mM.

by-products for all substrate contents. At 360 min, TOC was reduced by 72.1%, 82.3%, 90.1% and 79.3% in EF and 92.2%, 95.4%, 97.5% and 88.8% in PEF for 0.21, 0.51, 1.03 and 2.06 mM, respectively. The best performance was achieved for the 1.03 mM solution, further declining. Worth noting, a larger TOC amount was removed at greater substrate concentration. After 360 min of EF and PEF, for example, 158.6 and 177.5 mg L^{-1} TOC were destroyed when starting with 2.06 mM, values much greater than 100 mg L^{-1} TOC corresponding to the 1.03 mM solution.

The enhancement of the oxidation ability at higher substrate concentrations is easily corroborated from the corresponding MCE values given in Fig. 5a and b. In both treatments, the highest efficiency was obtained for 2.06 mM. Since the same amount of hydroxyl radicals is expected to be produced in all treatments at equal j , a larger number of organic molecules react with BDD($\bullet\text{OH}$) and $\bullet\text{OH}$, thus decelerating parasitic Reactions (10)–(13). Note again the continuous drop of MCE values over time, as also stated above.

In conclusion, the powerful PEF leads to an almost total mineralization of 4-hydroxyphenylacetic acid solutions, with 98% TOC removal as maximal. This is due to the large photolytic action of UVA radiation to destroy photoactive by-products that are slowly removed by hydroxyl radicals in EF.

3.3. Decay kinetics of 4-hydroxyphenylacetic acid in sulfate medium by EF and PEF

The reaction of 4-hydroxyphenylacetic acid with generated oxidants was monitored by reversed-phase HPLC. Fig. 6 illustrates the exponential concentration decay for a 1.03 mM substrate solution in 0.050 M Na_2SO_4 at pH 3.0 treated by EF and PEF at 33.3 mA cm^{-2} , disappearing in 60 and 40 min, respectively. One can infer that the main oxidant in EF and PEF is $\bullet\text{OH}$ in the bulk. The slightly faster

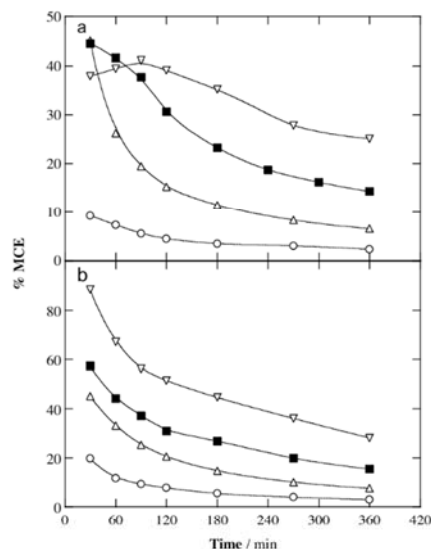


Fig. 5. Time course of mineralization current efficiency for the assays of Fig. 4.

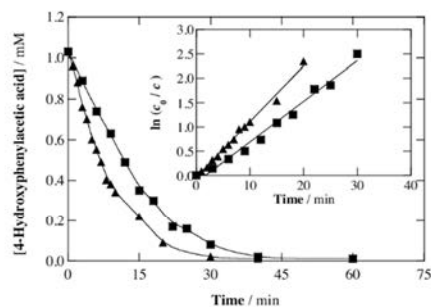


Fig. 6. Decay of 4-hydroxyphenylacetic acid concentration with electrolysis time for the (■) EF and (▲) PEF degradations of 100 mL of pollutant solutions in 0.050 M Na_2SO_4 with 0.50 mM Fe^{2+} at pH 3.0 using a BDD/air-diffusion cell at 33.3 mA cm^{-2} and 35°C . The inset panel presents the kinetic analysis assuming a pseudo-first-order reaction for 4-hydroxyphenylacetic acid.

destruction in PEF can then be ascribed to the generation of additional amounts of $\bullet\text{OH}$ by photolytic Reaction (8).

The inset panel of Fig. 6 presents the good fitting for the drop of substrate concentrations according to a pseudo-first-order kinetic equation. From these straight lines, apparent rate constants (k_1) of $1.4 \times 10^{-3} \text{ s}^{-1}$ ($R^2 = 0.990$) for EF and $1.9 \times 10^{-3} \text{ s}^{-1}$ ($R^2 = 0.992$) for PEF were obtained. This behavior suggests the attack of a steady and low $\bullet\text{OH}$ concentration on 4-hydroxyphenylacetic acid obeying the following second-order reaction rate (r):

$$r = k_2[\bullet\text{OH}][\text{R}] = k_1[\text{R}] \quad (14)$$

where $k_2 (= k_1/[\bullet\text{OH}])$ is the absolute or second-order rate constant and R denotes the 4-hydroxyphenylacetic acid. Taking into account that $k_2 = 7.02 \times 10^8 \text{ M}^{-1} \text{ s}^{-1}$ for this reaction [11], one can estimate

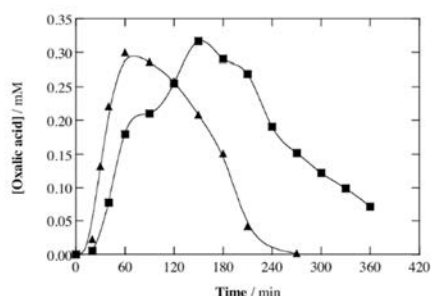


Fig. 7. Evolution of the concentration of oxalic acid detected during the treatments shown in Fig. 6: (■) EF and (▲) PEF.

the action of average $\cdot\text{OH}$ concentrations ($=k_1/k_2$) of 2.0×10^{-11} and 2.7×10^{-11} M for EF and PEF, respectively.

3.4. Time-course of final carboxylic acids during EF and PEF in sulfate medium

Ion-exclusion chromatograms revealed the accumulation of large concentrations of oxalic acid during the EF and PEF treatments. It is a typical short-chain carboxylic acid by-product that forms Fe(III) complexes that can be directly converted into CO_2 [21,27,33,34]. Fig. 7 depicts the evolution of oxalic acid concentration during the treatment of a 1.03 mM 4-hydroxyphenylacetic acid solution at 33.3 mA cm^{-2} . In EF it was progressively accumulated up to 0.32 mM at 150 min, whereupon it dropped drastically to 0.072 mM at the end of the electrolysis. This corresponds to 1.70 mg L^{-1} TOC, which accounts for 17.1% of the remaining TOC (see Fig. 2a). The final solution of EF then contained a large proportion of by-products that are even more hardly oxidized by BDD($\cdot\text{OH}$) and/or $\cdot\text{OH}$ than final carboxylic acids. In contrast, Fig. 7 shows that in PEF oxalic acid was much more rapidly accumulated, up to 0.32 mM in 60 min, and completely removed in 240 min because of the rapid photolysis of Fe(III)-oxalate complexes by UVA light via Reaction (9). At that time, the solution contained 18.7 mg L^{-1} TOC (see Fig. 2b), which was reduced to 2.5 mg L^{-1} at 360 min. This means that the combined action of BDD($\cdot\text{OH}$), $\cdot\text{OH}$ and UVA light over remaining photoactive by-products strongly enhances the mineralization process.

3.5. Degradation of 4-hydroxyphenylacetic acid in a real OOMW matrix

The study of the degradation of 4-hydroxyphenylacetic acid was extended to a real OOMW, the matrix that conveys the pollutant to the aquatic environment. Table 1 summarizes the physico-chemical properties of the OOMW sample. The raw sample had: (i) neutral pH, (ii) very low conductivity and (iii) high turbidity, TOC, COD, TSS and TS. After filtration with an $18 \mu\text{m}$ filter, the conditioned OOMW showed a drastic removal of turbidity, TSS and TS. Its phenol index was low, with larger contents of oil and grease. The $\text{BOD}_5/\text{COD} = 0.334$ for the conditioned OOMW spiked with 1.03 mM 4-hydroxyphenylacetic acid informed about its low biodegradability. The conditioned OOMW also contained: (i) a very high concentration of SO_4^{2-} compared to the very small contents of NO_3^- and Cl^- as anions and (ii) the predominance of K^+ and Na^+ among the cations, with an insignificant content of Fe^{2+} . On the other hand, its GC-MS analysis revealed the presence of a large variety of compounds like 7 phenolic molecules, including

Table 1
Main physicochemical characteristics of the raw and conditioned OOMW sample to be further used for electrochemical treatment.

Parameter (units)	OOMW
pH	6.8 ± 0.1^a
Conductivity (mS cm^{-1})	1.5 ± 0.1^a
Turbidity (NTU)	245.7 ± 14.0^b
	24.0 ± 0.1^b
TOC (mg L^{-1})	598 ± 42^a
	505 ± 31^b
COD ($\text{mg O}_2 \text{ L}^{-1}$)	2368 ± 1^c
BOD_5 ($\text{mg O}_2 \text{ L}^{-1}$)	790 ± 42^c
BOD_5/COD	0.334 ± 0.012^c
TSS (mg L^{-1})	3712 ± 398^a
	82 ± 41^b
TS (mg L^{-1})	5852 ± 284^a
	2107 ± 51^b
Phenol index (mg L^{-1})	9.3 ± 0.21^b
Oil and grease (mg L^{-1})	60^b
NO_2^- (mg L^{-1})	$<0.012^{bd}$
NO_3^- (mg L^{-1})	0.51^b
SO_4^{2-} (mg L^{-1})	910.31^b
Cl^- (mg L^{-1})	2.91^b
Fe^{2+} (mg L^{-1})	1.35^b
Ca^{2+} (mg L^{-1})	15.11^b
Mg^{2+} (mg L^{-1})	16.41^b
K^+ (mg L^{-1})	76.81^b
Na^+ (mg L^{-1})	387.81^b

^a Raw OOMW sample.

^b After filtration with an $18 \mu\text{m}$ filter.

^c After filtration (as in b) and addition of 1.03 mM 4-hydroxyphenylacetic acid.

^d Limit of quantification.

4-hydroxyphenylacetic acid, 1 heteroaliphatic alcohol as well as 4 aromatic and 4 aliphatic (1 cyclic and 3 linear) carboxylic acids, as summarized in Table 2.

The EAOPs were then applied to the degradation of the conditioned OOMW after spiking or not 1.03 mM 4-hydroxyphenylacetic acid, as well as spiked OOMW samples diluted to 60% and 20% (v/v) with ultrapure water. The initial pH was adjusted to 3.0 with H_2SO_4 and trials were carried out at 16.7 mA cm^{-2} for 540 min. This small j was chosen because of the large potential difference of the cell arising from the low conductivity of the raw OOMW (see Table 1). Trials were performed with the conditioned sample to avoid the influence of suspended solids, particularly on the absorption of the irradiated UVA light.

Fig. 8a–c depict the same relative oxidation ability of the EAOPs in the sequence $\text{AO-H}_2\text{O}_2 < \text{EF} < \text{PEF}$ for all the media tested. Partial mineralization of the conditioned undiluted OOMW (not spiked) was obtained with final TOC reductions of 71.8%, 79.5% and 83.4% for the above treatments. This indicates an effective attack of BDD($\cdot\text{OH}$) on the organics contained in the real OOMW in $\text{AO-H}_2\text{O}_2$, which was enhanced under the parallel action of $\cdot\text{OH}$ in EF and became even more efficient upon photolysis of photoactive by-products in PEF. This behavior was also found after spiking 1.03 mM 4-hydroxyphenylacetic acid to the undiluted OOMW (100% (v/v)) and to diluted OOMW samples. Fig. 8a–c highlights a slight enhancement of the normalized TOC abatement when decreasing the organic concentration of the treated effluent. The quickest mineralization was achieved for the 20% (v/v) solution reaching 82.5%, 83.0% and 86.4% TOC decay by $\text{AO-H}_2\text{O}_2$, EF and PEF, respectively. However, since the initial TOC decreased significantly from 605 mg L^{-1} corresponding to the 100% (v/v) solution, one can infer that all the treatments were more efficient at greater organic load, confirming the deceleration of their parasitic Reactions (10)–(13).

The decay kinetics of the spiked 4-hydroxyphenylacetic acid in the above assays was followed by reversed-phase HPLC and compared with that obtained in $0.050 \text{ M Na}_2\text{SO}_4$. Fig. 9a and b illustrates the exponential abatement of the concentration of this compound

Table 2
Organic compounds identified by GC-MS using a non-polar column for a lyophilized real OOMW sample after filtration with an 18 μm filter.


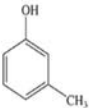
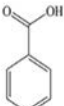
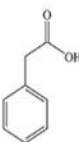
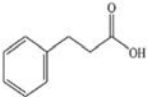
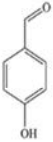
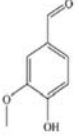
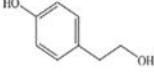
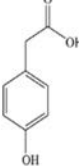
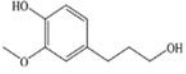
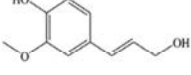
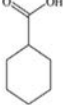
Compound	Molecular structure	t_r (min)	Main fragmentation ions (m/z)
Phenol		9.3	94, 74, 66
3-Methylphenol		12.3	108, 90, 79, 77
Benzoic acid		15.2	122, 105, 77, 51
Benzeneacetic acid		17.4	136, 91, 65
Benzenepropanoic acid		20.1	150, 104, 91, 65
4-Hydroxybenzaldehyde		21.6	121, 93, 65, 39
Vanillin		22.1	151, 137, 123, 109, 81
4-Hydroxyphenylethanol		23.0	138, 107, 91, 77
4-Hydroxyphenylacetic acid		23.2	152, 107, 77
Homovanillyl alcohol		25.3	168, 137, 122
4-((1E)-3-Hydroxy-1-propenyl)-2-methoxyphenol (Coniferyl alcohol)		30.2	180, 163, 137, 124, 103, 91
Cyclohexanecarboxylic acid		14.5	128, 110, 73, 55, 41

Table 2 (Continued)

Compound	Molecular structure	t_r (min)	Main fragmentation ions (m/z)
2-(2-butoxyethoxy)-ethanol		16.2	132, 101, 87, 75, 57, 45
<i>n</i> -Heptanoic acid		5.0	130, 87, 73, 60
<i>n</i> -Hexadecanoic acid (Palmitic acid)		34.1	256, 213, 171, 157, 129, 97, 73, 60, 43
Oleic acid		37.2	282, 264, 129, 111, 97, 83, 69, 55, 41

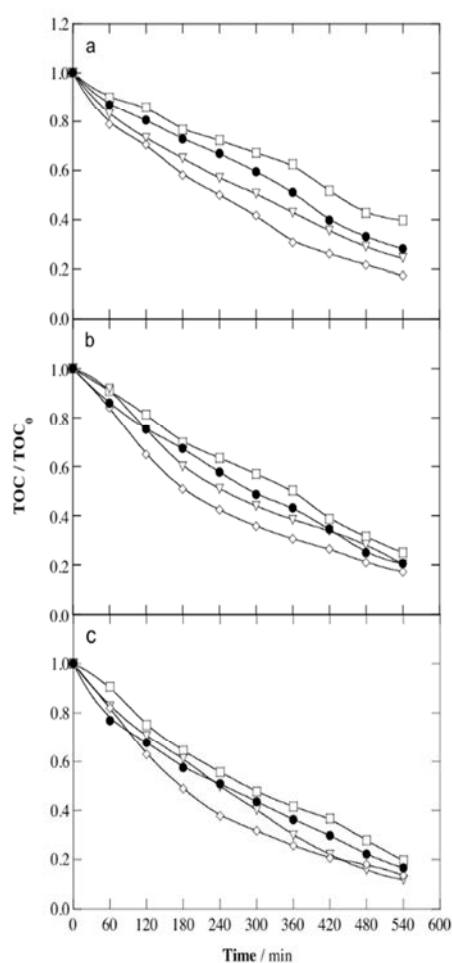


Fig. 8. Normalized TOC removal vs. electrolysis time for: (a) AO-H₂O₂, (b) EF with 0.50 mM Fe²⁺ and (c) PEF with 0.50 mM Fe²⁺ and 6W UVA radiation treatments of 100 mL of solutions with (●, □) 100%, (▽) 60% and (◇) 20% (v/v) of filtered (18 μm) real OOMW, in the (●) absence or (□, ▽, ◇) presence of 1.03 mM 4-hydroxyphenylacetic acid at pH 3.0 using a stirred BDD/air-diffusion tank reactor at 16.7 mA cm⁻² and 35 °C.

under all experimental conditions, always obeying a pseudo-first-order kinetics, as depicted in their inset panels. Under AO-H₂O₂ conditions (see Fig. 9a), the slow destruction by BDD(•OH) led to the complete removal of 4-hydroxyphenylacetic acid in 540 min

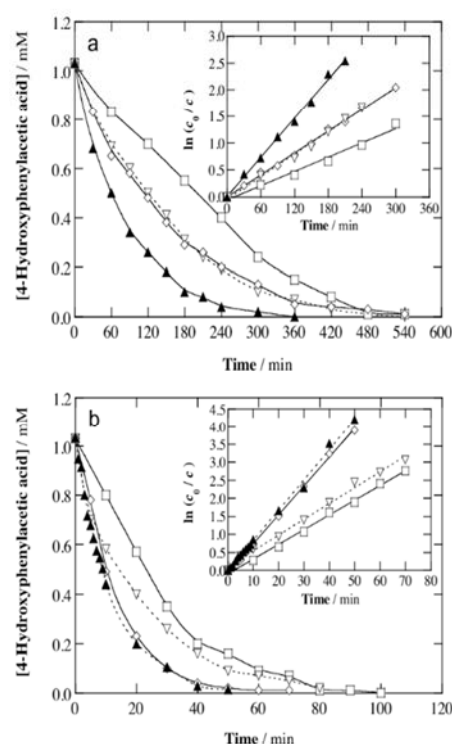


Fig. 9. 4-Hydroxyphenylacetic acid abatement with electrolysis time for the (a) AO-H₂O₂ and (b) PEF treatments of 100 mL of 1.03 mM 4-hydroxyphenylacetic acid solutions in (□) 100%, (▽) 60% and (◇) 20% (v/v) of filtered (18 μm) real OOMW, as well as in (▲) 0.050 M Na₂SO₄, all at pH 3.0 using a stirred BDD/air-diffusion tank reactor at 16.7 mA cm⁻² and 35 °C. The corresponding kinetic analysis considering a pseudo-first-order decay for the pollutant is shown in the inset panels.

for all the OOMW solutions, although its removal was faster at a gradually smaller organic load. Accordingly, the substrate disappeared completely in about 360 min in 0.050 M Na₂SO₄. The k_1 values varied between $7.3 \times 10^{-5} \text{ s}^{-1}$ ($R^2 = 0.985$) for the 100% (v/v) solution and $2.0 \times 10^{-4} \text{ s}^{-1}$ ($R^2 = 0.992$) for 0.050 M Na₂SO₄. Assuming that Reaction (14) is verified for BDD(•OH), its average content can be estimated as k_1/k_2 , with $k_2 = 7.02 \times 10^8 \text{ M}^{-1} \text{ s}^{-1}$, growing from 1.0×10^{-13} to 2.8×10^{-13} M. As expected, the substrate decay was much faster by PEF due to the more active •OH formed from Reactions (7) and (8). Fig. 9b reveals that time for total disappearance varied from 100 to 70 min when going from 100% to 20% (v/v) solutions, decreasing to 50 min for 0.050 M Na₂SO₄. The corresponding k_1 values increased from $6.8 \times 10^{-4} \text{ s}^{-1}$ ($R^2 = 0.993$) for

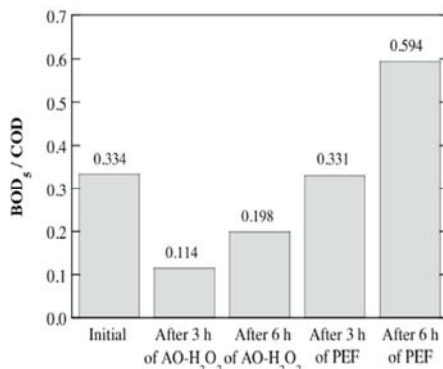


Fig. 10. Change of BOD₅/COD ratio of the raw OOMW sample (filtered with an 18 μm filter) once spiked with 1.03 mM 4-hydroxyphenylacetic acid and treated for 3 and 6 h by either AO-H₂O₂ or PEF with 0.50 mM Fe²⁺ and 6 W UVA radiation.

the 100% (v/v) solution to $1.4 \times 10^{-3} \text{ s}^{-1}$ ($R^2 = 0.993$) for 0.050 M Na₂SO₄, with an average •OH content between 9.7×10^{-13} and 2.0×10^{-12} M. This corroborates the enhanced oxidation of aromatic products by •OH than BDD(•OH) in PEF.

The change in biodegradability of the treated solutions was also evaluated. The initial BOD₅/COD ratio was 0.334 for the conditioned OOMW spiked with 1.03 mM 4-hydroxyphenylacetic acid, which is close to the biodegradability threshold of 0.4 needed for biological treatment [44]. Fig. 10 shows a decay of the initial BOD₅/COD ratio after 180 and 360 min of the AO-H₂O₂ treatment, indicating the generation of biorefractory species during electrolysis as well as the effect of accumulated H₂O₂. In contrast, the PEF degradation caused a strong enhancement of the biodegradability, with a final BOD₅/COD value near 0.6 after 360 min of treatment. This means that PEF is not only the most powerful EAOP to decontaminate OOMW, spiked or not with 4-hydroxyphenylacetic acid, but it can also be an optimum process for coupling with biological processes. This suggests a much faster and efficient degradation of this kind of wastewater by means of the coupled PEF/biological process, if compared to a single step biological treatment, as recently shown for the EF/biological degradation of antibiotics furosemide and ranitidine in aqueous medium [44].

4. Conclusions

PEF process is the most powerful EAOP for treating 4-hydroxyphenylacetic acid and, what is more relevant for future application, its high performance is maintained in a real wastewater matrix like OOMW. The quick mineralization in PEF was achieved thanks to the photolytic action of UVA radiation on photoactive by-products, as observed for the quick removal of Fe(III)-oxalate complexes formed. The increase in *j* accelerated the mineralization in all media tested, but with loss of MCE owing to the parasitic reactions that consume the hydroxyl radicals. An enhancement of the oxidation ability of all EAOPs with increasing organic load was always found, with the consequent rise in MCE. This favors the degradation rate of real OOMW with high organic content. 4-Hydroxyphenylacetic acid decay always obeyed a pseudo-first-order kinetics. About 98% and 80% TOC reductions were achieved for the PEF treatment of 1.03 mM 4-hydroxyphenylacetic acid in 0.050 M Na₂SO₄ and in the real OOMW, respectively. In the latter case, the PEF process also led to a greater biodegradability.

Acknowledgements

The authors acknowledge financial support from project CTQ2013-48897-C2-1-R (MINECO, FEDER, EU). The PhD fellowship awarded to N. Flores by SENESCYT (Ecuador) is acknowledged as well.

References

- [1] S. Magdich, C. Ben Ahmed, R. Jarboui, B. Ben Rouina, M. Boukhris, E. Ammar, Dose and frequency dependent effects of olive mill wastewater treatment on the chemical and microbial properties of soil, *Chemosphere* 93 (2013) 1896–1903.
- [2] S. Dermeche, M. Nadour, C. Larroche, F. Mouti-Mati, P. Michaud, Olive mill wastes: biochemical characterizations and valorization strategies, *Process Biochem.* 48 (2013) 1532–1552.
- [3] M. DellaGreca, L. Previtera, F. Temussi, A. Zarrelli, Low-molecular-weight components of olive oil mill waste-waters, *Phytochem. Anal.* 15 (2004) 184–188.
- [4] J.M. Ochando-Pulido, M.D. Victor-Ortega, G. Hodaifa, A. Martinez-Ferez, Physicochemical analysis and adequation of olive oil mill wastewater after advanced oxidation process for reclamation by pressure-driven membrane technology, *Sci. Total Environ.* 503–504 (2014) 113–121.
- [5] D. Pham Minh, P. Gallezot, S. Azabou, S. Sayadi, M. Besson, Catalytic wet air oxidation of olive oil mill effluents, *Appl. Catal. B: Environ.* 84 (2008) 749–757.
- [6] C. Belaid, M. Kallel, M. Khadhraoui, G. Lalleve, B. Elleuch, J.F. Fauvarque, Electrochemical treatment of olive mill wastewaters: removal of phenolic compounds and decolorization, *J. Appl. Electrochem.* 36 (2006) 1175–1182.
- [7] C. Belaid, M. Khadraoui, S. Mseddi, M. Kallel, B. Elleuch, J.F. Fauvarque, Electrochemical treatment of olive mill wastewater: treatment extent and effluent phenolic compounds monitoring using some uncommon analytical tools, *J. Environ. Sci.* 25 (2013) 220–230.
- [8] P.P. Liebgott, M. Labat, A. Amouric, J.L. Tholozan, J. Lorquin, Tyrosol degradation via the homogentisic acid pathway in a newly isolated *Halomonas* strain from olive processing effluents, *J. Appl. Microbiol.* 105 (2008) 2084–2095.
- [9] S. Ammar, M.A. Oturan, L. Labiadh, A. Guersalli, R. Abdelhedi, N. Oturan, E. Brillas, Degradation of tyrosol by a novel electro-Fenton process using pyrite as heterogeneous source of iron catalyst, *Water Res.* 74 (2015) 77–87.
- [10] I. Sanchez, F. Stueber, A. Fabregat, J. Font, A. Fortuny, C. Bengoa, Degradation of model olive mill contaminants of OMW catalysed by zero-valent iron enhanced with a chelant, *J. Hazard. Mater.* 199–200 (2012) 328–335.
- [11] F.J. Benitez, J.L. Acero, F.J. Real, F.J. Rubio, A. Leal, The role of hydroxyl radicals for the decomposition of p-hydroxy phenylacetic acid in aqueous solutions, *Water Res.* 35 (2001) 1338–1343.
- [12] M. Panizza, G. Cerisola, Direct and mediated anodic oxidation of organic pollutants, *Chem. Rev.* 109 (2009) 6541–6569.
- [13] I. Sirés, E. Brillas, Remediation of water pollution caused by pharmaceutical residues based on electrochemical separation and degradation technologies: a review, *Environ. Int.* 40 (2012) 212–229.
- [14] I. Sirés, E. Brillas, M.A. Oturan, M.A. Rodrigo, M. Panizza, Electrochemical advanced oxidation processes: today and tomorrow. A review, *Environ. Sci. Pollut. Res.* 21 (2014) 8336–8367.
- [15] S. Vasudevan, M.A. Oturan, Electrochemistry: as cause and cure in water pollution—an overview, *Environ. Chem. Lett.* 12 (2014) 97–108.
- [16] I. Sirés, P.L. Cabot, F. Centellas, J.A. Garrido, R.M. Rodríguez, C. Arias, E. Brillas, Electrochemical degradation of clofibrate acid in water by anodic oxidation. Comparative study with platinum and boron-doped diamond electrodes, *Electrochim. Acta* 52 (2006) 75–85.
- [17] M. Hamza, R. Abdelhedi, E. Brillas, I. Sirés, Comparative electrochemical degradation of the triphenylmethane dye Methyl Violet with boron-doped diamond and Pt anodes, *J. Electroanal. Chem.* 627 (2009) 41–50.
- [18] E.B. Cavalcanti, S. Garcia-Segura, F. Centellas, E. Brillas, Electrochemical incineration of omeprazole in neutral aqueous medium using a platinum or boron-doped diamond. Degradation kinetics and oxidation products, *Water Res.* 47 (2013) 1803–1815.
- [19] L. Ciriaco, C. Anjo, J. Correia, M.J. Pacheco, A. Lopes, Electrochemical degradation of ibuprofen on Ti/Pt/PbO₂ and Si/BDD electrodes, *Electrochim. Acta* 54 (2009) 1464–1472.
- [20] P. Cañizares, J. Lobato, R. Paz, M.A. Rodrigo, C. Saez, Electrochemical oxidation of phenolic compound wastes with BDD anodes, *Water Res.* 39 (2005) 2687–2703.
- [21] E. Brillas, I. Sirés, C. Arias, P.L. Cabot, F. Centellas, R.M. Rodríguez, J.A. Garrido, Mineralization of paracetamol in aqueous medium by anodic oxidation with a boron-doped diamond electrode, *Chemosphere* 58 (2005) 399–406.
- [22] A. Özcan, Y. Şahin, A.S. Kopalal, M.A. Oturan, Prophan mineralization in aqueous medium by anodic oxidation using boron-doped diamond anode. Experimental parameters' influence on degradation kinetics and mineralization efficiency, *Water Res.* 42 (2008) 2889–2898.
- [23] V. Santos, J. Diogo, M.J.A. Pacheco, L. Ciriaco, A. Morão, A. Lopes, Electrochemical degradation of sulfonated amines on Si/BDD electrodes, *Chemosphere* 79 (2010) 637–645.

- [24] N. Oturan, E. Brillas, M.A. Oturan, Unprecedented total mineralization of atrazine and cyanuric acid by anodic oxidation and electro-Fenton with a boron-doped diamond anode, *Environ. Chem. Lett.* 10 (2012) 165–170.
- [25] A. El-Ghenymy, J.A. Garrido, R.M. Rodríguez, P.L. Cabot, F. Centellas, C. Arias, E. Brillas, Degradation of sulfanilamide in acidic medium by anodic oxidation with a boron-doped diamond anode, *J. Electroanal. Chem.* 689 (2013) 149–157.
- [26] C.I. Brinzila, N. Monterio, M.J. Pacheco, L. Ciriaco, I. Siminicéanu, A. Lopes, Degradation of tetracycline at a boron-doped diamond anode: influence of initial pH, applied current intensity and electrolyte, *Environ. Sci. Pollut. Res.* 21 (2014) 8457–8465.
- [27] A. Bedolla-Guzman, I. Sirés, A. Thiam, J.M. Peralta-Hernández, S. Gutiérrez-Granados, E. Brillas, Application of anodic oxidation, electro-Fenton and UVA photoelectro-Fenton to decolorize and mineralize acidic solutions of Reactive Yellow 160 azo dye, *Electrochim. Acta* 206 (2016) 307–316.
- [28] P. Cañizares, R. Paz, C. Sáez, M.A. Rodrigo, Electrochemical oxidation of alcohols and carboxylic acids with diamond anodes. A comparison with other advanced oxidation processes, *Electrochim. Acta* 53 (2008) 2144–2153.
- [29] K. Cruz-González, O. Torres-López, A. García-León, E. Brillas, A. Hernández-Ramírez, J.M. Peralta-Hernández, Optimization of electro-Fenton/BDD process for decolorization of a model azo dye wastewater by means of response surface methodology, *Desalination* 286 (2012) 63–68.
- [30] A. Wang, J. Qu, H. Liu, J. Ru, Mineralization of an azo dye Acid Red 14 by photoelectro-Fenton process using an activated carbon fiber cathode, *Appl. Catal. B: Environ.* 84 (2008) 393–399.
- [31] A. Khataee, A. Akbarpour, B. Vahi, Photoassisted electrochemical degradation of an azo dye using Ti/RuO₂ anode and carbon nanotubes containing gas-diffusion cathode, *J. Taiwan Inst. Chem. Eng.* 45 (2014) 930–936.
- [32] N. Daneshvar, S. Aber, V. Vatanpour, M.H. Rasoulifard, Electro-Fenton treatment of dye solution containing Orange II: influence of operational parameters, *J. Electroanal. Chem.* 615 (2008) 165–174.
- [33] A. Dirany, I. Sirés, N. Oturan, A. Özcan, M.A. Oturan, Electrochemical treatment of the antibiotic sulfaclozopyridazine: kinetics, reaction pathways, and toxicity evolution, *Environ. Sci. Technol.* 46 (2012) 4074–4082.
- [34] A. El-Ghenymy, R.M. Rodríguez, E. Brillas, N. Oturan, M.A. Oturan, Electro-Fenton degradation of the antibiotic sulfanilamide with Pt/carbon-felt and BDD/carbon-felt cells. Kinetics reaction intermediates, and toxicity assessment, *Environ. Sci. Pollut. Res.* 21 (2014) 8368–8378.
- [35] M.S. Yahya, N. Oturan, K. El Kacemi, M. El Karbane, C.T. Aravindakumar, M.A. Oturan, Oxidative degradation study on antimicrobial agent ciprofloxacin by electro-Fenton process: kinetics and oxidation products, *Chemosphere* 117 (2014) 447–454.
- [36] I. Sirés, F. Centellas, J.A. Garrido, R.M. Rodríguez, C. Arias, P.L. Cabot, E. Brillas, Mineralization of clofibrac acid by electrochemical advanced oxidation processes using a boron-doped diamond anode and Fe²⁺ and UVA light as catalysts, *Appl. Catal. B: Environ.* 72 (2007) 373–381.
- [37] S. Garcia-Segura, A. El-Ghenymy, F. Centellas, R.M. Rodríguez, C. Arias, J.A. Garrido, P.L. Cabot, E. Brillas, Comparative degradation of the diazo dye Direct Yellow 4 by electro-Fenton, photoelectro-Fenton and photo-assisted electro-Fenton, *J. Electroanal. Chem.* 681 (2012) 36–43.
- [38] A. Thiam, I. Sirés, J.A. Garrido, R.M. Rodríguez, E. Brillas, Decolorization and mineralization of Allura Red AC aqueous solutions by electrochemical advanced oxidation processes, *J. Hazard. Mater.* 290 (2015) 34–42.
- [39] A. Thiam, I. Sirés, F. Centellas, P.L. Cabot, E. Brillas, Decolorization and mineralization of Allura Red AC azo dye by solar photoelectro-Fenton: identification of intermediates, *Chemosphere* 136 (2015) 1–8.
- [40] A.D. Eaton, L.S. Clesceri, E.W. Rice, A.E. Greenberg (Eds.), *Standard Methods for the Examination of Water and Wastewater*, 21 st ed., American Public Health Association (APHA), American Water Works Association (AWWA), Water Environment Federation (WEF), Washington D.C., USA, 2005.
- [41] E.J. Ruiz, A. Hernández-Ramírez, J.M. Peralta-Hernández, C. Arias, E. Brillas, Application of solar photoelectro-Fenton technology to azo dyes mineralization: effect of current density, Fe²⁺ and dye concentrations, *Chem. Eng. J.* 171 (2011) 385–392.
- [42] B. Boye, P.A. Michaud, B. Marselli, M.M. Dieng, E. Brillas, C. Cominellis, Anodic oxidation of 4-chlorophenoxyacetic acid on synthetic boron-doped diamond electrodes, *N. Diamond Front. Carbon Technol.* 12 (2002) 63–72.
- [43] B. Marselli, J. Garcia-Gomez, P.A. Michaud, M.A. Rodrigo, C. Cominellis, Electrogeneration of hydroxyl radicals on boron-doped diamond electrodes, *J. Electrochem. Soc.* 150 (2003) D79–D83.
- [44] H. Olvera-Vargas, N. Oturan, D. Buisson, M.A. Oturan, A coupled bio-EF process for mineralization of the pharmaceuticals furosemide and ranitidine: feasibility assessment, *Chemosphere* 155 (2016) 606–613.

9. SUMMARY

The decontamination of OOMW is very difficult due its complex nature and variety of organic components. One way to enhance the decontamination of this kind of wastewater would be to understand the processes involved in the removal of single components. In this Thesis and for the first time, the degradation and mineralization of three aromatic acids generally found in olive oil mill wastewater were studied by different EAOPs.

The destruction of *trans*-cinnamic, *trans*-ferulic and 4-hydroxyphenylacetic acids was performed under similar experimental conditions, separately. Solutions of 100 mL of each acid in 0.050 M Na₂SO₄ at acidic pH 3.0 and constant temperature of 35 °C were treated by anodic oxidation with electrogenerated H₂O₂ (AO-H₂O₂), electro-Fenton (EF), UVA photoelectro-Fenton (PEF) and solar photoelectro-Fenton (SPEF) using a stirred tank reactor equipped with a 3 cm² boron-doped diamond (BDD) anode and a 3 cm² carbon-polytetrafluoroethylene air-diffusion cathode. After establishing the best conditions for the mineralization of the acids in each EAOP tested, 4-hydroxyphenylacetic acid was chosen as a model component. This acid was spiked into the OOMW in order to study the matrix effect, including aqueous mixtures with different percentages of this wastewater, over its degradation performance.

In AO-H₂O₂, each acid and its intermediates were pre-eminently destroyed by •OH formed at the BDD surface via reaction (45). In EF, the removal of organic matter was enhanced by the additional production of •OH in the bulk from Fenton's reaction (12) between H₂O₂ generated at the cathode and Fe²⁺ added at the beginning of experiment (0.50 mM). In the case of PEF, the process was accelerated thanks to the photocatalytic action of UVA radiation provided by a 6 W lamp. In SPEF, the solution was directly exposed to sunlight illumination. In each treatment, the influence of current density and initial acid concentration on total organic carbon (TOC) decay was thoroughly assessed. Additionally, the chemical oxygen demand (COD) and the 5-day biochemical oxygen demand (BOD₅) were followed in the runs performed with OOMW. Short-chain aliphatic carboxylic acids generated during treatments were identified and quantified by ion-exclusion HPLC, whereas aromatic intermediates were identified by GC-MS. A reaction pathway for each acid was finally proposed based on all the detected intermediates.

Preliminary experiments were made to clarify the behavior of the cathode and the anode during the electrogeneration of H₂O₂ in an undivided electrolytic cell using a carbon-polytetrafluoroethylene (PTFE) air-diffusion cathode and a Pt anode, each with an immersed area of 3 cm². The conditions for all the assays were: 100 mL of a 0.050 M Na₂SO₄ solution at pH 3.0 kept at 25 °C, under AO-H₂O₂, EF and PEF conditions. A concentration 0.50 mM of Fe²⁺ was added when using EF and PEF; furthermore, the solution was exposed to a 6 W UVA lamp with $\lambda_{\max} = 360$ nm in PEF. The increase in current density (j) from 33.3 to 100 mA cm⁻², caused the accumulation of higher H₂O₂ concentration, which always tended to a steady value that was achieved when its generation rate from reaction (35) became equal to its destruction rate, including its oxidation at the anode from reactions (39) and (40), in the bulk from Fenton's reaction (12) in EF and from photolytic reaction (21) in PEF. As a result, the accumulation of H₂O₂ in the cell dropped in the sequence:

AO-H₂O₂ > EF > FEF, in agreement with its quicker removal. The current efficiency was very high at the beginning of the electrolysis, but decayed dramatically as the treatment was prolonged due to the enhancement of destruction reactions. These results confirmed that H₂O₂ concentration attained was enough to further destroy the organic pollutants in all the EAOPs in an effective manner.

Several trials were carried out using Pt as the anode for *trans*-cinnamic acid, *trans*-ferulic acid and 4-hydroxyphenylacetic acid degradation. However, experiments made at $j = 33.3 \text{ mA cm}^{-2}$ for 360 min revealed a very low degradation of these acids (< 20% TOC decay). Since similar production of H₂O₂ was expected using the more powerful BDD (see section 1.6.1), this anode was employed to degrade the organic matter in subsequent assays.

The degradation of synthetic aqueous solutions containing 0.926 mM of *trans*-cinnamic acid (100 mg L⁻¹ TOC) and 0.050 M Na₂SO₄ at acidic pH 3.0 and 25 °C was studied for j values varying between 16.7 and 100 mA cm⁻². In all the EAOPs tested, TOC was gradually reduced along the electrolysis. In AO-H₂O₂ this can be accounted for by the large generation of BDD(•OH) via reaction (45), reaching a maximum TOC reduction of 66.7% when applying 100 mA cm⁻². In EF, the great amounts of •OH formed from Fenton's reaction (12) yielded a higher TOC abatement, attaining 90% at 100 mA cm⁻². In order to attain this value in PEF, a j as low as 16.7 mA cm⁻² was required. This could be explained by the fact that most by-products formed at the end of electrolysis were photosensitive, leading to a 98% TOC reduction at the other j values applied in PEF. Consequently, the oxidation ability of EAOPs increased in the sequence: AO-H₂O₂ < EF < PEF. For each method, the mineralization was enhanced at increasing current density. The most potent method, PEF, allowed reaching 98% mineralization after 180 min at 33.3 and 66.7 mA cm⁻², meaning that UVA light is a powerful tool for the decontamination of this typical component of OOMW. However, the mineralization current efficiency (MCE) for each EAOP diminished as j rose. In AO-H₂O₂, the MCE was practically the same for all the treatments, suggesting a constant removal of organics with the low amounts of BDD(•OH) produced. Maximum current efficiencies were found in EF and PEF during the first 120 min of electrolysis, thanks to the quick destruction of *trans*-cinnamic acid and the formation of intermediates that are attacked by •OH in the bulk. In PEF, once the recalcitrant intermediates were removed, the photosensitive compounds were gradually mineralized under UVA irradiation, yielding a high MCE of 73% after 90 min at 16.7 mA cm⁻².

Another important parameter was the *trans*-cinnamic acid concentration, whose effect on TOC removal was carefully assessed. To this purpose, solutions with concentrations of 0.185, 0.463, 0.926 and 1.852 mM of this acid were electrolyzed at 33.3 mA cm⁻². The amount of TOC removed grew when the concentration of the acid increased: in AO-H₂O₂, from 68% to 81%, in EF, from 75% to 81% and, in PEF, from 87% to 97%, thus making the process much more efficient. Since greater organic load led to higher quantities of TOC removed, higher MCE values were always found. For example, the MCE values at 120 min varied from 8.6% to 60% in AO-H₂O₂, from 5.1 to 53% in EF and from 8.6% to 60% in PEF. Since a similar j was applied in all the treatments, analogous •OH was produced under EF and PEF conditions. The enhancement in TOC abatement can then be attributed to the deceleration of parasitic reactions (51)-(53) and hence, more hydroxyl radicals could react with the initial contaminant and its intermediates, which in turn

promoted the formation of photosensitive compounds and their quicker elimination under the action of UVA light. The optimum conditions for the PEF process were 0.926 mM *trans*-cinnamic acid at 33.3 mA cm⁻², yielding 98% mineralization and 16% MCE. It should be noted that even higher acid concentrations did not improve the TOC reduction.

To elucidate the mineralization pathways of *trans*-cinnamic acid, samples were withdrawn after 90 min of AO-H₂O₂ treatment using 0.926 mM of the acid at pH 3.0 and 33.3 mA cm⁻², and were subsequently analyzed by GC-MS. The results informed about the presence of some intermediates such as coumarin, benzeneacetaldehyde and 3-phenylpropanoic acid, which are formed from an internal cyclization of the carboxylic group, decarboxylation and oxidation of double bond to a single one, respectively. 4-Hydroxyphenylacetic acid, benzaldehyde and benzoic acid proceeding from further decomposition of benzeneacetaldehyde were also detected. HPLC chromatograms of all electrolyzed solutions exhibited well-defined peaks related to the destruction of the parent molecule and its intermediates yielding final short-chain carboxylic acids such as to oxalic, acetic and fumaric acids. The two latter acids are formed from the cleavage of the benzene ring of aromatic derivatives, then being oxidized to oxalic acid, which is completely mineralized to CO₂ after 240 min in PEF. These products are the result of the oxidation with BDD([•]OH) formed from water oxidation at the BDD surface in AO-H₂O₂, the additional destruction with [•]OH produced in the bulk from Fenton's reaction (12) between generated H₂O₂ and added Fe²⁺ in EF, and the additional photolysis of Fe(III)-carboxylate complexes, like Fe(III)-oxalate species, upon UVA irradiation in PEF (reaction (22)).

The decay kinetics of *trans*-cinnamic acid was studied for a 0.962 mM solution at pH 3.0 and 33.3 mA cm⁻², treated by AO-H₂O₂, EF and PEF and using reversed-phase HPLC. The complete removal of the acid occurred after 360 min in AO-H₂O₂, whereas only 42 min were needed in EF and PEF. This could be explained by the rapid reaction of the acid with [•]OH radicals present in the medium produced by Fenton's reaction (12) in comparison with the slow reaction with BDD([•]OH) radicals. Moreover, the photolytic action of UVA light does not seem to play an important role during PEF process. The apparent rate constant (k_1) was 0.012 min⁻¹ in AO-H₂O₂, 0.052 min⁻¹ in EF and 0.050 min⁻¹ in PEF. These values corroborated that both, EF and PEF were able to quickly remove *trans*-cinnamic acid thanks to the production of [•]OH in the bulk. Some experiments were also performed at lower acid concentration, namely 0.185 and 0.463 mM, requiring a shorter time for complete disappearance. This led to an increase of k_1 to 0.014 min⁻¹ in AO-H₂O₂ and 0.58 min⁻¹ in EF in the case of 0.185 mM *trans*-cinnamic acid. This suggests that the reaction does not follow a true pseudo-first-order reaction. Since similar amounts of [•]OH and BDD([•]OH) are produced during all the treatments at the same j value, a greater quantity of these radicals can effectively react with the intermediates generated as the initial content of the parent compound is increased, reducing their ability to attack *trans*-cinnamic acid.

The next step of the Thesis was focused on the degradation of the *trans*-ferulic acid at 35 °C, following the experimental conditions chosen for the OOMW components. To determine the kinetics of *trans*-ferulic acid degradation, several electrolyses were performed with solutions containing 0.167, 0.417 and 0.834 mM of the acid at a current density of 33.3-100 mA cm⁻². During the trials, a drop in pH

from 3.0 to 2.8 could be observed due to the generation of carboxylic acids. The reduction of *trans*-ferulic acid concentration for a 0.834 mM solution was very slow in AO-H₂O₂, reaching 95% after 360 min, whereas it took 15 min in EF and 10 min in PEF due to the additional action of •OH in the medium. The similar time need for total removal in EF and PEF showed that there was a little participation of UVA light to generate more •OH radicals in the medium and thus degrade the acid faster. It is noticeable that the concentration decays always obeyed a pseudo-first-order kinetics, which could be due to a stable generation of radicals (•OH and BDD (•OH)). The k_1 values were similar for EF (0.32 min⁻¹) and PEF (0.34 min⁻¹), being three orders of magnitude higher than that of AO-H₂O₂ (7.2 × 10⁻³ min⁻¹). The kinetic studies with solutions containing 0.167 and 0.417 mM of the acid, made at 33.3 mA cm⁻², required shorter time for total disappearance. Therefore, they yielded a higher k_1 value that indicates that the acid degradation did not obey a true pseudo-first-order kinetics. This can be again accounted for the reaction of •OH and BDD (•OH) with a larger number of intermediates that are formed during the degradation of the higher contents of the parent molecule.

Once clarified the degradation of *trans*-ferulic acid solutions, their mineralization was comparatively studied by means of AO-H₂O₂, EF, PEF and SPEF monitoring the TOC abatement. It was found that, under comparable conditions, the oxidation power of the methods increased in the sequence: AO-H₂O₂ < EF < PEF < SPEF. For example, at 33.3 mA cm⁻², the treatment of 0.834 mM *trans*-ferulic acid solutions yielded TOC abatements of 98% in PEF, 80% in EF and 72% in AO-H₂O₂. Nevertheless, at 180 min of PEF, a 95% mineralization was already attained, which is related to the photolysis of the intermediates and the photodecomposition of Fe(III)-carboxylate complexes by reaction (22).

The next parameter to be analyzed was the current density. The electrolyses were carried with solutions of 0.834 mM at j values from 16.7 to 100 mA cm⁻² for 360 min. In AO-H₂O₂ and EF, a gradual enhancement of mineralization was found with the progressive increase of j . This can be accounted for by the expected larger formation of BDD(•OH) in AO-H₂O₂ and •OH in EF from Fenton's reaction (12). However, the PEF process was faster within the early stages, and in only 180 min the TOC was reduced by more than 95% regardless of the current density. This is an evidence of the positive photolytic action of UVA light, which photolyzed more rapidly the intermediates when they were formed more quickly upon action of higher amounts of BDD(•OH) and •OH. By increasing j , the MCE was gradually reduced due to the faster destruction of the excess of hydroxyl radicals in their parasitic reactions (51)-(53).

The influence of initial *trans*-ferulic acid concentration within the range 0.167-1.668 mM was assessed at a j value of 33.3 mA cm⁻². Analyzing the results, it was possible to notice a greater TOC decay at higher initial concentration, which was accompanied by a higher MCE. For example: at the highest substrate concentration, maximum TOC abatements of 74%, 80% and 98% were obtained in AO-H₂O₂, EF and PEF, respectively. Therefore, the PEF process exhibited the highest oxidation power. In all these treatments, performed at the same j , a similar amount of hydroxyl radicals was expected to be produced. Consequently, at higher organic matter content, the reaction between the •OH or BDD(•OH) and the oxidation products was favored, thus hampering the occurrence of parasitic reactions. Additionally, in the PEF process there was a rapid photodecomposition

of the intermediates upon the action of UVA radiation.

SPEF trials showed a rapid destruction of *trans*-ferulic acid. This process was even faster than classical PEF under similar conditions, due to the higher intensity of UVA radiation provided by sunlight. A solution with 0.834 mM *trans*-ferulic acid underwent a 93% mineralization at 33.3 mA cm⁻², after 120 min, and it only required half of this time when j rose to 100 mA cm⁻². This can be explained by the high production of •OH in the medium combined with the faster photolysis of intermediates during electrolysis. When the acid concentration was reduced to 0.417 mM and the same j was applied in SPEF, TOC decreased by 84% and become stable over time. This lower TOC reduction in SPEF compared to 94% obtained in PEF under similar conditions resulted from the quicker photolysis of some intermediates in SPEF, producing highly recalcitrant compounds that were accumulated at the end of the electrolysis. The most efficient SPEF treatment with maximum 44% MCE was obtained by electrolyzing a 0.834 mM acid solution for 120 min at 33.3 mA cm⁻², achieving a 93% TOC abatement.

Identification of intermediates during *trans*-ferulic acid mineralization was performed by GC-MS at 30 and 90 min of electrolysis, employing a solution with 0.834 mM at 33.3 mA cm⁻². The following intermediates were detected: 2-methoxy-4-vinylphenol, 4-ethyl-2-methoxyphenol, 1-(2,4-dihydroxyphenyl)ethanone, and vanillin. The former product was formed from the decarboxylation of *trans*-ferulic acid, whereas 4-ethyl-2-methoxyphenol and vanillin are produced from its subsequent oxidation. In addition, the cleavage of the benzene ring of the aromatic compound gave rise to a mixture of carboxylic acids such as fumaric, acetic and oxalic, which were detected by ionic-exclusion HPLC. These acids form complexes with Fe(III) that are quite persistent, since BDD(•OH) and •OH find it difficult to degrade them, but they can be photodecarboxylated under UVA irradiation in PEF, especially the final Fe(III)-oxalate complexes that are converted into CO₂, regenerating Fe²⁺.

The last typical compound of OOMW to be treated by EAOPs in this Thesis was the 4-hydroxyphenylacetic acid. First, the effect of j on TOC removal in AO-H₂O₂ was studied, since j determines the amount of reactive BDD(•OH) radical acting at given experimental conditions. For this, 100 mL of synthetic solutions containing 1.03 mM of this substrate were electrolyzed at increasing j , from 16.7 to 100 mA cm⁻², for 360 min. As expected, the increase in j yielded a higher mineralization rate. The percentage of TOC removal increased from 69.1% to 95% when j rose from 16.7 to 100 mA cm⁻², thanks to the concomitant acceleration of reaction (45).

The mineralization of 4-hydroxyphenylacetic acid solutions followed a pseudo-first-order kinetics, governed by the low content of oxidants generated and the mass transport of the acid and its derivatives towards the anode. The apparent rate constant (k_{TOC}) was 3.4x10⁻³, 3.9x10⁻³, 6.6x10⁻³ and 7.9x10⁻³ min⁻¹ at j values of 16.7, 33.3, 66.7 and 100 mA cm⁻², respectively. From the small increase of k_{TOC} with j , a progressive efficiency reduction at greater j can be inferred. This behavior was verified by calculating the MCE for 1.03 mM acid solutions at different j . The most efficient process was obtained at 16.7 mA cm⁻², with 28.4% current efficiency after the first 60 min of electrolysis. The MCE underwent a progressive decay along electrolysis time in all cases. This can be attributed to the gradual disappearance of the organic matter in the medium and the formation of by-products that are more difficult to degrade by BDD(•OH). When raising j , the

mineralization rate of 4-hydroxyphenylacetic acid increased, but MCE decreased. Under these conditions, parasitic reactions consume more largely the main oxidant BDD(\bullet OH), with the consequent waste of current in reactions that do not contribute to the destruction of organic matter in the cell.

The specific energy consumption per unit TOC mass (EC_{TOC}) was another parameter analyzed during the degradation of this acid since it determines if the process can be viable for practical applications. Higher EC_{TOC} values were found at higher j , which was expected because of the great increase in cell voltage. Values of $4.30 \text{ kWh (g TOC)}^{-1}$ and $0.325 \text{ kWh (g TOC)}^{-1}$ were determined at j of 100 and 16.7 mA cm^{-2} , respectively. Based on these data and electricity cost in Spain, the best AO- H_2O_2 treatment for 1.03 mM 4-hydroxyphenylacetic acid had a cost of 0.030 euros per gram of TOC, with 69% TOC removal and 29.1% MCE at 16.7 mA cm^{-2} .

Solutions of 4-hydroxyphenylacetic acid were also treated at different concentrations, ranging from 0.21 to 2.06 mM, at a j value of 33.3 mA cm^{-2} for 360 min in order to study the effect of substrate concentration on AO- H_2O_2 performance. The rate of the 4-hydroxyphenylacetic acid mineralization depended on its initial content, since an equal amount of oxidant BDD(\bullet OH) was theoretically produced during all the experiments at a given j . TOC removal from these solutions increased with increasing concentration, thus achieving a TOC abatement of 67.0%, 82.6%, 75.5% and 64.1% at 0.21, 0.51, 1.03 and 2.06 mM, respectively. At the highest concentration of 2.06 mM, a decrease in the percentage of TOC removal was clearly found, although a larger amount of TOC was removed from the medium because more molecules of 4-hydroxyphenylacetic acid and its derivatives present in the media reacted with BDD(\bullet OH), minimizing its parasitic non-oxidizing reaction. This trend was more evident when MCE values were analyzed, since 2.15%, 6.54%, 21.9% and 20.3% of efficiency was obtained after 360 min of treatment at concentrations of 0.21, 0.51, 1.03 and 2.06 mM. These values highlight that MCE increased when the 4-hydroxyphenylacetic acid content was raised. When the EC_{TOC} values were analyzed, a gradual drop was determined when the acid concentration was increased. For example, $0.59 \text{ kWh (g TOC)}^{-1}$ were consumed to remove 64.1% of TOC from a 2.06 mM concentration with 20.3% MCE. This indicates that the AO- H_2O_2 process became efficient enough with lower energy consumption if concentrated solutions were treated.

The kinetics of 4-hydroxyphenylacetic acid decay was analyzed using reversed-phase HPLC using a 1.03 mM acid solution at $j = 33.3 \text{ mA cm}^{-2}$, achieving almost total removal after 360 min. However, there were still remaining intermediates in the final solution. The data allowed determining a pseudo-first-order rate constant of $1.0 \times 10^{-2} \text{ min}^{-1}$ for this reaction. This value suggests that 4-hydroxyphenylacetic acid was degraded by a constant concentration of BDD(\bullet OH) radicals. This is feasible by the short lifetime of this radical, around 10^{-9} s , which allows the presence of a very small steady concentration during the whole AO- H_2O_2 process. Since the absolute second order rate constant of 4-hydroxyphenylacetic acid was $7.02 \times 10^8 \text{ M}^{-1} \text{ s}^{-1}$, it was possible to estimate that the concentration of BDD(\bullet OH) radical was approximately $2.4 \times 10^{-13} \text{ M}$, which acted in the anode vicinity.

The aromatic intermediates formed during degradation of 1.03 mM 4-hydroxyphenylacetic acid at $j = 33.3 \text{ mA cm}^{-2}$ were identified by means of GC-MS. Two aromatic intermediates were found, namely 4-hydroxybenzenemethanol and

4-hydroxybenzaldehyde, in addition to acetic acid. It can then be assumed that the BDD(\bullet OH) radical decarboxylated the 4-hydroxyphenylacetic acid with hydroxylation to produce the diol 4-hydroxybenzenemethanol, which was subsequently oxidized to 4-hydroxybenzaldehyde, whereas acetic acid was the product of oxidation of the aromatic intermediates by cleavage of their benzenic ring. Other carboxylic acids were also detected by ionic-exclusion HPLC, such as acetic acid in traces and oxalic acid, which attained a concentration of 0.71 mM after 240 min of electrolysis.

The study of 4-hydroxyphenylacetic acid destruction was followed by considering the EF and PEF processes. The experiments were performed under the same conditions used in AO-H₂O₂, but adding 0.50 mM Fe²⁺ in the two latter processes and exposing the solution to a 6 W UVA lamp in PEF. Two operation parameters were studied to know their effect on the performance of both EAOPs: the 4-hydroxyphenylacetic acid concentration and the current density. The first effect was studied from 0.21 to 2.06 mM and the second one by increasing j from 16.7 to 100 mA cm⁻².

Experiments with 1.03 mM 4-hydroxyphenylacetic acid in 0.050 M Na₂SO₄ at 16.7 mA cm⁻² exhibited a continuous TOC reduction with time, reaching a maximum of 69%, 86% and 98% in AO-H₂O₂, EF and PEF. This tendency clearly indicates that the PEF process was the most effective treatment to mineralize the organic load. This is related to the oxidation power of the BDD(\bullet OH) radical, along with that of peroxodisulfate and ozone formed during AO-H₂O₂, whereas in EF the greater amount of \bullet OH radical produced via Fenton's reaction (12) increased the oxidation ability of the method. In PEF, greater mineralization was obtained thanks to the photolysis of some intermediates that are formed during the electrolysis and the photoreduction of iron-carboxylate complexes by the action of UVA light through reaction (22).

The concentration of generated hydroxyl radicals in EF and PEF depends on the current density. Experiments performed in the range 16.7-100 mA cm⁻² showed a greater TOC decay at higher j . For example, in EF, TOC abatements of 85.7%, 90.1%, 93.5% and 94.8% were obtained at 16.7, 33.3, 66.7 and 100 mA cm⁻², respectively. The same tendency was observed in PEF, although the mineralization was at least as high as 97.5% at all current densities. PEF led to a very fast mineralization and, in only 180 min, the TOC removal was > 78.8% at lower j values, performing better at growing current density. The difference in the amount of TOC reduced when comparing EF and PEF was 12.6 mg L⁻¹ upon application of 16.7 mA cm⁻² and 15.1 mg L⁻¹ at 100 mA cm⁻², which can be explained by the rapid formation of photosensitive intermediates at higher j , being quickly removed by UVA light.

A drop in MCE values with increasing j was observed for all the processes. Maximum current efficiencies of 54% in EF and 49.9% in PEF were found at 16.7 mA cm⁻², further dropping at higher current densities. In all cases, the mineralization current efficiency decreased almost exponentially along the last 180 min of electrolysis due to the loss of organic load and the formation of more recalcitrant by-products. However, at the lowest j there was a peak of efficiency in EF and PEF at around 120-180 min, due to the smaller amounts of hydroxyl radicals produced that destroy slowly the recalcitrant benzenic by-products.

The substrate concentration is another important variable since it affects the attack of oxidants on organics and the extent of parasitic reactions. The assays by increasing the content of parent compound confirmed again that PEF was the most efficient treatment to remove 4-hydroxyphenylacetic acid, achieving an almost complete mineralization with 98% of TOC removal, even at high concentrations. At 360 min, TOC was reduced by 72.1%, and 79.3% in EF and 92.2% and 88.8% in PEF for solutions containing 0.21 and 2.06 mM of acid, respectively. A larger amount of TOC was removed from more concentrated solutions. In the case of PEF, for example, 100 mg L⁻¹ of TOC were abated from a solution with 1.03 mM, whereas in a solution with an initial concentration of 2.06 mM a much higher quantity of 175 mg L⁻¹ was removed. This is due to the positive photolytic action of UVA light that destroyed greater quantities of photoactive intermediates formed at higher 4-hydroxyphenyl acid concentration.

The reaction of 4-hydroxyphenylacetic acid with generated oxidants was monitored by reversed-phase HPLC. The concentration of 4-hydroxyphenylacetic acid decayed exponentially for a 1.03 mM solution under EF and PEF conditions at 33.3 mA cm⁻². This acid disappeared after 60 min in EF, and slightly more rapidly, after 45 min, in PEF. This indicates that the main oxidant in these processes was the •OH radical in the bulk, with contribution from the photolysis of Fe(OH)²⁺ species via reaction (21) in PEF. The decay of 4-hydroxyphenylacetic acid obeyed a pseudo-first-order kinetics with a k_1 value of 1.4x10⁻³ s⁻¹ in EF and 1.9x10⁻³ s⁻¹ in PEF. This behavior suggests that 4-hydroxyphenylacetic acid was predominantly attacked by a steady and low concentration of •OH in the bulk.

Final short-chain acids generated during EF and PEF treatments of 4-hydroxyphenylacetic acid were identified and quantified by ion-exclusion HPLC. The most important linear aliphatic acid accumulated from 1.03 mM of the substrate at $j = 33.3$ mA cm⁻² was oxalic. This final product was completely mineralized by PEF in only 270 min, but in EF it remained in the solution even after 360 min of electrolysis. This means that the combined action of BDD(•OH), •OH and UVA light onto the remaining photoactive by-products strongly enhanced the mineralization process.

Once the degradation of three highly recalcitrant components of OOMW, such as *trans*-cinnamic, *trans*-ferulic and 4-hydroxyphenylacetic acids, was exhaustively studied, it could be assumed that these acids would also be degraded by such EAOPs if they were contained in real OOMW samples. However, when 1.03 mM of each acid was spiked into a OOMW sample, only 4-hydroxyphenylacetic acid was easily dissolved. This acid was then chosen to clarify the effect of the OOMW matrix on the degradation performance of the EAOPs.

The mineralization of 4-hydroxyphenylacetic acid was studied using OOMW/water mixtures with ratios varying between 20/80 to 100/0 v/v. The experimental conditions were the same as those employed with 0.050 M Na₂SO₄, being utilized 100 mL of each matrix at pH 3.0 and 35 °C that were treated in a stirred tank reactor equipped with a 3 cm² BDD anode and a 3 cm² air-diffusion cathode.

The real OOMW sample was provided by a local company of olive oil production, which was physically and chemically characterized before use. Its analysis yielded the following results: pH 6.8, 505.35 mg L⁻¹ of TOC, 2368 mg O₂ L⁻¹ of COD, 1600 mg O₂ L⁻¹ of DBO₅, 5852 mg L⁻¹ of TS, 3712 mg L⁻¹ of TDS, 1.51 mS of conductivity, 245.7 NTU of turbidity, 9.3 mg L⁻¹ of phenol index, 60 mg L⁻¹ of oil and grease and

the presence of several ions such as SO_4^{2-} , NO_3^- , Cl^- , Na^+ , K^+ and a very small Fe^{2+} concentration ($< 1 \text{ mg L}^{-1}$). The sample also presented a grey color and strong odor. As a first step, the OOMW was filtered with a $18 \mu\text{m}$ cloth to avoid interferences in the TOC measurements. The GC-MS analysis revealed the presence of several phenolic compounds like 4-hydroxyphenylacetic acid, 1 heteroaliphatic alcohol as well as 4 aromatic and 4 aliphatic (1 cyclic and 3 linear) carboxylic acids.

OOMW was treated by EAOPs obtaining TOC reductions of 71.8% in AO- H_2O_2 , 79.5% in EF and 83.4% in PEF. The ability of the EAOPs was upgraded in the sequence AO- $\text{H}_2\text{O}_2 < \text{EF} < \text{PEF}$ due to attack of BDD($\cdot\text{OH}$) in AO- H_2O_2 , which was enhanced by $\cdot\text{OH}$ produced in bulk by Fenton's reaction (12) in EF and the photolysis of photoactive by-products in PEF. This was also found when 1.03 mM 4-hydroxyphenylacetic acid was added to the OOMW sample.

The degradation of 1.03 mM of 4-hydroxyphenylacetic acid in matrices containing OOMW showed that the normalized TOC removal slightly increased when the OOMW percentage of the treated effluent decreased. The quickest mineralization was achieved for the 20% v/v solution with a TOC decay of 82.5% by AO- H_2O_2 , 83.0% by EF and 86.4% by PEF. Since the initial TOC content decreased in each diluted solution, it is possible to conclude that all the treatments were more efficient at greater organic load because of the deceleration of their parasitic reactions.

The pseudo-first-order kinetics for the 4-hydroxyphenylacetic acid decay was monitored by reversed-phase HPLC. In AO- H_2O_2 , the acid disappeared after 540 min in all matrices containing OOMW in contrast to 360 min required in 0.050 M Na_2SO_4 . The degradation was faster at lower content of organics in the medium. The k_1 values gradually increased from $7.3 \times 10^{-5} \text{ s}^{-1}$ for the 100% OOMW to $2.0 \times 10^{-4} \text{ s}^{-1}$ for 0.050 M Na_2SO_4 . The process was faster in PEF where it disappeared in only 50 min for 0.050 M Na_2SO_4 , 70 min for 20% OOMW matrix and 100 min for 100% OOMW. The PEF process also increased the biodegradability of the samples making possible its future coupling with a biological post-treatment.

10. CONCLUSIONS

This Thesis has led to the following conclusions:

- I. In a cell equipped with a Pt or BDD anode and an air-diffusion cathode operating with 0.050 M Na₂SO₄ at pH 3.0 and 25 °C, a high concentration of hydrogen peroxide was accumulated, with good current efficiency, under AO-H₂O₂, EF and PEF conditions. This concentration is sufficient to carry out the EF and PEF degradation of organic matter.
- II. The concentration of accumulated hydrogen peroxide is higher in AO-H₂O₂ than in EF or PEF at all current densities. In all cases, a steady concentration of H₂O₂ was reached when its rate of generation at the cathode becomes equal to its rate of destruction on the anode in AO-H₂O₂. Further decrease was found by Fenton's reaction in EF and also by the additional action of UVA light in PEF.
- III. It has been demonstrated that the EAOPs checked in this Thesis using a cell with a BDD anode and an air-diffusion cathode under comparable experimental conditions were capable of degrading solutions of *trans*-cinnamic, *trans*-ferulic and 4-hydroxyphenyl acetic acids with 0.050 M Na₂SO₄ at pH 3.0 and constant temperature. The information obtained in is very useful for a deeper understanding of OOMW decontamination by these techniques.
- IV. The decay kinetics of *trans*-cinnamic, *trans*-ferulic and 4-hydroxyphenylacetic acids always obeyed a pseudo-first-order reaction. The apparent rate constant increased with raising current density because of the formation of a larger number of hydroxyl radicals. Conversely, an increase in substrate concentration led to a slower degradation, although a large quantity of the parent acid was removed.
- V. The percentage of TOC removal from *trans*-cinnamic, *trans*-ferulic and 4-hydroxyphenylacetic acid solutions increased in the order AO-H₂O₂ < EF < PEF under comparable conditions. The oxidative action of the physisorbed BDD(•OH) radical at the anode surface in AO-H₂O₂ was enhanced by the formation of hydroxyl radicals in the bulk from Fenton's reaction in EF. The higher oxidation power of the PEF method was related to the additional photolysis of intermediates under UVA light irradiation.
- VI. The mineralization rate of *trans*-cinnamic, *trans*-ferulic and 4-hydroxyphenylacetic acids rose at higher current density for all the methods tested. However, the mineralization current efficiency decreased since the parasitic non-oxidizing reactions that consume hydroxyl radicals were largely accelerated.
- VII. The increase in concentration of *trans*-cinnamic, *trans*-ferulic and 4-hydroxyphenylacetic acids caused a higher loss of total organic carbon with

higher mineralization current efficiency because the presence of more organic matter favored the reaction of the acids and their by-products with hydroxyl radicals, thus decelerating their wasting reactions.

- VIII. Reaction pathways have been established to explain the *trans*-cinnamic mineralization by EAOPs. The acid is initially converted into coumarin, benzeneacetaldehyde and 3-phenylpropanoic acid. Further oxidation of benzeneacetaldehyde yields 4-hydroxyphenylacetic acid, benzaldehyde and benzoic acid. All these products then evolve to short-linear aliphatic carboxylic acids due to the cleavage of their benzene rings. Finally, these carboxylic acids generate oxalic acid that is directly converted into CO₂.
- IX. A reaction sequence for *trans*-ferulic acid mineralization has been proposed based on the products detected by HPLC and GC-MS. The decarboxylation of this acid yields 2-methoxy-4-vinylphenol, which is subsequently oxidized to 4-ethyl-2-methoxyphenol, 1-(2,4-dihydroxyphenyl) ethanone and vanillin. The cleavage of the aromatic products leads to fumaric, acetic and oxalic acids, the latter one being directly oxidized to CO₂.
- X. During the treatment of 4-hydroxyphenylacetic acid by AO-H₂O₂, few products were detected. The substrate was initially decarboxylated and hydroxylated to the diol 4-hydroxybenzenemethanol, which was oxidized to 4-hydroxybenzaldehyde. The degradation of these aromatics yielded acetic acid, whereas oxalic acid was accumulated and slowly removed.
- XI. The mineralization of 4-hydroxyphenylacetic acid in a synthetic matrix with 0.050 M Na₂SO₄ becomes more cost-effective if a low *j* is used. The best AO-H₂O₂ results in 21.9 % mineralization current efficiency with a specific energy consumption of 0.325 kWh (g TOC)⁻¹, which were obtained at 16.7 mA cm⁻² with a low TOC removal of 67.6 %.
- XII. The current efficiency for 4-hydroxyphenylacetic acid mineralization using AO-H₂O₂ was upgraded when the substrate concentration was increased, although smaller percentage of total organic carbon removal was obtained. Lower specific energy consumption was required.
- XIII. The method with higher oxidation power was PEF, which led to an almost total mineralization of *trans*-cinnamic, *trans*-ferulic and 4-hydroxyphenylacetic acids.
- XIV. The SPEF treatment of *trans*-ferulic acid solutions accelerated the mineralization process compared with PEF due to the greater UV intensity of sunlight.
- XV. 4-Hydroxyphenylacetic acid can be effectively destroyed either from raw OOMW or aqueous matrices containing a percentage of OOMW by means of EAOPs, especially by PEF where > 97% mineralization was achieved.
- XVI. The percentage of OOMW in the aqueous matrix affected the percentage of total organic carbon removal as well the 4-hydroxyphenylacetic acid

degradation rate. For each EAOP, higher mineralization rate was found as the OOMW content was increased in the mixture due to the enhancement of the reactions of components present in OOMW since they consume more rapidly the generated hydroxyl radicals.

- XVII. The PEF process yielded a greater biodegradability of OOMW and its aqueous mixtures. In conclusion, EAOPs like AO, EF and PEF are an interesting alternative for the remediation of real olive oil mill wastewater, as single technologies or in combination with pre- or post-treatments that could decrease the required time or the total costs.

11. REFERENCIAS

- Agabo, C., Hodaifa, G., 2017. Real olive oil mill wastewater treatment by photo-Fenton system using artificial ultraviolet light lamps. *J. Clean. Prod.* 162, 743–753. doi:10.1016/j.jclepro.2017.06.088
- Agència Catalana de l'Aigua, Generalitat de Catalunya, 2016. El precio del agua en Cataluña, 2016. URL: http://aca-web.gencat.cat/aca/documents/DocuWeb/estudis/observatori_preus_2016_es.pdf (acceso 06/12/17).
- Aggoun, M., Arhab, R., Cornu, A., Portelli, J., Barkat, M., 2016. Olive mill wastewater microconstituents composition according to olive variety and extraction process. *Food Chem.* 209, 72–80. doi:10.1016/j.foodchem.2016.04.034
- Alver, A., Baştürk, E., Kılıç, A., Karataş, M., 2015. Use of advance oxidation process to improve the biodegradability of olive oil mill effluents. *Process Saf. Environ. Prot.* 98, 319–324. doi:10.1016/j.psep.2015.09.002
- Amaral, C., Lucas, M.S., Sampaio, A., Peres, J.A., Dias, A.A., Peixoto, F., Anjos, M. do R., Pais, C., 2012. Biodegradation of olive mill wastewaters by a wild isolate of *Candida oleophila*. *Int. Biodeterior. Biodegrad.* 68, 45–50. doi:10.1016/j.ibiod.2011.09.013
- Andreozzi, R., Caprio, V., Insola, A., Marotta, R., 1999. Advanced oxidation processes (AOP) for water purification and recovery. *Catal. Today* 53, 51–59. doi:10.1016/S0920-5861(99)00102-9
- Angus, J.C., 2011. Electrochemistry on Diamond: History and Current Status, in: Brillas, E., Martínez-Huitle, C.A. (Eds.), *Synthetic Diamond Films: Preparation, Electrochemistry, Characterization, and Applications*. John Wiley & Sons, Inc., New Jersey, pp. 1–19. doi:10.1002/9781118062364.ch1
- Arenas-Sánchez, A., Rico, A., Vighi, M., 2016. Effects of water scarcity and chemical pollution in aquatic ecosystems: State of the art. *Sci. Total Environ.* 572, 390–403. doi:10.1016/j.scitotenv.2016.07.211
- Arvanitoyannis, I.S., Kassaveti, A., 2008. Olive Oil Waste Management: Treatment Methods and Potential Uses of Treated Waste, in: *Waste Management for the Food Industries*. Academic Press, Amsterdam, pp. 453–552. doi:10.1016/B978-0-12-373654-3.50011-0
- Asociación Española de Abastecimientos de Agua y Saneamiento, A., 2017. Día Mundial del Agua - Informe sobre aguas residuales en España. URL: <http://www.asoaeas.com/sites/default/files/Documentos/Informe sobre aguas residuales AEAS.pdf> (acceso el 06/11/17).
- Azaizeh, H., Halahlh, F., Najami, N., Brunner, D., Faulstich, M., Tafesh, A., 2012. Antioxidant activity of phenolic fractions in olive mill wastewater. *Food Chem.* 134, 2226–2234. doi:10.1016/j.foodchem.2012.04.035
- Badawy, M.I., Gohary, F.E., Ghaly, M.Y., Ali, M.E., 2009. Enhancement of olive mill wastewater biodegradation by homogeneous and heterogeneous photocatalytic oxidation. *J. Hazard. Mater.* 169, 673–679. doi:10.1016/j.jhazmat.2009.04.038
- Barbera, A.C., Maucieri, C., Cavallaro, V., Ioppolo, A., Spagna, G., 2013. Agricultural water management effects of spreading olive mill wastewater on



- soil properties and crops, a review. *Agric. Water Manage.* 119, 43–53. doi:10.1016/j.agwat.2012.12.009
- Barnaby, W., 2009. Do nations go to war over water? *Nature* 458, 282–283. doi:10.1038/458282a
- Belaid, C., Khadraoui, M., Mseddi, S., Kallel, M., Elleuch, B., Fauvarque, J.F., 2013. Electrochemical treatment of olive mill wastewater: Treatment extent and effluent phenolic compounds monitoring using some uncommon analytical tools. *J. Environ. Sci.* 25, 220–230. doi:10.1016/S1001-0742(12)60037-0
- Bickers, D., Calow, P., Greim, H., Hanifin, J.M., Rogers, A.E., Saurat, J.H., Sipes, I.G., Smith, R.L., Tagami, H., 2005. A toxicologic and dermatologic assessment of cinnamyl alcohol, cinnamaldehyde and cinnamic acid when used as fragrance ingredients. *Food Chem. Toxicol.* 43, 799–836. doi:10.1016/j.fct.2004.09.013
- Borja, R., Alba, J., Banks, C.J., 1997. Impact of the main phenolic compounds of olive mill wastewater (OMW) on the kinetics of acetoclastic methanogenesis. *Process Biochem.* 32, 121–133. doi:10.1016/S0032-9592(96)00055-6
- Brillas, E., Bastida, R.M., Llosa, E., Casado, J., 1995. Electrochemical destruction of aniline and 4-chloroaniline for waste-water treatment using a carbon-PTFE O₂-fed cathode. *J. Electrochem. Soc.* 142, 1733–1741. doi:10.1149/1.2044186
- Brillas, E., Calpe, J.C., Casado, J., 2000. Mineralization of 2,4-D by advanced electrochemical oxidation processes. *Water Res.* 34, 2253–2262. doi:10.1016/S0043-1354(99)00396-6
- Brillas, E., Mur, E., Casado, J., 1996. Iron (II) catalysis of the mineralization of aniline using a carbon PTFE O₂-fed cathode. *J. Electrochem. Soc.* 143, L49. doi:10.1149/1.1836528
- Brillas, E., Sirés, I., Oturan, M.A., 2009. Electro-Fenton process and related electrochemical technologies based on Fenton's reaction chemistry. *Chem. Rev.* 109, 6570–6631. doi:10.1021/cr900136g
- Cañizares, P., Lobato, J., Paz, R., Rodrigo, M.A., Sáez, C., 2007. Advanced oxidation processes for the treatment of olive-oil mills wastewater 67, 832–838. doi:10.1016/j.chemosphere.2006.10.064
- Catley-Carlson, M., 2011. Environment: Water, water everywhere... *Nature* 473, 27–28. doi:10.1038/473027a
- Cermola, F., DellaGreca, M., Iesce, M.R., Montella, S., Pollio, A., Temussi, F., 2004. A mild photochemical approach to the degradation of phenols from olive oil mill wastewater. *Chemosphere* 55, 1035–41. doi:10.1016/j.chemosphere.2003.12.016
- Chalmers, R.A., Valman, H.B., Liberman, M.M., 1979. Measurement of 4-hydroxyphenylacetic aciduria as a screening test for small-bowel disease. *Clin. Chem.* 25, 1791–1794.
- Chatzisyneon, E., Xekoukoulotakis, N.P., Diamadopoulou, E., Katsaounis, A., Mantzavinos, D., 2009a. Boron-doped diamond anodic treatment of olive mill wastewaters: Statistical analysis, kinetic modeling and biodegradability. *Water Res.* 43, 3999–4009. doi:10.1016/j.watres.2009.04.007
- Chatzisyneon, E., Xekoukoulotakis, N.P., Mantzavinos, D., 2009b. Determination of key operating conditions for the photocatalytic treatment of olive mill wastewaters. *Catal. Today* 144, 143–148. doi:10.1016/j.cattod.2009.01.037
- Chen, G., 2004. Electrochemical technologies in wastewater treatment. *Sep. Purif. Technol.* 38, 11–41. doi:10.1016/j.seppur.2003.10.006



- Chowdhury, A., Akratos, C.S., Vayenas, D. V., Pavlou, S., 2013. Olive mill waste composting: A review. *Int. Biodeterior. Biodegrad.* 85, 108–119. doi:10.1016/j.ibiod.2013.06.019
- Clodoveo, M.L., Camposeo, S., De Gennaro, B., Pascuzzi, S., Roselli, L., 2014. In the ancient world, virgin olive oil was called "liquid gold" by Homer and "the great healer" by Hippocrates. Why has this mythic image been forgotten? *Food Res. Int.* 62, 1062–1068. doi:10.1016/j.foodres.2014.05.034
- Comninellis, C., 1994. Electrocatalysis in the electrochemical conversion/combustion of organic pollutants for waste water treatment. *Electrochim. Acta* 39, 1857–1862. doi:10.1016/0013-4686(94)85175-1
- Cooley, J.K., 1984. The War over Water. *Foreign Policy* 3. doi:10.2307/1148352
- Coskun, T., Debik, E., Demir, N.M., 2010. Treatment of olive mill wastewaters by nanofiltration and reverse osmosis membrane. *Desalination* 259, 65–70. doi:10.1016/j.desal.2010.04.034
- D'Antuono, I., Kontogianni, V.G., Kotsiou, K., Linsalata, V., Logrieco, A.F., Tasioula-Margari, M., Cardinali, A., 2014. Polyphenolic characterization of olive mill wastewaters, coming from Italian and Greek olive cultivars, after membrane technology. *Food Res. Int.* 65, 301–310. doi:10.1016/j.foodres.2014.09.033
- Daâssi, D., Lozano-Sánchez, J., Borrás-Linares, I., Belbahri, L., Woodward, S., Zouari-Mechichi, H., Mechichi, T., Nasri, M., Segura-Carretero, A., 2014. Olive oil mill wastewaters: Phenolic content characterization during degradation by *Corioloopsis gallica*. *Chemosphere* 113, 62–70. doi:10.1016/j.chemosphere.2014.04.053
- Dai, Q., Zhou, J., Meng, X., Feng, D., Wu, C., Chen, J., 2016. Electrochemical oxidation of cinnamic acid with Mo modified PbO₂ electrode: Electrode characterization, kinetics and degradation pathway. *Chem. Eng. J.* 289, 239–246. doi:10.1016/j.cej.2015.12.054
- Danés, C., Ruza, J., Bordas, M.A., Espinosa, G., Puig, A., 2007. Manual para la Gestión de Vertidos - Autorización de vertido, 1st Ed. Fareso, S.A., Madrid.
- De Marco, E., Savarese, M., Paduano, A., Sacchi, R., 2006. Analytical, nutritional and clinical methods characterization and fractionation of phenolic compounds extracted from olive oil mill wastewaters. *Anal. Nutr. Clin. Methods* 104, 858–867. doi:10.1016/j.foodchem.2006.10.005
- De Martino, A., Arienzo, M., Iorio, M., Vinale, F., Lorito, M., Prenzler, P.D., Ryan, D., Obied, H.K., 2011. Detoxification of olive mill wastewaters by zinc–aluminium layered double hydroxides. *Appl. Clay Sci.* 53, 737–744. doi:10.1016/j.clay.2011.07.003
- DellaGreca, M., Previtera, L., Temussi, F., Zarrelli, A., 2004. Low-molecular-weight components of olive oil mill waste-waters. *Phytochem. Anal.* 15, 184–188. doi:10.1002/pca.766
- Dermeche, S., Nadour, M., Larroche, C., Moulti-Mati, F., Michaud, P., 2013. Olive mill wastes: Biochemical characterizations and valorization strategies. *Process Biochem.* 48, 1532–1552. doi:10.1016/j.procbio.2013.07.010
- Dhouib, A., Aloui, F., Hamad, N., Sayadi, S., 2006. Pilot-plant treatment of olive mill wastewaters by *Phaerochaete chrysosporium* coupled to anaerobic digestion and ultrafiltration. *Process Biochem.* 41, 159–167. doi:10.1016/j.procbio.2005.06.008
- Eaton, A.E.A., Clesceri, L.S., Rice, E.W., 2005. Standard Methods for the Examination of Water and Wastewater, 21st Ed. American Public Health Association (APHA), American Water Works Association (AWWA), Water



- Environment Federation (WEF), Washington D.C., EEUU.
- Eisenberg, G.M., 1943. Colorimetric determination of hydrogen peroxide. *Ind. Eng. Chem. Anal. Ed.* 15 (5), 327–328. doi:10.1021/i560117a011
- El Hajjouji, H., Barje, F., Pinelli, E., Bailly, J.-R., Richard, C., Winterton, P., Revel, J.-C., Hafidi, M., 2008. Photochemical UV/TiO₂ treatment of olive mill wastewater (OMW). *Bioresour. Technol.* 99, 7264–7269. doi:10.1016/j.biortech.2007.12.054
- El Hajjouji, H., Pinelli, E., Guisresse, M., Merlina, G., Revel, J., Hafidi, M., 2007. Assessment of the genotoxicity of olive mill waste water (OMWW) with the *Vicia faba* micronucleus test 634, 25–31. doi:10.1016/j.mrgentox.2007.05.015
- El-Gohary, F.A., Badawy, M.I., El-Khateeb, M.A., El-Kalliny, A.S., 2009. Integrated treatment of olive mill wastewater (OMW) by the combination of Fenton's reaction and anaerobic treatment. *J. Hazard. Mater.* 162, 1536–1541. doi:10.1016/j.jhazmat.2008.06.098
- El-Gohary, F., Tawfik, A., Badawy, M., El-Khateeb, M.A., 2008. Potentials of anaerobic treatment for catalytically oxidized olive mill wastewater (OMW). *Bioresour. Technol. J.* 100, 2147–2151. doi:10.1016/j.biortech.2008.10.051
- Elkacmi, R., Boulmal, N., Kamil, N., Bennajah, M., 2017. Techno-economical evaluation of a new technique for olive mill wastewater treatment. *Sustain. Prod. Consum.* 10, 38–49. doi:10.1016/j.spc.2016.12.004
- Enache, T.A., Chiorcea-Paquim, A.-M., Fatibello-Filho, O., Oliveira-Brett, A.M., 2009. Hydroxyl radicals electrochemically generated in situ on a boron-doped diamond electrode. *Electrochem. Commun.* 11, 1342–1345. doi:10.1016/j.elecom.2009.04.017
- Ergül, F.E., Sargin, S., Ngen, G., Sukan, F.V., 2008. Dephenolisation of olive mill wastewater using adapted *Trametes versicolor*. *Int. Biodeterior. Biodegrad.* 63, 1–6. doi:10.1016/j.ibiod.2008.01.018
- Espinoza, C., Romero, J., Villegas, L., Cornejo-Ponce, L., Salazar, R., 2016. Mineralization of the textile dye acid yellow 42 by solar photoelectro-Fenton in a lab-pilot plant. *J. Hazard. Mater.* 319, 24–33. doi:10.1016/j.jhazmat.2016.03.003
- Fajardo, A.S., Rodrigues, R.F., Martins, R.C., Castro, L.M., Quinta-Ferreira, R.M., 2015. Phenolic wastewaters treatment by electrocoagulation process using Zn anode. *Chem. Eng. J.* 275, 331–341. doi:10.1016/j.cej.2015.03.116
- Fiestas, J.A., De Ursinos, R., Borja-Padilla, 1997. Biomethanization. *Int. Biodeterior. Biodegrad.* 38, 145–153. doi:doi.org/10.1016/S0964-8305(96)00043-1
- Fujishima, A., Einaga, Y., Rao, T.N., Tryk, D.A., 2005. *Diamond Electrochemistry*, 1st Ed. BKC INC, Elsevier, Tokio.
- Galiatsatou, P., Metaxas, M., Arapoglou, D., Kasselouri-Rigopoulou, V., 2002. Treatment of olive mill waste water with activated carbons from agricultural by-products. *Waste Manage.* 22, 803–812. doi: 10.1016/S0956-053X(02)00055-7
- Gebreyohannes, A.Y., Mazzei, R., Giorno, L., 2016. Trends and current practices of olive mill wastewater treatment: Application of integrated membrane process and its future perspective. *Sep. Purif. Technol.* 162, 45–60. doi:10.1016/j.seppur.2016.02.001
- González-González, A., Cuadros, F., 2015. Effect of aerobic pretreatment on anaerobic digestion of olive mill wastewater (OMWW): An ecoefficient treatment. *Food Bioprod. Process.* 95, 339–345.



- doi:10.1016/j.fbp.2014.10.005
- Gozzi, F., Sirés, I., Thiam, A., De Oliveira, S.C., Junior, A.M., Brillas, E., 2017. Treatment of single and mixed pesticide formulations by solar photoelectro-Fenton using a flow plant. *Chem. Eng. J.* 310, 503–513. doi:10.1016/j.cej.2016.02.026
- Gupta, P., Lakes, A., Butterfield, A.D., 2016. Chapter One – A Free Radical Primer, *Oxidative Stress and Biomaterials*. Elsevier, London. doi:10.1016/B978-0-12-803269-5.00001-2
- Gutiérrez Duarte, M.V., Rodríguez López, Á., Galván Vallina, J., 2013. Objetivos y principios de la política ambiental europea. *Rev. Int. Mundo Económico y Derecho* 6, 37–69.
- Haber, F., Weiss, J., 1934. The catalytic decomposition of hydrogen peroxide by iron salts. *Proc. Royal Soc. London. Ser. A Math. Phys. Sci.* 147, 333–351. doi:10.1098/rspa.1934.0221
- Hartley, R.D., Jones, E.C., 1975. Effect of ultraviolet light on substituted cinnamic acids and the estimation of their *cis* and *trans* isomers by gas chromatography. *J. Chromatogr. A* 107, 213–218. doi:10.1016/S0021-9673(00)82768-5
- Hodaifa, G., Ochando-Pulido, J.M., Rodríguez-Vives, S., Martínez-Ferez, A., 2013. Optimization of continuous reactor at pilot scale for olive-oil mill wastewater treatment by Fenton-like process. *Chem. Eng. J.* 220, 117–124. doi:10.1016/j.cej.2013.01.065
- Hodaifa, G., Páez, J.A., Agabo, C., Ramos, E., Gutiérrez, J.C., Rosal, A., 2015. Flocculation on the treatment of olive mill wastewater: Pretreatment. *Int. J. Chem. Mol. Nucl. Mater. Metall. Eng.* 9, 645–650.
- Iamarino, G., Rao, M.A., Gianfreda, L., 2008. Dephenolization and detoxification of olive-mill wastewater (OMW) by purified biotic and abiotic oxidative catalysts. *Chemosphere* 74, 216–223. doi:10.1016/j.chemosphere.2008.09.061
- Inan, H., Dimoglo, A., Simsek, H., Karpuzcu, M., 2004. Olive oil mill wastewater treatment by means of electro-coagulation. *Sep. Purif. Technol.* 36, 23–31. doi:10.1016/S1383-5866(03)00148-5
- Instituto Nacional de Estadísticas, 2016. Estadística sobre el suministro y saneamiento del agua. Serie 2000-2014. URL: <http://www.ine.es/jaxi/Datos.htm?path=/t26/p067/p01/serie/10/&file=01004a.px> (acceso 05/29/17).
- Instituto Nacional de Estadística, 2017. INEbase / Agricultura y medio ambiente / Agua / Estadística sobre el suministro y saneamiento del agua / Últimos datos. URL: http://www.ine.es/dyngs/INEbase/es/operacion.htm?c=Estadistica_C&cid=1254736176834&menu=ultiDatos&idp=1254735976602 (acceso 06/12/17).
- International Olive Council, 2017. Olive Oil World Figures. Olive oil exportations. 2017. URL: <http://www.internationaloliveoil.org/estaticos/view/131-world-olive-oil-figures> (acceso 05/14/17).
- Ioannou-Ttofa, L., Michael-Kordatou, I., Fattas, S.C., Eusebio, A., Ribeiro, B., Rusan, M., Amer, A.R.B., Zuraiqi, S., Waismand, M., Linder, C., Wiesman, Z., Gilron, J., Fatta-Kassinou, D., 2017. Treatment efficiency and economic feasibility of biological oxidation, membrane filtration and separation processes, and advanced oxidation for the purification and valorization of olive mill wastewater. *Water Res.* 114, 1–13. doi:10.1016/j.watres.2017.02.020
- Jaouani, A., Vanthourhout, M., Penninckx, A.M.J., 2005. Olive oil mill wastewater purification by combination of coagulation-flocculation and biological



- treatments. Environ. Technol. 266, 633–642. doi:10.1080/09593330.2001.9619503
- Juretic, H., Montalbo-Lombay, M., Van Leeuwen, H., Cooper, W.J., Grewell, D., 2015. Hydroxyl radical formation in batch and continuous flow ultrasonic systems. Ultrason. Sonochem. 22, 600–606. doi:10.1016/j.ultsonch.2014.07.003
- Khoufi, S., Aloui, F., Sayadi, S., 2006. Treatment of olive oil mill wastewater by combined process electro-Fenton reaction and anaerobic digestion. Water Res. 40, 2007–2016. doi:10.1016/j.watres.2006.03.023
- Kodera, F., Kuwahara, Y., Nakazawa, A., Umeda, M., 2007. Electrochemical corrosion of platinum electrode in concentrated sulfuric acid. J. Power Sources 172, 698–703. doi:10.1016/j.jpowsour.2007.05.016
- Kontos, S.S., Koutsoukos, P.G., Paraskeva, C.A., 2014. Removal and recovery of phenolic compounds from olive mill wastewater by cooling crystallization. Chem. Eng. J. 251, 319–328. doi:10.1016/j.cej.2014.04.047
- Kraft, A., 2007. Doped diamond: A compact review on a new, versatile electrode material. Int. J. Electrochem. Sci. 2, 355–385.
- Kumar, N., Pruthi, V., 2014. Potential applications of ferulic acid from natural sources. Biotechnol. Reports 4, 86–93. doi:10.1016/j.btre.2014.09.002
- Lafi W.K., Shannak, B., Al-Shannag, M., Al-Anber, Z-, Al-Hasan, M., 2009. Treatment of olive mill wastewater by combined advanced oxidation and biodegradation. Sep. Purif. Technol. 70, 141–146. doi:10.1016/j.seppur.2009.09.008
- Lafka, T.I., Lazou, A.E., Sinanoglou, V.J., Lazos, E.S., 2011. Phenolic and antioxidant potential of olive oil mill wastes. Food Chem. doi:10.1016/j.foodchem.2010.08.041
- Letizia, C.S., Cocchiara, J., Lapczynski, A., Lalko, J., Api, A.M., 2005. Fragrance material review on cinnamic acid. Food Chem. Toxicol. doi:10.1016/j.fct.2004.09.015
- Lu, G.H., Chan, K., Leung, K., Chan, C.L., Zhao, Z.Z., Jiang, Z.H., 2005. Assay of free ferulic acid and total ferulic acid for quality assessment of *Angelica sinensis*. J. Chromatogr. A 1068, 209–219. doi:10.1016/j.chroma.2005.01.082
- Lu, H., Wang, J., Wang, T., Wang, N., Bao, Y., Hao, H., 2017. Crystallization techniques in wastewater treatment: An overview of applications. Chemosphere 173, 474–484. doi:10.1016/j.chemosphere.2017.01.070
- Luong, J.H.T., Male, K.B., Glennon, J.D., 2009. Boron-doped diamond electrode: synthesis, characterization, functionalization and analytical applications. Analyst 134, 1965–1979. doi:10.1039/b910206j
- Magdich, S., Abid, W., Boukhris, M., Rouina, B., Ammar, E., 2016. Effects of long-term olive mill wastewater spreading on the physiological and biochemical responses of adult *Chemlali* olive trees (*Olea europaea* L.). Ecol. Eng. 97, 122–129. doi:10.1016/j.ecoleng.2016.09.004
- Malten, K.E., 1976. Cinnamic acid. Food Cosmet. Toxicol. 16, 687–690. doi:10.1016/S0015-6264(78)80073-X
- Mancuso, C., Santangelo, R., 2014. Ferulic acid: Pharmacological and toxicological aspects. Food Chem. Toxicol. 65, 185–195. doi:10.1016/j.fct.2013.12.024
- Mantzavinos, D., Kalogerakis, N., 2005. Treatment of olive mill effluents Part I. Organic matter degradation by chemical and biological processes—an overview. Environ. Int. 31, 289–295. doi:10.1016/j.envint.2004.10.005



- MAPAMA, 2016. Directiva 91/271/CEE sobre el tratamiento de las aguas residuales urbanas. Manual de interpretación y elaboración de informes. URL: http://www.mapama.gob.es/es/agua/publicaciones/03_Manual_Directiva_91_271_CEE_tcm7-28959.pdf (acceso 06/13/17).
- MAPAMA, 2017. Aceite de oliva - Aceite de oliva y aceituna de mesa - Producciones agrícolas - Agricultura - mapama.es. URL: <http://www.mapama.gob.es/es/agricultura/temas/producciones-agricolas/aceite-oliva-y-aceituna-mesa/aceite.aspx> (acceso 05/14/17).
- Martínez-Huitle, C.A., Brillas, E., 2009. Decontamination of wastewaters containing synthetic organic dyes by electrochemical methods: A general review. *Appl. Catal. B: Environ.* 87, 105–145. doi:10.1016/j.apcatb.2008.09.017
- Mcnamara, C.J., Anastasiou, C.C., O'Flaherty, V., Mitchell, R., 2008. Bioremediation of olive mill wastewater. *Int. Biodeterior. Biodegrad.* 61, 127–134. doi:10.1016/j.ibiod.2007.11.003
- Mert, B.K., Yonar, T., Kiliç, M.Y., Kestioglu, K., 2010. Pre-treatment studies on olive oil mill effluent using physicochemical, Fenton and Fenton-like oxidations processes. *J. Hazard. Mater.* 174, 122–128. doi:10.1016/j.jhazmat.2009.09.025
- Minh, D.P., Aubert, G., Gallezot, P., Besson, M., 2007. Degradation of olive oil mill effluents by catalytic wet air oxidation: 2-Oxidation of *p*-hydroxyphenylacetic and *p*-hydroxybenzoic acids over Pt and Ru supported catalysts. *Appl. Catal. B: Environ.* 73, 236–246. doi:10.1016/j.apcatb.2006.12.014
- Ministerio de Medio Ambiente, 2007. El Plan Nacional de Calidad de la Aguas: Saneamiento y Depuración 2007-2015. URL: http://www.mapama.gob.es/es/agua/planes-y-estrategias/PlanNacionalCalidadAguas_tcm7-29339.pdf (acceso 05/13/17).
- Ministerio de Obras Públicas y Urbanismo, 1989. Real Decreto 849/1986, de 11 de abril, por el que se aprueba el Reglamento del Dominio Público Hidráulico, que desarrolla los títulos Preliminar, I, IV, V, VI y VII de la Ley 29/1985, de 2 de agosto, de Aguas. BOE 103, 34496–34500.
- Miranda, M.T., Cabanillas, A., Rojas, S., Montero, I., Ruiz, A., 2006. Combined combustion of various phases of olive wastes in a conventional combustor. *Fuel* 86, 367–372. doi:10.1016/j.fuel.2006.07.026
- Montoya, F.G., Baños, R., Meroño, J.E., Manzano-Agugliaro, F., 2016. The research of water use in Spain. *J. Clean. Prod.* 112, 4719–4732. doi:10.1016/j.jclepro.2015.06.042
- Moreira, F.C., Boaventura, R.A.R., Brillas, E., Vilar, V.J.P., 2017. Electrochemical advanced oxidation processes: A review on their application to synthetic and real wastewaters. *Appl. Catal. B: Environ.* 202, 217–261. doi:10.1016/j.apcatb.2016.08.037
- Moreno-Casillas, H.A., Cocke, D.L., Gomes, J.A.G., Morkovsky, P., Parga, J.R., 2007. Electrocoagulation mechanism for COD removal. *Sep. Purif. Technol.* 56, 204–211. doi:10.1016/j.seppur.2007.01.031
- Mota, F.L., Queimada, A.J., Pinho, S.P., Macedo, E.A., 2008. Aqueous solubility of some natural phenolic compounds. *Ind. Eng. Chem. Res.* 47, 5182–5189. doi:10.1021/ie071452o
- National Center for Biotechnology Information, 2004. 4-hydroxyphenylacetic acid. PubChem Compd. Database; CID=127. URL <https://pubchem.ncbi.nlm.nih.gov/compound/127> (acceso 06/05/17).



- Niaounakis, M., Halvadakis, C.P., 2006. Olive Processing Waste Management, Waste Management Series. Elsevier. doi:10.1016/S0713-2743(06)80004-8
- Nidheesh, P.V, Gandhimathi, R., 2012. Trends in electro-Fenton process for water and wastewater treatment: An overview. *Desalination* 299, 1–15. doi:10.1016/j.desal.2012.05.011
- Nieto, L.M., Hodaifa, G., Rodríguez, S., Giménez, J.A., Ochando, J., 2011. Degradation of organic matter in olive-oil mill wastewater through homogeneous Fenton-like reaction. *Chem. Eng. J.* 173, 503–510. doi:10.1016/j.cej.2011.08.022
- Ntougias, S., Gaitis, F., Katsaris, P., Skoulika, S., Iliopoulos, N., Zervakis, G.I., 2013. The effects of olives harvest period and production year on olive mill wastewater properties - Evaluation of *Pleurotus* strains as bioindicators of the effluent's toxicity. *Chemosphere* 92, 399–405. doi:10.1016/j.chemosphere.2013.01.033
- Ochando-Pulido, J.M., Martínez-Ferez, A., 2015. On the recent use of membrane technology for olive mill wastewater purification. *Membranes (Basel)*. 5, 513–531. doi:10.3390/membranes5040513
- Ochando-Pulido, J.M., Pimentel-Moral, S., Verardo, V., Martínez-Ferez, A., 2017. A focus on advanced physico-chemical processes for olive mill wastewater treatment. *Sep. Purif. Technol.* 179, 161–174. doi:10.1016/j.seppur.2017.02.004
- Ochando-Pulido, J.M., Verardo, V., Segura-Carretero, A., Martínez-Ferez, A., 2015. Technical optimization of an integrated UF/NF pilot plant for conjoint batch treatment of two-phase olives and olive oil washing wastewaters. *Desalination* 364, 82–89. doi:10.1016/j.desal.2014.10.040
- Oller, I., Malato, S., Sánchez-Pérez, J.A., 2011. Combination of advanced oxidation processes and biological treatments for wastewater decontamination—A review. *Sci. Total Environ.* 409, 4141–4166. doi:10.1016/j.scitotenv.2010.08.061
- Olvera-Vargas, H., Oturan, N., Oturan, M.A., Brillas, E., 2015. Electro-Fenton and solar photoelectro-Fenton treatments of the pharmaceutical ranitidine in pre-pilot flow plant scale. *Sep. Purif. Technol.* 146, 127–135. doi:10.1016/j.seppur.2015.03.046
- Ozdemir, Y., Ozdemir, B.A., Ozkan, M., 2012. Comparative view on the pollution effect of wastewaters from olive oil and table industries, in: PROSODOL (Ed.), *Proceedings Symposium on “Olive Mill Wastes and Environmental Protection.”* Chania, Greece, pp. 59–77.
- Panizza, M., 2010. Importance of Electrode Material in the Electrochemical Treatment of Wastewater Containing Organic Pollutants, in: Comninellis, C., Chen, G. (Eds.), *Electrochemistry for the Environment*. Springer New York, New York, NY, pp. 25–54. doi:10.1007/978-0-387-68318-8_1
- Patel, P.S., Bandre, N., Saraf, A., Ruparelia, J.P., 2013. Electro-catalytic Materials (Electrode Materials), in: *Electrochemical Wastewater Treatment*. *Procedia Eng.* 51, 430–435. doi:10.1016/j.proeng.2013.01.060
- Pawar, R., Lee, C.S., 2015. Basics of Photocatalysis, In *Heterogeneous Nanocomposite-Photocatalysis for Water Purification*. William Andrew Publishing, Boston, Chapter 1, pp. 1–23. doi:10.1016/B978-0-323-39310-2.00001-1
- Pelendridou, K., Michailides, M.K., Zagklis, D.P., Tekerlekopoulou, A.G., Paraskeva, C.A., Vayenas, D. V., 2014. Treatment of olive mill wastewater using a



- coagulation-flocculation process either as a single step or as post-treatment after aerobic biological treatment. *J. Chem. Technol. Biotechnol.* 89, 1866–1874. doi:10.1002/jctb.4269
- Piazzon, A., Forte, M., Nardini, M., 2010. Characterization of phenolics content and antioxidant activity of different beer types. *J. Agric. Food Chem.* 58, 10677–10683. doi:10.1021/jf101975q
- Pignatello, J.J., 1992. Dark and photoassisted Fe³⁺-catalyzed degradation of chlorophenoxy herbicides by hydrogen peroxide. *Environ. Sci. Technol.* 26, 944–951. doi: 10.1021/es00029a012
- Pipi, A.R.F., Sirés, I., De Andrade, A.R., Brillas, E., 2014. Application of electrochemical advanced oxidation processes to the mineralization of the herbicide diuron. *Chemosphere* 109, 49–55. doi:10.1016/j.chemosphere.2014.03.006
- PROSODOL, 2012. Integrated Strategy of actions, measures and means suitable for Mediterranean Countries. URL: http://www.prosodol.gr/sites/prosodol.gr/files/ACT15_1.pdf (acceso 05/15./17).
- Ratnayaka, D.D., Brandt, M.J., Johnson, K.M., Twort, A.C., 2009. CHAPTER 1 – The Demand for Public Water Supplies, in: *Water Supply*. Butterworth-Heinemann, pp. 1–35. doi:10.1016/B978-0-7506-6843-9.00009-3
- Rozzi, A., Malpei, F., 1996. Treatment and disposal of olive mill effluents. *Int. Biodeterior. Biodegrad.* 135, 135–144.
- Sabbatini, V., 2014. The supply function of olive oil: a case study of Italy. *Procedia Econ. Financ.* 14, 553–558. doi:10.1016/S2212-5671(14)00755-2
- Shakeel, F., Salem-Bekhit, M.M., Haq, N., Siddiqui, N.A., 2017. Solubility and thermodynamics of ferulic acid in different neat solvents: Measurement, correlation and molecular interactions. *J. Mol. Liq.* 236, 144–150. doi:10.1016/j.molliq.2017.04.014
- Shimadzu Corporation, 2003. TOC-VCPH/CPN & TOC-Control V Software User Manual 384.
- Sirés, I., Brillas, E., 2012. Remediation of water pollution caused by pharmaceutical residues based on electrochemical separation and degradation technologies: A review. *Environ. Int.* 40, 212–229. doi:10.1016/j.envint.2011.07.012
- Sirés, I., Brillas, E., Oturan, M.A., Rodrigo, M.A., Panizza, M., 2014. Electrochemical advanced oxidation processes: Today and tomorrow. A review. *Environ. Sci. Pollut. Res.* 21, 8336–8367. doi:10.1007/s11356-014-2783-1
- Sirés, I., Garrido, J.A., Rodríguez, R.M., Brillas, E., Oturan, N., Oturan, M.A., 2007. Catalytic behavior of the Fe³⁺/Fe²⁺ system in the electro-Fenton degradation of the antimicrobial chlorophene. *Appl. Catal. B: Environ.* 72, 382–394. doi:10.1016/j.apcatb.2006.11.016
- Skoumal, M., Rodríguez, R.M., Cabot, P.L., Centellas, F., Garrido, J.A., Arias, C., Brillas, E., 2009. Electro-Fenton, UVA photoelectro-Fenton and solar photoelectro-Fenton degradation of the drug ibuprofen in acid aqueous medium using platinum and boron-doped diamond anodes. *Electrochim. Acta* 54, 2077–2085. doi:10.1016/j.electacta.2008.07.014
- Soto, M.L., Moure, A., Domínguez, H., Parajó, J.C., 2011. Recovery, concentration and purification of phenolic compounds by adsorption: A review. *J. Food Eng.* 105, 1–27. doi:10.1016/j.jfoodeng.2011.02.010
- Suna, A., Yay, E., Oral, H.V., Onay, T.T., Yenigün, O., 2011. A study on olive oil mill wastewater management in Turkey: A questionnaire and experimental



- approach. *Resour. Conserv. Recycl.* 60, 64–71. doi:10.1016/j.resconrec.2011.11.009
- Takeda, K., Fujisawa, K., Nojima, H., Kato, R., Ueki, R., Sakugawa, H., 2017. Hydroxyl radical generation with a high power ultraviolet light emitting diode (UV-LED) and application for determination of hydroxyl radical reaction rate constants. *J. Photochem. Photobiol. A Chem.* 340, 8–14. doi:10.1016/j.jphotochem.2017.02.020
- Teh, C.Y., Budiman, P.M., Shak, K.P.Y., Wu, T.Y., 2016. Recent advancement of coagulation–flocculation and its application in wastewater treatment. *Ind. Eng. Chem. Res.* 55, 4363–4389. doi:10.1021/acs.iecr.5b04703
- Tezcan Un, U., Ugur, S., Koparal, A.S., Bakir Ogutveren, U., 2006. Electrocoagulation of olive mill wastewater. *Sep. Purif. Technol.* 52, 136–141. doi:10.1016/j.seppur.2006.03.029
- Topi, D., Beqiraj, I., Seiti, B., Halimi, E., 2014. Environmental impact from olive mills waste disposal, chemical analysis of solid wastes and wastewaters. *J. Hyg. Eng. Des.* 7, 44–48.
- Torrecilla, J.S., 2010. Phenolic Compounds in Olive Oil Mill Wastewater, in: Watson, V.R.P. and R.R. (Ed.), *Olives and Olive Oil in Health and Disease Prevention*. Academic Press, San Diego, pp. 357–364. doi:10.1016/B978-0-12-374420-3.00040-1
- United Nations, 1987. *Our Common Future: Report of the World Commission on Environment and Development*. URL: <http://www.un-documents.net/our-common-future.pdf> (acceso 06/08/17).
- United Nations, 2007. *GEO 4, Global Environment Outlook, environment for development*, Unep. Progress Press Ltd., Valleta, Malta. doi:9789280728361
- Vidal, J., Huiliñir, C., Salazar, R., 2016. Removal of organic matter contained in slaughterhouse wastewater using a combination of anaerobic digestion and solar photoelectro-Fenton processes. *Electrochim. Acta* 210, 163–170. doi:10.1016/j.electacta.2016.05.064
- Walling, C., 1975. Fenton's reagent revisited. *Acc. Chem. Res.* 8, 125–131. doi:10.1021/ar50088a003
- Wan, L., Wang, C., Cai, W., 2016. Impacts on water consumption of power sector in major emitting economies under INDC and longer term mitigation scenarios: An input-output based hybrid approach. *Appl. Energy* 184, 26–39. doi 10.1016/j.apenergy.2016.10.013
- Wang, N., Zheng, T., Zhang, G., Wang, P., 2016. A review on Fenton-like processes for organic wastewater treatment. *J. Environ. Chem. Eng.* 4, 762–787. doi:10.1016/j.jece.2015.12.016
- Welcher, F.J., 1967. *Standard Methods of Chemical Analysis. Instrumental Analysis.*, 6th Ed. D. VAN Nostrand Company, Inc., Princeton, New Jersey.
- World Water Council, 2000. *The Use of Water Today*, 1st Ed. Earthscan Publications Ltd, London, UK.
- WTW, 2001. *Determination of Biochemical Oxygen Demand (BOD). User's Manual*.
- WWAP, 2006. *Water: a shared responsibility - The United Nations world water development report 2, executive summary*.
- Yahiaoui, O., Lounici, H., Abdi, N., Drouiche, N., Ghaffour, N., Pauss, A., Mameri, N., 2011. Treatment of olive mill wastewater by the combination of ultrafiltration and bipolar electrochemical reactor processes. *Chem. Eng. Process. Process Intensif.* 50, 37–41. doi: 10.1016/j.cep.2010.11.003
- Yangui, A., Abderrabba, M., Sayari, A., 2016. Amine-modified mesoporous silica



- for quantitative adsorption and release of hydroxytyrosol and other phenolic compounds from olive mill wastewater. *J. Taiwan Inst. Chem. Eng.* 70, 111–118. doi:10.1016/j.jtice.2016.10.053
- Zabela, V., Sampath, C., Oufir, M., Moradi-Afrapoli, F., Butterweck, V., Hamburger, M., 2016. Pharmacokinetics of dietary kaempferol and its metabolite 4-hydroxyphenylacetic acid in rats. *Fitoterapia*. doi:10.1016/j.fitote.2016.10.008
- Zagklis, D.P., Vavouraki, A.I., Kornaros, M.E., Paraskeva, C.A., 2015. Purification of olive mill wastewater phenols through membrane filtration and resin adsorption/desorption. *J. Hazard. Mater.* 285, 69–76. doi:10.1016/j.jhazmat.2014.11.038
- Zhang, L.W., Al-Suwayeh, S.A., Hsieh, P.W., Fang, J.Y., 2010. A comparison of skin delivery of ferulic acid and its derivatives: Evaluation of their efficacy and safety. *Int. J. Pharm.* 399, 44–51. doi:10.1016/j.ijpharm.2010.07.054
- Zhang, Y., Wang, A., Tian, X., Wen, Z., Lv, H., Li, D., Li, J., 2016. Efficient mineralization of the antibiotic trimethoprim by solar assisted photoelectro-Fenton process driven by a photovoltaic cell. *J. Hazard. Mater.* 318, 319–328. doi:10.1016/j.jhazmat.2016.07.021
- Zorpas, A.A., Costa, C.N., 2010. Combination of Fenton oxidation and composting for the treatment of the olive solid residue and the olive mill wastewater from the olive oil industry in Cyprus. *Biosource Technol.* 101, 7984–7987. doi:10.1016/j.biortech.2010.05.030



